# METHODS FOR GAS CHROMATOGRAPHY/TANDEM MASS SPECTROMETRY ON THE QUADRUPOLE ION TRAP

By

NATHAN A. YATES

A DISSERTATION PRESENTED TO THE GRADUATE SCHOOL
OF THE UNIVERSITY OF FLORIDA IN PARTIAL FULFILLMENT
OF THE REQUIREMENTS FOR THE DEGREE OF
DOCTOR OF PHILOSOPHY

UNIVERSITY OF FLORIDA

1994

LD
1780
1994
.Y33

To my high school science teacher Linda Ingling, my academic hero Professor Anthony LoBello, and my loving parents.

ACKNOWLEDGEMENTS

I would like to express my sincere gratitude to Dr. Rick Yost for his guidance, friendship, and patience over the past five years. I am very glad to have had the pleasure of working in his laboratory, and the freedom he gives all of his students to pursue their own directions. I would also like to acknowledge Drs. Peggy Borum and Jodie Johnson for their collaboration and input into my work at the University of Florida.

In addition, I feel very fortunate to have worked with the Finnigan MAT research and development team. I would like to thank Drs. Mike Story and George Stafford for overseeing my employment and maintaining corporate support for my research. I would also like to thank Steve Bradshaw, Don Hoekman and David Tucker for teaching me how to write and modify the ion trap software that was developed as part of my dissertation.

Dr. Pete Palmer has also been a great friend and enthusiastic colleague. Thank you for funding this work and sharing a memorable summer in Northern California. I wish you the best of luck in your new career as a university professor.

I would also like to credit Jeanne Karalby, Beverly Lisk, and Donna Balkcom for the extra steps they took to help make my graduate career less stressful. I would also like to thank Russ Pierce for designing, building, and repairing much of the special electronics that were required for my experiments. I am also very grateful to have worked with Joe Shalosky who taught me how to machine the custom parts that I often needed.

I would also like to express my most sincere appreciation to my fellow graduate students whom I worked with and learned from on a daily basis. Their knowledge and

friendship made the lab an exciting place to work and Gainesville a great place to live. In particular, I want to thank Tim Griffin for the many hours that he spent writing the gatorware code. It is difficult to imagine how I would have achieved my goals without your help. I also need to acknowledge my collaborators Jim Stephenson and Matt Booth for co-authoring a book chapter on ion trap GC/MS/MS.

Thanks go to my friends for all of the pizza nights, camping trips, beach parties, and other distractions that made the last five years so memorable. Finally, I would like to thank my wife, Jan, for her love, patience, and understanding. I couldn't have done it without your help!

TABLE OF CONTENTS

page

ACKNOWLEDGEMENTS ..... iii

LIST OF TABLES ..... viii

LIST OF FIGURES ..... ix

ABSTRACT ..... xv

CHAPTERS

1 OVERVIEW ..... 1

The Quadrupole Ion Trap ..... 2
Ion Storage and the Mathieu Stability Diagram ..... 4
Mass Selective Instability Scan ..... 7
The Ion Trap Scan Program ..... 12
Overview of Dissertation ..... 14

2 PRACTICAL ION TRAP TECHNOLOGY: GC/MS AND GC/MS/MS ..... 18

Introduction ..... 18
Instrumentation and Methods of Operation ..... 20
GC/MS and GC/MS/MS Applications ..... 41
Operational Principles for Ion Trap GC/MS ..... 49
Space Charge Effects ..... 51
Space Charge and Automatic Ionization Control ..... 55
EI Scan Segments ..... 57
Scan Repetition Rate ..... 59
Single Ion Monitoring vs. Full Scan ..... 63
Ion-Molecule Reactions ..... 66
Mass Spectral Skewing ..... 72
Advances in Ion Trap GC/MS and GC/MS/MS ..... 73
Methods for Reducing Background Interferences ..... 74
Single-frequency resonance ejection ..... 75
Multiple-frequency resonance ejection ..... 76
RF/DC ..... 82

External Ionization GC/MS ..... 84
Tuning Methods for GC/MS/MS ..... 94
Frequency Shifts, Resonant Excitation Methods, and CID .. 97
Benchtop GC/MS/MS Instruments ..... 105
Summary ..... 110

3 ION ISOLATION ..... 113

Introduction ..... 113
Experimental ..... 118
Instrumentation ..... 118
Apex Isolation Scan Program ..... 120
Two-step Isolation Scan Program ..... 126
$E_{iso}$ and $E_{EJ}$ Measurements ..... 133
Acquiring $E_{iso}$ and $E_{EJ}$ Data as a Function of DC Voltage . 135
$E_{iso}$ and $E_{EJ}$ Measurements at a Series of $q_z$ Values ..... 135
Storage Time Studies ..... 136
Supplementary AC Voltage Studies ..... 136
Results and Discussion ..... 137
$E_{EJ}$ and $E_{iso}$ for Apex and Two-step Isolation ..... 141
Two-step Isolation and the Sharpness of the Stability Diagram Edges ..... 149
Storage Time Studies ..... 154
Effect of the Supplementary AC Voltage Applied During Isolation ..... 163
Practical Considerations for Apex and Two-step Isolation . 166
Summary ..... 167

4 ION EXCITATION ..... 169

Introduction ..... 169
Frequency-Assignment Pre-Scan ..... 171
Frequency Modulated Broadband Excitation ..... 176
SWIFT Broadband Excitation ..... 178
Experimental ..... 180
Instrumentation ..... 181
Frequency Shift Measurements ..... 181
Frequency Modulation on the ITMS ..... 182
Frequency-Assignment Pre-Scan ..... 183
Frequency Modulated Broadband Excitation ..... 185
SWIFT Broadband Excitation ..... 186
Results and Discussion ..... 187
MS/MS Efficiencies and Frequency Shifts ..... 187
Frequency-Assignment Pre-Scan ..... 196
Frequency Modulated Broadband Excitation ..... 206
SWIFT Broadband Excitation ..... 212
Summary ..... 215

5 A BENCHTOP ION TRAP FOR GC/MS/MS ..... 218

Introduction ..... 218
Instrumentation ..... 219
GC/MS Hardware ..... 219
Hardware Modifications ..... 220
Software ..... 225
Scan Editor and Acquisition Software ..... 226
SWIFT Software ..... 231
Software Integration ..... 233
Experimental ..... 234
AGC-EI Calibration Studies ..... 234
ARC-CI Calibration Studies ..... 237
Fixed Ionization Time Studies ..... 237
Carnitine Analyses ..... 237
ARC-CI Cocaine Analyses ..... 241
AGC-EI Petroleum Analyses ..... 241
ARC-CI Barbiturate Analyses ..... 245
Results and Discussion ..... 245
AGC-EI Calibration Studies ..... 247
AGC-CI/MS/MS Calibration Studies ..... 262
Fixed Ionization Time Studies ..... 271
Carnitine Analyses ..... 274
Additional GC/MS/MS Analyses ..... 291
Summary ..... 303

6 CONCLUSIONS AND FUTURE WORK ..... 306

REFERENCE LIST ..... 311

BIOGRAPHICAL SKETCH ..... 320

LIST OF TABLES


| Table | | page |
|---|---|---|
| Table 3-1. | Summary of apex isolation scan program. | 122 |
| Table 3-2. | Summary of two-step isolation scan program. | 129 |
| Table 5-1. | AGC-EI/MS/MS scan program list. | 229 |
| Table 5-2. | AGC-EI parameters for the analysis of benzophenone. | 236 |
| Table 5-3. | ARC-CI parameters for the analysis of benzophenone. | 238 |
| Table 5-4. | Fixed EI parameters for the analysis of benzophenone. | 239 |
| Table 5-5. | Summary of carnitine test mixture. | 241 |
| Table 5-6. | Summary of instrument parameters for the analysis of camitine. | 242 |
| Table 5-7. | Summary of parameters for the analysis of cocaine. | 243 |
| Table 5-8. | ARC-EI parameters for the analysis of petroleum. | 244 |
| Table 5-9. | Summary of parameters for the analysis of barbiturates. | 246 |

LIST OF FIGURES


| Figure | | page |
|---|---|---|
| 1-1. | Ion trap electrodes. | 4 |
| 1-2. | A portion of the quadrupole ion trap Mathieu stability diagram that is used to describe the stability and motion of ions stored in a quadrupolar field. | 7 |
| 1-3. | Diagram of the mass-selective instability scan showing the RF amplitude as a function of time. | 12 |
| 1-4. | Ion trap scan program used to acquire EI mass spectra for m/z 60 - m/z 100. | 14 |
| 2-1. | EI/MS profile spectra of ionized perflourotributylamine $(C_4F_9)_3N$ (MW = 642). | 23 |
| 2-2. | Background subtracted full-scan mass spectra for the injection of 10 ng amobarbital (MW = 226). | 25 |
| 2-3. | Ion trap scan program used to acquire CI mass spectra for m/z 50 - 650. | 27 |
| 2-4. | AGC (EI) automatic ionization control scan program. | 30 |
| 2-5. | ARC (CI) automatic ionization control scan program. | 32 |
| 2-6. | EI/MS calibration curve for m/z 284 of hexachlorobenzene (MW = 284). | 34 |
| 2-7. | Ion trap scan program used to acquire EI/MS/MS product ion spectra for m/z 134. | 37 |
| 2-8. | Background subtracted EI/MS/MS product ion spectrum for $M^{+\cdot}$ ion (m/z 134) of n-butylbenzene (MW = 134); 1 pg injected. | 39 |
| 2-9. | EI/MS profile spectra of ionized perflourotributylamine $(C_4F_9)_3N$ (MW = 642). | 41 |

2-10. GC/MS data of the trimethylsilyl-enol trimethylsilyl derivative of norandrosterone isolated from a urine sample and analyzed by the ion trap detector in the positive-ion CI mode. . . . . 46

2-11. GC full-scan MS/MS analysis of an extract of plasma initially spiked at 1 ng/g. . . . . 49

2-12. Separate background subtracted centroid mass spectra for hexachlorobenzene. . . . . 55

2-13. Ion trap scan program used to acquire EI mass spectra from m/z 60 - m/z 650 using four scan segments. . . . . 59

2-14. Scan repetition rate (scan/s) for an EI/MS segmented scan program as a function of the number of µscans. . . . . 63

2-15. Relationship between the acquisition range and the maximum number of µscans that can be averaged for an AGC-EI/MS scan program with a scan repetition rate of 1 scan/s. . . . . 66

2-16. Mass spectrum for 100 ng of benzophenone (MW = 182) analyzed using standard GC/ion trap MS configuration, showing excessive (M+1) abundance and adduct formation due to ion-molecule reactions. . . . . 69

2-17. Tendency of fragment ions from methyl deconate to donate a proton to the neutral ester. . . . . 72

2-18. Resonant ejection mass-selective instability scan of a 37.1 pmol sample of substance P. . . . . 79

2-19. Comparison of GC/MS data for 200 pg of cocaine (MW = 303) in the presence of a 100 ng of PAH background. . . . . 82

2-20. Internal and external ionization hardware. . . . . 86

2-21. Total ion chromatogram and mass spectrum for 1 ng of benzophenone analyzed on the GC/ion trap MS system using external ionization. . . . . 89

2-22. Comparison of the (M+1)/(M) ratio for the analysis of benzophenone using both internal and external ionization systems. . . . . 91

2-23. Mass spectrum for 500 ng of benzophenone analyzed using GC/ion trap MS with external ionization, showing correct (M+1) abundance and no adduct formation. . . . . 94

2-24. Ion signal as a function of excitation frequency. . . . . 99

2-25. Product ion spectra as a function of ionization time, showing the effect on MS/MS efficiency. . . . . 102

2-26. Random noise excitation spectrum. . . . . 105

3-1. Stability diagram in ($a_z$,$q_z$) space for the quadrupole mass filter. . . . . 116

3-2. Calibration curve for the DC output of the ITMS selective mass storage electronics relative to the software set voltage. . . . . 120

3-3. Stability diagram in ($a_z$,$q_z$) space showing the inner region that corresponds to mathematically stable ion trajectories in the quadrupole ion trap. . . . . 124

3-4. Ion trap scan program used to isolate m/z 157 at the apex of the stability diagram. . . . . 126

3-5. Stability diagram in ($a_z$,$q_z$) space showing the inner region that corresponds to mathematically stable ion trajectories in the quadrupole ion trap. . . . . 131

3-6. Ion trap scan program used to isolate m/z 157 using a two-step isolation sequence. . . . . 133

3-7. Two-step isolation of bromobenzene. . . . . 139

3-8. Two-step isolation of 1-octene. . . . . 141

3-9. Relationship between $E_{ISO}$ vs. $E_{EJ}$ for the isolation of m/z 157 of bromobenzene at the apex of the stability diagram. . . . . 143

3-10. $E_{ISO}$ versus the $E_{EJ}$ for (a) m/z 158, and (b) m/z 156 for two-step isolation of m/z 157 of bromobenzene. . . . . 146

3-11. $E_{ISO}$ versus $E_{EJ}$ curves for the isolation of m/z 40 and the ejection of m/z for 1-octene. . . . . 149

3-12. $E_{ISO}$ for m/z 40 of 1-octene at various points along the $\beta_z = 0$ and $\beta_r = 0$ stability diagram edge. . . . . 152

3-13. Stability diagrams in (RF, DC) space showing the inner region that corresponds to mathematically stable ion trajectories for m/z 100 and m/z 120 in the quadrupole ion trap. . . . . 154

3-14. Relationship between ion intensities of $156^+$, $157^+$, $158^+$ for ionized bromobenzene and the DC pulse time applied during scan tables 8 and 11 for two-step isolation of m/z 157. . . . . 158

3-15. Relationship between ion intensities of $156^+$, $157^+$, $158^+$ for ionized bromobenzene and the DC pulse time applied during scan table 8 for apex isolation of m/z 157. . . . . 160

3-16. Relationship between the two-step isolated ion intensity (m/z 157) and time observed after the power for the ITMS electronics had been turned on. . . 163

3-17. Isolation efficiency as a function of resonant excitation. . . . . 166

4-1. Frequency breakdown curves for isopherone obtained by incrementing the frequency of the supplementary AC voltage from 110,000 Hz to 122,475 Hz at 25 Hz increments. . . . . 174

4-2. Comparison of mass spectra obtained by an RF amplitude scan and supplementary AC frequency scan. . . . . 176

4-3. Diagram of the computational procedure used to generate stored waveform inverse Fourier transform (SWIFT) broadband excitation waveforms. . . . . 180

4-4. Frequency-assignment pre-scan scan program. . . . . 185

4-5. Comparison of MS/MS spectra taken at three different ionization times. . 189

4-6. Secular frequency versus ionization time. . . . . 193

4-7. Comparison of the total and selected mass chromatograms for the parent ion $139^+$ and product ions $110^+$ and $69^+$ of isopherone. . . . . 196

4-8. Frequency-assignment pre-scan signals. . . . . 198

4-9. Frequency for maximum ejection versus resonant excitation voltage for m/z 156 from bromobenzene. . . . . 201

4-10. Frequency for maximum ejection versus frequency sweep rate for m/z 156 of bromobenzene with an increasing frequency scan. . . . . 204

4-11. Comparison of three MS/MS product ion spectra obtained using the frequency-assignment pre-scan for m/z 134 of n-butylbenzene at ionization times of (a) 5 ms, (b) 85 ms, and (c) 200 ms. . . . . 206

4-12. GC/MS/MS product ion data for m/z 134 of n-butylbenzene (800 pg injected), obtained using broadband excitation over a 10 kHz frequency range centered at 118 kHz. . . . . 209

4-13. GC/MS/MS results obtained for the injection of 140 ng of n-butylbenzene. . . . . 212

4-14. Comparison of the average power spectra for SWIFT and single frequency resonant excitation signals as measured by a digital spectrum analyzer. . 215

5-1. Block diagram of a modified ITS40 GC/MS/MS ion trap. . . . . 222

5-2. Schematic diagram of the active dipolar excitation circuit used to mix the supplementary AC voltages into two signals of equal magnitude that are phase shifted by 180°. . . . . 225

5-3. Screen captures for the scan editor software interface used to create AGC-EI/MS/MS and ARC-CI/MS/MS scan programs. . . . . 228

5-4. Ion trap scan program used to acquire GC/MS/MS EI mass spectra on a modified ITS40. . . . . 231

5-5. Background subtracted AGC-EI/MS spectrum of 3.56 ng of benzophenone (MW = 182) and structure showing fragmentation of the carbon-carbon bond α to the carbonyl to yield the two major fragment ions. . . . . 249

5-6. Background subtracted AGC-EI/MS/MS 182⁺ product ion spectrum of 3.56 ng of benzophenone (MW = 182). . . . . 251

5-7. Calibration curve for benzophenone (MW = 182).. . . . . 255

5-8. EI ion chromatograms for benzophenone. . . . . 260

5-9. Background subtracted spectra for 23 pg of benzophenone. . . . . 262

5-10. Calibration curve for benzophenone (MW = 182). . . . . 265

5-11. Background subtracted spectra for 290 pg of benzophenone. . . . . 268

5-12. CI ion chromatograms for benzophenone. . . . . 271

5-13. Benzophenone EI ion chromatograms for the three predominant EI and 182⁺ product ions are plotted for AGC-EI/MS and EI/MS/MS scan modes. . . . . 274

5-14. Background subtracted ARC-CI/MS mass spectrum and structure for the N-demethylated tertiarybutyldimethylsilyl derivative of isobutyrylcarnitine (MW = 331). . . . . 277

5-15. Fragmentation pathways for N-demethylated tertiarybutyldimethylsilyl derivatives of acylcarnitines. . . . . 280

5-16. AGC-EI/MS chromatograms for nine carnitine standard TBDMS derivatives.. . . . . 282

5-17. AGC-EI/MS/MS chromatograms for nine carnitine standard TBDMS derivatives. . . . . 284

5-18. AGC-EI/MS chromatograms for a TBDMS derivitized liver tissue extract containing nine carnitine standards. . . . . 287

5-19. AGC-EI/MS/MS chromatograms for a TBDMS derivitized liver tissue extract containing nine carnitine standard. . . . . 289

5-20. AGC-EI/MS/MS chromatograms for a TBDMS derivitized liver tissue extract. . . . . 291

5-21. Background subtracted CI spectra for 1.25 ng of cocaine (MW = 303). . . 294

5-22. AGC-EI/MS chromatogram for the injection of petroleum oil that was diluted 1:100 (v:v) in hexane. . . . . 296

5-23. AGC-EI/MS/MS background subtracted mass spectrum for the injection of petroleum oil that was diluted 1:100 (v:v) in hexane. . . . . 298

5-24. Total ion chromatogram for a barbiturate test mixture containing five barbiturates at 2 ng/μL level that was analyzed with a ARC-CI/MS scan program. . . . . 301

5-25. Total ion chromatogram for a barbiturate test mixture containing five barbiturates at 2 ng/μL level that was analyzed with a ARC-CI/MS/MS $227^{+}$ product ion scan program. . . . . 303

Abstract of Dissertation Presented to the Graduate School
of the University of Florida in Partial Fulfillment of the
Requirements for the Degree of Doctor of Philosophy

# METHODS FOR GAS CHROMATOGRAPHY/TANDEM MASS SPECTROMETRY ON THE QUADRUPOLE ION TRAP

By

Nathan A. Yates

April 1994

Chairperson: Richard A. Yost
Major Department: Chemistry

The specific aim of this study was to develop a quadrupole ion trap mass spectrometer for gas chromatography/tandem mass spectrometry (GC/MS/MS) analyses. This work was carried out in three stages. First, the problems associated with the coupling of gas chromatography (GC) and tandem mass spectrometry (MS/MS) on the ion trap were characterized. Second, new ion isolation and ion excitation methods that improve the performance of GC/MS/MS experiments were developed. Finally, a benchtop ion trap mass spectrometer was constructed that combines these new methods into a functional instrument.

The new ion trap utilizes a two-step isolation procedure that allows ions of a specific mass-to-charge-ratio (m/z) to be selectively stored in the ion trap while ions of other m/z are eliminated. Comparison of the two-step isolation technique with traditional isolation methods shows that two-step isolation is more efficient and is simpler to optimize. Additionally, three ion activation methods, single frequency excitation, frequency

modulated (FM) broadband excitation, and stored waveform inverse Fourier transform (SWIFT) broadband excitation, are used to effect dissociation of parent ions in MS/MS experiments. FM and SWIFT broadband excitation are observed to be better suited for GC/MS/MS experiments because they are not affected by shifts in an ion's secular frequency of motion that occur as compounds elute into the ion trap from the GC.

The quadrupole ion trap mass spectrometer constructed in this study represents one of the first ion trap instruments capable of performing GC/MS/MS and was used to characterize the analytical advantages and limitations of ion trap GC/MS/MS. Comparison of several figures of merit reveals that ion trap GC/MS/MS can be used to increase the selectivity over that of GC/MS while obtaining lower limits of detection and a comparable linear dynamic range. Example acylcarnitine, cocaine, petroleum, and barbiturate analyses demonstrate that while the new instrument greatly improves the feasibility of ion trap GC/MS/MS, ion-molecule reactions and inefficient ion isolation may limit the utility of the instrument for some samples.

# CHAPTER 1
# OVERVIEW

The recent emergence of the quadrupole ion trap as a high performance mass analyzer is perhaps the most important advancement to occur in the area of mass spectrometric instrumentation in recent decades. Benchtop mass spectrometers based on the softball sized quadrupole ion trap exhibit ultralow detection limits that are less than or equal to those of the most sensitive mass spectrometers available today. In addition to high sensitivity, numerous operational modes such as tandem mass spectrometry, external ionization, extended mass range, and high resolution have been developed that demonstrate the "high performance" potentials and versatility of ion traps. The ion trap's simple mechanical design also makes it one of the least expensive mass spectrometers available. The combination of tremendous performance, miniature size, and affordable price is expected to make the ion trap the future mass spectrometer of choice.

At present, "high performance" ion trap mass spectrometers are in the early stages of development. One current limitation of today's ion traps is that the "high performance" capabilities, like tandem mass spectrometry, can be spoiled if sample pressures inside the mass spectrometer fluctuate. For this reason, some of the most common sample inlet systems, such as gas and liquid chromatography, complicate the use of the ion trap's advanced features.

Gas chromatography/tandem mass spectrometry (GC/MS/MS) based on a different type of instrument, the triple quadrupole mass spectrometer, is an important analytical tool for the analysis of trace constituents present in complex matrices. The development of practical GC/MS/MS techniques on the ion trap mass spectrometer would have a large impact on analytical mass spectrometry and analytical chemistry as a whole. Potential applications include high confidence drug testing procedures, rapid on-site environmental pollutant screening, and continuous real-time environmental and process monitoring.

The specific aim of this study was to investigate new methods for achieving practical GC/MS/MS on the quadrupole ion trap. New techniques and instrumentation have been developed to overcome many of the problems that have restricted the ion trap's use for GC/MS/MS analyses. In particular, three problems have made ion trap GC/MS/MS impractical: shifts in an ion's secular frequency of motion due to changing ion abundances, the need for real-time ionization control to limit space charge for tandem mass spectrometry (MS/MS) experiments, and complicated setup and tuning procedures required for MS/MS scan programs. A benchtop GC/MS/MS ion trap mass spectrometer, based on the Finnigan MAT ITS-40, has been constructed and tested. The instrument employs automatic ionization control, two-step isolation, stored waveform inverse Fourier transform broadband excitation, and sophisticated instrument control and data processing software.

## The Quadrupole Ion Trap

Figure 1-1 shows a cross sectional and a three dimensional view of a set of quadrupole ion trap electrodes used in commercial ion trap mass spectrometers.

Figure 1-1. Ion trap electrodes. Cross section and three dimensional view of the hyperbolic ring and endcap electrodes used in commercial ion trap instruments.[1]

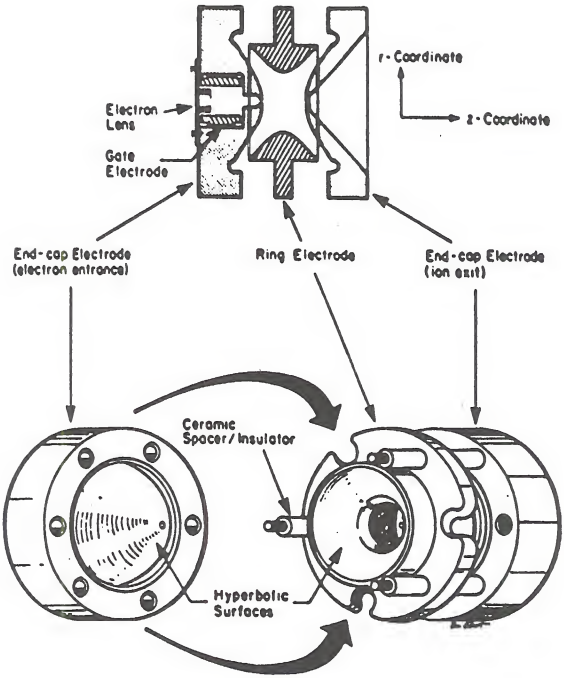
r - Coordinate
z - Coordinate
Electron Lens
Gate Electrode
End-cap Electrode (electron entrance)
Ring Electrode
End-cap Electrode (ion exit)
Ceramic Spacer/Insulator
Hyperbolic Surfaces

Three rotationally symmetric electrode surfaces define the ion trap's inner cavity. The electrodes are commonly referred to as the ring and endcap electrodes. By applying an oscillating electrical signal of the proper amplitude and frequency to the ring electrode, a quadrupole field is created that can be used to confine charged particles or ions in the center of the device (hence the name "ion trap.")

The quadrupole ion trap was first disclosed in 1953 by Paul and Steinwedel who were later awarded the 1991 Nobel prize in physics for their invention. Quadrupole Storage Mass Spectrometry by March and Hughes provides a historical account of the development of the ion trap.[2] Many modes of operation have been employed since the ion trap's inception to manipulate ions of various mass-to-charge ratios (m/z), but the development of a truly practical method of obtaining a mass spectrum was only recently developed. The mass-selective instability scan allowed a complete mass spectrum to be obtained from a single ionization event and led to the commercialization of the ion trap as a GC/MS detector in 1984.[3]

## Ion Storage and the Mathieu Stability Diagram

The equations governing ion storage and motion in a quadrupolar field are presented in several manuscripts and review articles.[4-7] A thorough discussion of this subject is not presented here as it is not required for the comprehension of the material in this dissertation. Instead, the principles that control the ion motion with respect to the Mathieu stability diagram are summarized.

The portion of the Mathieu stability diagram for the quadrupole ion trap that is relevant to the ion trap's operation as a mass spectrometer is shown in Figure 1-2. The Mathieu parameters $a_z$ and $q_z$ are plotted on the ordinate and abscissa,

Figure 1-2. A portion of the quadrupole ion trap Mathieu stability diagram that is used to describe the stability and motion of ions stored in a quadrupolar field.[2]

## Ion Trap Stability Diagram

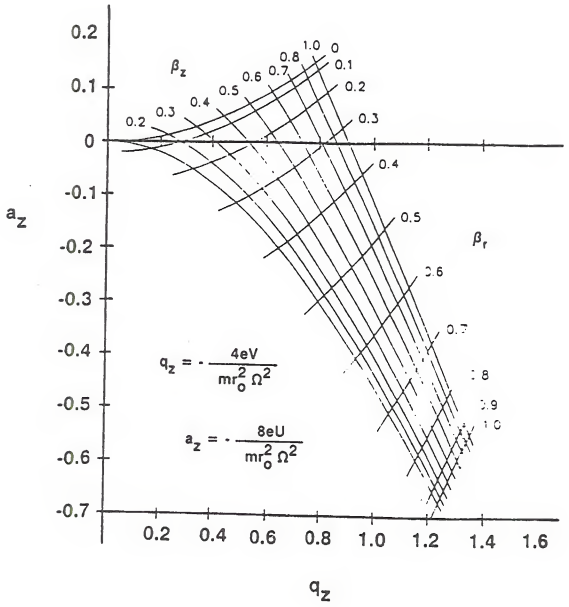

respectively. These parameters define an ion's stability or instability to the ion trap's physical and electrical characteristics. Simply stated, ions that have $a_z$ and $q_z$ values that fall within the outer boundaries of the stability diagram will be stored in the ion trap. Ions possessing an $a_z$ and $q_z$ coordinate outside the outer boundaries of the stability diagram will follow an unstable trajectory and will not be stored in the device. The equations used for calculating an ion's $a_z$ and $q_z$ values are shown in Figure 1-2, where e is the charge on an electron, V is the amplitude of the radio frequency (RF) voltage that is applied to the ring electrode, m is the mass of the ion, $r_o$ is the inner radius of the ring electrode, $\Omega$ is the frequency of the RF voltage and U is the DC potential applied to the ring electrode. Examination of these equations reveals that $q_z$ and $a_z$ are proportional to the amplitude of the RF voltage and potential of the DC voltages that are applied to the ion trap ring electrode, respectively. Additional information contained in the Mathieu stability relates to the motion of the ions that are stored in or exit the ion trap.

Ions contained in a quadrupole field are not stationary. Instead, trapped ions follow complicated orbits around the center of the ion trap. Movement in the axial direction or z-direction refers to ions traveling away from one endcap and towards the other. Movement in the radial or r-direction refers to ions traveling in the direction of the ring electrode. The rate with which trapped ions traverse back and forth in either the z-direction or r-direction is described as the ion's frequency in the z-direction or r-direction. Simply stated, an ion has a high frequency in the z direction if it oscillates back and forth from endcap to endcap at a rapid rate. Likewise, an ion has a high frequency in the r-direction if its path of motion follows the inner circumference of the ring electrode at a rapid rate. The Mathieu stability diagram shown in Figure 1-2

contains iso-beta lines, $\beta_z$ and $\beta_r$, that correspond to an ion's frequency of motion in the z-direction and the r-direction, respectively. The iso-beta lines are shown as the lines that criss-cross the Mathieu stability diagram. Ions that have $a_z$ and $q_z$ coordinates near the iso-beta line $\beta_z$=1 have a high frequency of motion in the z-direction, and conversely ions that have $a_z$ and $q_z$ coordinates near the iso-beta line $\beta_z$=0 have a low frequency of motion in the z-direction. A similar relationship holds for the iso-beta lines $\beta_r$=1 and $\beta_r$=0. The frequency of motion in the z-direction is often referred to as an ion's secular frequency of motion.

Understanding the following statements will help reaffirm the material presented in this section.

1. Ions with $a_z$ and $q_z$ coordinates that fall within the Mathieu stability diagram follow theoretically stable trajectories and are stored in the ion trap.

2. For an ion trap of fixed dimensions, fixed RF amplitude, fixed DC voltage, and fixed RF frequency, more massive ions will have a lower $q_z$ value than less massive ions.

3. Increasing the applied RF amplitude will increase the $q_z$ values for all ions.

4. Increasing the applied DC potential will increase the absolute magnitude of $a_z$ for all ions.

5. Increasing the applied RF potential will increase the frequency of ion motion in the z direction for all ions in the ion trap.

6. The application of an RF amplitude without the use of a DC potential results in all ions having an $a_z$ value equal to zero. (RF-only mode)

7. If an ion of m/z 20 has the Mathieu coordinates $a_z$ = 0 and $q_z$ = 0.9 all ions above m/z 20 will have stable $a_z$ and $q_z$ coordinates, allowing a wide mass range of ions to be trapped.

8. For an ion trap of fixed dimensions, voltages, and frequencies, ions of high m/z are positioned to the left of the stability diagram and ions of low m/z are positioned to the right of the stability diagram.

9. For an ion trap of fixed dimensions, voltages, and frequencies, ions of high m/z have lower secular frequencies of motion than low m/z ions.

## Mass Selective Instability Scan

The mass selective instability scan is a simple and ingenious method of obtaining a mass spectrum of the ions contained in a quadrupole ion trap by increasing the amplitude of the RF voltage. When the ion trap is operated in RF-only mode (DC = 0V), ions of sequential m/z lie along the $a_z = 0$ line of the Mathieu stability diagram. By increasing the RF amplitude, the $q_z$ of all the ions is increased. When an ion exceeds a $q_z$ of 0.91, it falls outside the stability diagram and is no longer trapped. A fortunate result is that ions that pass over the $q_z = 0.91$ coordinate leave the ion trap in the z-direction. This ion current can be detected by placing a detector behind a hole in either of the endcap electrodes. Thus, a mass spectrum can be obtained by collecting the ion current that is ejected from the trap as the RF amplitude is increased. A representation of this process is shown in Figure 1-3.

## The Ion Trap Scan Program

Unlike conventional mass spectrometers that mass analyze a continuous beam of sample ions, the quadrupole ion trap operates as a pulsed mass spectrometer, mass analyzing discrete packets of sample ions. A timing diagram of the ion trap's pulsed scan sequence, referred to here as the scan program, is shown in Figure 1-4. The scan program starts with an empty ion trap that contains only neutral sample molecules. Next, the trapping voltages are turned on and an electron beam is gated into the ion trap. Sample ions are formed by electron ionization (EI) and the beam is turned off. Following ionization, the RF amplitude is raised to exclude all background ions below a variable m/z ratio prior to mass analysis. Finally, a mass spectrum of the

Figure 1-3. Diagram of the mass-selective instability scan showing the RF amplitude as a function of time. The simulated spectrum for perflourotributylamine demonstrates the timing sequence used to acquire a mass spectrum.

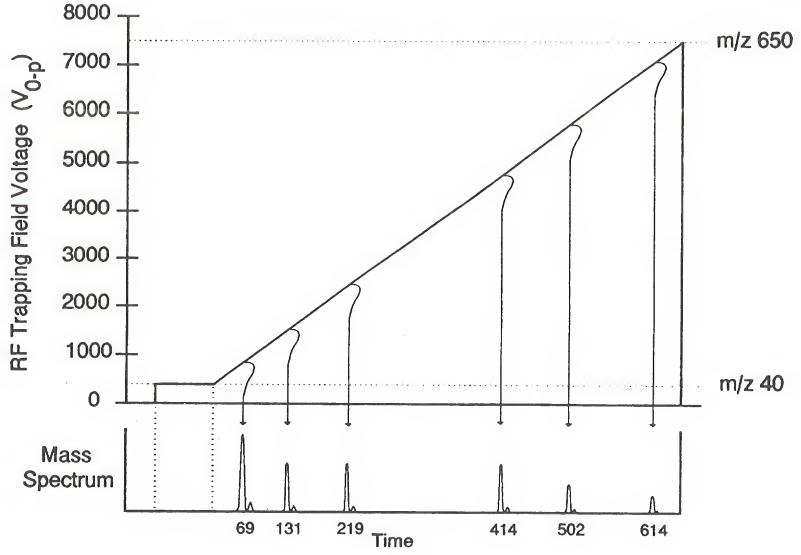
8000
7000
6000
5000
4000
3000
2000
1000
0
RF Trapping Field Voltage ($V_{0-p}$)
m/z 650
m/z 40
Mass Spectrum
69
131
219
414
502
614
Time

Figure 1-4. Ion trap scan program used to acquire EI mass spectra for m/z 60 - m/z 100. Ions are generated during period I, background ions below a selected m/z are ejected at point B, and the mass analysis scan is performed during stage S. The RF level (maximum of 650 m/z or 15,000 $V_{p-p}$) is directly related to the strength of the trapping field and determines the lowest m/z stored in the trap. Ions reaching the detector during stage B are not acquired by the data acquisition software. A supplementary AC voltage frequency of 530 kHz on the ITMS and 485 kHz on the ITS40 is applied during period S to effect axial modulation (frequency not drawn to scale). Axial modulation is not included on ITD700 and ITD800 scan programs. Multiplier settings of 0 V and 2000 V represent on and off values and do not correspond to the actual analog voltages applied. The ion signal shown corresponds to the actual ion signal observed for 1-octene and the peak widths and data acquisition rate are drawn to scale.

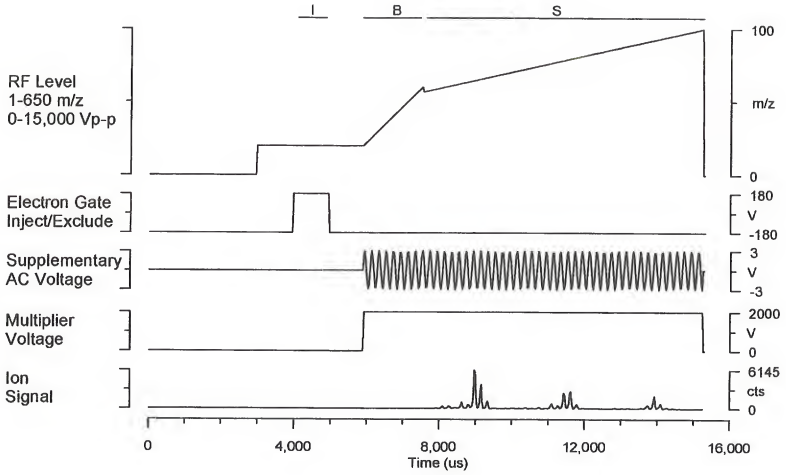
I
B
S
RF Level
1-650 m/z
0-15,000 Vp-p
100
m/z
0
Electron Gate
Inject/Exclude
180
V
-180
Supplementary
AC Voltage
3
V
-3
Multiplier
Voltage
2000
V
0
Ion
Signal
6145
cts
0
0
4,000
8,000
12,000
16,000
Time (us)

remaining ions is obtained with a mass-selective instability scan that causes ions of increasing m/z to be ejected from the ion trap, through a hole in the endcap, and detected at the electron multiplier.

Much of the versatility of commercial ion traps is due to the "software intensive" design of these microprocessor controlled instruments. Switching between EI, chemical ionization (CI), and MS/MS scan modes is accomplished by altering the scan program executed by the ion trap electronics. Similarly, the mass range and resolution of the ion trap can be controlled through modification of the scan program. In many ways, the versatility of the microprocessor controlled ion traps is similar to that of the personal computer; to switch from text editing to data analysis on a PC one simply has to exit the word processor software and load a spreadsheet program. Analogously, to change the scan mode of the ion trap from EI to CI or MS to MS/MS, only a simple modification of the scan program is required to manipulate the duration, amplitude, and frequency of the applied signals.

## Overview of Dissertation

Chapter 2 contains excerpts prepared for a book chapter titled Practical Ion Trap Technology: GC/MS and GC/MS/MS and is structured in the following fashion: a short discussion of the commercial ion trap instruments is presented to provide a basis for those who may be unfamiliar with each instrument's features and methods of operation. Next, several GC/MS and GC/MS/MS application examples are summarized. The operational principles and characteristics of GC/MS ion traps are described, with attention given to the underlying differences between the ion trap and the quadrupole mass filter. Following this, new methods are presented that reduce

space charge effects, decrease the extent of ion-molecule reactions, and further the applicability of GC/MS and GC/MS/MS. Finally, GC/MS/MS results from two unique ion traps are presented. The aim of this discussion is to convey the key issues underlying GC/MS and GC/MS/MS on the ion trap and to provide an appreciation of the applicability of both techniques.

Chapter 3 focuses on the isolation of ions in the quadrupole ion trap. Ion isolation is an important step in the GC/MS/MS experiment. The isolation requirements, as well as the characteristics of an ideal isolation technique, are discussed. A new two-step isolation technique is described, as is the more common apex isolation method. Results from a comparative study of the two techniques are presented. Since the development of practical GC/MS/MS on the ion trap was the goal of this work, operation and automation considerations are discussed. A summary of the presented results is included.

Chapter 4 examines the ion excitation stage of the MS/MS experiment. The most common method of ion excitation, single frequency dipolar excitation, is discussed, and the limitations of this approach for GC/MS/MS are addressed. The shifts in the secular frequency of ion motion are measured as a function of ion population. The detrimental effects of these frequency shifts for GC/MS/MS experiments are discussed. Three instrumental approaches are described that compensate for frequency shifts. MS/MS results are presented for each technique, and the advantages and disadvantages are summarized.

Chapter 5 covers the development of a new benchtop ion trap for GC/MS/MS that incorporates several of the new techniques discussed in Chapters 3 and 4. The instrument hardware is described, particularly the modifications that were required to

adapt the GC/MS ion trap for GC/MS/MS analyses. New software was written to control the instrument, and the methods of operation including the instrumental settings used are outlined. Results from a comparative study of GC/MS and GC/MS/MS are presented. Electron ionization and chemical ionization methods are investigated. The performance of each step of the GC/MS/MS experiment is characterized. Results from example applications are presented. A summary of the GC/MS/MS results is also included.

Chapter 6 concludes by discussing the potentials and limitations of the approaches presented in this dissertation for GC/MS/MS on the quadrupole ion trap. In particular, new questions that arise from this work are addressed and future studies are suggested. Finally, the upcoming commercial introduction of a GC/MS/MS ion trap is discussed and the potential capabilities of these instruments are examined.

# CHAPTER 2
# PRACTICAL ION TRAP TECHNOLOGY: GC/MS AND GC/MS/MS

The second chapter of this dissertation is intended as a means of summarizing the ion trap's current capabilities for gas chromatography/mass spectrometry (GC/MS) and highlighting new advances that may be incorporated into the next generation of commercial instruments. Although many new ion trap capabilities have been reported in the literature, such as parent and neutral loss scans,[8,9] high resolution,[10] and accurate mass measurement,[11,12] few of these methods have been reduced to practice. These features are not covered here. Instead, this chapter will emphasize what GC/MS ion traps currently excel at, what their present limitations are, and what they should be capable of in the near future.

## Introduction

In recent years, the quadrupole ion trap has grown from a novel ion storage device into a widely used mass analyzer used for gas chromatography/mass spectrometry (GC/MS). The development of the mass selective instability scan in 1984 by Stafford revolutionized the ion trap's use as a mass analyzer.[13] Commercial instruments that are based on this convenient method of mass analysis exhibit unit resolution, a mass range of 650 u, and high sensitivity.[3,14] Several ion trap applications include the monitoring of priority pollutants in environmental chemistry,[15] the

identification of drugs and their metabolites from biological matrixes in clinical chemistry,[16] and the analysis of rock extracts in geochemistry.[17] With 3500 instruments sold worldwide, the ion trap has become the second most widely used mass analyzer for GC/MS.

Although GC/MS has been the driving force behind the commercial development of the quadrupole ion trap, many expect that the ion trap's use for gas chromatography/tandem mass spectrometry (GC/MS/MS) will become important as well. The ion trap's tandem-mass-spectrometry (MS/MS) capabilities were first demonstrated by Louris et al.[18] Many research groups have further developed this technique in the last several years.[19-27] Efficient fragmentation and detection are primary advantages of ion trap MS/MS. Full-scan MS/MS spectra have been obtained for 1000 times less sample than could be observed on a triple quadruple tandem mass spectrometer.[28] These techniques, which are powerful characterization and identification tools for the chemist, are not in general use for gas chromatographic applications.[29] However, the development of new instrumental methods that make GC/MS/MS practical is ongoing. With the commercialization of new ion isolation and excitation techniques, the next generation of GC/ion-trap instruments is expected to incorporate powerful MS/MS capabilities into a benchtop gas chromatographic detector.

This chapter is structured in the following way. A short discussion of the commercial ion trap instruments is presented to provide a basis for those who may be unfamiliar with each instruments features and methods of operation. Next, several GC/MS and GC/MS/MS application examples are summarized. The operational principles and characteristics of GC/MS ion traps are described, with attention given to the underlying differences between the ion trap and the quadrupole mass filter.

Following this, new methods are presented that reduce space charge effects, decrease the extent of ion-molecule reactions, and further the applicability of GC/MS and GC/MS/MS. The aim of this discussion is to convey the key issues underlying GC/MS and GC/MS/MS on the ion trap and to provide an appreciation of the applicability of both techniques.

## Instrumentation and Methods of Operation

The ITD700® (Finnigan) was the first ion trap mass spectrometer commercially available.[14] Capable of acquiring full-scan and selected-ion electron ionization (EI) mass spectra over a 650 u mass range, the ITD700 shared similar features with other low cost GC/MS detectors, such as small size and simple software controlled operation.[14] A heated transfer line coupled the GC to the ion trap via an open-split interface. Sample effluent passed through this interface and into the internal volume of the ion trap. The scan sequence was made up of three steps that were performed in rapid succession: (1) ionization and storage of all sample ions above a particular m/z limit, (2) ejection of background ions below a low m/z cut off, and (3) the ejection and detection of ions in order of increasing m/z to produce a mass spectrum. A diagram of this scan program sequence, also referred to as a scan function, is shown in Figure 1-4. This example scan program produces mass spectra for ions between m/z 60 and m/z 100. Full-scan spectra covering m/z 60 - m/z 650 were acquired using a segmented EI scan program that is discussed later in this section. The execution of a single scan program is referred to as a microscan (μscan). During a GC/MS acquisition, the data for each μscan are summed, and an averaged spectrum is returned to the data system and recorded as a single analytical scan.[13] The ion trap is

operated with 1 mtorr of helium buffer gas that serves to damp the motion of trapped ions as well as to enhance the mass resolution and sensitivity.[3] The buffer gas is introduced through the GC column and made up by an open split interface. The ionization time controls the number of ions that are created and trapped for a given sample pressure. Figure 2-1 compares four profile mass spectra that were acquired with (a) 50 μs, (b) 350 μs, (c) 1 ms and (d) 5 ms ionization times. For the 350 μs - 5 ms cases, the loss of resolution observed for ions of low m/z is a result of too many ions being contained in the ion trap. Resolution improves for high m/z ions because the low m/z ions are scanned out of the trap before the high m/z ions are detected. These space charge effects reduce the performance of the ion trap and are discussed in a following section of this chapter. Calibration curves generated with the ITD700 typically exhibited a linear dynamic range of two to three orders of magnitude. Although the introduction of the ITD700 represented a breakthrough in ion trap technology, the manual adjustment of the ionization time and the narrow linear dynamic range were clear drawbacks for routine GC/MS.

The ITD800® (Finnigan) was an upgraded version of the ITD700 that included chemical ionization (CI) capabilities and improved on several of the ITD700's most apparent limitations. ITD800s were also sold with the ATD50/8000 name-plate by Perkin Elmer, and upgrade kits were available for ITD700 users. Positive chemical ionization is carried out by forming an excess of CI reagent ions that can react further to produce protonated sample.[30,31] Figure 2-2 compares the background subtracted full-scan spectra for 10 ng of amobarbital (MW = 226) using (a) EI and (b) low pressure methane CI. The CI scan program is shown in Figure 2-3. Note that the CI scan begins with an EI ionization event that produces the reagent ions that react

Figure 2-1. EI/MS profile spectra of ionized perflourotributylamine $(C_4F_9)_3N$ (MW = 642). Acquired with ionization times of (a) 50 μs, (b) 350 μs, (c) 1 ms, and (d) 5 ms. Intensity (cts) correspond directly to the ion current measured by the electrometer circuit without the application of a scaling factor for ionization time.

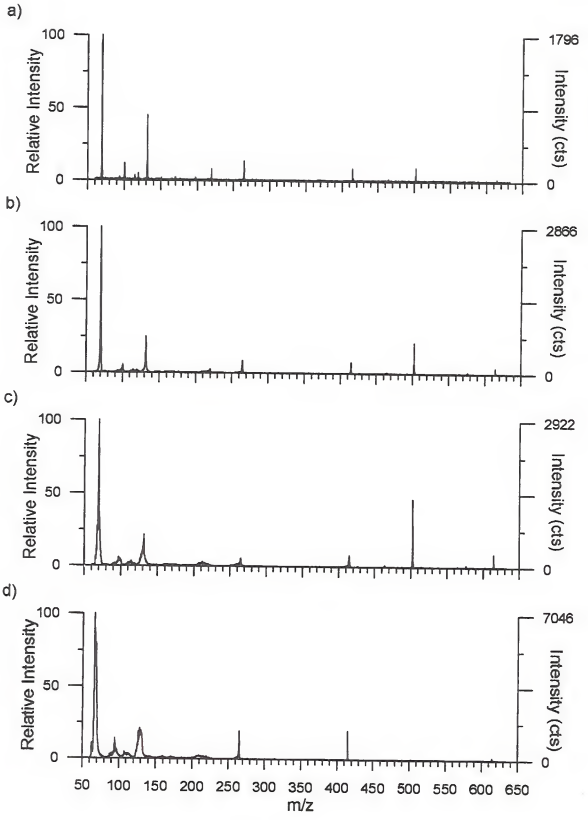
a)
b)
c)
d)
Relative Intensity
Intensity (cts)
100
50
0
1796
2866
2922
7046
50 100 150 200 250 300 350 400 450 500 550 600 650
m/z

Figure 2-2. Background subtracted full-scan mass spectra for the injection of 10 ng amobarbital (MW = 226). Acquired with (a) EI, and (b) methane CI.

a)

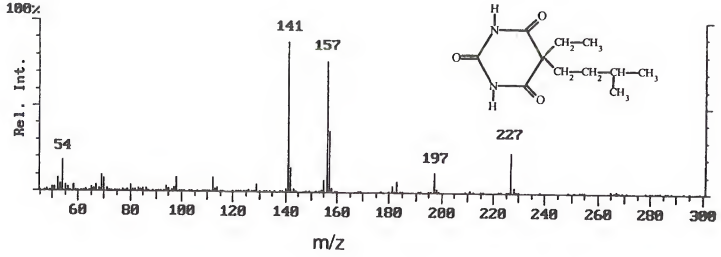
100%
Rel. Int.
141
157
54
197
227
60 80 100 120 140 160 180 200 220 240 260 280 300
m/z

b)

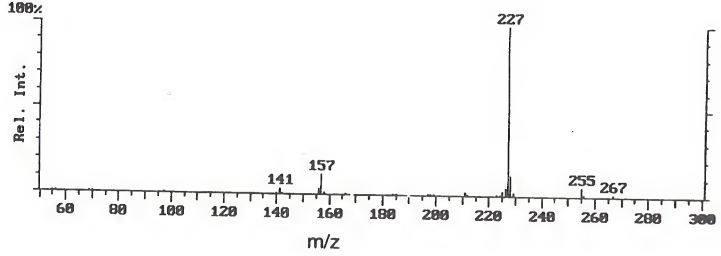
100%
Rel. Int.
227
141
157
255
267
60 80 100 120 140 160 180 200 220 240 260 280 300
m/z

Figure 2-3. Ion trap scan program used to acquire CI mass spectra for m/z 50 - 650. CI reagent ions are generated during period I, $[M+H]^+$ ions form during interval R, background ions are ejected at point B, and the mass analysis scan is performed during stage S.

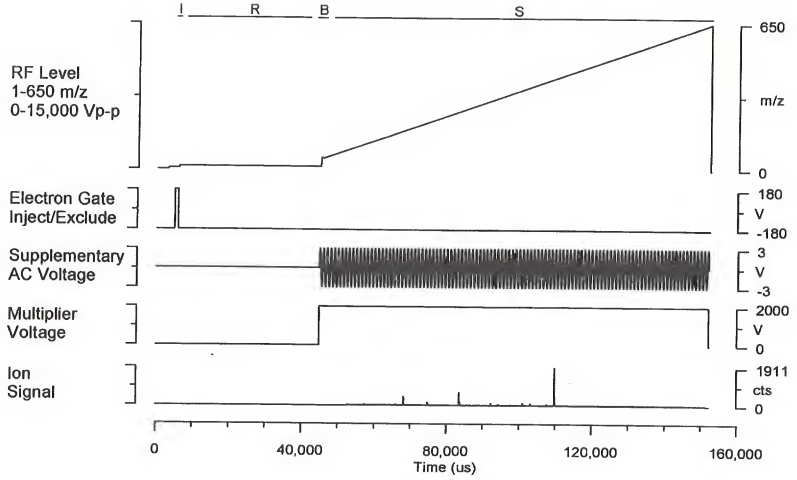
I
R
B
S
RF Level
1-650 m/z
0-15,000 Vp-p
650
m/z
0
Electron Gate
Inject/Exclude
180
V
-180
Supplementary
AC Voltage
3
V
-3
Multiplier
Voltage
2000
V
0
Ion
Signal
1911
cts
0
0
40,000
80,000
120,000
160,000
Time (us)

further to form $[M+H]^+$ ions. The number of $[M+H]^+$ ions produced in a CI experiment is controlled by the length of time available for the CI reaction to take place. Importantly, the EI spectrum shows a much larger 227 $[M+H]^+$ peak than an $M^+$ peak due to self-CI.

In addition to the ITD800s CI capabilities, automatic ionization control routines were introduced that eliminated the manual adjustment of the ionization time. Automatic gain control (AGC) and automatic reaction control (ARC) set the ionization and reaction times for EI and CI GC/MS analyses, respectively.[32,33] The AGC and ARC pre-scans, shown in Figure 2-4 and Figure 2-5, determine the total ion signal for a fixed ionization period. Using this measurement, the ion trap's microprocessor calculates the proper ionization time for the next μscan. To correct for the effect of variable ionization times, all ion intensity data are normalized to a 25 ms ionization time. AGC and ARC allow sample amounts ranging from the low picogram to the high nanogram levels to be injected without the manual adjustment of the ionization time. Figure 2-6 shows a calibration curve for hexachlorobenzene that was created with AGC. Note that the linear dynamic range extends over six orders of magnitude. With the addition of CI and the automatic ionization control techniques, ITD800 users found that the sensitivity, spectral quality, dynamic range, and ease of operation were significantly improved compared to the ITD700.[34]

The ITMS® (Finnigan) is a multi-purpose research instrument. Approximately 50 ITMS instruments have been produced. The main use of the ITMS has been in the development and characterization of new ion trap capabilities, although some GC/ITMS applications have been shown. MS/MS,[1,21,23,24,35-36] ion injection,[37-42] chemical ionization,[30,31,43,44] mass range extension,[45,46] and high resolution[10,47-49] are several examples of the "high performance" features that have been studied using the ITMS.

Figure 2-4. AGC (EI) automatic ionization control scan program. Pre-scan ionization is performed during stage I', background ions are ejected at point B', and the total ion current is collected during interval T'. Total ion current measurements can be made by rapidly raising the RF amplitude to its maximum value (as shown here, and as used on the ITS40) or by dropping the amplitude to 0V (as used on the ITD800 and ITMS). The ion signal obtained during T' is used to set the ionization time (I") for the next μscan. B', B" and S denote the background ejection and mass analysis stage for the μscan.

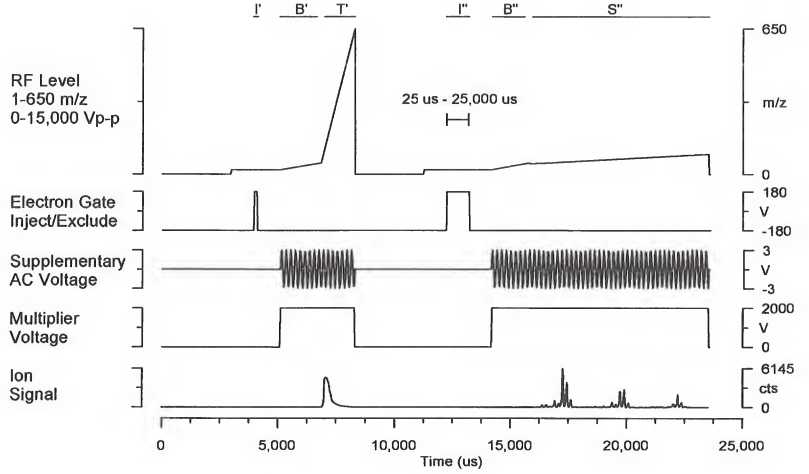
I'
B'
T'
I"
B"
S"
RF Level
1-650 m/z
0-15,000 Vp-p
25 us - 25,000 us
650
m/z
0
Electron Gate
Inject/Exclude
180
V
-180
Supplementary
AC Voltage
3
V
-3
Multiplier
Voltage
2000
V
0
Ion
Signal
6145
cts
0
0
5,000
10,000
15,000
20,000
25,000
Time (us)

Figure 2-5. ARC (CI) automatic ionization control scan program. Pre-scan ionization is performed during stage I', background ions are ejected at point B', and the total ion current is collected during interval T'. The ion signal obtained during T' is used to set the reaction time (R") for the next μscan. B', B" and S denote the background ejection and mass analysis stage for the μscan. R' and R" indicate the CI reaction periods for the ARC pre-scan and μscan respectively.

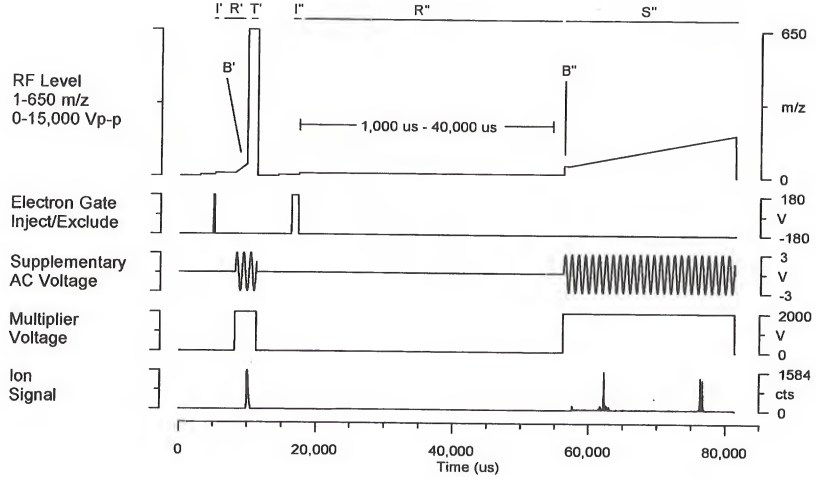
I' R' T'
I"
R"
S"
B'
B"
1,000 us - 40,000 us
RF Level
1-650 m/z
0-15,000 Vp-p
650
m/z
0
Electron Gate
Inject/Exclude
180
V
-180
Supplementary
AC Voltage
3
V
-3
Multiplier
Voltage
2000
V
0
Ion
Signal
1584
cts
0
0
20,000
40,000
60,000
80,000
Time (us)

Figure 2-6. EI/MS calibration curve for m/z 284 of hexachlorobenzene (MW = 284). Each data point (▲) represents three replicate injections. Error bars correspond to ± 2 standard deviation. The best fit line was determined by linear regression using the data points between 0.02 ng and 100 ng.

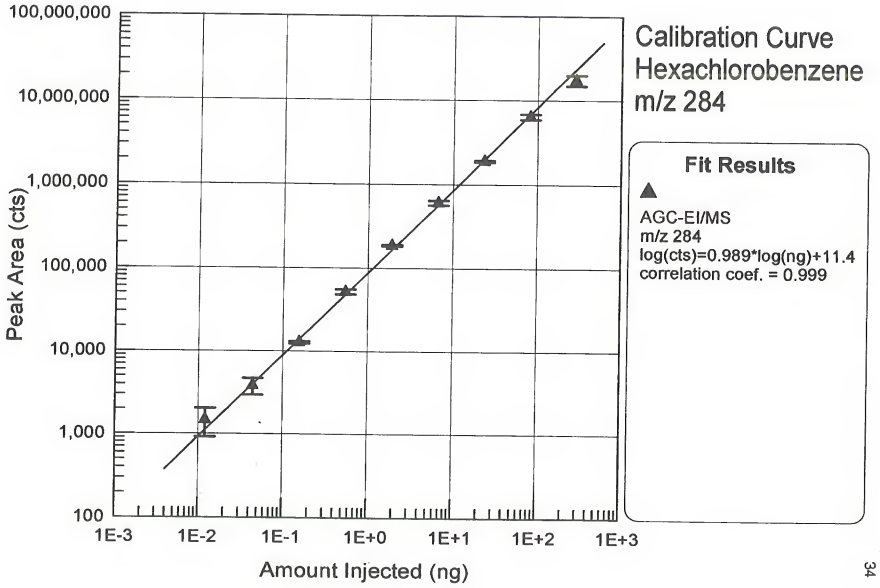
Calibration Curve
Hexachlorobenzene
m/z 284
Fit Results
AGC-EI/MS
m/z 284
log(cts)=0.989*log(ng)+11.4
correlation coef. = 0.999
Peak Area (cts)
100,000,000
10,000,000
1,000,000
100,000
10,000
1,000
100
1E-3
1E-2
1E-1
1E+0
1E+1
1E+2
1E+3
Amount Injected (ng)

The ion trap analyzer, electronics, and GC/MS transfer-line interface are similar to those of the ITD700 and ITD800. Hardware differences include a large multi-port UHV vacuum system, a probe lock, a heated solids probe, and a programmable DC supply and frequency synthesizer. In addition to the standard EI and CI scan programs shown in Figures 1-4 and 2-3, the ITMS provides versatile software for creating custom scan programs. Figure 2-7 shows a custom MS/MS scan program that was created using the ITMS scan editor software. The ion trap MS/MS experiment has been described in detail previously.[1,19,20] Briefly, MS/MS is performed in four steps; (a) ionization of the sample molecules, (b) isolation of the parent ion, (c) activation of the parent ion to promote collision-induced dissociation (CID), and (d) collection of the resulting product ion spectrum. The isolation step (b) is accomplished by the application of a combination of RF and DC voltages the ring electrode of the ion trap.[20,50-52] The CID step (c) is achieved by applying a supplementary AC voltage across the ion trap's endcap electrodes.[19,53] The frequency of the supplementary AC voltage is adjusted to match the ion's secular frequency of motion. This method of resonant excitation accelerates the parent ions in the axial direction. CID occurs when the collisions between the accelerated ions and the helium buffer gas impart sufficient energy to break the bonds of individual ions. Figure 2-8 shows the MS/MS product ion spectrum for the molecular ion m/z 134, of n-butylbenzene. The supplementary AC voltage is also applied during the mass selective instability scan. This method of axial modulation improves the resolution and dynamic range by increasing the efficiency with which ions are ejected from the ion trap.[52] Figure 2-9 compares two spectra that were acquired with and without the use of axial modulation. Note that unit m/z peak widths are observed with axial modulation and that the peak height observed for m/z

Figure 2-7. Ion trap scan program used to acquire EI/MS/MS product ion spectra for m/z 134. Periods I, M, C, and S correspond to ionization, mass selection, CID, and mass analysis, respectively. Positive and negative DC voltages are applied to the ring electrode to isolate the ion of interest using the $\beta_z = 0$ and $\beta_z = 1$ stability edges respectively. Typical values for the resonant excitation signal are 100 kHz - 200 kHz and 0.5 - 2.0 $V_{p\text{-}p}$ (frequency not drawn to scale).

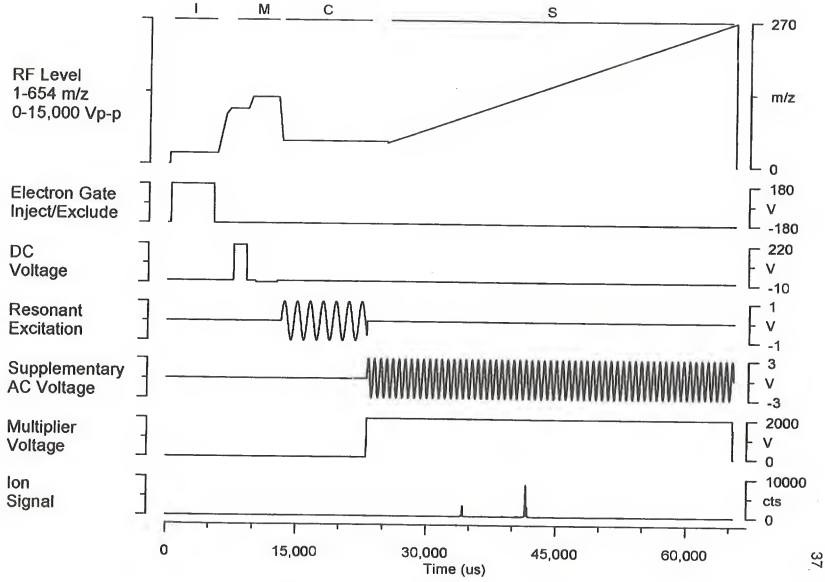
I
M
C
S
RF Level
1-654 m/z
0-15,000 Vp-p
270
m/z
0
Electron Gate
Inject/Exclude
180
V
-180
DC
Voltage
220
V
-10
Resonant
Excitation
1
V
-1
Supplementary
AC Voltage
3
V
-3
Multiplier
Voltage
2000
V
0
Ion
Signal
10000
cts
0
0
15,000
30,000
45,000
60,000
Time (us)

Figure 2-8. Background subtracted EI/MS/MS product ion spectrum for $M^{+\cdot}$ ion (m/z 134) of n-butylbenzene (MW = 134); 1 pg injected.

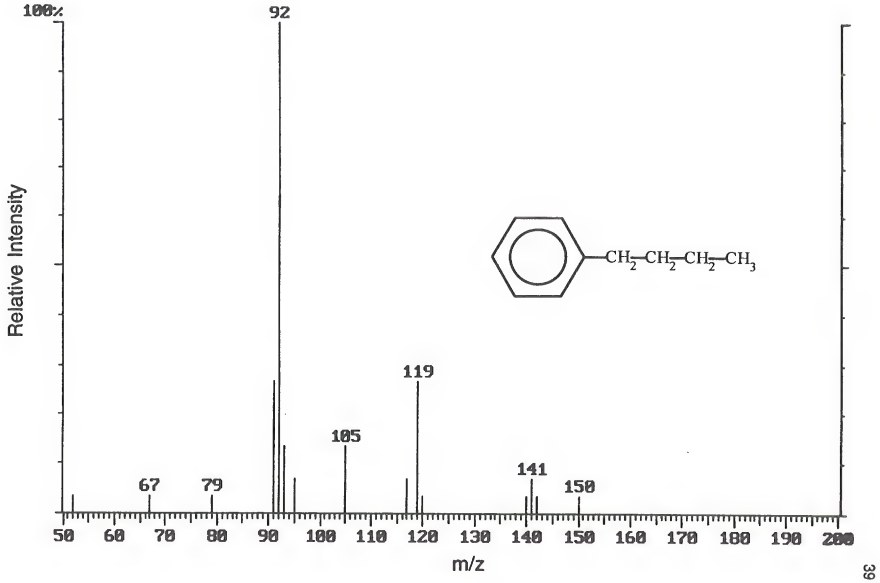
100%
92
Relative Intensity
119
105
67
79
141
150
50 60 70 80 90 100 110 120 130 140 150 160 170 180 190 200
m/z
39

Figure 2-9. EI/MS profile spectra of ionized perflourotributylamine $(C_4F_9)_3N$ (MW = 642). Acquired (a) without axial modulation and (b) with axial modulation of 6.0 $V_{p-p}$ at 530 kHz. A fixed ionization time of 150 μs was used to acquire both spectra. Intensities (cts) correspond directly to the ion current measured by the electrometer circuit without the application of a scaling factor for ionization time.

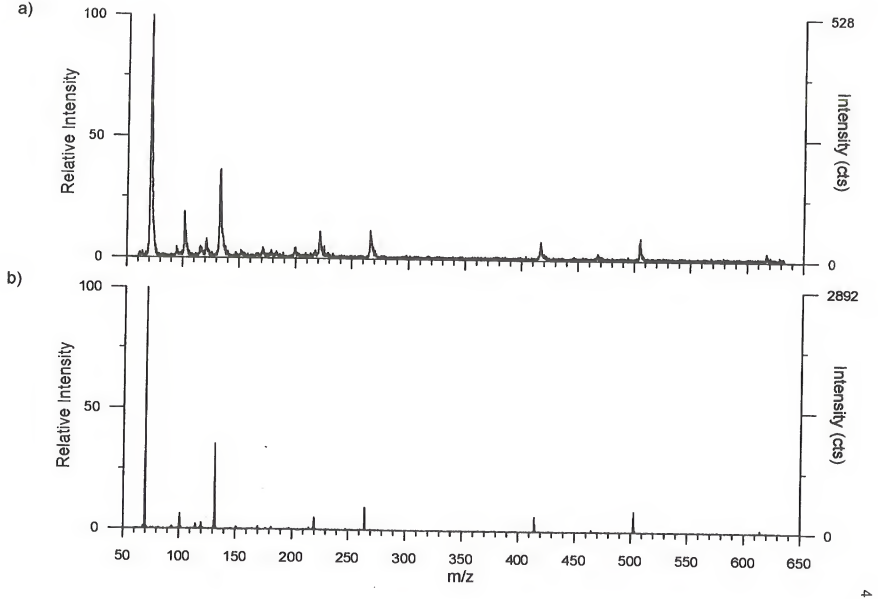
a)
b)
Relative Intensity
Intensity (cts)
100
50
0
528
2892
50
100
150
200
250
300
350
400
450
500
550
600
650
m/z

69 is five times greater than the peak height recorded without the use of axial modulation.

Although the ITMS is a versatile instrument for tandem mass spectrometry, several problems limit the use of MS/MS with gas chromatographic sample introduction. One problem is that the AGC and ARC routines, which improve GC/MS performance, are not integrated into the scan editor software that is used to create MS/MS scan programs. Tuning MS/MS scan programs for GC analyses is very time consuming since multiple sample injections are required. Although some GC/MS/MS applications have appeared in the literature,[21,28,35,54,55] the ITMS is best suited for fundamental studies where sample pressures can be controlled and maintained constant.

The ITS40® ion trap (Finnigan) is a benchtop GC/MS system designed for routine analyses. The hardware for the MAGNUM® (Finnigan) and SATURN® (Varian) instruments are functionally identical to that of the ITS40. The open-split interface used on the ITD and ITMS instruments is replaced by a heated transfer-line that directs all of the column effluent into the ion trap analyzer. Additionally, both manufacturers use an open-split interface for air monitoring work, and a jet separator for volatiles. A fixed frequency crystal oscillator and balun transformer supply the axial modulation signal that improves ion detection, reproducibility, and ion statistics. The ITS40's scan acquisition processor (SAP) board centroids the profile spectra before transferring them to the data system. This reduces the time that the instrument spends communicating with the data system, resulting in a higher scan repetition rate. Both systems also use a new data system which integrates the control of an optional autosampler, the GC, and the mass spectrometer into an easy-to-use package. The

standard EI and CI scan programs are supported, but the ability to create custom scan programs is not available. Both AGC and ARC are included. In addition, the MAGNUM and SATURN III instruments use new techniques that remove EI ions above the m/z of the CI reagent ions. In summary, the ITS40 based instruments are refined GC/MS ion traps that are capable of generating full-scan EI and CI spectra over a wide dynamic range with very high sensitivity.

## GC/MS and GC/MS/MS Applications

Of the commercial ion traps sold, greater than 97% are dedicated GC/MS instruments. It is impossible in the limited space of this chapter to present a complete summary of the many applications in which GC/MS ion traps have been used. This problem, therefore, has been mitigated by selecting examples that demonstrate the ion trap's use in several areas of chemistry.

The identification of priority pollutants in complex matrices has been one of the primary applications of GC/MS. Ion trap GC/MS is employed for many environmental applications,[15,56-60] including the United States Environmental Protection Agency (US EPA) ground water monitoring methods (624, 625) and drinking water methods (524.2, 525). The determination of trace levels of herbicides and their degradation products in surface and ground waters was demonstrated by Pereira, et al.[61] Calibration curves were linear from 0.06 to 6 μg/mL for the analytes of interest. The lower of detection of the analytes was 60 pg (with a signal-to-noise ratio greater than 10:1). Full-scan mass spectra were routinely obtained for 1 ng of analyte and the author notes that the ion trap is rapid, specific, sensitive, inexpensive, and could be easily automated as a screening method. Ground water samples were observed to be less difficult to analyze

than surface water samples because of reduced matrix interference problems. Mass spectra obtained for approximately 1 ng of the compounds selected for this study demonstrate the ability of this technique to provide absolute and unambiguous identification of environmental organic contaminants.[61] Canela and Muehleisen applied headspace GC/MS to the measurement of industrial air emissions.[58] Detection with an ITD improved the identification and determination of priority pollutants with LOD's of 0.50 and 0.12 mg/m$^3$ for passive and active adsorption, respectively.

GC/MS ion traps have also been applied to an assortment of clinical and pharmaceutical studies.[16,21,34,44,62-67] De Boer compared the performance of an ITD to a Hewlett Packard mass selective detector (MSD) for the analysis of TMS-enol, TMS ether, methoxime TMS, and pentafluoropropionic ester derivatives of the main urinary metabolite of a nandrolone, norandrosterone.[62] Figure 2-10 shows the ITD chromatographic data and full scan mass spectrum for derivatized norandrosterone. The ITD's sensitive full-scan and selective chemical ionization capabilities are observed to be the two main advantages of the ITD for this application. However, the MSD gave better sensitivity, with SIM mode, for norandrosterone extracted from urine because of the ITD's limited ability to handle background interferences. Genin and Lehrer used the ITD for anti-doping studies to determine low levels of drugs and their metabolites in biological matrices.[68] The ITD allowed complete CI mass spectra to be obtained from less sample compared with other MS methods. Full-scan analyses of seven drugs resulted in improved sensitivity and specificity compared to multiple ion detection methods. Horman, et al. have demonstrated routine GC/MS analysis of fatty acid methyl esters using the ITD.[69] They obtained full-scan EI mass spectra that gave good correlation with literature reference spectra for sample amounts from 2 pg to 225

Figure 2-10. GC/MS data of the trimethylsilyl-enol trimethylsilyl derivative of norandrosterone isolated from a urine sample and analyzed by the ion trap detector in the positive-ion CI mode. Figure includes (a) the mass chromatograms at m/z 421 and 331, and (b) the full-scan mass spectrum for scan 833.[62]

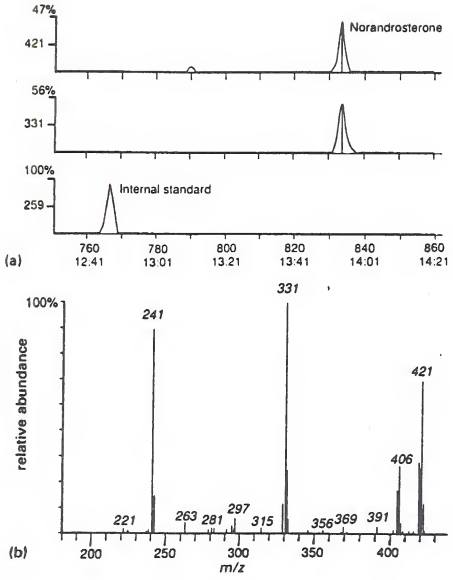
47%
421
Norandrosterone
56%
331
100%
259
Internal standard
760
12:41
780
13:01
800
13:21
820
13:41
840
14:01
860
14:21
(a)
100%
relative abundance
241
331
421
406
221
263
281
297
315
356
369
391
200
250
300
350
400
m/z
(b)

ng. Enhanced $[M+1]^+$ ions are formed at levels above 50 ng due to self-CI, but this did not prevent identification.

Compared to GC/MS, relatively few GC/MS/MS ion trap applications appear in the literature.[21,28,29,35,54,55,70-72] One reason for this discrepancy is that less than 2% of all ion traps sold have MS/MS capabilities. Of these instruments, few have been used for GC/MS/MS applications. The second reason for such a small number of GC/MS/MS applications is that several problems currently limit the usefulness of GC/MS/MS on the ion trap. Johnson et al. compared GC/MS/MS on the ITMS and the triple quadrupole mass spectrometer (TQMS).[28] Full-scan product ion spectra could be obtained for the injection of 15 pg and 1.5 ng of diisopropyl methylphosphonate (DIMP) standards on the ITMS and TQMS, respectively. The maximum efficiency of CID was observed to be 90% on the ITMS (compared to 56% on the TQMS), but the overall MS/MS efficiency, including the efficiency of isolation of the parent ion, was not determined. MS/MS log-log calibration curves obtained for DIMP on the ITMS show a slope of 0.53 (compared to the ideal of 1.0) demonstrating the first limitation of GC/MS/MS on the ITMS. Strife and Simms evaluated the quantitative analysis of tebufelon (TE) in crude plasma extracts by MS/MS with an ITMS in an effort to determine the analytical utility of the technique.[55] Quantitation, using an internal standard method previously described by Strife, resulted in a correlation coefficient ($r^2$) of 1.000 for the TE calibration curve. The authors note that the only practical choice for GC/MS/MS quantitation on the ITMS is the use of internal standards, due to the ITMS's non-linear external calibration curves. RF/DC isolation was observed to be important for the analysis of real samples because it reduces space charge caused by the presence of the matrix ions. Figure 2-11 shows the analysis of a plasma extract for a sample

Figure 2-11. GC full-scan MS/MS analysis of an extract of plasma initially spiked at 1 ng/g. The ionization time for tebufelone is 10 ms. The upper trace is a sum of all MS/MS product ion current as a function of time. The lower trace is reconstructed from product ions of m/z 233 only.[28]

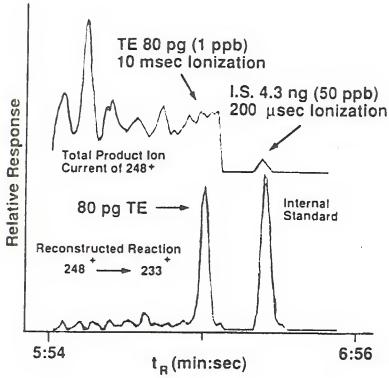
TE 80 pg (1 ppb)
10 msec Ionization
I.S. 4.3 ng (50 ppb)
200 µsec Ionization
Total Product Ion
Current of 248+
80 pg TE
Internal
Standard
Reconstructed Reaction
248+ → 233+
Relative Response
5:54
6:56
tR (min:sec)

spiked at 1 ppb of TE. Note that the upper trace is the sum of the product ion current, which would be equivalent to the ion signal for m/z 248 using SIM. The reconstructed ion current for the reaction of $248^+$ -> $233^+$ demonstrates the enhancement in signal-to-noise ratio (S/N) that can be obtained with MS/MS relative to SIM. A limitation for practical GC/MS/MS, as noted by Strife[55] and Johnson,[28] is that, when the ITMS is operated in MS/MS mode, the instrument software does not support the automatic ionization control techniques that significantly improves the usefulness of ion trap GC/MS. Several examples of GC/MS/MS using automatic ionization control have been demonstrated on modified ITS40 instruments.[70,73,74] These and other results aimed at practical GC/MS/MS are examined later in this chapter.

Although ion trap MS is a relatively new technique compared to the more conventional MS methods, the ion trap's use for GC/MS has been widespread. The driving force behind this growth has been the ability to obtain full-scan spectra with high sensitivity. Full-scan spectra can improve the certainty of an identification relative to selected ion monitoring methods. Secondly, switching from EI to CI is accomplished through software, and does not require hardware changes such as swapping ion-volumes. The altemating EI and CI scan capabilities provides a powerful method for obtaining molecular weight and structural information in a single experiment[75]. A current limitation that has been observed in environmental and clinical GC/MS applications is the loss in sensitivity that occurs when background chemical interferences are high. Additionally, negative ion CI cannot performed in the ion trap's standard configuration. Several reports have noted differences between ion trap and quadrupole EI spectra.[69,76,77] While differences between ion trap and quadrupole spectra exist, these variations are analogous to the differences that are commonly

observed for spectra obtained on differing types of instruments. Practical methods for performing GC/MS/MS on the ion trap are under development, but are not as yet commercially available. Clearly, the development of an affordable and easy to use benchtop GC/MS/MS ion trap is expected to expand use of the ion trap to a new class of research applications.

## Operational Principles for Ion Trap GC/MS

### Space Charge Effects

Space charge, defined as the electrostatic forces that exist between ions that are held in close proximity to each other, can severely degrade the ion trap's performance as a mass spectrometer.[52,78-81] The effects of space charge are commonly observed as losses in mass resolution and/or mass shifts.[82,83] Although space charge can degrade the performance of most types of mass spectrometers, space charge effects are particularly apparent with the long ion residence times employed with the ion trap.

A few simple models can help explain space charge effects in the ion trap. Confinement of the ions within the ion trap increases the effect of space charge; in many ways, this is analogous to tossing a handful of marbles into a mixing bowl, where they will be trapped. Compare this situation with that of a linear quadrupole, which can be likened to inserting marbles into one end of a length of tubing; the marbles will roll through the tube and be gone. Ions entering the quadrupole with a typical energy of 4 eV will traverse the 20 cm quadrupole length in approximately 20 μs. In the bowl (ion trap), they will be confined for periods 1,000 to 100,000 times longer. Thus, ions that are formed at the beginning of a 1 ms ionization period will remain in the ion trap to

interact with ions that are formed at the end of the ionization step, and continue to interact during ion storage. Clearly the storage of ions adds to the ion trap's susceptibility for space charge. In addition, friction will damp the marbles' trajectories toward the bottom of the bowl. Similarly, collisions with buffer gas (He) will "frictionally" cool the ions toward the center of the trap, forcing the ions together and increasing space charge effects.

Furthermore, space charge effects are more noticeable with the ion trap because typically all of the ions above a particular m/z are stored at the same time. To illustrate how this situation contributes to space charge, consider a crowded elevator that is carrying people from the basement of a building up to their respective floors. Initially, people getting off at the lower levels must push past the others to get out of the elevator. As the car travels upward and people continue to get off, however, it becomes easier to get out of the elevator. The crowding in this example is analogous to the space charge that exists when the ion trap is operated in the selective instability mode. Initially all of the ions that are stored and available for detection are formed during the ionization event, and space charge is high. As low m/z ions are scanned out of the ion trap, space charge caused by the presence of all the higher m/z ions can affect their detection. By the time the high m/z ions are themselves scanned out of the ion trap, space charge has lessened because most of the ions have previously been ejected from the ion trap. Figure 2-1 clearly shows how resolution improves with increasing mass as space charge is reduced during a mass analysis scan.

Although space charge is normally associated with loss in resolution, it can affect the ion trap operation in a variety of ways. For example, low levels of space

charge can be observed as a slight shift in an ion's secular frequency.[28,53,71,84,85] Fulford et al. used these frequency shifts as a sensitive method of measuring the number of ions in the ion trap.[53] At moderate space charge levels, peak broadening (2-3 u) is observed, particularly for low m/z ions. Good GC/MS performance is maintained under moderate space charge conditions when axial modulation is used. Gross space charge effects may be observed as very broad peaks, with widths ranging from 5 to 25 u. Gross space charge may also decrease the efficiency with which ions can be stored in the ion trap and increase the ion losses that occur during ionization. Since space charge limits the ion trap's ability to produce identifiable mass spectra, it becomes difficult to determine how it affects other stages of ion trap operation. For example, Eades et al. recently demonstrated that space charge increases the magnitude of "black holes" arising from ion losses due to non-linear resonances.[86] Because space charge limits the efficiency with which ions are detected, fundamental questions such as how many ions can be stored in the ion trap, and with what efficiency these ions can be detected, have proved difficult to answer.

While a complete appreciation of space charge will undoubtedly assist the development of new GC/MS methods in the future, being able to recognize the effects of space charge in GC/MS experiments is important. Recognizing space charge effects in GC/MS data is complicated because the current commercial instruments are limited to only acquiring centroided mass spectra. Profile spectra can be viewed when the instrument is tuned, but they cannot be collected to a data file. After profile data have been converted to centroid data, it becomes difficult to characterize changes in resolution, peak shape, and mass assignment that may be caused by space charge. Figure 2-12 shows EI mass spectra for the injection of 2.0 and 81 ng of

Figure 2-12. Separate background subtracted centroid mass spectra for hexachlorobenzene. Sample amounts of (a) 2.0 ng and (b) 81 ng of hexachlorobenzene were injected. Note the differences in the relative intensity of m/z 282 and m/z 283 for the two spectra. Ionization times were set by AGC.

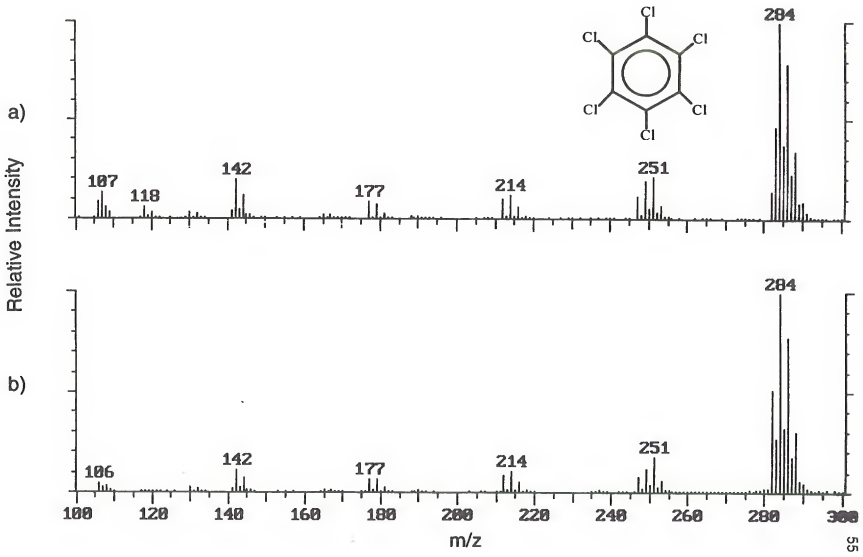
a)
b)
Relative Intensity
m/z
284
251
214
177
142
118
107
106
100
120
140
160
180
200
220
240
260
280
300
Cl

hexachlorobenzene. For both amounts, the hexachlorobenzene spectra are easily identified. However, it is difficult to differentiate between unit resolved peaks and peak broadening/shifts that are caused by space charge (compare the relative intensity of m/z 283 and m/z 284 in both spectra). For GC/MS/MS experiments, space charge and the lack of profile acquisition make it difficult to asses how well the parent ion has been mass isolated prior to CID. Calibration curves are often the best indication of space charge for GC/MS experiments. Non-linearities at high concentrations show when the efficiency of ion detection begins to drop off and provide the most straightforward method of estimating the mass resolution and peak shape for samples of lower concentration.

Space Charge and Automatic Ionization Control

Automatic ionization control, which we refer to here by Finnigan's term AGC,[32,33] is a method of reducing space charge by limiting the number of ions that are created at different points along a chromatographic run. When the AGC pre-scan returns a large total ion current (TIC) measurement, the ionization time for the subsequent µscan is reduced. Conversely, when the AGC pre-scan TIC measurement is low, the ionization time for the µscan is increased. Thus, AGC improves the linear dynamic range of the ion trap in two ways. First it minimizes space charge when sample pressures are high, and second it enhances sensitivity when sample pressures are low.

Although the development of AGC significantly improved the ion trap's usefulness for GC/MS, background interferences can cause AGC to reduce the ionization time which diminishes sensitivity for the analyte. When the ratio of background molecules to analyte molecules in the ion trap is high, the majority of the

ions formed during the AGC pre-scan are background ions. If the background ions are present in large amounts, the AGC pre-scan shortens the ionization to prevent space charge caused by the background ions. This reduction in ionization time also decreases the number of analyte ions that are formed and detected. Similar problems can occur when co-eluting internal standards are used for quantitation. Large discrepancies in the quantities of deuterated internal standard and analyte can adversely affect the detection of the less abundant compound. Thus, a high background-to-analyte ion ratio can reduce the sensitivity of GC/MS on the ion trap. It is important to note that the use of internal standards that are structural analogs helps to eliminate these problems because coelution is less common. The use of sequential RF/DC isolation steps have also been demonstrated as a suitable method for obtaining a linear calibration curve for an analyte and its isotopically labeled internal standard that coelute with vastly different partial pressures.[87]

EI Scan Segments

Full-scan EI spectra covering a wide m/z range are normally acquired with a segmented EI scan program. Figure 2-13 shows the scan program diagram for a segmented EI scan over a scan range of m/z 60 - m/z 650. This scan program produces a complete mass spectrum by combining the spectra obtained from each of the four scan segments. Each scan segment resembles a separate scan program, including the ionization, low m/z ejection, and data acquisition steps. Although a single scan segment could be used to obtain full scan EI data, the segmented scan program helps to reduce self-CI ions that can be observed in EI spectra due to ion-molecule reactions. Breaking long scan programs into four shorter scan segments, reduces the

Figure 2-13. Ion trap scan program used to acquire EI mass spectra from m/z 60 - m/z 650 using four scan segments. Periods labeled I correspond to the ionization step for each of the four scan segments S1 - S4. The m/z values for the segment breaks can be set manually; the default values are shown. The supplementary AC voltage is available on ITMS and ITS40 based ion traps only (frequency not drawn to scale). The ion signal shown corresponds to the actual ion signal observed for perflourotributylamine and the peak widths and data acquisition rate are drawn to scale.

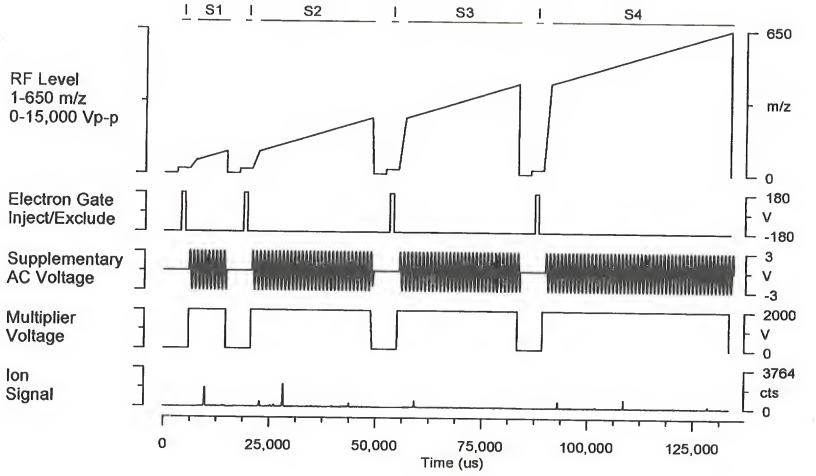
S1
S2
S3
S4
RF Level
1-650 m/z
0-15,000 Vp-p
650
m/z
0
Electron Gate
Inject/Exclude
180
V
-180
Supplementary
AC Voltage
3
V
-3
Multiplier
Voltage
2000
V
0
Ion
Signal
3764
cts
0
0
25,000
50,000
75,000
100,000
125,000
Time (us)

time between an ion's formation and when it is scanned out to the detector. By minimizing the amount of time available for ion-molecule reactions to occur, the intensity of ion-molecule reaction products in EI spectra may be reduced.

The segmented scan program also allows different ionization settings to be used for different sections of the mass spectrum. To alter the intensity of ions in a particular scan segment the scaling factor and/or RF ionization level can be adjusted. The scaling factors allow shorter ionization levels to be used during the low m/z scan segments and longer ionization times to be used for the high m/z scan segments. This helps to reduce the number of ions that are in the ion trap when the low m/z ions are scanned out and increase the number of high m/z ions that are detected. The adjustment of the RF ionization level corrects for the dependence of the efficiency of ionization on m/z.[88] Together, the proper adjustment of the scaling factor and the RF ionization level for each segment of the EI scan program can improve the sensitivity of the ion trap for GC/MS.

Scan Repetition Rate

Here the ion trap's scan repetition rate (scans/s) is defined as the number of scans that can be acquired to disk in one second. The justification for the use of repetition rate instead of scan rate is that scan rate commonly describes the speed of the acquisition step for a scan program (u/s). In the ion trap software, the term scan rate is incorrectly used to refer to the time required for a scan to be performed (s/scan), which is not a rate but a time. To avoid further confusion, the term "repetition rate" will be used to describe the number of scans that are acquired each second (e.g. 1.3 scans/s).

For GC/MS, the repetition rate is important because it defines the number of scans that can be acquired over a GC peak. A minimum repetition rate of 1 scan/s is required for most GC/MS applications. However, higher repetition rates increase the number of data points that define the shape of the GC peak profile and can improve quantitation precision.

Figure 2-14 shows the relationship between the scan repetition rate, the number of μscans, and the acquisition range for an ITS40 EI scan program. In general, the repetition rate may be increased in one of two ways: reducing the number of μscans or decreasing the duration of the μscan. Communication delays also affect the repetition rate, but they cannot be easily reduced. Reducing the number of μscans that are averaged to produce a spectrum will increase the scan repetition rate. However, a loss in S/N and mass spectral reproducibility is observed. In practice the signal averaging benefits of using 3 or more μscans outweigh the gains that are made in repetition rate by using 1 μscan. The scan repetition rate can also be increased by reducing the duration of the scan program. This can be accomplished by eliminating the AGC pre-scan or reducing the acquisition range. By judiciously choosing an acquisition range that minimizes the number of scan segments, large gains in repetition rate can be effected. For example, the repetition rate increases dramatically when the end m/z is changed from m/z 200 to m/z 199 because this decreases the number of scan segments from three to two.

The largest gains in scan repetition rate are obtained when a single scan segment is used. Figure 2-15 shows that repetition rates approach 10 scans/s when a 2 u wide acquisition range is used. Also, scan repetition rates are usually higher for CI and MS/MS scan programs because these scan modes use a single scan segment.

Figure 2-14. Scan repetition rate (scan/s) for an EI/MS segmented scan program as a function of the number of μscans. Unfilled data points include the extra scan time for the AGC pre-scan, and solid data points correspond to the repetition rate without AGC. All scan rates were calculated by the ITS40 software.

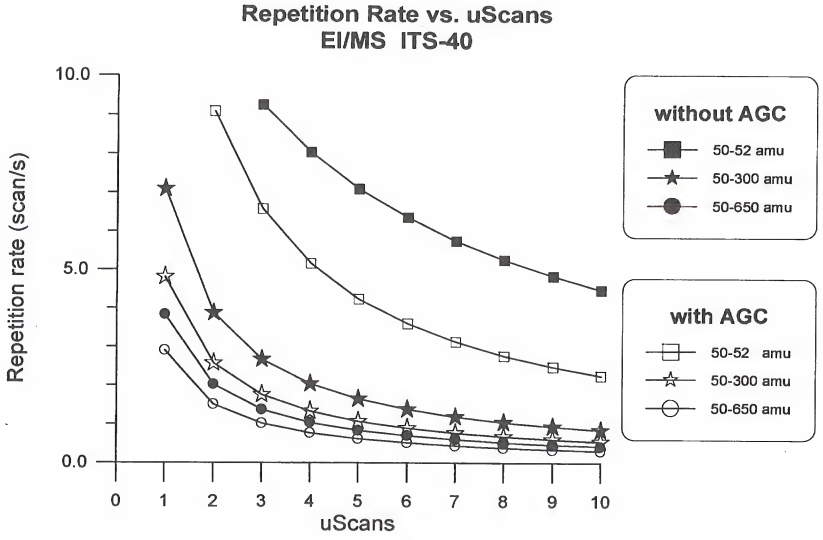
Repetition Rate vs. uScans
EI/MS ITS-40
Repetition rate (scan/s)
10.0
5.0
0.0
0
1
2
3
4
5
6
7
8
9
10
uScans
without AGC
50-52 amu
50-300 amu
50-650 amu
with AGC
50-52 amu
50-300 amu
50-650 amu

Single Ion Monitoring vs. Full Scan

The trade-offs between full-scan and single ion monitoring (SIM) modes are different for ion trap and quadrupole mass spectrometers. SIM improves sensitivity for beam-type mass spectrometers by continuously collecting current for a single m/z, thus enhancing the S/N. As an example, if a quadrupole mass filter is scanned over a 200 u mass range every second, 1/200 of this time (0.005 s) is spent collecting the ion current for each m/z. By changing to SIM and monitoring the ion current for a single m/z continuously, the observed S/N would typically be enhanced by $\sqrt{200} = 14.4$. For the ion trap, reducing the acquisition range to cover a single m/z only shortens one part of the scan program, thus the reduction in scan time is small. Since SIM on the ion trap does not monitor a single m/z continuously, only modest gains in S/N are observed as detailed below.

In practice, switching from full-scan to SIM on the ion trap eliminates the information available in full-scan spectra for only a slight gain in sensitivity. Figure 2-15 shows how the number of μscans that can be acquired changes with acquisition range for a 1 second AGC-EI/MS scan program. When full-scan data are acquired over a m/z range of 650, 3 μscan can be acquired in one second. For an acquisition m/z range of 1, 23 μscans can be acquired. By switching from full-scan to SIM, the ion current observed for SIM would be expected to be 8 times greater, which results in a S/N enhancement of 2.7. While this modest gain in S/N may be beneficial in some cases, the additional information that would have been provided by a full-scan spectrum is typically more significant. Although the limited sensitivity enhancements afforded by SIM on the ion trap appear to be a significant drawback for GC/MS, this is

Figure 2-15. Relationship between the acquisition range and the maximum number of μscans that can be averaged for an AGC-EI/MS scan program with a scan repetition rate of 1 scan/s. A fixed start mass (m/z 50) was used for each acquisition range and the large decreases in the number of μscan at acquisition ranges of 50, 200, and 350 correspond to the segment breaks at m/z 100, m/z 250, and m/z 400 respectively.

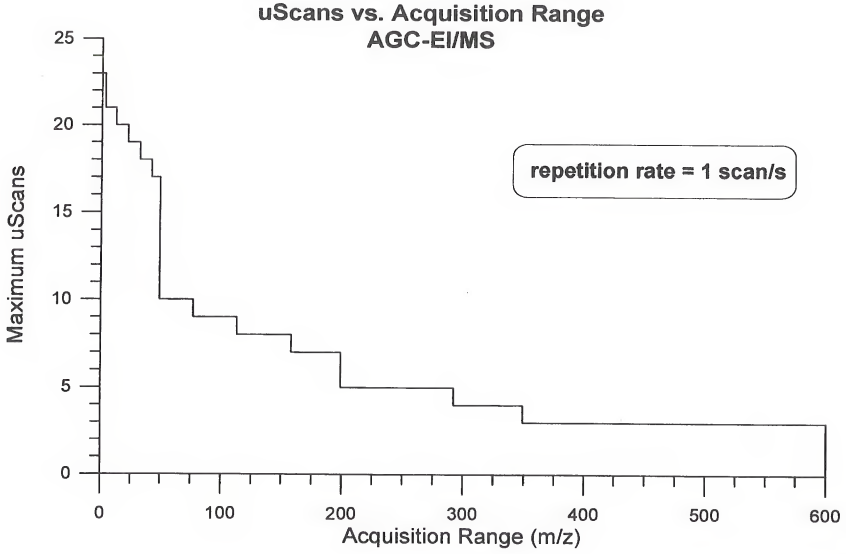
uScans vs. Acquisition Range
AGC-EI/MS
repetition rate = 1 scan/s
Maximum uScans
25
20
15
10
5
0
0
100
200
300
400
500
600
Acquisition Range (m/z)

not the case. The inherent high sensitivity of the ion trap allows full scan spectra to be obtained at lower levels than can be detected with SIM on conventional instruments.

SIM does benefit ion trap operation in several other ways. By reducing the acquisition range, SIM increases the scan repetition rate. As we have seen in the previous section, this can improve quantitation by more accurately reproducing the GC peak profile. Additionally, several SIM methods have been discussed in the literature that eject background interference ions from the ion trap prior to mass analysis. This serves to enhance sensitivity because longer ionization times may be employed without space charge effects. One group observed 1000 times more signal using this approach.[89] The use of SIM to eliminate background interferences is covered later in this chapter.

Ion-Molecule Reactions

Several researchers have addressed the problem of ion-molecule reactions that can occur when performing GC/MS with an ion trap.[82,83,90,91] These reactions, which are commonly termed "self-CI" for self-induced chemical ionization, result in excessive $[M+1]^+/M^+$ ratios and adduct peaks for many classes of compounds that are typically analyzed by GC/MS (see Figure 2-16). The presence of these spectral artifacts can lead to difficulties in unambiguously identifying a compound. It is important to recognize their presence and understand what causes these artifacts to appear.

The types of compounds for which self-CI effects appear at lower sample pressures are those that can readily either donate or accept a proton. Examples of compounds with this type of behavior are aliphatic molecules containing oxygen or nitrogen (i.e. aliphatic alcohols, amines, ketones, and esters), since the alkyl fragment

Figure 2-16. Mass spectrum for 100 ng of benzophenone (MW = 182) analyzed using standard GC/ion trap MS configuration, showing excessive (M+1) abundance and adduct formation due to ion-molecule reactions.

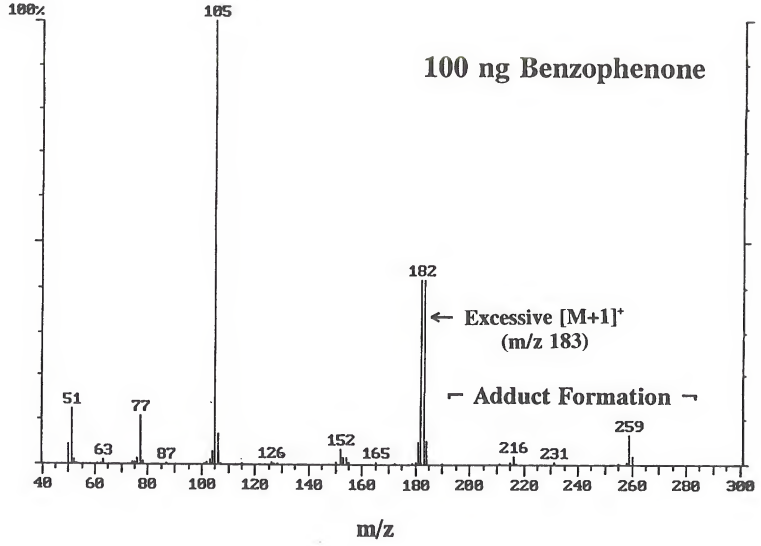
100%
105
100 ng Benzophenone
182
← Excessive [M+1]+
(m/z 183)
⌐ Adduct Formation ¬
51
77
63
87
126
152
165
216
231
259
40
60
80
100
120
140
160
180
200
220
240
260
280
300
m/z

ions for these types of compounds have relatively high gas-phase acidities. For example, Ratnayake et al.[91] observed increased $[M+1]^+/[M]^+$ ratios and other differences in the spectra of certain lipids including fatty acid esters when performing ITD analyses.

As discussed by Pannell et al.,[82] proton transfer reactions are typically observed for compounds that have a large number of alkyl fragments which have conjugate bases of low proton affinity. Since these are bimolecular reactions, the even-electron fragment ions can react with neutral compounds to form even-electron products through proton and alkyl group transfer (leading to the presence of "self-CI" product ions), while odd-electron fragment ions can react with neutral compounds through charge exchange (leading to $M^+$ ions). In the case of methyl decanoate, Pannell et al. found that the tendency for even-electron fragment ions to donate a proton to the neutral molecule was greatest for the lower mass fragment ions as shown in Figure 2-17.[82] In the case of the m/z 41 fragment ion, they also observed subsequent fragmentation of the $[M+H]^+$ ion formed from the proton transfer reaction due to the very low proton affinity of this fragment ions conjugate base. Losses of $H_2$ and methanol also were observed for this reaction.

McLuckey et al. also described the conditions for which self-CI is observed in the ion trap.[83] Although the partial pressure of neutral molecules [M] varies with the GC peak profile under GC/MS conditions, a standard rate equation was used to approximate the likelihood of self-CI occurring since typical GC peak widths are on the order of 1-5 s, and [M] changes relatively slowly for each individual scan. They concluded that a 50 ng sample of a substance capable of reacting with itself or its fragment ions with a rate constant of ca. $3 \times 10^{-9}$ $cm^3/(molecule\ s)$ and with a reaction

Figure 2-17. Tendency of fragment ions from methyl deconate to donate a proton to the neutral ester. A 50 ng sample of methyl deconate was injected onto a DB-1 column.

Methyl Decanoate 50ng Injected on DB-1

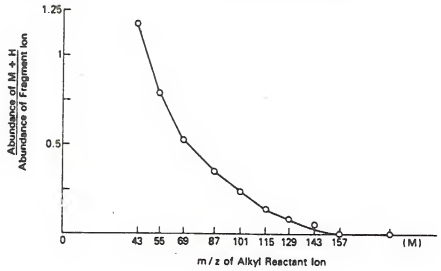

time of ca. 50 ms in the ion trap would show about 13% excess $[M+1]^+/M^+$ as it elutes from a typical GC column.

The authors mentioned above have made the important point that AGC has no effect in reducing the potential for self-CI. The relative degree of self-CI is governed by the extent of ion-molecule reactions, and thus by the partial pressure of neutrals and the reaction time for a fixed number of ions. The use of segmented scan programs helps to reduce the degree of self-CI because of the reduction in reaction time.

Mass Spectral Skewing

The ion trap does not exhibit the mass spectral distortions (skewing) that result from changes in the partial pressure of the sample in the ion source during the mass spectral scan. Mass spectral "skewing" is observed when the ions are continuously formed in the ion source and the time required to obtain a mass spectrum is a significant fraction of the GC peak width.[92] Since the ion trap creates all of the ions that are available for detection at the same time, the short (1-25 ms) ionization period produces a accurate snapshot of the sample molecules that are present in the ion trap at the beginning of the scan. Thus, changes in the partial pressure of the sample that occur during mass analysis do not cause mass spectra skewing because no ions are being formed during this period.

## Advances in Ion Trap GC/MS and GC/MS/MS

Although the ion trap is considered by many to be the most sensitive mass spectrometer for EI and PCI GC/MS, the development of new techniques that further

enhance instrument performance are actively being pursued. Of the many new developments in ion trap mass spectrometry, techniques that reduce background interferences, minimize ion-molecule reactions, and improve on-line MS/MS, appear to hold the greatest potential for GC/MS applications. This section summarizes some of the recent advancements that have been made in these areas.

Methods for Reducing Background Interferences

Several researchers have addressed the problem of background interference ions that can reduce the sensitivity and dynamic range of ion trap GC/MS experiments.[29,52,93-96] The presence of high levels of background ions normally requires that shorter ionization times be used so that space charge effects can be avoided. However, shortening the ionization time also reduces the number of analyte ions that are available for detection, resulting in a loss of sensitivity and dynamic range. Space charge effects caused by background interference ions can be reduced by ejecting these ions from the ion trap prior to collecting a mass spectrum. In most cases, it is preferable to remove these ions during ionization, or shortly thereafter, because gross space charge may also affect the ion trap's storage efficiency. Although many of these methods have been developed using a variety of inlet systems and ionization techniques, they are equally useful for GC/MS. In general, these methods reduce the effects of background interferences, and can boost sensitivity by as much as three orders of magnitude in certain cases.[89]

Single-frequency resonance ejection

Single-frequency resonance ejection removes ions of a particular m/z by applying a sine wave to the endcap electrodes at the ion's secular frequency of motion. As these ions absorb sufficient power from the applied field, they are ejected from the ion trap in the axial direction. Although single-frequency resonant ejection is mass selective, either the excitation frequency can be varied or the ion's secular frequency can be varied (by changing the RF amplitude) so that ions over a m/z range are ejected.

McLuckey et al. described several single-frequency resonance ejection techniques that use a combination of RF voltages and swept-frequency resonant ejection to effect selective ion isolation/ejection over a broad m/z range.[93] As an example of the use of these techniques, matrix ions were removed from a spectrum of 2,4,6-trinitrotoluene (TNT) using swept-frequencies to eject ions from m/z 46 - m/z 120 during ion injection from an air sampling source. The ejection amplitude in these studies was 30 $V_{p-p}$. The authors also observed that the use of swept-frequency resonance ejection during ion accumulation does not completely remove all of the matrix ions since ions begin to accumulate after the frequency sweep has passed over the frequency necessary to eject them.

To effect simultaneous ejection over a wide m/z range during ionization, Eades et al. demonstrated a broadband excitation technique that rapidly switched between discrete frequencies that cover a 300 kHz range.[94] The ITMS's programmable frequency synthesizer and special instrument control software were used to generate 300 kHz wide broadband excitation signals.[97] Compared to swept-frequency resonant ejection, broadband ejection over a 300 u mass range (375 kHz - 75 kHz @ 6 $V_{p-p}$)

during ionization does not allow ions to reform because the entire frequency range is excited in rapid succession.

These studies demonstrate that single-frequency resonant ejection can reduce space charge effects by ejecting background interference ions both during and after ionization. However, only modest gains in sensitivity are observed when single-frequency ejection methods are used in conjunction with long ionization times. McLuckey et al. noted that the analyte signal for TNT could only be increased by a factor of 8 with a 150 fold increase in ion accumulation time, even though frequency sweeps were used to prevent gross space charge affects.[93] Eades et al. also observed a non-linear relationship between ionization time and detected ion signal using the broadband ejection methods.[94] These results suggest that the efficiency with which single-frequency methods can be used to remove ions over a wide m/z range may not be sufficient to produce large gains in sensitivity for a single ion. This is a logical result since the frequency sweep and broadband excitation methods excite ions of only one m/z at a time. Instead, single-frequency ejection methods may be better suited to eliminating a single m/z.

Multiple-frequency resonance ejection

Multiple-frequency resonance ejection methods use non-sinusoidal waveforms containing a spectrum of frequencies. These methods eject ions of different m/z simultaneously. Excitation waveforms are created by numerical methods that provide greater control over the excitation process. These digital waveforms are then converted into analog signals by means of a high speed digital to analog converter (DAC). Commercial arbitrary (ARB) waveform generators offer a convenient method

for producing these types of analog signals. The main advantage of multiple-frequency resonance ejection over single-frequency techniques is that they continuously excite the selected ions, keeping them from accumulating to any appreciable level.

Stored waveform inverse Fourier transform (SWIFT) broadband excitation, as developed by Marshall et al. is a powerful tool for the manipulation of ions that are held in ion cyclotron resonance (ICR) or quadrupole ion traps.[98] SWIFT on the ICR has been used to isolate/eject ions with high resolution and efficiency. Figure 2-18 demonstrates the use of SWIFT on the quadrupole ion trap for the elimination of matrix ions that prevented the detection of 37 pmol of substance P using desorption ionization.[95] A limitation of the SWIFT approach is that it is computationally intensive. Thus, the time required to calculate and download a single SWIFT waveform restricts the use of multiple waveforms during a GC analyses. Also, because SWIFT pulses have a finite duration, the length of excitation is limited. As an example, an 8192 point SWIFT pulse that is output at a rate of 2 µs/point lasts approximately 16 ms. During the 16 ms pulse, ions are only excited for ca. 12 ms due to the reduced amplitude during the leading and tailing edges of the waveform. Multiple SWIFT excitation pulses can be linked together to form longer ejection periods, but it is important to note that the excitation is not continuous. Thus, ions formed between SWIFT pulses are not immediately ejected from the ion trap. The time-varying nature of SWIFT waveforms may also affect the resolution with which an ion can be isolated since the resolution of other resonance ejection techniques is observed to improve as the length of the excitation pulse is increased.[99]

A second type of multiple-frequency resonant ejection applies a filtered noise field (FNF) to the ion trap to isolate/eject ions of specific m/z.[89] The FNF method uses

Figure 2-18. Resonant ejection mass-selective instability scan of a 37.1 pmol sample of substance P. Ions are created via desorption ionization from glycerol-thioglycerol matrix. The sample was bombarded by a 7-kV $Cs^+$ beam for 80 ms during which time ions were injected into the trap: (a) no SWIFT pulse applied; this spectrum shows the severe effect of space charge, with low parent ion intensity; (b) SWIFT pulse applied during ion injection.[95]

a)

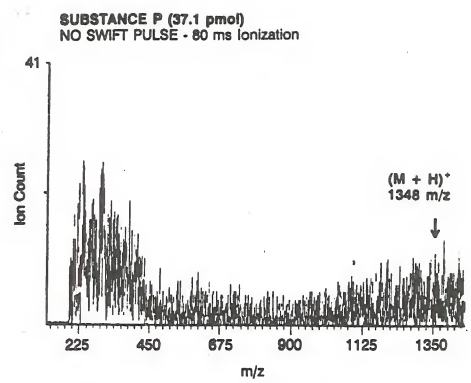
SUBSTANCE P (37.1 pmol)
NO SWIFT PULSE - 80 ms Ionization
41
Ion Count
(M + H)+
1348 m/z
225
450
675
900
1125
1350
m/z

b)

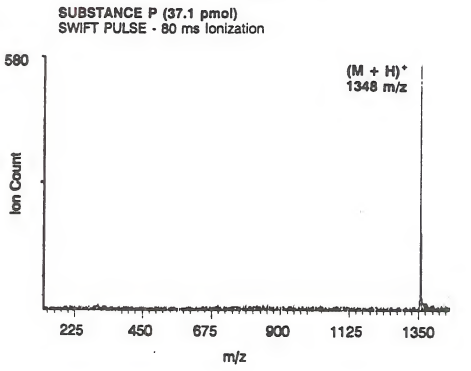
SUBSTANCE P (37.1 pmol)
SWIFT PULSE - 80 ms Ionization
580
Ion Count
(M + H)+
1348 m/z
225
450
675
900
1125
1350
m/z

a single excitation waveform containing all frequencies to excite all of the ions in the ion trap. Then, before this waveform is converted to an analog signal, rapid digital filtering methods are applied to remove selected frequencies from the noise spectrum. By selecting filters that mask the m/z of interest, FNF removes all of the other ions from the ion trap. FNF has been shown to enhance GC/MS sensitivity by as much as 1000 times over GC/MS alone.[89] Figure 2-19 shows two sets of ion chromatograms for the molecular and fragment ions of cocaine present in a mixture of polyaromatic hydrocarbons. An advantage of the FNF approach is that the digital filters can be exchanged rapidly, allowing different ions to be isolated/ejected at different points during the chromatogram. Figure 2-20 also demonstrates that the FNF technique can be used to isolate multiple m/z windows, allowing more than a single ion to be monitored at high sensitivity.

The commercial introduction of ion isolation/ejection methods that reduce background interferences is expected to further improve ion trap performance for GC/MS and GC/MS/MS. The FNF electronics are currently the only electronics commercially available that can be interfaced to existing ion trap instruments. A similar method that also uses complex waveforms has been demonstrated by Varian Associates and is expected to be available for the SATURN instruments.[96] Alternatively, the availability of inexpensive arbitrary waveform generators, digital function generators, and personal computers offer a practical means for implementing the SWIFT and single-frequency resonant ejection methods on existing ion trap hardware. It is important to point out that while these multiple-frequency techniques appear to improve upon the ion trap's current capabilities, detailed studies that characterize the isolation efficiency, ejection efficiency, sensitivity, and linear dynamic

Figure 2-19. Comparison of GC/MS data for 200 pg of cocaine (MW = 303) in the presence of a 100 ng of PAH background. Acquired with (a) AGC and (b) FNF selected ion monitoring modes.

a)

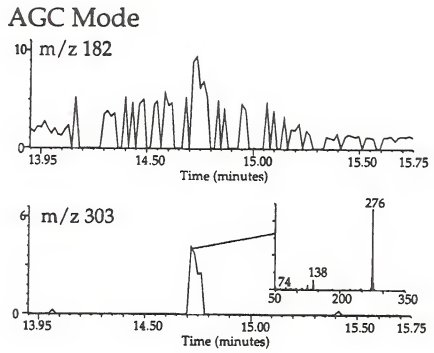
AGC Mode
m/z 182
10
0
13.95
14.50
15.00
15.50
15.75
Time (minutes)
m/z 303
6
0
276
138
74
50
200
350
13.95
14.50
15.00
15.50
15.75
Time (minutes)

b)

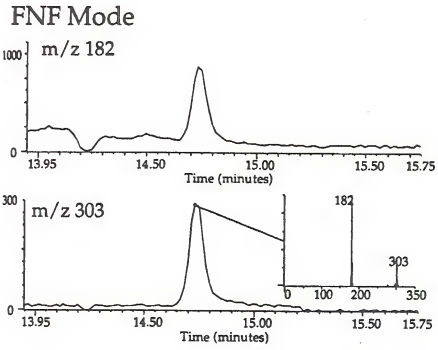
FNF Mode
m/z 182
1000
0
13.95
14.50
15.00
15.50
15.75
Time (minutes)
m/z 303
300
0
182
303
0
100
200
350
13.95
14.50
15.00
15.50
15.75
Time (minutes)

range for GC/MS have not been published.

RF/DC

RF/DC methods can be used to remove interference ions from the ion trap by operating at RF and DC voltages that preclude high or low m/z ions from having stable trajectories. An important difference between resonance ejection and RF/DC methods is that before resonance ejection can occur, the ions must assume regular trajectories at their secular frequency. RF/DC methods exclude ions from having stable trajectories, which prevents prolonged storage of these ions. The rapid nature of RF/DC ejection would appear to make it a more efficient method for eliminating matrix ions. However, the large RF and DC voltages that are commonly associated with RF/DC methods perturb the energy and trajectories of the ionizing electrons and in turn reduce the efficiency with which analyte ions are created and trapped. Nevertheless, RF/DC methods have been shown to be useful for reducing certain types of background interferences.

The application of a small positive DC voltage (5 V - 20 V) during electron ionization can be used to efficiently remove high m/z ions from the ion trap. For chemical ionization experiments, the ejection of high mass EI ions that are formed at the same time that the CI reagent ions are formed can improve CI sensitivity and eliminate the EI ions from CI spectra. Eades showed that the application of a small positive DC voltage could be used to eject all ions above m/z 50.[94] This allowed ionization time to be increased from 1 ms to 50 ms and resulted in a 20-fold increase in ion signal for m/z $41^+$.

Several RF/DC methods have been demonstrated that reduce background interferences by isolating the ion of interest after the ionization event. Strife showed that the sequential ionization and isolation of an analyte and its internal standard dramatically improved the ion trap's ability to detect compounds that co-elute at vastly different concentrations.[29] In a subsequent article, Klientop et al. used sequential RF/DC isolation steps to obtain a calibration curve for an analyte and its isotopically labeled internal standard for sample amounts that spanned six orders of magnitude.[67]

External Ionization GC/MS

In the standard ion trap configuration (see Figure 2-20a), GC effluent is introduced into the body of the ion trap, and electrons emitted from a filament located external to the ion trap are gated into the trap. Ions formed by electron ionization are stored and then mass analyzed by ramping the rf voltage placed on the ring electrode. In this process, neutral molecules are present in the same region as the ions that are being stored and analyzed. Reaction times of around 50 ms are typically encountered; this can lead to ion-molecule reactions ("self-CI") as previously discussed. Both proton transfer (creating excessive $[M+1]^+$ abundances) and alkyl group transfer (creating adduct ion peaks) can clearly be seen in the ion trap mass spectrum of benzophenone (see Figure 2-16).

Perhaps the best solution to the problem of self-CI occurring during GC/ITMS analyses is to limit the number of neutral molecules (either analyte, solvent, or contaminants) present in the ion trap during storage and scanning. This can be accomplished by creating the ions in a conventional ion source and injecting them into the ion trap. Injecting ions from an external ion source into an ion trap in order to

Figure 2-20. Internal and external ionization hardware. Schematic of (a) standard GC/ion trap MS configuration using internal ionization and (b) external ion source used for GC/ion trap MS. Helium is directly introduced into the trap (a) via the GC and (b) by an additional gas line. The external ion source was constructed from a Finnigan 4500 series ion source. Lens 3 (L3) has a tube lens that helps pass ions from the ion source to the entrance endcap. The pressure in the ion trap was maintained 10 times greater than the surrounding vacuum system via the conductance spacers that are located between the ring and endcap electrodes.

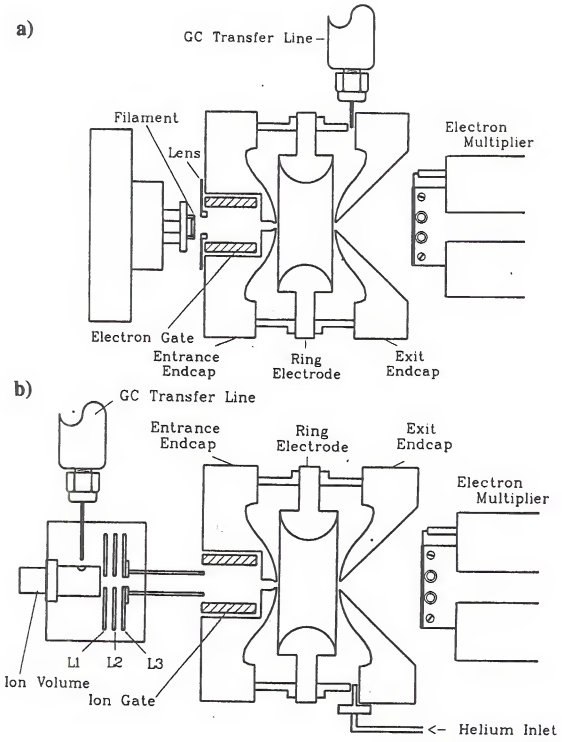
a)
GC Transfer Line
Filament
Lens
Electron Multiplier
Electron Gate
Entrance Endcap
Ring Electrode
Exit Endcap
b)
GC Transfer Line
Entrance Endcap
Ring Electrode
Exit Endcap
Electron Multiplier
L1
L2
L3
Ion Volume
Ion Gate
<- Helium Inlet

introduce samples from a high pressure source into the ion trap has been used by many researchers since the original work done by Louris et al.[37] Some of this work includes atmospheric sampling glow discharge ionization,[100] particle beam liquid chromatography,[101] supercritical fluid chromatography,[102] and electrospray ionization.[103]

Figure 2-20b shows an external ion-source/ion-trap GC/MS interface that was recently described.[104] For this work, a Finnigan 4500 ion source was directly coupled to a Finnigan ITMS-style ion trap. Injection of ions was accomplished by grounding the ion source and floating the endcap and ring electrodes of the ion trap by a variable potential. A standard ITS40 electron gate electrode was used as the ion gate for this system. The electron gate TTL signal produced by the ion trap electronics was inverted and amplified using a custom circuit and a variable power supply to produce the ion gate voltage. For this work, a standard EI AGC scan program was used.

Since benzophenone forms both the protonated molecule (m/z 183) and adduct ions (m/z 216 and 259) under EI conditions, it was used to evaluate the GC/MS performance of this system. Figure 2-21 shows the total ion chromatogram and mass spectrum of 1 ng benzophenone analyzed on the GC/ion injection ion trap system. Figure 2-22 compares the $[M+1]^+/[M]^+$ ratio for the analysis of benzophenone using both internal and external ionization systems. As can be seen from this figure, the $[M+1]^+/[M]^+$ ratio remains constant and very close to the theoretical value for the GC/ion injection ion trap system. The data for internal ionization, in contract, show that even at 0.5 ng benzophenone, the proper $[M+1]^+/[M]^+$ ratio is never reached. At low concentrations, this may be due to lower mass ions from the column bleed that were present during the analysis. These ions also have relatively high gas-phase acidities, and can donate protons to neutral benzophenone. At the higher concentrations of

Figure 2-21. Total ion chromatogram and mass spectrum for 1 ng of benzophenone analyzed on the GC/ion trap MS system using external ionization. Ion injection times were controlled by AGC.

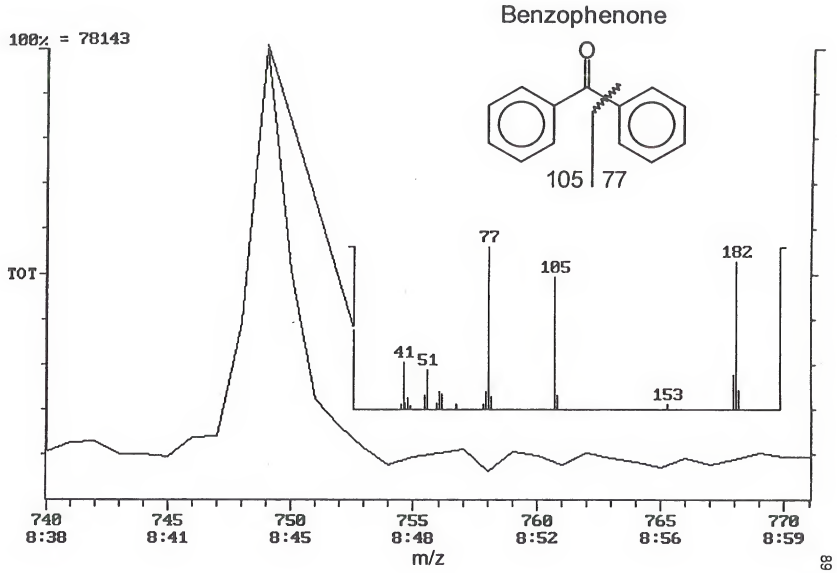
Benzophenone
100% = 78143
TOT
105
77
77
105
182
41
51
153
740
8:38
745
8:41
750
8:45
755
8:48
760
8:52
765
8:56
770
8:59
m/z

Figure 2-22. Comparison of the (M+1)/(M) ratio for the analysis of benzophenone using both internal and external ionization systems. The theoretical peak area ratio of 14.6% assumes that only $^{13}C$ contributes to $[M+1]^+$.

## (M + 1)/(M) Ratio vs. Amount Injected

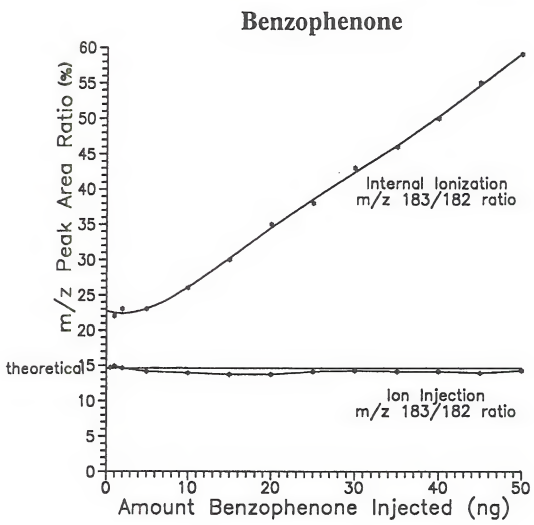

benzophenone, self-protonation occurs, leading to a linear relationship between the (M+1)/(M) ratio and the amount of benzophenone injected.

Figure 2-16 shows the mass spectrum for 100 ng of benzophenone analyzed on the GC/internal ionization ion trap system. At this concentration, both the protonated benzophenone molecule (m/z 183) and adduct ions (m/z 216 and 259) can be seen. Figure 2-23 shows the mass spectrum for 500 ng of benzophenone analyzed on the GC/ion injection ion trap system. Even at this high concentration, the proper $[M+1]^+/[M]^+$ ratio is obtained, and there are no adduct ions observed in this spectrum.

It is important to note that only minor modifications to a standard ITS40 GC/MS ion trap system were needed in order to use an external ion source. For this system, differential pumping was not required; a tube lens was added to the third lens of the ion source, and helium was added directly into the ion trap.

Although this system does show that it is capable of delaying the onset of ion-molecule reactions, it is important to realize that all mass spectrometers are susceptible to ion-molecule reactions. Besides reducing ion-molecule reactions, another potential benefit in using an external ion source is that negative ion chemical ionization (NICI) may be performed. NICI cannot be performed when using internal ionization because of the lack of thermal electrons due to the presence of the ion trap's high voltage RF storage field.[105] NICI is particularly useful when analyzing compounds with very electronegative functional groups, such as halogenated pesticides and PCBs.

The major drawback to using an external ion source is the added complexity of operation. The external ion source requires a slightly larger vacuum system than the standard configuration, and the source requires an extra set of power supplies to drive

Figure 2-23. Mass spectrum for 500 ng of benzophenone analyzed using GC/ion trap MS with external ionization, showing correct (M+1) abundance and no adduct formation.

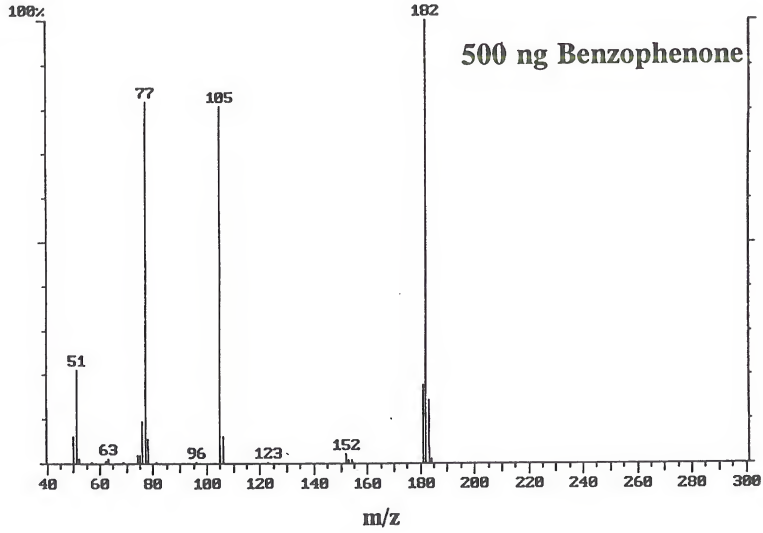
100%
182
500 ng Benzophenone
77
105
51
63
96
123
152
40
60
80
100
120
140
160
180
200
220
240
260
280
300
m/z

the lenses. Additionally, changing between EI and CI ionization modes involves hardware adjustments with an external ionization source (e.g. changing ion volumes), in contrast to the minor software modifications that are required when internal ionization is used. Even with these limitations, the development of commercial external ionization source GC/ion trap systems will expand the ion trap's use for applications the require reduced ion-molecule reactions and additional ionization modes.

Tuning Methods for GC/MS/MS

Creating and tuning a MS/MS scan program is currently a time consuming process that can restrict the usefulness of GC/MS/MS on the ion trap. Several parameters may be adjusted, including ionization time, rf level for ionization, RF and DC voltages for isolation, isolation times, rf level for CID, excitation frequency, excitation time, and excitation voltage. For GC sample introduction, tuning time is limited to the width of the chromatographic peak, typically 2-3 seconds over the course of the GC run. Thus, if 50 manual adjustments are required, 50 repetitive sample injections would also need to be performed. Repetitive injections require a lot of time, and can be impractical even if only a few injections are needed. Additionally, either standards must be available or the sample must be of sufficient volume and concentration to allow tuning to be performed. Alternatively, standards of sufficient volatility can be introduced via a variable leak valve to allow for off-line tuning of the scan program. Clearly the amount of tuning that is currently required to analyze a single compound, present at a known concentration in a clean sample matrix, makes general use of ion trap GC/MS/MS impractical.

Todd et al. demonstrated a sophisticated set of programs that automatically adjusted MS/MS scan program parameters.[106] With the use of the dynamically programmed scan method, complete MS/MS fragmentation data maps were constructed automatically. However, the rate at which these types of experiments were performed, 5 min to 15 min, would limit their applicability on a GC time scale.

New software developed for the ITMS simplifies the process of setting up MS/MS scan programs by automatically scaling a template of an MS/MS scan program for a parent m/z of interest.[71,97] This software adjusts the RF voltages, table times, and scan program structure without tuning. The need to tune the resonant excitation frequency is obviated by the use of broadband excitation (discussed in the following section). Additionally, the DC voltage used for isolation is calculated empirically. After proper calibration of the DC voltage, these methods can automatically isolate a 2-3 u wide window between m/z 70 - m/z 300. Fine tuning of the isolation voltages to isolate a single m/z still requires manual adjustment and remains the biggest limitation for tuning MS/MS scan programs for GC analyses. The use of a scan program template also restricts the versatility of the software to particular types of MS/MS scan programs. Regardless of these limitations, this software simplifies many of the tuning requirements for MS/MS scan programs and can save a considerable amount of time compared to creating new scan programs.

Yates et al. have developed several sophisticated programs that automatically tune MS/MS scan programs for an ITS40 that has been modified for GC/MS/MS experiments.[73,97] This software uses the Mathieu parameters $a_z$ and $q_z$ and the modified field equations for the ion trap's stretched geometry to calculate the RF and DC voltage for each stage of the scan.[107] This allows scan tables to be scaled for a

particular m/z of interest. Additionally, versatile automatic ionization control techniques for EI and CI are included that eliminate the adjustment of the ionization time. Creation of an MS/MS scan program for m/z 303 begins with the creation of a MS/MS scan program for m/z 264 of perfluorotributylamine (PFTBA). PFTBA is employed as a calibration gas that can be readily introduced into the ion trap via a leak valve. Once the $a_z$, $q_z$, and table time parameters have been manually adjusted for PFTBA, the scan program can be scaled to the m/z of interest with a software toggle. Although the isolation of a single m/z can be erratic, 2-3 u m/z windows can be isolated with good reproducibility. In most cases these programs allow MS/MS scan programs to be created without the need for repetitive injections.

The process of performing GC/MS/MS on the ion trap is limited in part by the current complexity of tuning MS/MS experiments. However the development of more accurate electronics and sophisticated tuning methods should make switching from MS to MS/MS as simple as pushing a button.

Frequency Shifts, Resonant Excitation Methods, and CID

Shifts in an ion's secular frequency of motion that occur when the number of ions in the ion trap change have been investigated by several groups.[26,53,71,84,85] Figure 2-24 contains three frequency breakdown curves for the molecular ion of n-butylbenzene, m/z 134. The minimum of each curve corresponds to the most efficient resonant excitation frequency, and may be interpreted as the ion's secular frequency of motion in the axial direction. Interestingly, the secular frequency shifts to lower values as the number of ions is increased by elevating the ionization time from 5 ms to 85 ms. These frequency shifts complicate single-frequency resonant excitation

Figure 2-24. Ion signal as a function of excitation frequency. Comparison of three frequency breakdown curves for m/z 134 of n-butylbenzene at ionization times of (a) 5 ms, (b) 40 ms, and (c) 85 ms. Resonant excitation parameters include amplitude = 400 mV, duration = 10 ms, frequency 116000 - 119000 @ 23 Hz increments.

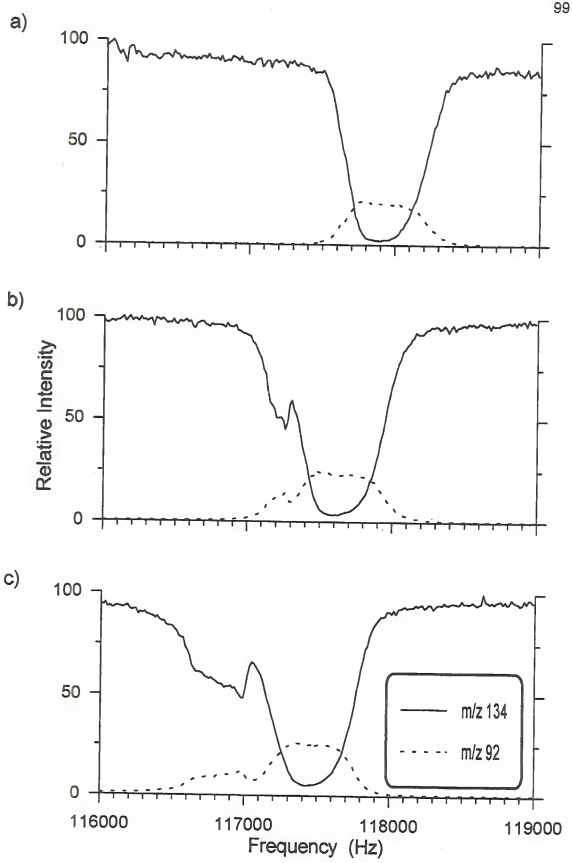
a)
100
50
0
b)
100
50
0
Relative Intensity
c)
100
50
0
m/z 134
m/z 92
116000
117000
118000
119000
Frequency (Hz)

experiments, since the excitation frequency must match the ion's secular frequency. To illustrate what happens when the excitation frequency does not match the ion's secular frequency, Figure 2-25 shows three product ion spectra for m/z 134 of n-butylbenzene. These spectra were acquired using (a) 5 ms, (b) 40 ms, and (c) 85 ms ionization times, and a resonant excitation frequency of 117900 Hz. Note that as the ionization time (and thus the number of ions in the ion trap) increases, the efficiency of CID for $134^+$ decreases due to shifts in the ion's secular frequency of motion.

For GC/MS/MS, the dependance of CID efficiency on the number of ions in the ion trap can be particularly bothersome since the number of ions continually changes during a GC run. Tuning single-frequency resonant excitation scan programs for GC can also be complicated because it is difficult to determine from a CID spectrum whether the excitation frequency was too high or low. To simplify CID on the GC time scale, several methods have been developed that compensate for the effects of frequency shifts, as detailed in chapter 4.

Briefly, the frequency-assignment pre-scan corrects for frequency shifts by performing two rapid pre-scans prior to each analytical scan to determine the parent ion's secular frequency of motion.[71] Each pre-scan employs a 10 ms frequency sweep that determines the parent ion's secular frequency of motion by ejecting the parent ion to the detector. By correlating the observed ion signal with the frequency sweep rate, the secular frequency of motion may be determined. The frequency-assignment pre-scan is discussed in detail in chapter 4 of this dissertation.

Broadband excitation compensates for frequency shifts by exciting a range of frequencies that cover the expected magnitude of the frequency shift.[71] On the ITMS, broadband excitation may be implemented by programming the frequency synthesizer

Figure 2-25. Product ion spectra as a function of ionization time, showing the effect on MS/MS efficiency. MS/MS product ion spectra for m/z 134 of n-butylbenzene at ionization time of (a) 5 ms, (b) 40 ms, and (c) 85 ms. Resonant excitation parameters of 400 mV, 117900 Hz, and 10 ms were used.

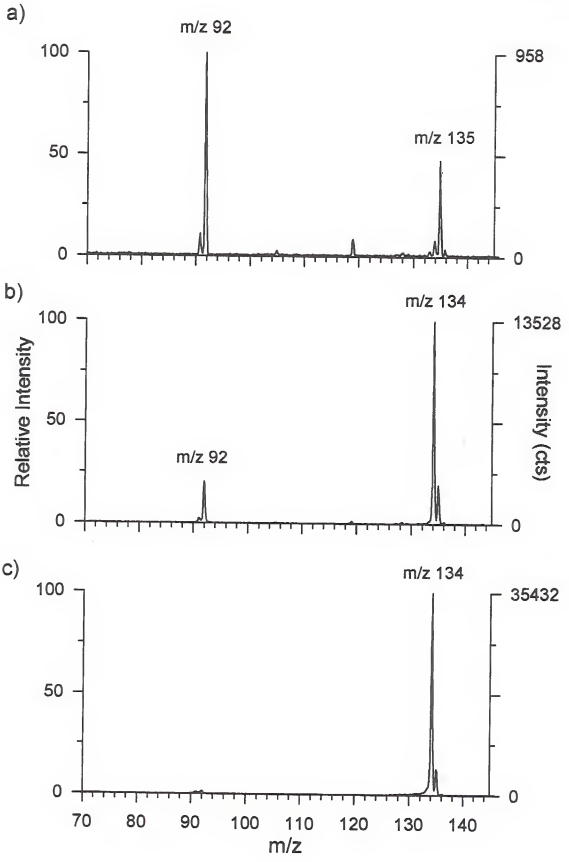
a)
m/z 92
100
50
0
958
m/z 135
0
b)
m/z 134
100
13528
Relative Intensity
50
Intensity (cts)
m/z 92
0
0
c)
m/z 134
100
35432
50
0
0
70
80
90
100
110
120
130
140
m/z

to switch between selected frequencies in a phase continuous manner. A typical broadband excitation pulse switches between 1400 discrete frequencies covering a 10 kHz wide range. Centering this broadband excitation signal at 118 kHz excites a 1.2 u wide m/z range at $q_z$ = 0.3 on the ITMS. Frequency modulated and SWIFT broadband excitation methods are discussed in chapter 4 of this dissertation.

Random noise excitation is a simple method for resonantly exciting ions over a wide m/z range that is also unaffected by frequency shifts. The technique can be implemented with a commercial noise generator that produces a random noise signal with a flat power spectrum from 10 Hz-500 kHz.[108] Although low-pass filters can be used to alter this power spectrum, the technique is not m/z selective. Figure 2-26 shows the power spectrum of a random noise source that has been attenuated by several low-pass filters. Note that for a low m/z cutoff of 35, a frequency range from 10 kHz-530 kHz corresponds to a m/z 35 - m/z 1000. Thus, random noise excitation results in the simultaneous activation of all of the ions in the ion trap.

Since random noise excitation is not m/z selective, parent ions undergo CID to form product ions that are also excited and fragment to form other product ions, etc. Thus, random noise may produce more fragment ions and more structural information in a single experiment than is observed for mass selective CID methods. However, additional fragmentation does not always provide more structural information because formation of low m/z fragment ions are often less useful for structure elucidation studies. Additional fragmentation may also lead to the production of ions below the low m/z cut off of the ion trap. In this case, both the CID efficiency and sensitivity are reduced due to the exclusion of low m/z ions from the ion trap.

Figure 2-26. Random noise excitation spectrum. Relative noise power versus frequency as a function of - 3 dB roll-off frequency for several low pass filters: (a) no filter, (b) $f_c$ = 300 kHz, (c) $f_c$ = 100 kHz, (d) $f_c$ = 30 kHz. Mass-to-charge values are also indicated for a low mass cutoff corresponding to m/z 35.[108]

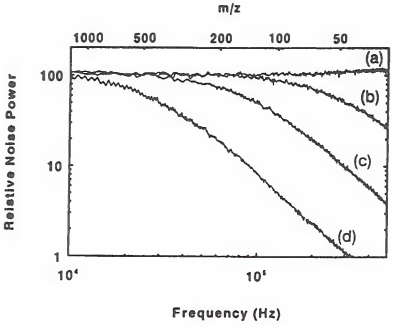
m/z
1000
500
200
100
50
(a)
(b)
(c)
(d)
100
10
1
Relative Noise Power
10⁴
10⁵
Frequency (Hz)

Increased ion losses due to resonant ejection may also be observed when random noise is used for CID. Although the average power spectrum of a random noise source exhibits a flat response, discrete segments of the random noise signal may exhibit irregularities in the time domain. Individual ions may be unaffected, excited, or ejected, depending on the instantaneous phase and frequency of the noise source and the ion's velocity, position, and m/z. Thus, random noise excitation may be more erratic than single frequency methods which exhibit a smooth activation process. Additionally, with single frequency excitation all of the parent ions can be excited without exciting the product ions. Because noise fields excite both the parent and product ions, it is difficult to completely excite the parent ion without loosing a fraction of the product ions. In practice, ion losses are 40-60 % greater for random noise relative to single frequency resonant excitation.[108]

The filtered noise field (FNF) method that is used for the removal of background matrix ions can also be applied as an excitation method for GC/MS/MS. FNF broadband excitation can be implemented by applying a digital filter to the noise field that masks all of the frequencies except for a 10 kHz wide window centered at the frequency of motion of the parent ion of interest. Digital methods also allow the phase relationship of the unfiltered noise field to be controlled so that ion activation is a smooth process rather than an erratic one. Although many of details of the FNF method have yet to be described, the ion isolation and broadband excitation capabilities of FNF appear to make it a powerful technique for GC/MS/MS.

DC pulse axial activation can be used to effect ion activation and dissociation in the quadrupole ion trap.[109] The method employs short (2 μs) DC pulses that are applied to the endcaps of the analyzer to accelerate the ions in the axial direction.

Excitation is not mass selective and must be combined with isolation to perform MS/MS experiments. Interestingly, the maximum internal energy that can be deposited has been shown to be considerably higher than is possible with resonant excitation methods.[109] Dissociation efficiencies are less than those typically observed for resonant excitation, ranging from 50% - 5% as the amplitude of excitation is increased.

Wang et al. demonstrated a similar non-resonant ion activation method that employs low frequency (100 Hz - 500 Hz) excitation signals.[110] Ions are excited by applying a 56 V 200 Hz square wave signal across the endcap electrodes for 10 ms. This signal corresponds to two 5 ms long DC pulses of altemating polarity. High CID efficiencies and considerable internal energy deposition were demonstrated. The detection of 100 pg of n-butylbenzene was demonstrated using non-resonant excitation GC/MS/MS. Interestingly, the internal energy deposition was noticeably less for the GC/MS/MS results, as indicated by the intensity ratio for the product ions m/z $91^+/92^+$. Although these DC pulse axial activation methods are relatively new tools for affecting CID, their simplicity, energy deposition, and lack of dependence on the parent ion's frequency of motion, appear to make them a good choice for GC/MS/MS experiments.

## Benchtop GC/MS/MS Instruments

Based on the present understanding of the ion trap's GC/MS and MS/MS capabilities, several criteria for practical GC/MS/MS analyses can be identified.

The first criterion for practical GC/MS/MS is the ability to analyze sample amounts that extend over a wide dynamic range without manually adjusting the ionization time. Automatic ionization control methods have been affective for GC/MS and would appear to be a reasonable approach for limiting space charge, maximizing parent ion intensity, and enhancing dynamic range for GC/MS/MS experiments. External ionization would help to reduce ion-molecule reactions and allow selective ionization modes like electron capture negative CI to be used.

The second criterion for practical GC/MS/MS is the ability to analyze samples regardless of high levels of chemical interferences. The incorporation of isolation methods that reduce background interferences by ejecting matrix ions from the ion trap should help to limit space charge affects for complex samples. Consequently, isolation of the m/z of interest is also a necessary first step for any MS/MS experiment. Thus, MS/MS analyses should be less affected by space charge because of the reduced number of ions that are analyzed compared to MS analyses.

The third criterion for practical GC/MS/MS is that the method of ion activation yields high CID efficiencies regardless of the number of ions in the ion trap. Many of the broadband excitation methods that have been developed appear to be viable methods for effecting CID over a GC peak.

Perhaps the most important criterion for practical GC/MS/MS on the ion trap is simplified operation. By using improved methods of operation the need for repetitive sample injections can be reduced. The development of software that automatically handles the creation and tuning of scan programs would reduce the level of sophistication that is currently required to take advantage of the ion trap's MS/MS capabilities.

Although no ion traps currently incorporate all of these features, several groups have strived to improve the usefulness of GC/MS/MS on the ion trap in order to demonstrate the analytical utility of the technique. Van Berkel et al. recently demonstrated the use of random noise excitation on a modified ITS40.[70] Product ion spectra were obtained by triggering the random noise signal during the CI reaction period of a ARC-CI/MS scan program. CID spectra for GC peaks that correspond to amphetamine and methamphetamine were obtained. The authors also point out that while the random noise technique is simple to implement, the ITS40 software was intended for GC/MS experiments and can be restrictive for GC/MS/MS analyses. For instance, the ITS40 EI segmented scan program does not hold the ions a fixed RF level for an extended period of time, thus random noise CID experiments cannot be performed using EI.

An important advantage of random noise CID is observed when complete chromatographic separation is achieved. That is, the same scan program can be used to produce product ion spectra for each compound, regardless of the parent ion m/z. Additionally, toggling the random noise on or off with each scan would allow molecular weight and structural information to be obtained in a single experiment.

A disadvantage of random noise CID on the ITS40 is that the parent ions are not mass selected prior to CID; thus, this is not a true MS/MS experiment. CID/MS experiments like these can only perform "orphan scans" not "daughter scans", because there is no way of determining the m/z of the parent ions from the product ion spectra. Most importantly, the analytical utility of CID/MS and MS/MS are not the same. In contrast to MS/MS, CID/MS produces product ions for all of the ions in the ion trap, including matrix ions. Thus, chemical noise will not be reduced and no gains in selectivity or signal-to-noise (S/N) ratio should be observed.

GC/MS/MS was recently demonstrated on a modified ITS40 that employs automatic ionization control (AGC and ARC), RF/DC two-step isolation, SWIFT broadband excitation, and new instrument control software that automatically scales MS/MS scan programs for the parent m/z of interest. The development of this benchtop GC/MS/MS instrument and the GC/MS/MS results obtained are discussed in chapter 5 of this dissertation.

## Summary

The quadrupole ion trap has undergone a renaissance from a novel ion storage device to a conventional mass analyzer used for GC/MS. Although GC/MS has been the driving force behind the commercial development of the quadrupole ion trap, many expect that the ion trap's use for GC/MS/MS will become important as well. In this chapter, the instrument's features and methods of operation for the commercial ion trap instruments have been reviewed and GC/MS and GC/MS/MS application examples have been summarized. An explanation of the underlying differences between ion trap and quadrupole mass filter mass spectrometers has been presented to give those that

are less familiar with the ion trap an appreciation of this unique mass analyzer's strengths and limitations.

Several new methods of operation are currently being developed that aim to further improve the ion trap's GC/MS capabilities. The use of single-frequency and multi-frequency excitation signals to selectively isolate the ion of interest while ejecting interference ions shows a strong potential for improving the ion trap's ability to analyze trace analytes that coelute in complex mixtures. The development of ion activation methods such as SWIFT and FNF broadband excitation that are capable of dissociating ions without a loss in efficiency or the need for extensive manual tuning will also improve the ion trap's capabilities for GC/MS/MS. DC pulse axial activation appears to be a promising method for accessing higher fragmentation energies.

The benefits of external ionization and ion injection may also prove to be very useful for complicated GC analyses. In particular, the reduction of the sample pressure in the ion trap reduces the intensity of ion-molecule reaction products in ion trap spectra. The observation that ion-molecule reactions can be significantly reduced without differential pumping is important because it should reduce the cost and complexity of the instrumentation. Secondly, the use of external ionization sources allows highly selective ionization methods such as electron capture negative CI to be used with the ion trap.

Finally, the development of sophisticated ion trap systems that are not only powerful mass spectrometers, but also simple to operate, is needed before the ion trap's high performance capabilities can be accessed by a wide range of users. The current commercial instruments, which are aimed at the single quadrupole (GC/MS) market, tend to disguise the underlying differences between linear quadrupoles and ion

traps. This prevents the casual user from gaining a complete understanding of the unique principles that govern ion trap operation. This is unfortunate because many of the benefits of ion trap mass spectrometry, such as the full-scan sensitivity and MS/MS, arise from these differences. Perhaps the greatest gains in ion trap mass spectrometry can be made by taking advantage of the ion trap's unique abilities while appreciating the underlying limitations of this marvelous ion storage device.

# CHAPTER 3
# ION ISOLATION

## Introduction

The isolation of one m/z or a narrow m/z range is an important step in many of the experiments that can be performed with the quadrupole ion trap mass spectrometer. For tandem mass spectrometry, the mass selection of an ion of interest represents the first stage of mass analysis in an MS/MS experiment.[20,29,50,93,99,111,112] The ability to isolate reactant ions in the ion trap is also an important tool for studying gas phase kinetics and ion-molecule reaction pathways.[113-115] In addition, the isolation of ions has been shown to be an affective method of reducing space charge and improving the sensitivity and dynamic range of the quadrupole ion trap.[21,87,94]

Traditionally, quadrupole mass analyzers select a single m/z by operating at an RF amplitude and DC potential that define an operating line that passes through the apex of the Mathieu stability diagram. Figure 3-1 shows the stability diagram for a quadrupole mass filter including the "RF/DC" operating line. Ions with m/z values defined by the (a,q) coordinates at the intersection of the stability diagram apex and the operating line will pass through the mass filter. Similarly, ions of a single m/z can be mass selected in the quadrupole ion trap using several "RF/DC" operation modes.

This chapter describes experiments that were performed to characterize two RF/DC methods, apex isolation and two-step isolation. These methods are used for

isolating one m/z or a narrow m/z range in the quadrupole ion trap. The scan programs for implementing apex and two-step isolation are also described. Two new figures of merit that relate the efficiency of isolation and ejection for the isolation of ions in the quadrupole ion trap are used to compare the experimental data collected in this study. Using these figures of merit, the efficiency of the apex and two-step isolation methods are characterized for several ions that range from m/z 40 to m/z 157. Experimental results that show the relative "sharpness" of stability diagram edges are presented. Additionally, an empirical model is used to described why certain stability edges exhibit sharper stable/unstable transitions. Finally, several practical considerations including ease-of-use, tuning, and electronic stability are discussed for both isolation techniques.

Two criteria for an "ideal" mass isolation technique have been defined. First, an ideal isolation technique would be able to eject all ions other than the m/z of interest from the ion trap. Secondly, all of the ions of the m/z of interest that were formed during the ionization period should remain in the ion trap following the isolation step. Here we define two new terms, the efficiency of isolation ($E_{ISO}$) and the efficiency of ejection ($E_{EJ}$), that measure these criteria. $E_{ISO}$ is defined as,

$$E_{ISO} = \frac{I_P}{I_P^\circ} * 100\% \qquad (3\text{-}1)$$

where $I_p$ is the intensity of the isolated ion and $I_p^\circ$ is the intensity of the ion of interest without isolation. Thus, $E_{ISO}$ measures the percentage of the ion of interest that remains in the ion trap following isolation. The extent of isolation is expressed in terms of the percent of an adjacent ion (next to or near the ion of interest) that is ejected from the ion trap. This term is called the efficiency of ejection, $E_{EJ}$, and is defined as,

Figure 3-1. Stability diagram in ($a_z$,$q_z$) space for the quadrupole mass filter. The intersection of the RF/DC operating line with the apex of the stability diagram (point A) indicates the m/z of the ions that will follow stable trajectories and pass through the mass filter.

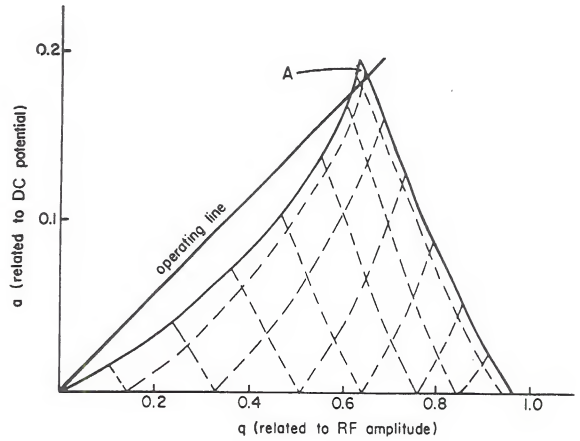
0.2
0.1
A
operating line
a (related to DC potential)
0.2
0.4
0.6
0.8
1.0
q (related to RF amplitude)

$$E_{EJ} = [1 - \frac{I_{P-1}}{I^{\circ}_{P-1}}] * 100\% \quad \textit{for } P\text{-}1 \tag{3-2}$$

and

$$E_{EJ} = [1 - \frac{I_{P+1}}{I^{\circ}_{P+1}}] * 100\% \quad \textit{for } P\text{+}1 \tag{3-3}$$

where the subscripts (P+1) and (P-1) correspond to the nearest m/z ion above and below the m/z of interest.

The phrase "unit resolution" has also been used to characterize the isolation of ions in the ion trap[18]. Several ambiguities arise from this convention. First, resolution is defined as the ratio m/$\Delta$m where m and m + $\Delta$m are the m/z values of two adjacent peaks in the mass spectrum. Because this definition requires the observation of two peaks of different m/z it cannot be used after one ion has been isolated. When a single m/z is isolated in the ion trap, resolution may be measured using a peak-width definition.[92] For the ion trap, the peak widths are a measure of the performance of the mass selective instability scan and provide little information about the isolation process. Additionally, resolution does not adequately describe the ion losses that must also be considered when comparing ion isolation techniques.

The isolation of one m/z and the mathematical terms used to characterize the isolation process are dependent on how close (in terms of m/z) and how intense adjacent ions are, and are thus dependent on the sample and matrix ions in the ion trap. For example, the isolation of one m/z is easily accomplished when the ion of interest and the nearest adjacent ions are separated by several m/z units. In this case, the ions above and below the m/z of the interest can be removed without

bringing the ion of interest near an instability limit; $E_{ISO}$ and $E_{EJ}$ would approach 100%. However, when the m/z of the adjacent ions are within 1 u of the ion of interest, the instability limit used to remove the adjacent ions can also influence the intensity of the ion of interest. Here, the $E_{ISO}$ and $E_{EJ}$ would be lower than in the previous examples. Additionally, the relative intensities of the ion of interest and the adjacent ions will also influence isolation. For these reason, comparisons of the $E_{ISO}$ and $E_{EJ}$ values for two isolation techniques must be performed using the same compounds and chemical background.

## Experimental

### Instrumentation

A Finnigan MAT ITMS was used for these studies. The instrument was equipped with the selective mass storage option that allows RF/DC operation modes to be implemented on the ITMS. The maximum magnitude of the DC potential that could be applied to the ring electrode was ± 700 V. The DC potential was measured at the base of the ITMS's RF coil using a digital multimeter (Fluke model# 75). The relationship between the software settings and the actual DC voltage is shown in Figure 3-2. The actual DC voltage is observed to be 93.0 % of the software set voltage; DC calibration slopes recorded over a 3 year period have remained constant within ± 0.06 %. The ITMS was controlled using a pre-release version of the ICMS© instrument control software.[97,116] A positive slew rate of 1.0 V/μs was measured for the selective mass storage using a oscilloscope (Tektronix model# 5440).

Batch inlet samples were introduced into the ITMS vacuum chamber via a fine metering valve (Granville Phillips) that was connected to a hollow sample insertion

Figure 3-2. Calibration curve for the DC output of the ITMS selective mass storage electronics relative to the software set voltage.

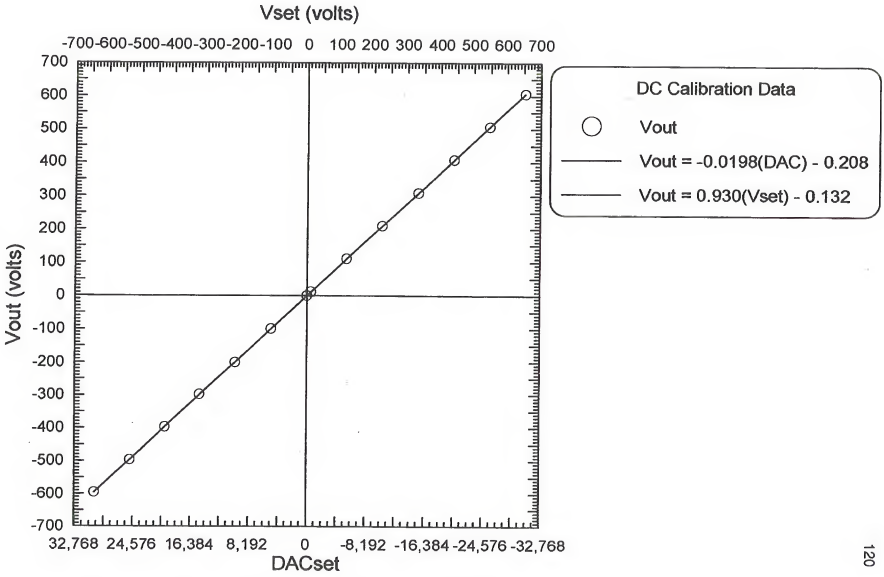
Vset (volts)
-700 -600 -500 -400 -300 -200 -100 0 100 200 300 400 500 600 700
Vout (volts)
700
600
500
400
300
200
100
0
-100
-200
-300
-400
-500
-600
-700
32,768 24,576 16,384 8,192 0 -8,192 -16,384 -24,576 -32,768
DACset
DC Calibration Data
Vout
Vout = -0.0198(DAC) - 0.208
Vout = 0.930(Vset) - 0.132

probe. GC samples were introduced into the internal volume of the ion trap with a heated transfer line probe that positioned the end of the GC column on the inside of the ion trap's rulon fitting. The ion trap was operated at a helium buffer gas pressure of 1 mtorr with the helium introduce directly into the ITMS vacuum chamber.

Apex Isolation Scan Program

Table 3-1 list the individual stages (scan tables) of an ion trap scan program that isolates 157* using apex isolation. Each μscan is initiated with a trigger table that maintains the RF and DC voltage at zero for a duration of 0.14 ms. This assures that all of the ions that remained in the ion trap from the previous μscan are removed. Next, the start and end m/z are set to 20, which corresponds to the RF voltage that is necessary to position m/z 20 at $q_z$=0.908 and $a_z$=0.0. At this voltage, all ions that have a m/z ≥ 20 are stored in the ion trap when the ion trap is operated in the "RF-only" mode. Scan table 3 creates EI ions by gating electrons that are formed by an extemal filament into the ion trap. Scan table 4 is a pause table. Pause tables are often inserted into a scan program to give the ions additional time to interact with the helium buffer gas so that their trajectories are damped towards the center of the ion trap. Ions traveling near outer edges of the ion trap have a greater chance of hitting an electrode and being lost. Scan tables 5 and 6 increase the RF voltage so that the low-mass-cut-off is 134.6 u. This RF level positions m/z 157 at a $q_z$ = 0.78 which is directly below the upper apex of the ion trap stability diagram. At this point, all ions that have a m/z ≥ 134.6 exhibit stable trajectories in the ion trap. Next, a DC potential of -173.5 V is applied to the ring electrode during scan table 8. This positions m/z 157 at a working point just below the upper apex of the stability diagram. Here, all ions other than 157*

Table 3-1. Summary of apex isolation scan program.

| # | Scan Table | Start m/z | End m/z | DC V | AC kHz | AC V | Time ms |
|---|---|---|---|---|---|---|---|
| 1 | Trigger | 0.0 | 0.0 | | | | 0.50 |
| 2 | Pause | 20.0 | 20.0 | | | | 0.20 |
| 3 | Ionize | 20.0 | 20.0 | | | | 5.00 |
| 4 | Pause | 20.0 | 20.0 | | | | 0.50 |
| 5 | RF Ramp #1 | 20.0 | 130.0 | | | | 1.00 |
| 6 | RF Ramp #2 | 130.0 | 134.6 | | | | 1.50 |
| 7 | Pause | 134.6 | 134.6 | | | | 1.00 |
| 8 | DC Pulse (A) | 134.6 | 134.6 | -173.5 | | | 1.00 |
| 9 | RF Ramp #3 | 134.6 | 20.0 | | | | 1.00 |
| 10 | Mult. On | 20.0 | 20.0 | | 530 | 6.0 | 2.00 |
| 11 | Acquire | 20.0 | 200.0 | | 530 | 6.0 | 33.12 |
| 12 | Empty Trap | 0.0 | 0.0 | | | | 1.00 |

fall outside the boundaries of the stability diagram and are ejected from the ion trap. At this point in the μscan, m/z 157 is isolated in the ion trap. Following isolation, the 157$^+$ ions can be scanned out (as shown in scan tables 9-12), or reacted or fragmented for MS/MS.

Figure 3-3 shows the Mathieu stability diagram for the quadrupole ion trap in (a,q) space. The upper RF and DC axes correspond to the RF amplitude and DC potential that are required to position m/z 157 at different working points in (a,q) space. The open circle and dashed lines show the path that the m/z 157 ion follows during the apex isolation scan program. The (a,q) coordinates for the apex of the stability diagram are indicated.

Figure 3-4 shows an ion trap scan program diagram for the scan program listed in Table 3-1. Note that the additional time required to isolate m/z 157 is minimal

Figure 3-3. Stability diagram in ($a_z$, $q_z$) space showing the inner region that corresponds to mathematically stable ion trajectories in the quadrupole ion trap. The dashed line indicates the path taken by m/z 157 during an apex isolation sequence. The RF and DC axes show the RF amplitude ($V_{p-p}$) and DC potential (V) applied to the ring electrode that correspond to the $a_z$ and $q_z$ coordinates for m/z 157. Point (a) marks the stability diagram apex used to simultaneously eject ions above and below m/z 157.

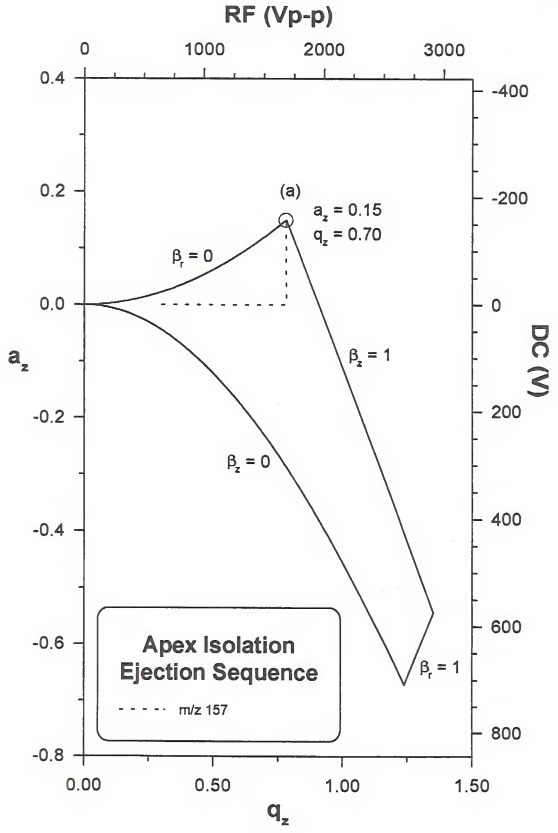
RF (Vp-p)
0
1000
2000
3000
0.4
0.2
0.0
-0.2
-0.4
-0.6
-0.8
-400
-200
0
200
400
600
800
DC (V)
$a_z$
$q_z$
0.00
0.50
1.00
1.50
(a)
$a_z$ = 0.15
$q_z$ = 0.70
$\beta_r$ = 0
$\beta_z$ = 1
$\beta_z$ = 0
$\beta_r$ = 1
Apex Isolation
Ejection Sequence
m/z 157

Figure 3-4. Ion trap scan program used to isolate m/z 157 at the apex of the stability diagram. Ions are generated during period I, m/z 157 is positioned at coordinates $a_z = 0$, $q_z = 0.78$ at point R, m/z 157 is isolated with a DC pulse applied during interval A, and the mass analysis scan is performed during stage S. The RF level (maximum of 650 m/z or 15,000 $V_{p-p}$) is directly related to the strength of the trapping field and determines the lowest m/z stored in the trap. A supplementary AC voltage frequency of 530 kHz on the ITMS is applied during period S to effect axial modulation (frequency not drawn to scale). The ion signal shown corresponds to the actual ion signal observed for m/z 157 of bromobenzene.

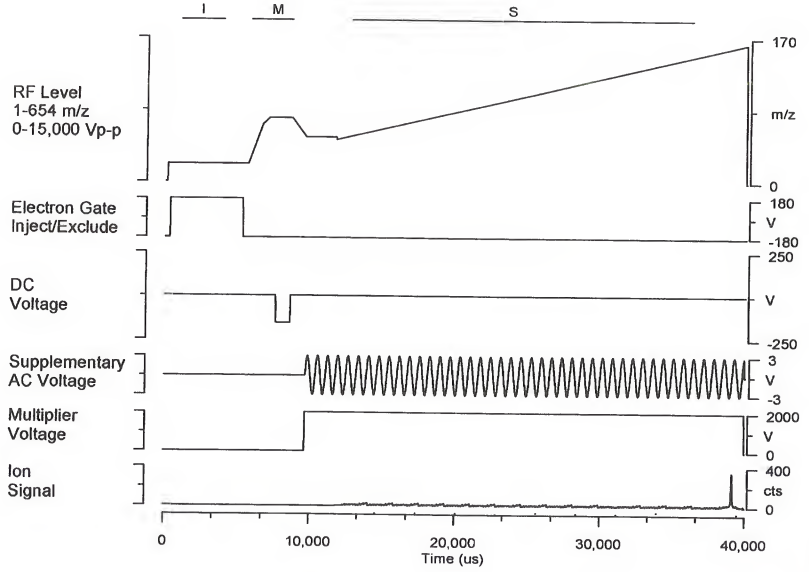
I
M
S
RF Level
1-654 m/z
0-15,000 Vp-p
170
m/z
0
Electron Gate
Inject/Exclude
180
V
-180
DC
Voltage
250
V
-250
Supplementary
AC Voltage
3
V
-3
Multiplier
Voltage
2000
V
0
Ion
Signal
400
cts
0
0
10,000
20,000
30,000
40,000
Time (us)

compared to that required for the mass analysis stage. Additionally, the scan program could be shortened considerably by obtaining a mass spectrum over a narrower mass range.

Manual adjustment of the RF and DC voltages is required if a single m/z is to be isolated. Initially, the start m/z and end m/z settings used in scan tables 6-9 are calculated to place the ion of interest at a $q_z = 0.78$. Next, the DC voltage is decreased from 0 V to -157 V for m/z 157. This corresponds to a working point that is well inside the upper apex of the ion trap stability diagram. At this point, the isolation window may be 5 - 30 m/z units wide depending on the low-mass-cut-off. Following this, the DC voltage is incremented in smaller steps and a mass spectrum is recorded between each adjustment to observe the change in the width of the isolated m/z window. As the width of the isolation window is reduced, the start and end m/z's in scan tables 6 - 9 are also adjusted so that the ion of interest remains in the center of the isolation window. The amount of manual adjustment that is needed depends on spacing and intensity of the nearest neighbor ions that are present in the full scan spectrum. To simplify this manual process, new software was developed that linked the RF and DC adjustments to the arrow keys on the data systems keyboard. Using the <up-arrow>, <down-arrow>, <left-arrow>, and <right-arrow> keys, the working point could be shifted to different positions inside the stability diagram apex until the best combination of RF and DC voltage for isolating a single m/z was found.

Two-step Isolation Scan Program

Because ions can be stored in the ion trap for extended periods, "RF/DC" isolation techniques are not restricted to the upper and lower apexes of the stability

diagram. Instead, multiple sets of (a,q) coordinates can be used to separately eject ions above and below the m/z of interest. Louris et al. suggested that the use of a combination of RF/DC ejection voltages with the addition of a supplementary AC field might offer the most practical approach towards improving the isolation of an ion in the ion trap.[20] Novel multi-step isolation techniques were demonstrated by Traldi et al.[117] and Yates et al..[51] Both techniques eliminate ions above and below the m/z of interest in separate steps, although the order of ejection was reversed for the two techniques.

Table 3-2 lists the scan tables for the two-step scan program employed by Yates et al.[51] to isolate m/z 157. Scan tables 1-4 are identical to the first four scan tables of the apex isolation scan previously described (see Table 3-1). Scan tables 5 and 6 increase the RF voltage so that the low-mass-cut-off is 122.0 u. This RF level positions m/z 157 at a $q_z$ = 0.70 on the ion trap stability diagram. At this point, all ions above m/z 122.0 exhibit stable trajectories in the ion trap. Scan table 7 is a pause table. Next, a DC potential of +249 V is applied to the ring electrode during scan table 8. This positions m/z 157 at a working point of $a_z$ = -0.23 and $q_z$ = 0.70 on stability diagram. Here, all ions that have a m/z greater than 157$^+$ fall outside the stability diagram and are ejected from the ion trap. Next, the DC voltage is returned to 0 V and the RF level is increased to position m/z 157 at $a_z$ = 0.00 and $q_z$ = 0.85 (scan tables 9,10). At this point in the μscan, a narrow m/z range from m/z 148 to m/z 157 has been isolated in the ion trap. Table 11 removes ions between m/z 148 and m/z 156 by applying a -59 V DC potential on the ring electrode. This positions m/z 157 at coordinates $a_z$ = 0.07 and $q_z$ = 0.85 on the Mathieu stability diagram. To increase the sharpness of the $\beta_z$ = 1 edge, a 530 kHz supplementary AC voltage with an amplitude of 6.0 $V_{p\text{-}p}$ is applied across the ion traps endcap electrodes. At this point, m/z 157 is

Table 3-2. Summary of two-step isolation scan program.

| # | Scan Table | Start m/z | End m/z | DC Volts | AC kHz | AC V | Time ms |
|---|---|---|---|---|---|---|---|
| 1 | Trigger | 0.0 | 0.0 | | | | 0.50 |
| 2 | Pause | 20.0 | 20.0 | | | | 0.20 |
| 3 | Ionize | 20.0 | 20.0 | | | | 5.00 |
| 4 | Pause | 20.0 | 20.0 | | | | 0.50 |
| 5 | RF Ramp #1 | 20.0 | 130.0 | | | | 1.00 |
| 6 | RF Ramp #2 | 130.0 | 150.0 | | | | 1.50 |
| 7 | Pause | 150.0 | 150.0 | | | | 1.00 |
| 8 | DC Pulse (H) | 150.0 | 150.0 | 174.6 | | | 0.50 |
| 9 | RF Ramp #3 | 150.0 | 155.0 | | | | 1.00 |
| 10 | Pause | 155.0 | 155.0 | | | | 0.50 |
| 11 | DC Pulse (L) | 155.0 | 155.0 | -11.8 | 530 | 6.0 | 0.05 |
| 12 | RF Ramp #4 | 155.0 | 20.0 | | | | 1.00 |
| 13 | Mult. On | 20.0 | 20.0 | | 530 | 6.0 | 2.00 |
| 14 | Acquire | 20.0 | 200.0 | | 530 | 6.0 | 33.12 |
| 15 | Empty Trap | 0.0 | 0.0 | | | | 1.00 |

isolated in the ion trap. Following isolation, the $157^+$ ion can be scanned out (as shown in scan tables 12-15), or used in a subsequent stage of mass spectrometry.

Figure 3-5 shows the path taken by m/z 157 in (a,q) space during the two-step isolation sequence detailed in Table 3-2. The upper RF and DC axes correspond to the RF amplitude and DC potential that are required to position m/z 157 at different working points in (a,q) space. The (a,q) coordinates used to eject ions from the trap are indicated.

Figure 3-6 shows the timing of an ion trap scan program that includes the two-step isolation method described in Table 3-2. Note that compared to apex isolation, more time is required to mass select an ion using the two-step isolation process.

Figure 3-5. Stability diagram in ($a_z$,$q_z$) space showing the inner region that corresponds to mathematically stable ion trajectories in the quadrupole ion trap. The dashed line (-------) indicates the path taken by m/z 157 during an two-step isolation sequence. The RF and DC axes show the RF amplitude ($V_{p-p}$) and DC potential (V) applied to the ring electrode that correspond to the $a_z$ and $q_z$ coordinates for m/z 157. Point (H) and (L) mark the working points used the eject ion of higher and lower m/z than the ion of interest. The dashed line (— — — —) locates the resonant ejection field created the supplementary AC voltage (530 kHz @ 6.0 $V_{p-p}$).

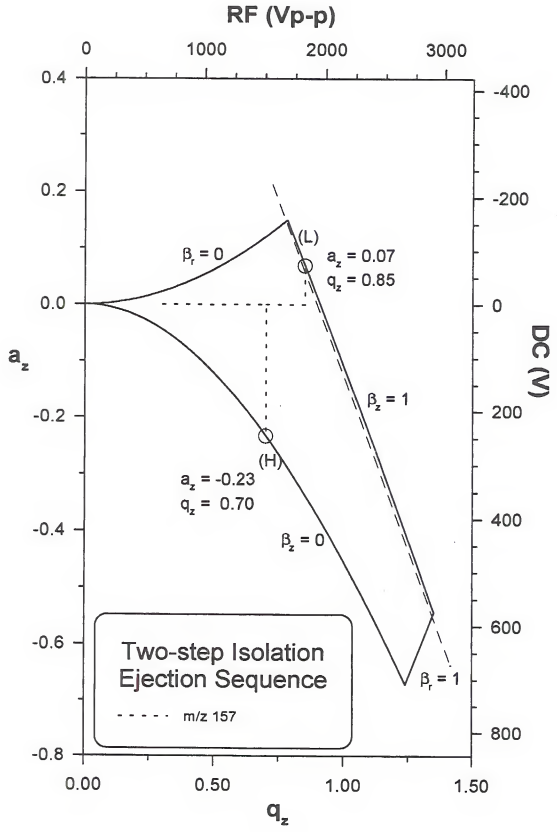
RF (Vp-p)
0
1000
2000
3000
0.4
0.2
0.0
-0.2
-0.4
-0.6
-0.8
$a_z$
-400
-200
0
200
400
600
800
DC (V)
$\beta_r = 0$
(L)
$a_z = 0.07$
$q_z = 0.85$
$\beta_z = 1$
(H)
$a_z = -0.23$
$q_z = 0.70$
$\beta_z = 0$
$\beta_r = 1$
Two-step Isolation
Ejection Sequence
m/z 157
0.00
0.50
1.00
1.50
$q_z$

Figure 3-6. Ion trap scan program used to isolate m/z 157 using a two-step isolation sequence. Ions are generated during period I, m/z 157 is positioned at coordinates $a_z = 0$, $q_z = 0.70$ at point R1, ions above m/z 157 are ejected with a DC pulse applied during interval H, m/z 157 is located at coordinates $a_z = 0$, $q_z = 0.70$ during interval R2, ions below m/z 157 are ejected with a DC pulse and supplementary AC voltage of 530 kHz (not drawn to scale) applied during interval L, and the mass analysis scan is performed during stage S.

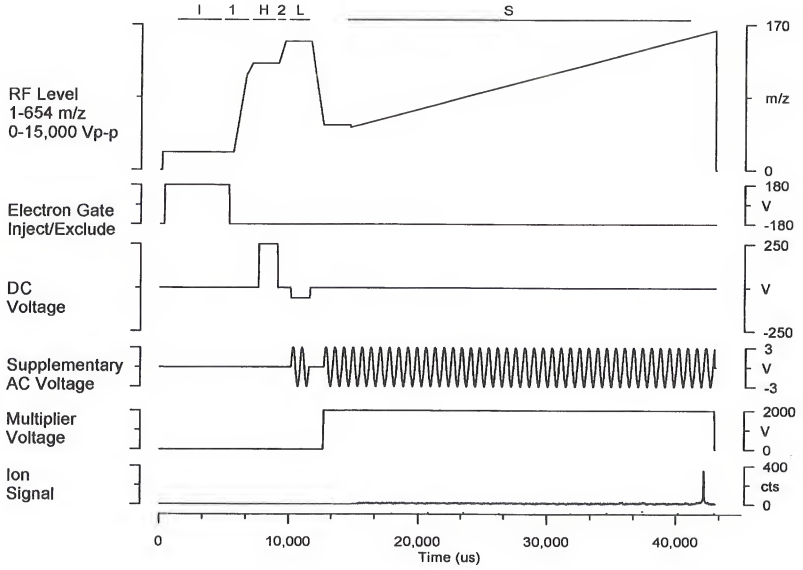
I
1
H
2
L
S
RF Level
1-654 m/z
0-15,000 Vp-p
170
m/z
0
Electron Gate
Inject/Exclude
180
V
-180
DC
Voltage
250
V
-250
Supplementary
AC Voltage
3
V
-3
Multiplier
Voltage
2000
V
0
Ion
Signal
400
cts
0
0
10,000
20,000
30,000
40,000
Time (us)

Additionally, the magnitude of the DC voltage that is required to eject the high m/z ions along the $\beta_z = 0$ edge at $q_z = 0.7$ is approximately 1.5 times greater than the voltage required for apex isolation.

The tuning procedure is slightly different for two-step isolation compared to apex isolation. Firstly, manual adjustment of the RF voltage is not required because two-step isolation does not need to be performed at a specific $q_z$. Secondly, because separate DC voltages are used to remove high and low m/z ions, the (a,q) value that ejects high m/z ions can be adjusted without compromising the ejection of the low m/z ions. Initially, the start and end m/z settings used in scan tables 6-9 are calculated to place the ion of interest at a $q_z = 0.70$. Next, the DC voltage used in table 8 is increased using large increments until the m/z of interest is ejected from the trap. Then the DC voltage is decreased until the ion of interest reappears in the mass spectrum. The DC voltage required to eject the low m/z ions is optimized in a similar fashion. Low mass ions can also be removed using the "RF-only" operation mode, but the 16-bit digital-to-analog converter (DAC) that controls the DC voltage affords finer adjustment than the RF voltage's 12-bit DAC.

$E_{ISO}$ and $E_{EJ}$ Measurements

To measure $E_{ISO}$ and $E_{EJ}$ a minimum of two spectra are required. A full-scan spectrum is used to determine the intensities of the ion of interest and the adjacent ions without isolation. Then an isolated mass spectrum is acquired to measure the intensity of the ion of interest and any adjacent ions that remain in the trap following mass isolation. Since the data from both spectra are to be related to one another, the

sample pressure and ionization parameters must remain constant over the course of the measurement.

Acquiring $E_{ISO}$ and $E_{EJ}$ Data as a Function of DC Voltage

An automated procedure was developed using the ITMS FORTH programming option to acquire a series of mass spectra for ions isolated at different $a_z$ (DC) values. The program uses two identical scan programs that include either an apex or two-step isolation sequence. The DC voltage used in the scan programs is reduce by ca. 7.0 V so that the intensity of the ion of interest and the adjacent ions was not affected by the DC pulses. Initially, the program acquires a single spectrum using the first scan program to measure the intensity of the ion of interest and the adjacent ions without isolation; this is termed a background spectrum. Next, the program switches to the second scan program, acquires 25 spectra, and increments the DC voltage used for isolation by 0.1 V. This acquisition process is repeated for 100 individual voltage steps, corresponding to a 10.0 V change in DC potential. A background scan is acquired between each DC increment to assure that the sample pressure and ion intensities remain constant during the course of the 30 minute measurement.

$E_{ISO}$ and $E_{EJ}$ Measurements at a Series of $q_z$ Values

Using the automated procedure described in the previous section, data were collected to measure the $E_{ISO}$ and $E_{EJ}$ for the ejection of ions of greater m/z than the ion of interest. For the stability diagram edge $\beta_z = 0$, $E_{ISO}$ and $E_{EJ}$ data were collected at $q_z = 0.2, 0.3, 0.4, 0.5, 0.6, 0.7$, and 0.8. For the $\beta_z = 0$ stability edge, $E_{ISO}$ and $E_{EJ}$ data were collected at $q_z = 0.2, 0.3, 0.4, 0.5, 0.6$, and 0.7. The EI fragment ion m/z 40

of 1-octene was selected as the ion of interest for this study, and the adjacent (P-1) and (P+1) ions were m/z 39 and m/z 41 respectively.

Storage Time Studies

The isolation of m/z 157 for ionized bromobenzene was used to determine the effect of several table times on the efficiency of isolation. For apex isolation, the duration of the pause (scan table 7) and DC pulse (scan table 8) were increased from the initial table time of 0.0 ms to 10.0 ms using a 0.1 ms increment. For two-step isolation, the duration of the pause (scan table 7) and both DC pulse (scan tables 8 and 11) were evaluated in a similar fashion. Background scans were collected to assure that the sample pressure remained constant during the course of the measurement.

Supplementary AC Voltage Studies

The effect of the 6.0 V supplementary AC voltage that is used to eject ions below the m/z of interest was investigated by measuring $E_{ISO}$ and $E_{EJ}$ for m/z 157 and m/z 156 respectively of ionized bromobenzene. The FORTH program that increments the DC voltage was used to increase the voltage of the DC pulse (scan table 11). This experiment was repeated with and without the addition of the supplementary AC voltage. Background scans were collected to assure that the sample pressure remained constant over the course of the measurement.

## Results and Discussion

Figure 3-7 shows (a) the full-scan mass spectrum of bromobenzene between m/z 20 and m/z 180, and (b) the isolated mass spectrum for m/z 157 of bromobenzene obtained with a two-step isolation scan program. The inset shows an expanded view of the molecular ion region in part (a) where m/z 156 corresponds to the $^{12}C$, $^{79}Br$ $M^{+\cdot}$ ion, m/z 157 corresponds to the $^{13}C$, $^{79}Br$ $M^{+\cdot}$ ion, m/z 158 corresponds to the $^{12}C$, $^{80}Br$ $M^{+\cdot}$ ion, and m/z 159 corresponds to the $^{13}C$, $^{80}Br$ $M^{+\cdot}$ ion. Note that space charge caused by m/z 158 broadens the peak shape of m/z 156 and distorts the relative peak heights from those predicted by natural isotopic abundances of Br. An $E_{ISO}$ for m/z 157 and $E_{EJ}$ for m/z 158 of approximately 45% and 95% (± 5%) were measured for spectra shown in this example.

Figure 3-8 shows (a) the full-scan mass spectrum of 1-octene between m/z 20 and m/z 120, and (b) the isolated mass spectrum for m/z 40 of 1-octene obtained with a two-step isolation scan program. An $E_{ISO}$ for m/z 40 and $E_{EJ}$ for m/z 41 of approximately 85% and 90% (± 5%) were measured for spectra shown in this example. The presence of m/z 39 in the isolated mass spectrum demonstrates that the efficiency of ejection for ions above the m/z of interest does not determine efficiency of ejection for ions below the m/z of interest. Thus, the $E_{EJ}$ must be evaluated for both the (P+1) and (P-1) ions when apex isolation or two-step isolation are used.

### $E_{EJ}$ and $E_{ISO}$ for Apex and Two-step Isolation

Figure 3-9 shows the $E_{ISO}$ vs. $E_{EJ}$ curves for the *apex* isolation of m/z 157 of bromobenzene. This figure compares the efficiency of isolation ($E_{ISO}$) for m/z 157 against (a) the efficiency of ejection ($E_{EJ}$) for m/z 158, and (b) the efficiency of ejection

Figure 3-7. Two-step isolation of bromobenzene. Profile mass spectra showing (a) the full scan EI mass spectrum for bromobenzene (MW = 156) and (b) the two-step isolation spectrum for m/z 157 of bromobenzene. The inset shows the molecular ion region including the bromine isotope peaks $156^+$ and $158^+$, and carbon isotope peaks $157^+$ and $159^+$. The isolation efficiency for m/z $157^+$ is ca. 45%.

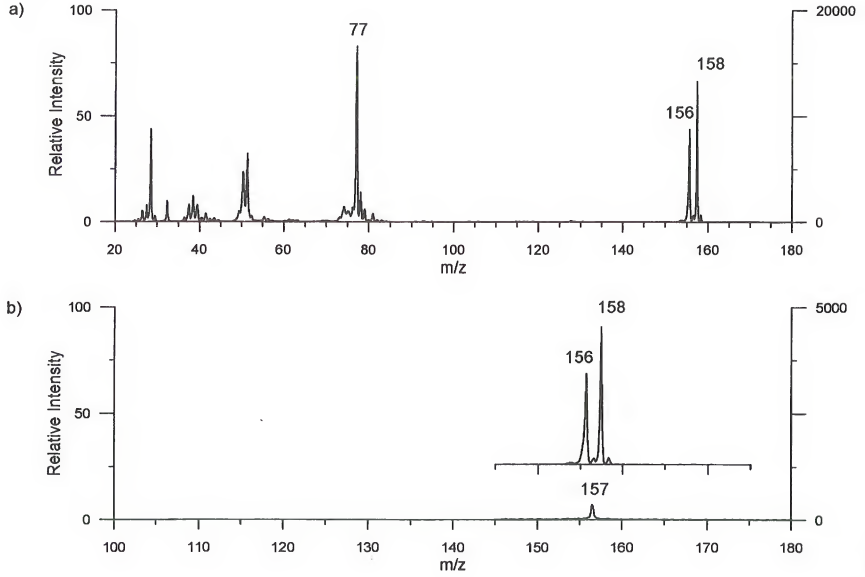
a)
100
50
0
Relative Intensity
77
158
156
20000
0
20
40
60
80
100
120
140
160
180
m/z
b)
100
50
0
Relative Intensity
158
156
157
5000
0
100
110
120
130
140
150
160
170
180
m/z

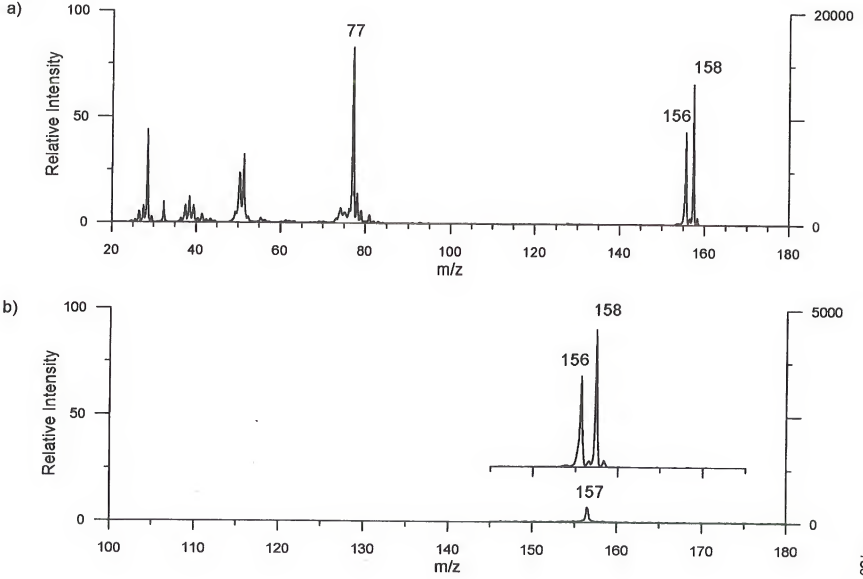
a)
Relative Intensity
100
50
0
77
158
156
20000
0
20
40
60
80
100
120
140
160
180
m/z
b)
Relative Intensity
100
50
0
158
156
157
5000
0
100
110
120
130
140
150
160
170
180
m/z

Figure 3-8. Two-step isolation of 1-octene. Profile mass spectra showing (a) the full-scan mass spectrum that contains the ions of 1-octene between m/z 20 and m/z 120, and (b) the isolated mass spectrum for m/z 40 of 1-octene obtained with a two-step isolation scan program.

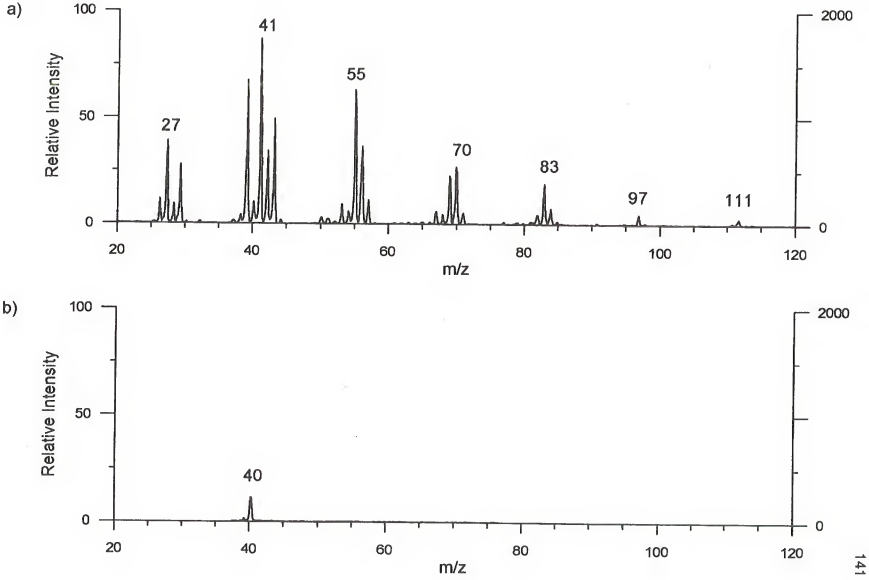
a)
Relative Intensity
100
50
0
2000
0
41
55
27
70
83
97
111
20
40
60
80
100
120
m/z
b)
Relative Intensity
100
50
0
2000
0
40
20
40
60
80
100
120
m/z

Figure 3-9. Relationship between $E_{ISO}$ vs. $E_{EJ}$ for the isolation of m/z 157 of bromobenzene at the apex of the stability diagram. The plots show the efficiency of isolation ($E_{ISO}$) for m/z 157 versus (a) the efficiency of ejection ($E_{EJ}$) for m/z 158, and (b) the efficiency of ejection ($E_{EJ}$) for m/z 156. Each data point (∘) corresponds to the average of 25 isolation spectra that are referenced to a corresponding background spectrum.

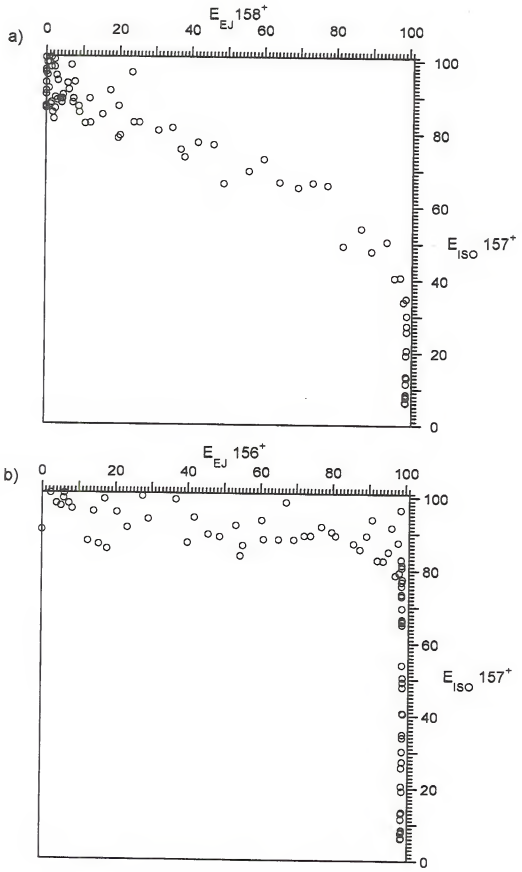
a)
$E_{EJ}$ $156^+$
0
20
40
60
80
100
$E_{ISO}$ $157^+$
b)
$E_{EJ}$ $156^+$
$E_{ISO}$ $157^+$

($E_{EJ}$) for m/z 156. The data for this figure were collected at a series of DC voltages that cause m/z 157 to successively approach the apex to the stability diagram. It is important to point out that each data point (•) represents 25 isolation spectra referenced to a corresponding background spectrum. Also, 25 μscans were averaged to improve the S/N of each acquired spectrum. The data points that lie outside the borders of the axis were not plotted. Attempts to obtain similar data using fewer spectra and less sophisticated background scan measurements resulted in increased deviations from the curve shown in Figure 3-9. Because the $E_{ISO}$ and $E_{EJ}$ measurements ratio small and large ion signals, the combined error can be great. However, with sufficient signal averaging a clear trend between the $E_{ISO}$ and $E_{EJ}$ is observed.

Figure 3-9 (a) shows that as the $E_{EJ}$ for m/z 158 approaches 100 %, the $E_{ISO}$ for m/z 157 drops to 40 %. Thus, to eliminate all of the $158^+$ ions from the ion trap using apex isolation 60 % of the $157^+$ ions would also be lost. Interestingly, Figure 3-9 (b) shows that as the $E_{EJ}$ for m/z 156 approaches 100 %, the $E_{ISO}$ for m/z 157 remains between 80 % - 90 %. This confirms the experimental observation made by Louris et al.[20] that the ejection of ions below the m/z of interest is more efficient than ejection of higher m/z ions at the apex of the stability diagram.

Figure 3-10 shows the $E_{ISO}$ vs. $E_{EJ}$ curves for *two-step* isolation of m/z 157 of bromobenzene. This figure relates the efficiency of isolation ($E_{ISO}$) for m/z 157 to (a) the efficiency of ejection ($E_{EJ}$) for m/z 158, and (b) the efficiency of ejection ($E_{EJ}$) for m/z 156. As $E_{EJ}$ for m/z 158 approaches 100 %, $E_{ISO}$ for m/z 157 is observed to approach 90 %. Thus, the intensity of $157^+$ that remains in the ion trap after m/z 158 has been ejected is two times greater than the intensity that remains following apex

Figure 3-10. $E_{ISO}$ versus the $E_{EJ}$ for (a) m/z 158, and (b) m/z 156 for two-step isolation of m/z 157 of bromobenzene. The plots show the efficiency of isolation ($E_{ISO}$) for m/z 157 versus (a) the efficiency of ejection ($E_{EJ}$) for m/z 158, and (b) the efficiency of ejection ($E_{EJ}$) for m/z 156. Each data point (•) corresponds to the average of 25 isolation spectra that are referenced to a corresponding background spectrum.

a)

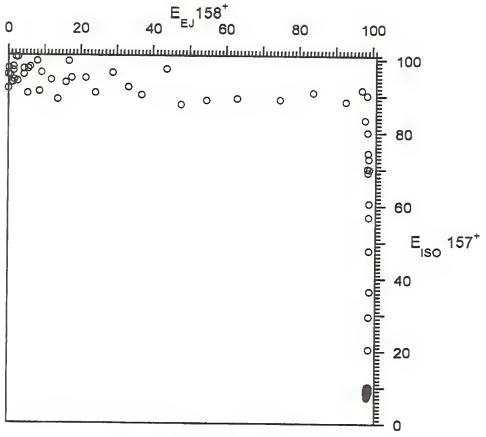
E EJ 158+
0
20
40
60
80
100
E ISO 157+

b)

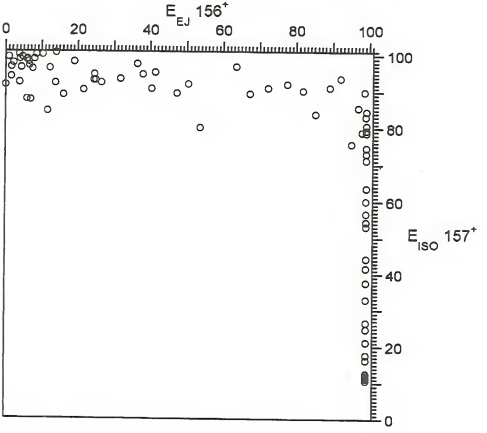
E EJ 156+
0
20
40
60
80
100
E ISO 157+

isolation. Figure 3-10 (b) shows that as the $E_{EJ}$ for m/z 156 approaches 100 %, $E_{ISO}$ for m/z 157 is observed to approach 90 %. Thus, the difference between the $E_{EJ}$ for m/z 156 is negligible for apex and two-step isolation techniques. The similar efficiencies observed for the ejection of m/z 156 for both isolation techniques is not surprising since both methods utilize the $\beta_z = 1$ edge of the stability diagram to eject ions below the m/z of interest.

Figure 3-11 compares the $E_{ISO}$ vs. $E_{EJ}$ curves for isolation of m/z 40 and the ejection of m/z 41 using (a) apex and (b) two-step isolation. For apex isolation, approximately 30 % of m/z 40 remains in the ion trap as the $E_{EJ}$ for m/z 41 approaches 100 %. Two-step isolation traps nearly 60 % of the $157^+$ ions when all of the m/z 158 ions are ejected. The corresponding curves for the ejection of m/z 39 (not shown) exhibit similar efficiencies (≥ 90 %) to the curves observed for the isolation of m/z 157 of bromobenzene (see Figure 3-9b and 3-10b). Thus, two-step isolation is observed to be nearly twice as efficient as apex isolation for the selection of m/z 40 of 1-octene.

Two-step Isolation and the Sharpness of the Stability Diagram Edges

The stability diagram edges $\beta_z = 1$ and $\beta_r = 1$ cause ions of below a specific m/z to be ejected from the ion trap in the axial and radial directions, respectively. The $\beta_z = 0$ and $\beta_r = 0$ stability diagram edges cause ions above a specific m/z to be ejected towards the ion trap's endcap and ring electrode, respectively. However, the stability diagram does not predict the edges that have the sharpest stability/instability transition.

The $\beta_z$=1 stability edge has been shown to exhibit a sharp low-mass-cut-off (refer to Figure 3-9b and 3-10b). This is a fortunate result since the $\beta_z = 1$ edge is used to obtain a mass spectrum in the mass selective instability mode. Similarly, the

Figure 3-11. $E_{iso}$ versus $E_{Ej}$ curves for the isolation of m/z 40 and the ejection of m/z 41 for 1-octene. Acquired using (a) apex and (b) two-step isolation. Each data point (∘) corresponds to the average of 25 isolation spectra that are referenced to a corresponding background spectrum.

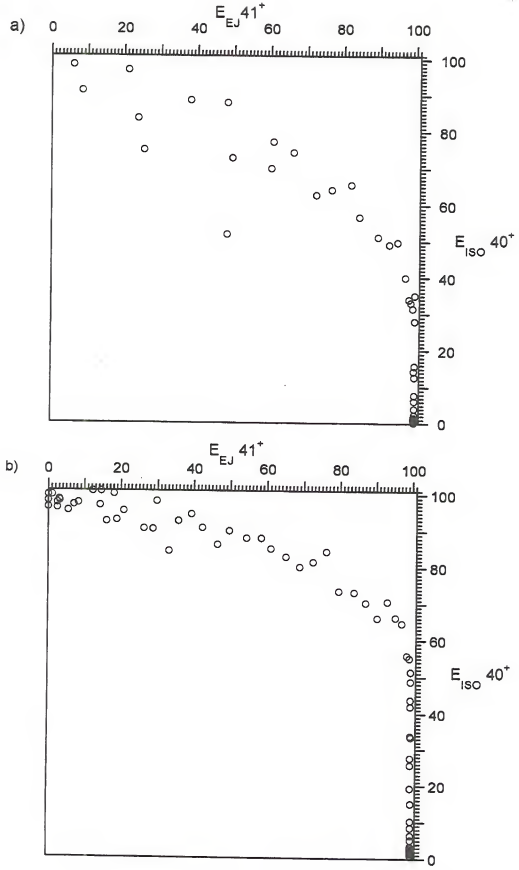
a)
$E_{EJ}$ $41^+$
0
20
40
60
80
100
$E_{iso}$ $40^+$
b)
$E_{EJ}$ $41^+$
$E_{iso}$ $40^+$

sharpness of stability/instability transition can be determine by measuring the efficiency of isolation ($E_{ISO}$) and efficiency of ejection ($E_{EJ}$) at several points along the $\beta_z = 0$ and $\beta_r = 0$ stability diagram edges.

Figure 3-12 compares the $E_{ISO}$ for m/z 40 of 1-octene at a constant $E_{EJ}$ for m/z 41 at a series of $q_z$ values along the $\beta_z = 0$ and $\beta_r = 0$ stability edges. In each case the efficiency of isolation of the $\beta_z = 0$ edge was observed to be greater than that of the $\beta_r = 0$ edge. This corresponds to the $\beta_z = 0$ edge having a sharper high-mass-cut-off than the $\beta_r = 0$ stability edge.

Figure 3-12 also shows that the efficiency of isolation for m/z 40 along the $\beta_z = 0$ and $\beta_r = 0$ stability edge increases with increasing $q_z$ values until a maximum of 66 % is reached at $q_z = 0.7$. It is important to remember that an increase in the efficiency of isolation simply means that the ion of interest is stored more efficiently at particular point in (a,q) than the adjacent ion is.

A simple model helps to explain why certain points along the edge of the stability diagram exhibit "sharper" stability/instability transitions. Figure 3-13 shows the outline of two stability diagrams for m/z 100 and m/z 120 plotted in "RF/DC" space. The relative separation between the stability diagram for m/z 100 and m/z 120 is proportional to the separation between two stability diagrams for ions 1 m/z apart. However, the magnitude of the separation for two stability diagrams 1 u apart is too small to observe on this scale.

Consider working point A on Figure 3-13 that corresponds to an RF amplitude and DC potential of approximately 300 $V_{p-p}$ and 10 V, respectively. At this point, the outlines of the stability diagrams for m/z 100 and m/z 120 closely parallel one another. Because the separation (voltage difference) is small between these two

Figure 3-12. $E_{iso}$ for m/z 40 of 1-octene at various points along the $\beta_z = 0$ and $\beta_r = 0$ stability diagram edge. $E_{iso}$ values were measured at $E_{e,j}$ of 95% for m/z 41.

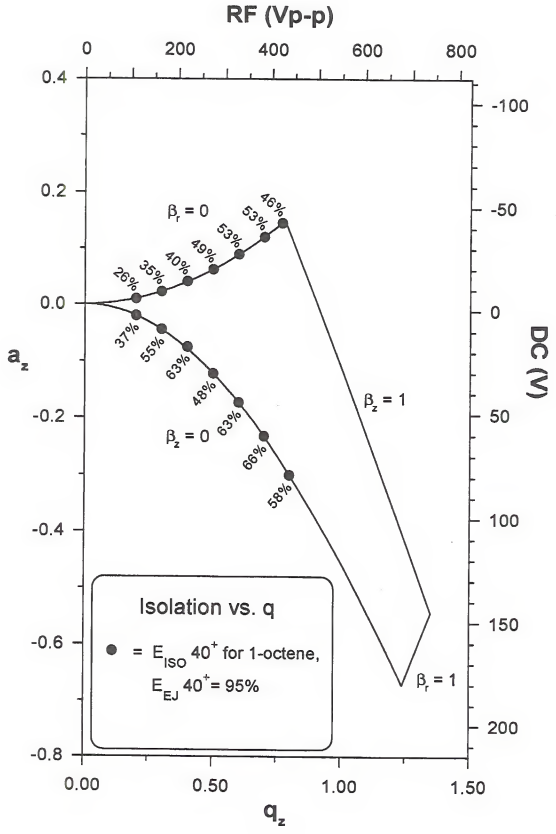
RF (Vp-p)
0
200
400
600
800
0.4
0.2
0.0
-0.2
-0.4
-0.6
-0.8
-100
-50
0
50
100
150
200
DC (V)
$a_z$
$q_z$
0.00
0.50
1.00
1.50
$\beta_r = 0$
$\beta_z = 1$
$\beta_z = 0$
$\beta_r = 1$
26%
35%
40%
49%
53%
53%
46%
37%
55%
63%
48%
63%
66%
58%
Isolation vs. q
● = $E_{ISO}$ $40^+$ for 1-octene,
$E_{EJ}$ $40^+$ = 95%

Figure 3-13. Stability diagrams in (RF, DC) space showing the inner region that corresponds to mathematically stable ion trajectories for m/z 100 and m/z 120 in the quadrupole ion trap.

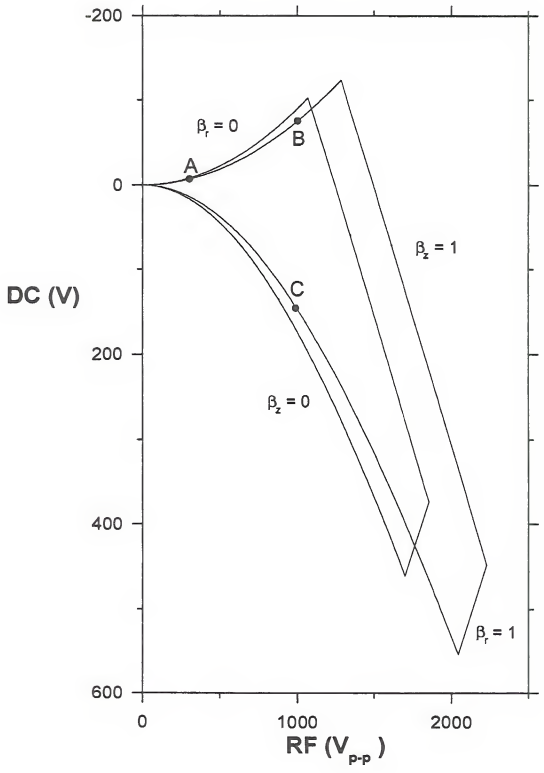
-200
0
200
400
600
DC (V)
0
1000
2000
RF ($V_{p-p}$)
$\beta_r = 0$
$\beta_z = 1$
$\beta_z = 0$
$\beta_r = 1$
A
B
C

stability/instability limits, ions of m/z 100 and m/z 120 would both exhibit partial or total ejection at this working point.

Compare working point A to working point B which corresponds to an RF amplitude and DC potential of 1000 $V_{p-p}$ and -70 V respectively. At point B, ions of m/z 120 are located outside of their stability diagram while ions of m/z 120 are located within their stability diagram. Thus, ions of m/z 120 would be ejected while ions of m/z 100 would follow stable trajectories and are stored in the ion trap. However, because m/z 100 is also close to its stability diagram edge, some ions of m/z 100 may be lost.

Now consider working point C on Figure 3-13 that corresponds to an RF amplitude and DC potential of 1000 $V_{p-p}$ and 150 V. At this point, ions of m/z 100 are also stable while ions of m/z 120 are unstable. However, the separation (voltage difference) between ion of m/z 100 and the m/z 100 stability diagram edge is greater than the separation observed at point B. Because m/z 100 is further away from its stability diagram edge, the possibility for ion losses are reduced. Thus, the use of working points that are located on stability edges that exhibit a large separation (voltage difference) between ions of adjacent m/z should also exhibit "sharp" stability/instability transitions and should produce higher $E_{iso}$ and $E_{EJ}$ values.

It is important to remember that separating m/z 100 from m/z 120 can be performed at almost any point along the outline of the stability diagram. However, smaller separations (voltage differences) are observed for stability diagrams for m/z 156 and m/z 157. Another important observation is that the $\beta_z = 1$ edge exhibits the larger separation of all the stability edges. Thus, the $\beta_z = 1$ stability edge should have the sharpest stability/instability transition. Experimentally, the $\beta_z = 1$ stability edge does exhibit the sharpest cut off with and without the use of axial modulation, which

also makes it a good edge for obtaining a mass spectrum with the mass selective instability scan.

Storage Time Studies

Figure 3-14 shows the ion intensity data for the two-step isolation of m/z 157 of bromobenzene as a function of the DC pulse time applied during scan tables 8 and 11. Initially, the intensity of the adjacent ions m/z 156 and m/z 158 are greater than the intensity of the ion of interest. The inefficient removal of adjacent ions is expected when short DC pulses (< 500 μs) are used because the slow rise time of the DC electronics prevents the DC voltage from reaching the level required for isolation. Once the duration of the DC pulse is increased to 1 ms the effect of the DC rise time is not observed and m/z 157 is the only ion left in the ion trap. Further increasing the DC pulse time to 10.0 ms results in a gradual loss in ion signal for m/z 157. Increased ion losses are expected for extended DC pulse times because the DC pulse positions the ion of interest near its instability limit. For a DC pulse time of 10 ms, the ion signal for the mass isolate $157^+$ ion decreases by 50 %. In practice, the DC pulse time is adjusted to assure that the DC supply has adequate time to reach the voltage selected. Longer DC pulse times result in decreased $E_{ISO}$ without a significant increase in $E_{EJ}$.

Similar ion losses are also observed with increased DC pulse times for apex isolation. Figure 3-15 shows the ion intensity data for the isolation of m/z 157 of bromobenzene as a function of DC pulse time. Here, the signal for m/z 157 decreases by approximately 80 % for a DC pulse time of 10 ms. This indicates that the ion losses at the apex of the stability diagram are greater than the ion losses observed

Figure 3-14. Relationship between ion intensities of $156^+$, $157^+$, $158^+$ for ionized bromobenzene and the DC pulse time applied during scan tables 8 and 11 for two-step isolation of m/z 157.

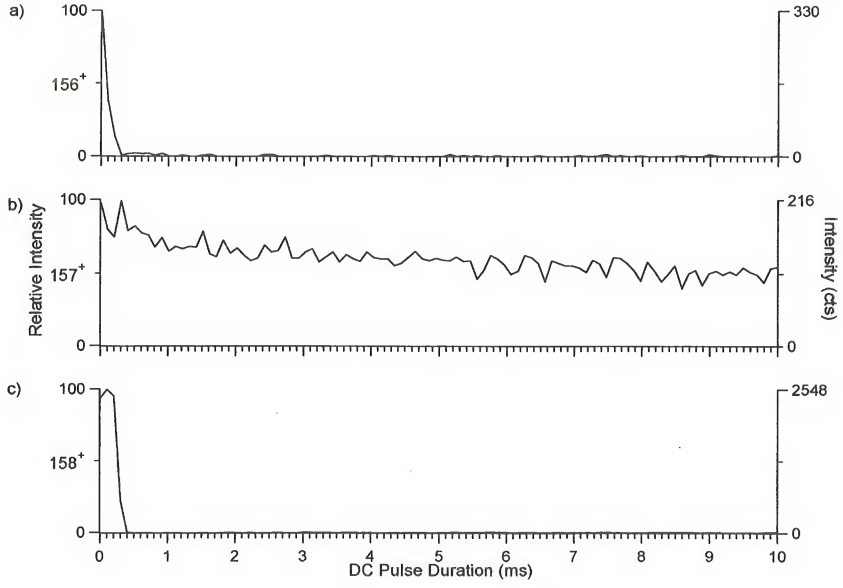
a)
100
330
156+
0
0
b)
100
216
157+
0
0
Relative Intensity
Intensity (cts)
c)
100
2548
158+
0
0
0
1
2
3
4
5
6
7
8
9
10
DC Pulse Duration (ms)

Figure 3-15. Relationship between ion intensities of $156^{+}$, $157^{+}$, $158^{+}$ for ionized bromobenzene and the DC pulse time applied during scan table 8 for apex isolation of m/z 157.

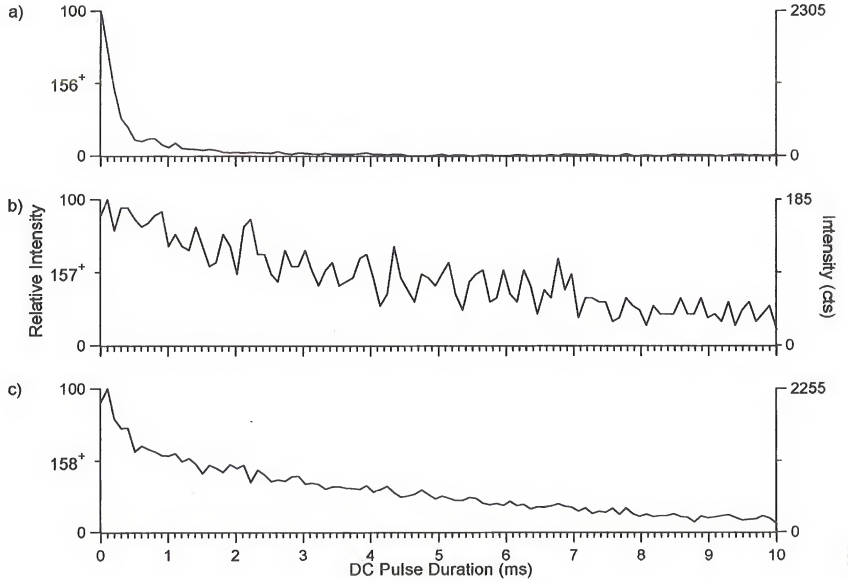
a)
100
2305
156+
0
0
b)
100
185
Relative Intensity
157+
Intensity (cts)
0
0
c)
100
2255
158+
0
0
0
1
2
3
4
5
6
7
8
9
10
DC Pulse Duration (ms)

along the $\beta_z$ = 0 stability edge (see Figure 3-14). Interestingly, rapid ejection of m/z 156 shows that the $\beta_z$ = 1 line (right edge) is "sharper" than the $\beta_z$ = 0 line (left edge) used for the ejection of m/z 158.

The durations of the RF ramp and pause tables that precede the DC pulse tables in the apex and two-step scan program sequences were also investigated to determine if they influenced the efficiency of isolation or ejection. In each case, the intensities of the ion of interest and the adjacent ions remained constant regardless of the duration of the preceding scan tables. Several researchers[93] have suggested that the addition of a pause table following the application of a DC pulse can improve the storage efficiency of the isolated ion; however, pause tables following the DC pulse were not investigated in this study.

A surprising result was observed when m/z 157 was isolated using the two-step isolation process immediately after the power for the RF and DC electronics had been turned on. As the electronics warmed up, the intensity of m/z 157 decreased from 36% of the base peak to less than 1 % of the base peak over a 25 minute period. Figure 3-16 shows the ion intensities for m/z 156, m/z 157, and m/z 158 of bromobenzene. Examination of the full-scan EI data confirmed that the sample pressure had not changed over the course of this experiment. Instead, the loss in ion intensity was observed as the ITMS electronics warmed up. By leaving the ITMS electronics on and replacing the instrument's cover which controls the flow of air over the electronics, m/z 157 could be isolated with constant efficiency over a time frame of several days. These observation indicates that improvements in the stability of the RF and DC electronics can affect ion isolation in the quadrupole ion trap.

Figure 3-16. Relationship between the two-step isolated ion intensity (m/z 157) and time observed after the power for the ITMS electronics had been turned on.

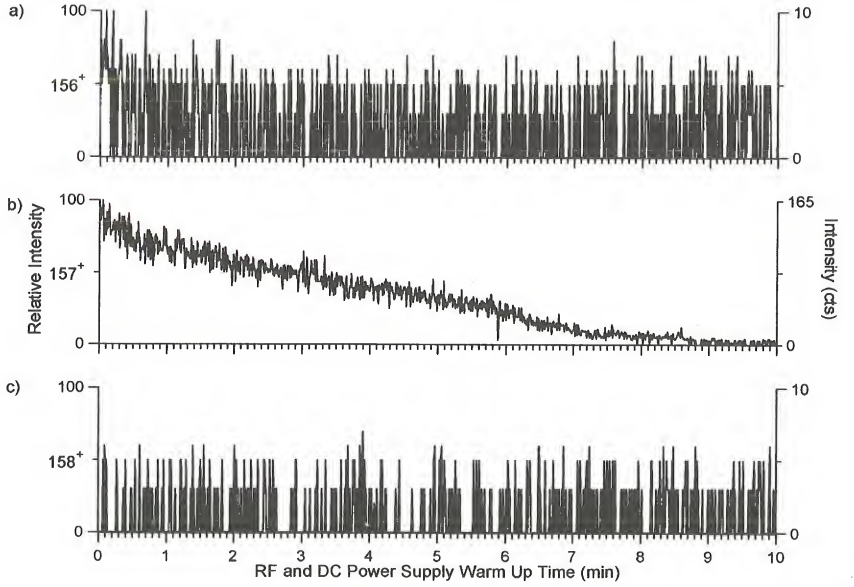
a)
100
156+
0
10
0
b)
100
157+
0
165
0
Relative Intensity
Intensity (cts)
c)
100
158+
0
10
0
0
1
2
3
4
5
6
7
8
9
10
RF and DC Power Supply Warm Up Time (min)

Effect of the Supplementary AC Voltage Applied During Isolation

Figure 3-17 shows the $E_{iso}$ vs. $E_{EJ}$ curves for two-step isolation of m/z 40 of ionized 1-octene. This figure compares the efficiency of isolation ($E_{iso}$) for m/z 40 with the efficiency of ejection ($E_{EJ}$) for m/z 39 (a) with, and (b) without the application of the supplementary AC voltage along the $\beta_z = 1$ stability diagram edge. Although both curves are similar, the $E_{iso}$ values obtained with the supplementary AC voltage are greater than those measured without it. Although this increase is minimal, the application of the supplementary AC voltage appears to improve the performance of two-step isolation when high levels of space charge are present in the ion trap.

Practical Considerations for Apex and Two-step Isolation

A benefit of two-step isolation that may not be recognized until it is used first hand is that less tuning is required to isolate the ion of interest. The first reason that two-step isolation scan programs are more easily tuned is due to the increased isolation efficiency observed for two-step isolation relative to apex isolation. This becomes clear when you consider that to obtain an $E_{iso}$ of 50% and an $E_{EJ}$ of 90 % with apex isolation, the RF and DC voltages must be set to the optimum values. Since two-step isolation affords higher isolation efficiencies, the adjustment of the RF and DC voltages is not as critical if an $E_{EJ}$ of only 50 % is desired. Secondly, two-step isolation scan programs are easier to tune because the DC voltage is the only parameter that needs to be adjusted. If the intensity of the ion of interest decreases after an adjustment of the DC voltage has been made, then the DC voltage adjustment was too large. For apex isolation, a loss in intensity of the ion of interest could indicate that the

Figure 3-17. Isolation efficiency as a function of resonant excitation. $E_{iso}$ for m/z 40 vs. $E_{EJ}$ for m/z 39 obtained (a) with, and (b) without the use of the supplementary AC voltage at 530 kHz @ 6 $V_{p-p}$. Each data point (∘) corresponds to the average of 25 isolation spectra that are referenced to a corresponding background spectrum.

a)

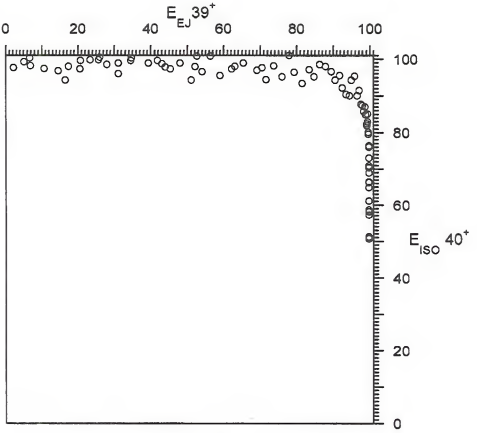
E_EJ 39+
0
20
40
60
80
100
E_iso 40+
0
20
40
60
80
100

b)

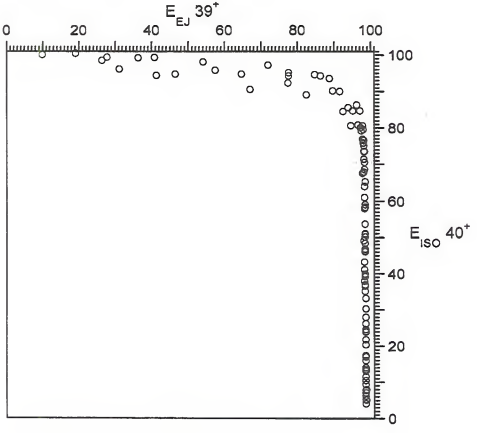
E_EJ 39+
0
20
40
60
80
100
E_iso 40+
0
20
40
60
80
100

DC voltage is too high or that the RF voltage is misadjusted so that the ion of interest is not aligned in the center of the stability diagram apex.

A consequence of using the $\beta_z = 0$ stability edge to remove ions above the m/z of interest is that larger DC voltages are required to reach the coordinates ($a_z = -0.23$, $q_z = 0.7$). Since the maximum voltage setting for the ITMS DC electronics is 700 V, the maximum m/z that can be isolated at this working point is ca. m/z 440. Increasing the output of the DC electronics to access higher voltages may not be a practical solution to this limitation because the higher voltages may cause arcing between the ion trap's electrodes. Instead, using a working point at a lower $q_z$ reduces the DC voltage required to eject ions above the m/z of the ion of interest.

Several reports have suggested that space charge causes shifts in the boundaries of the stability diagram.[80,81] Such shifts would certainly affect isolation procedures that use the stability diagram edges to eject ions from the ion trap. However, in these studies, the presence of shifts in the stability diagram have not been observed. Additionally, bringing an ion near a stability edge reduces space charge by ejecting ions above or below the m/z of interest. Thus, gross space charge effects are rarely observed when a single m/z is isolated in the ion trap.

## Summary

The results presented in this chapter characterize two RF/DC methods that have been developed for isolating ions of a single m/z in the quadrupole ion trap. Apex isolation and two-step isolation are powerful tools that can be used for tandem mass spectrometry experiments, as well as for ion-molecule reaction studies. The key benefit of the novel two-step isolation process is that one m/z can be isolated in the

ion trap with twice the efficiency of apex isolation. New figures of merit, $E_{EJ}$ and $E_{ISO}$, are described that can be used to gauge the performance of different types of isolation methods. Additionally, an empirical model is used to explain why certain stability edges exhibit "sharper" stability/instability transitions making them better for isolation. A final advantage of two-step isolation is that it is easier to set up and requires less manual tuning. This is one reason why two-step isolation is becoming the RF/DC isolation method of choice for the quadrupole ion trap.

# CHAPTER 4
# ION EXCITATION

## Introduction

The fourth chapter of this dissertation describes three methods of operating the ion trap mass spectrometer (ITMS) that eliminate the adjustment of the resonant excitation frequency required to effect collision-induced dissociation (CID). The first technique applies two rapid (50 ms) frequency pre-scans from which the frequency for ion excitation is determined. Deviations of less than 0.1% are observed between frequencies assigned by this method and manual procedures. The second ion activation technique, frequency modulated broadband excitation, excites a narrow range of frequencies to compensate for shifts in an ion's secular frequency of motion. Frequency modulated broadband excitation is shown to be an effective excitation method for GC/MS/MS with good correlation observed between product ion spectra obtained at the base and top of a GC peak. Stored waveform inverse Fourier transform (SWIFT) broadband excitation is the third ion activation method described in this chapter. SWIFT broadband excitation employs complex waveforms that contain a spectrum of frequencies to excite the parent ion of interest in MS/MS experiments. SWIFT broadband excitation is implemented with a commercial arbitrary waveform generator interfaced to a personal computer that is used to calculate and download the digital waveforms.

Tandem mass spectrometry (MS/MS) on the quadrupole ion trap mass spectrometer (ITMS) was first demonstrated by Louris et al.[31] and is described in detail in chapter 2. Of particular importance to the work described in this chapter is the method by which parent ions of a single m/z are excited in order to effect collision-induced dissociation (CID). Ions stored within the ion trap have characteristic orbital frequencies that are determined by the trapping field of the quadrupole analyzer.[2] Typically, excitation is carried out by applying a supplementary AC voltage across the end caps of the analyzer at a frequency resonant with the oscillations of the ion of interest in the axial direction. The amplitude of the orbital motion, and thereby the kinetic energy of the ion, increases as AC power is absorbed; CID results from energetic collisions between the ions and the helium buffer gas.

Ion trajectories have been simulated using the Mathieu theory [118-120], but the corresponding resonant excitation frequencies can only be approximated. Experimental frequencies differ from these solutions due to the influence of additional electric fields imposed by other ions in the trap.[85] The number and m/z of all the ions in the trap affect the actual frequency of ion motion. In practice, the calculated frequencies often differ significantly (up to 5 kHz) from those frequencies required to effect resonant excitation for CID. Thus, trial and error procedures are typically used to determine the best resonant frequency. This procedure can take as long as fifteen minutes to perform, during which time constant sample conditions are required. Automated procedures that follow similar trial and error approaches have reduced the time required to find the optimum resonant excitation frequency to a few minutes.[86] These approaches decrease the time required to set up procedures for performing MS/MS in the ion trap, but are limited to continuous sample introduction methods.

For gas chromatography/tandem mass spectrometry (GC/MS/MS), frequency assignment must be performed on the millisecond time scale. As the ion population within the ion trap changes over the chromatographic peak, the optimum resonant excitation frequency shifts. The frequency shifts that occur as the number of ions in the trap change is characterized in this chapter. In addition, three ion activation methods are described that promote CID regardless of these frequency shifts.

Frequency-Assignment Pre-Scan

The frequency-assignment pre-scan corrects for frequency shifts by rapidly measuring the secular frequency of motion of the ion of interest at the beginning of each μscan and adjusting the frequency of the supplementary AC voltage accordingly. Indirect measurements are used to determine an ion's secular frequency of motion. The most common method of measurement is to use the supplementary AC voltage to excite ions of a specific m/z in the axial direction. During resonant excitation, several processes can occur simultaneously. Energetic collisions between the ions and buffer gas may promote dissociation. Alternatively, power may be absorbed so rapidly by the ion that it escapes the analyzer's trapping field without undergoing fragmentation. Ion dissociation or ion ejection is detected by obtaining a mass spectrum of the ions that are present in the ion trap without resonant excitation and comparing it to a mass spectrum taken after the supplementary AC voltage is applied.

By plotting the ion intensity of one m/z for a series of spectra acquired at different supplementary AC frequencies, the relationship between the excitation frequency and the frequency at which the ion absorbs AC power is observed. This is commonly referred to as a frequency breakdown curve. Figure 4-1 shows several

frequency breakdown curves for isopherone. The minimum intensity for m/z 139 corresponds to the most efficient resonant excitation frequency, and may be interpreted as the ion's secular frequency of motion in the axial direction. Collecting the data for a frequency breakdown curve can be accomplished in several minutes using automated methods. However, this is too slow to be considered a real-time frequency assignment method for GC/MS/MS.

Alternatively, the relationship between the excitation frequency and an ion's motion can be measured with a single μscan that includes a frequency sweep. By scanning the resonant excitation frequency and recording the ions that are ejected from the ion trap to the detector, a mass spectrum can be recorded as a function of ion frequency. Figure 4-2 compares the spectra obtained for bromobenzene with (a) a mass selective instability scan, and (b) a swept frequency acquisition. Thus, frequency sweeps can be employed to obtain a mass spectrum, and swept frequency data can also yield the frequency at which the ions are most efficiently excited in the axial direction. Because frequency sweeps generate the entire frequency/excitation relationship from a single ionization event, they provide a rapid method of determining an ion's secular frequency of motion. The frequency-assignment pre-scan employs two rapid (10 ms) frequency sweeps to determine the resonant excitation frequency to be used in a subsequent MS/MS μscan.

Frequency Modulated Broadband Excitation

For ions stored at coordinates $a_z = 0.0$ and $q_z = 0.3$, the secular frequency of ion motion for ions stored in an ITMS is approximately 118 kHz. Frequency shifts caused by changes in ion population can typically span 500 Hz - 2,000 Hz, or

Figure 4-1. Frequency breakdown curves for isopherone obtained by incrementing the frequency of the supplementary AC voltage from 110,000 Hz to 122,475 Hz at 25 Hz increments. The displayed curves include the total ion current (TIC), parent ions m/z 139 and m/z 140, and product ions m/z 82 and m/z 69.

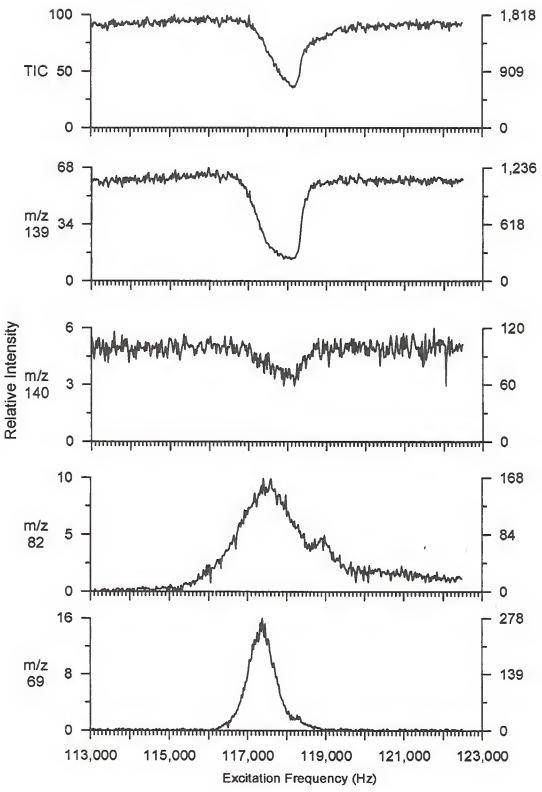
100
TIC 50
0
1,818
909
0
68
m/z 139 34
0
1,236
618
0
6
m/z 140 3
0
120
60
0
Relative Intensity
10
m/z 82 5
0
168
84
0
16
m/z 69 8
0
278
139
0
113,000
115,000
117,000
119,000
121,000
123,000
Excitation Frequency (Hz)

Figure 4-2. Comparison of mass spectra obtained by an RF amplitude scan and supplementary AC frequency scan. EI mass spectra of bromobenzene (MW = 156) obtained by (a) scanning the amplitude of the RF voltage at 128 $V_{p-p}$/s with a 6 $V_{p-p}$ AC signal fixed at 530,000 kHz, and (b) scanning the frequency of the 6 $V_{p-p}$ AC signal at -41.4 kHz/ms with a fixed RF amplitude of 1140 $V_{p-p}$.

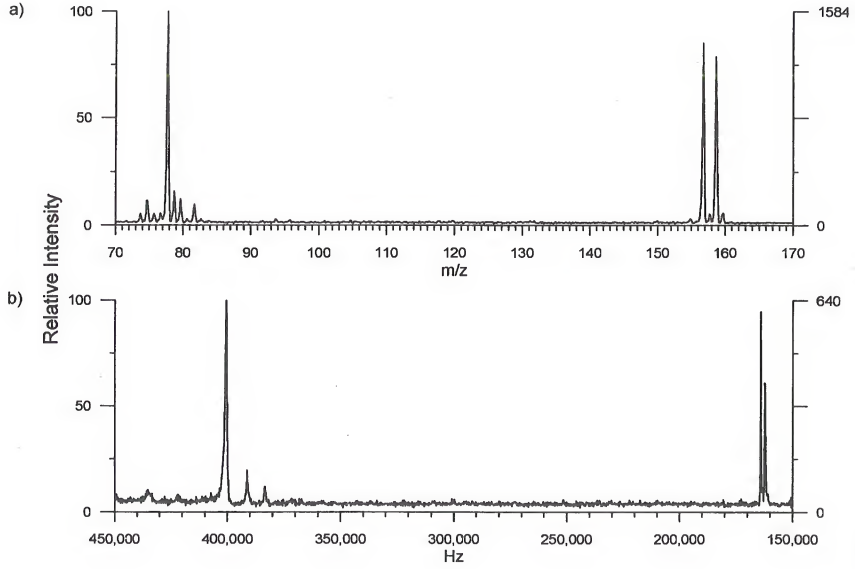
a)
100
50
0
1584
0
70
80
90
100
110
120
130
140
150
160
170
m/z
Relative Intensity
b)
100
50
0
640
0
450,000
400,000
350,000
300,000
250,000
200,000
150,000
Hz

approximately 0.5% to 2% of the secular frequency. Since the bandwidth of single frequency excitation used for CID is typically 5 - 10 Hz, the frequency of the applied excitation signal must match the ion's secular frequency of motion within 0.01% to effect CID. One approach that eliminates the need for exact frequency assignment is to use a broadband excitation signal that excites a narrow range of frequencies that covers the magnitude of the expected frequency shift. A broadband excitation signal covering a 10 kHz frequency range corresponds to a m/z range of 1.2 at $q_z = 0.3$.

Frequency modulation can be used to generate broadband excitation signals. By rapidly switching the output frequency of the supplementary AC voltage, a range of frequencies can be excited in rapid secession. Several types of frequency modulation patterns can be used to effect broadband excitation over a 10 kHz frequency range. Frequency sweeps excite a range of frequencies by scanning from a start frequency to a stop frequency at a variable frequency sweep rate. Random frequency excitation outputs sine waves of various frequencies between a start frequency and stop frequency. Additionally, ordered frequency patterns can be used to excite ions of different frequency in a controlled fashion. The frequency modulated broadband excitation pattern described here employs ordered patterns that are designed to impart equal power into ions that have a range of different secular frequencies of motion. It is important to note that broadband excitation methods based on sinusoidal waveforms can only excite one frequency at a time, but the effect of simultaneous excitation can be produced by using a fast frequency modulation rate (40 kHz).

SWIFT Broadband Excitation

Stored waveform inverse Fourier transform (SWIFT) broadband excitation simultaneously excites a spectrum of frequencies with the use of complex waveforms. The SWIFT technique, originally developed by Marshall et al. for ion excitation in ion cyclotron resonance mass spectrometers, has been previously described in detail.[98]

Briefly, the process of calculating a SWIFT broadband excitation waveform begins by specifying the start and end frequencies. Next, a magnitude and phase spectrum are calculated in the frequency domain for the specified frequency range. Figure 4-3 shows (a) the magnitude, and (b) the phase spectra for a 10 kHz wide excitation range centered at 112 kHz. Note that polar coordinates (magnitude and phase) are used to describe the SWIFT pulse in the frequency domain. Quadratic phase modulation is used to vary the phase relationship of the frequencies contained in the SWIFT waveform. The use of a constant phase relationship results in a time domain signal with a large dynamic range that cannot be easily produced electronically. Next, the magnitude and phase data are transformed from the frequency to the time domain via the inverse fast Fourier transform (IFFT). The resulting time domain data are reflected about their midpoint and apodized with a quarter-wave sine function to smooth the leading and trailing edges of the excitation signal to zero. Example data for the SWIFT broadband excitation signal are shown in Figure 4-3 (c). These data points are downloaded to an arbitrary waveform generator that produces the corresponding analog signal that is applied to the ion trap's endcaps to promote excitation in the axial direction.

Figure 4-3. Diagram of the computational procedure used to generate stored waveform inverse Fourier transform (SWIFT) broadband excitation waveforms. The broadband frequency domain spectrum (a) is subject to quadratic phase modulation (b) prior to being converted to a time domain excitation signal (c). The inverse fast Fourier transform (IFFT) is used to convert from the frequency (a, b) to time domain (c). The resulting time domain data is reflected and apodized as discussed by Marshall[98] prior to being downloaded to the arbitrary waveform generator.

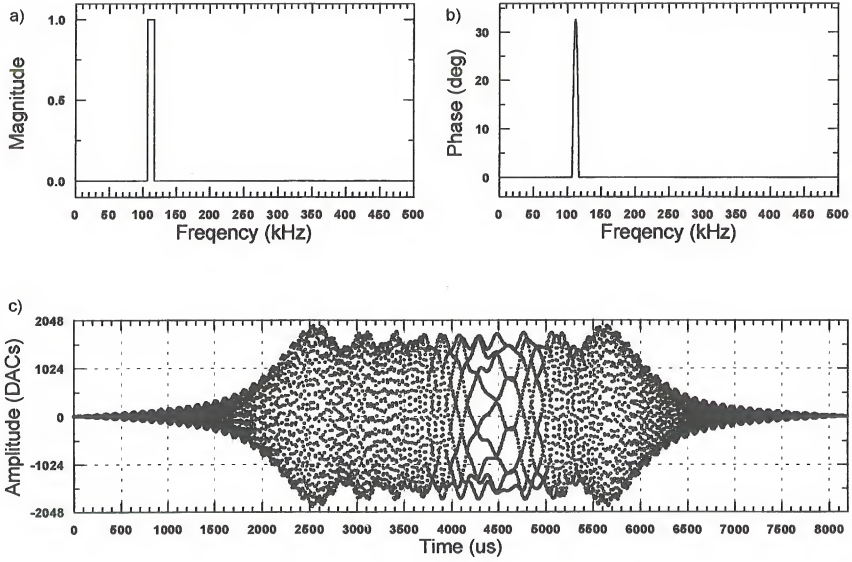
a)
Magnitude
1.0
0.5
0.0
0 50 100 150 200 250 300 350 400 450 500
Freqency (kHz)
b)
Phase (deg)
30
20
10
0
0 50 100 150 200 250 300 350 400 450 500
Freqency (kHz)
c)
Amplitude (DACs)
2048
1024
0
-1024
-2048
0 500 1000 1500 2000 2500 3000 3500 4000 4500 5000 5500 6000 6500 7000 7500 8000
Time (us)

## Experimental

### Instrumentation

An ITMS was used for the frequency-assignment pre-scan and frequency modulated broadband excitation studies. SWIFT broadband excitation was performed on a modified ITS40 instrument that is described in detail in chapter 5 of this dissertation. Samples of n-butylbenzene, perflourotributylamine (FC-43), and bromobenzene were introduced into the ITMS vacuum chamber via a Granville Phillips fine metering valve. Less volatile samples were injected onto a 30 M DB5 capillary GC column that was interfaced to both the ITMS and ITS40 with a heated transfer line that introduces the GC effluent directly into the ion trap's internal volume.

### Frequency Shift Measurements

Frequency breakdown curves were measured for m/z 134 of n-butylbenzene at ionization times of 5, 40, and 85 ms. The scan programs contained an RF pulse that ejected all of the ion below m/z 125 from the ion trap prior to the application of a supplementary AC voltage signal, for 10 ms. An excitation amplitude of 100 mV was used, and the frequency of the supplementary AC voltage was varied from 116 kHz - 119 kHz using 200 15 Hz increments.

Results for GC/MS/MS were obtained for 1 ng/uL of isopherone in methylene chloride. The scan program used included a 5 ms ionization period and two-step isolation of m/z 139. Single-frequency resonant excitation was performed at $q_z = 0.3$. The amplitude, frequency, and duration of the supplementary AC voltage were 500 mV, 117.9 kHz, and 10 ms, respectively.

Frequency Modulation on the ITMS

To permit rapid frequency modulation, software modifications to the ITMS firmware (assembly code running on the instrument's embedded microprocessor) and source code were made. Low level control software was added to take advantage of the rapid frequency switching capabilities of the ITMS's direct digital synthesizer (DDS) and to permit data acquisition during a frequency sweep. High level control of these new features was built into the ITMS scan editor program. These software modifications have been incorporated into the ICMS© software for the ITMS, which is distributed by the University of Florida.

The ICMS software implements rapid frequency modulation of the supplementary AC voltage with the DDS. A typical DDS can attain a frequency resolution of a fraction of a Hertz and phase-continuous switching rates in the nanosecond range[121]. The original ITMS scan editor could be used to set the output frequency of the DDS to the frequency of motion of a particular m/z ion, but it was limited to utilizing a single frequency per scan table. Thus, modulation of the AC frequency at a high rate over a large number of frequencies (>20) was not practical with the original scan editor.

The ICMS software allows the frequency of the supplementary AC voltage to be modulated over the frequency range from 0 to 1.5 MHz in 1 Hz increments. The frequency modulation rate of the DDS is fixed at approximately 40 kHz; the DDS can be programmed to strobe between 2000 discrete frequencies in a single scan table. For example, to implement broadband excitation over a 10 kHz range, 1400 different frequencies are strobed into the DDS at a rate of one frequency every 28 µs.

Frequency sweeps, frequency steps, multiple frequency bursts and other complex frequency modulation patterns can be created using the ICMS delta frequency pattern editor.

Frequency-Assignment Pre-Scan

The scan program containing the frequency-assignment pre-scan and subsequent MS/MS scan is shown in Figure 4-4. Following ionization and mass selection of the parent ion, the multiplier is turned on for a warmup period of 2 ms. During this time, the analog driver that controls the output voltage of the frequency synthesizer is warmed up at an initial amplitude of 2 $V_{p-p}$. With the multiplier and the analog driver stabilized, the frequency synthesizer is scanned up from 112 kHz to 122 Khz at a constant amplitude of 2 $V_{p-p}$ and a sweep rate of 600 kHz/s. This frequency range corresponds to a 1.2 u wide window at $q_z = 0.3$. Throughout the frequency scan, the ejected ion current is acquired with the ITMS's standard electrometer and A/D converter. These data are temporarily stored on the PC. A second frequency pre-scan is performed with the identical ionization and mass selection steps, but with the frequency scanned down from 122 kHz to 112 kHz and the data are returned to the data system. An algorithm locates the frequency corresponding to the maximum ejected ion current for each temporary data set and returns the maximum ejection frequencies. The average of these two values is calculated and used as the resonant excitation frequency in a subsequent MS/MS scan. The total time required to perform the entire frequency pre-scan procedure including two ionization, mass selection, frequency sweep, and calculation steps is less than 100 ms. The current implementation spends an additional 500 ms sending the frequency pattern to the

Figure 4-4. Frequency-assignment pre-scan scan program. The frequency-assignment pre-scan, steps I - F2, is performed prior to the MS/MS product ion scan to automatically determine an appropriate resonant excitation frequency to be used in step C. Ions are generated during the periods labeled I, parent ions are mass selected using two-step isolation during the stages labeled M, the parent ion's secular frequency of motion is determined with two frequency sweeps periods F1 and F2, the parent ions are dissociated during stage C, and mass analysis of the product ions is performed during period S. Increasing and decreasing frequency sweeps F1 and F2 (not drawn to scale) cover a 10 kHz range centered at 118 kHz. A supplementary AC voltage frequency of 530 kHz is applied during period S to affect axial modulation. The ion signals observed during the pre-scan and MS/MS scan are not shown on the same relative intensity scale.

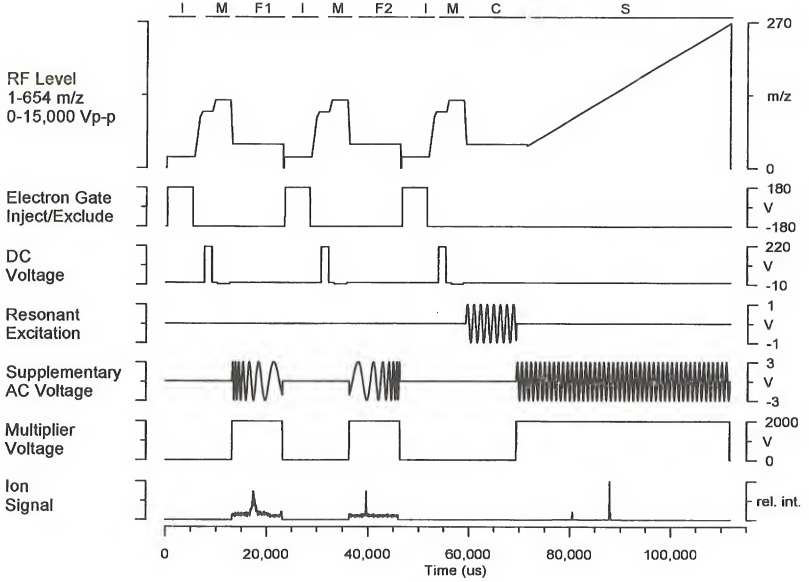
I
M
F1
I
M
F2
I
M
C
S
RF Level
1-654 m/z
0-15,000 Vp-p
270
m/z
0
Electron Gate
Inject/Exclude
180
V
-180
DC
Voltage
220
V
-10
Resonant
Excitation
1
V
-1
Supplementary
AC Voltage
3
V
-3
Multiplier
Voltage
2000
V
0
Ion
Signal
rel. int.
0
20,000
40,000
60,000
80,000
100,000
Time (us)

synthesizer's memory prior to each scan. This time was added as a developmental convenience that can be eliminated by sending the frequency sequence to the synthesizer before the beginning of an experiment.

Frequency Modulated Broadband Excitation

To implement broadband excitation over a 10 kHz range, 1400 frequencies are downloaded to the ITMS synthesizer memory and input into the DDS at a rate of one frequency every 28 μs. The frequencies used for broadband excitation comprise a 10 kHz range and are spaced 50 Hz apart. The order of the frequencies assures that the successive frequencies output by the synthesizer will be approximately 700 Hz apart. This frequency spacing assures that an ion is not doubly excited by two frequencies that are close to one another. Strobing through all 1400 frequencies produces a broadband excitation signal 40 ms long. The amplitude of the broadband excitation signal can be varied from 10 $mV_{p-p}$ - 6000 $mV_{p-p}$.

SWIFT Broadband Excitation

The initial SWIFT waveforms calculated for this work were developed using a mathematical software package (MathCAD 2.0). MathCAD is an equation solver program that simplifies the execution of complex numerical methods. However, MathCAD is too slow to be used for calculating multiple SWIFT waveforms. A program, named GTRSWIFT.EXE, was written in C++ that calculates and downloads SWIFT waveforms to an arbitrary waveform generator (Stanford Research Systems, model # DS345). A SWIFT waveform containing a maximum of 8192 points can be calculated in under a second, although 7 s are required to download the data over the

GPIB interface bus. The MathCAD program was used to aid the development and debugging of the GTRSWIFT.EXE program. Additionally, the IFFT routine used in the GTRSWIFT.EXE program was adapted from the IFFT program described in Numerical Recipes in C Second Edition.[122] The average power spectra produced by the SWIFT waveforms were recorded with a spectrum analyzer.

## Results and Discussion

### MS/MS Efficiencies and Frequency Shifts

Figure 4-5 shows three product ion spectra for m/z 134 of n-butylbenzene. These spectra were acquired using (a) 5 ms, (b) 40 ms, and (c) 80 ms ionization times with a resonant excitation frequency of 117900 Hz. Dissociation of the molecular ion ($M^{+\cdot}$) $134^+$ is achieved with the application of the supplementary AC voltage and forms the product ions $91^+$, $92^+$, $105^+$ and $119^+$. The ion observed at m/z 135 includes the protonated n-butylbenzene molecules $[M+H]^+$ and the $^{13}C$ molecular $M^{+\cdot}$ ions.

Note that the relative intensity of the remaining m/z 134 ions is much smaller than the m/z 135 peak. This indicates that nearly all of the $134^+$ ions have been resonantly excited and have undergone a m/z changing reaction or were ejected from the ion trap. The fragmentation efficiency ($E_F$), defined[123] as

$$E_F = \frac{\sum D_i}{P+\sum D_i} * 100\% \qquad (4\text{-}1)$$

where P is the intensity of the parent ion remaining following excitation and where $D_i$ is the intensity of the product ions. The $E_F$ measures the fraction of ions collected that are product ions. The $E_F$ observed for m/z 134 in Figure 4-5 (a) is ca. 88 ± 5 %

Figure 4-5. Comparison of MS/MS spectra taken at three different ionization times. MS/MS product ion spectra for m/z 134 of n-butylbenzene at ionization time of (a) 5 ms, (b) 85 ms, and (c) 200 ms. Resonant excitation amplitude and duration were 400 mV and 10 ms respectively. The excitation frequency used for resonant excitation was fixed at 117.9 kHz.

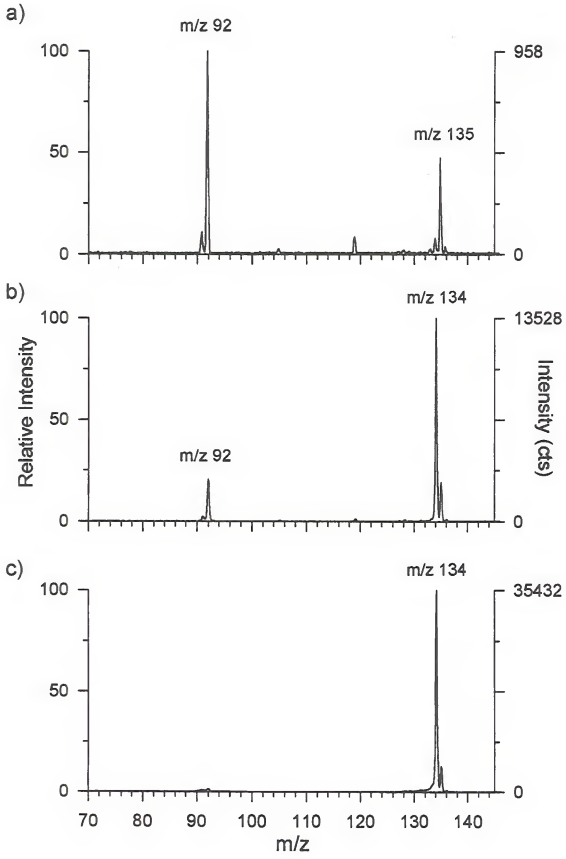
a)
m/z 92
100
50
0
958
m/z 135
0
b)
m/z 134
100
50
0
13528
Relative Intensity
Intensity (cts)
m/z 92
0
c)
m/z 134
100
50
0
35432
0
70
80
90
100
110
120
130
140
m/z

excluding the ions at m/z 135. The collection efficiency ($E_C$) for an MS/MS experiment is defined as

$$E_C = \frac{P_+ \sum D_I}{P_0} * 100\% \qquad (4\text{-}2)$$

where $P_0$ is the intensity of the parent ion without excitation. The $E_C$ measures the fraction of the initial parent ions that is collected as product ions. The $E_C$ for Figure 4-5 (a) is ca. 34 ± 5 %. This indicates that approximately 66 ± 5 % of the parent ion signal was lost as a result of the application of the supplementary AC voltage. The overall CID efficiency ($E_{CID}$) is defined as

$$E_{CID} = \frac{\sum D_I}{P_0} * 100\% = E_F * E_C \qquad (4\text{-}3)$$

and indicates the fraction of the initial parent ions that are collected as product ions. For the product ion spectrum shown in Figure 4-5 (a), the $E_{CID}$ is ca. 30 ± 5 %.

As the ionization time is increased from (a) 5 ms to (b) 40 ms the fragmentation efficiency ($E_F$) and the overall CID efficiency ($E_{CID}$) are reduced from 43 ± 5 % to 62 ± 5 %, respectively. A collection efficiency of 26 ± 5 % is observed for the spectrum shown in Figure 4-5 (b). The MS/MS product ion spectrum shown in Figure 4-5 (c) shows that increasing the ionization time to 85 ms produces an $E_F$ = 6 ± 5 %, $E_C$ = 93 ± 5 %, and $E_{CID}$ = 6 ± 5 %. Clearly, the increase in ionization time has reduced the effect of the supplementary AC voltage on the parent ion $134^+$, since fewer parent ions are lost and less product ions are formed and collected relative to the number of parent ions that were initially present.

The loss in overall MS/MS efficiency with increasing ionization times that is observed in Figure 4-5 is caused by shifts in an ion's secular frequency that occur as a result of space charge. As the number of the ions in the ion trap is increased, the increased space charge disturbs the ion trap's storage field and distorts the motion of the ions. Thus, as the number of ions in the trap increases, the secular frequency of motion of the parent ion shifts away from the frequency of the supplementary AC voltage, altering the efficiency of the MS/MS experiment.

Figure 4-6 compares three frequency breakdown curves for m/z 134 of n-butylbenzene that show the shift in an ion's secular frequency of motion that occurs as the number of ions contained in the ion trap is increased. The dashed line (----) shows the intensity of the product ion 92+. Note that the frequency shifts to lower values as the space charge, caused by the ions in the trap, increases. Interestingly, a reduction in the frequency of ion motion can also be caused by reducing the amplitude of the RF voltage or by applying a positive DC potential to the ring electrode of the ion trap. Since the RF amplitude and DC voltage were held constant for these experiments, the frequency shifts indicate that space charge, which is concentrated in the center of the ion trap, reduces the influence of the RF and DC voltage on ion motion.

Figure 4-6 also shows that although the frequency of ion motion shifts as a function of the ion population in the ion trap, the CID efficiency remains constant if the supplementary AC voltage is tuned to the correct frequency. This is an important observation because it indicates that MS/MS can be performed with similar efficiencies at both high and low levels of space charge.

For GC/MS/MS, the connection between CID efficiency and the number of ions in the ion trap can be particularly troublesome since the number of ions continually

Figure 4-6. Secular frequency versus ionization time: Comparison of three frequency breakdown curves for m/z 134 of n-butylbenzene at ionization times of (a) 5 ms, (b) 40 ms, and (c) 85 ms. Resonant excitation parameters include amplitude = 100 mV, duration = 10 ms, frequency 116,000 - 119,000 at 25 Hz increments.

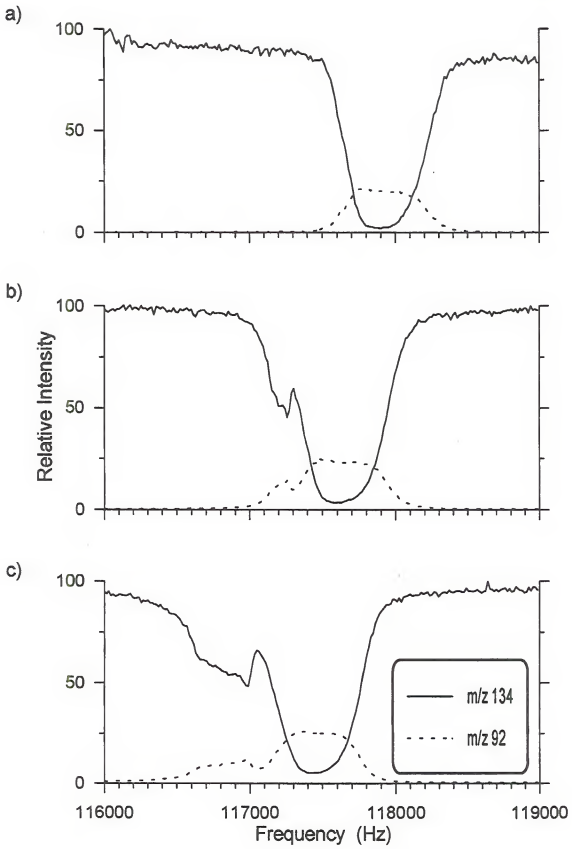
a)
b)
c)
100
50
0
Relative Intensity
m/z 134
m/z 92
116000
117000
118000
119000
Frequency (Hz)

changes as GC peaks elute. The frequency shifts that occur over a GC peak complicate the tuning of single-frequency resonant excitation scan programs to achieve consistent CID and thus result in variations in the MS/MS product spectra.

Figure 4-7 compares the total and selected ion chromatograms for the parent ion $139^+$ and product ions $110^+$ and $69^+$ of isopherone using single frequency excitation. Interestingly, the chromatographic profile for m/z 110 does not follow the profile of the $139^+$ or $69^+$ ions. At the base of the GC peak, the relative intensity of the product ion m/z 110 was higher than its intensity at the center of the GC peak. Shifts in $139^+$ secular frequency of motion could account for the difference observed between the GC peak profiles of the product ions. As the ion's secular frequency shifts in and out of resonance with the frequency of the supplementary AC voltage, the amount of energy deposited into the ion changes, leading to differing product ion intensities. Thus, frequency shifts can alter the relative intensities of the product ions observed, as well as reduce the efficiency of the MS/MS experiments.

Frequency-Assignment Pre-Scan

The frequency-assignment pre-scan corrects for frequency shifts by performing two rapid pre-scans prior to each analytical scan that determine the parent ion's secular frequency of motion. Each pre-scan employs a 10 ms frequency sweep that determines the parent ion's secular frequency of motion by ejecting the parent ion to the detector. By correlating the observed ion signal with the frequency sweep rate, the secular frequency of motion may be determined.

Figure 4-8 (a) shows the frequency breakdown curve for m/z 264 of perfluorotributylamine (MW = 642). The frequency breakdown curve shows that the

Figure 4-7. Comparison of the total and selected mass chromatograms for the parent ion $139^+$ and product ions $110^+$ and $69^+$ of isopherone. GC/MS/MS using single- frequency excitation at 117.9 kHz for 5 ms with an amplitude of 500 mV. The parent ion, m/z 139, was isolated at a $q_z = 0.3$ prior to dissociation.

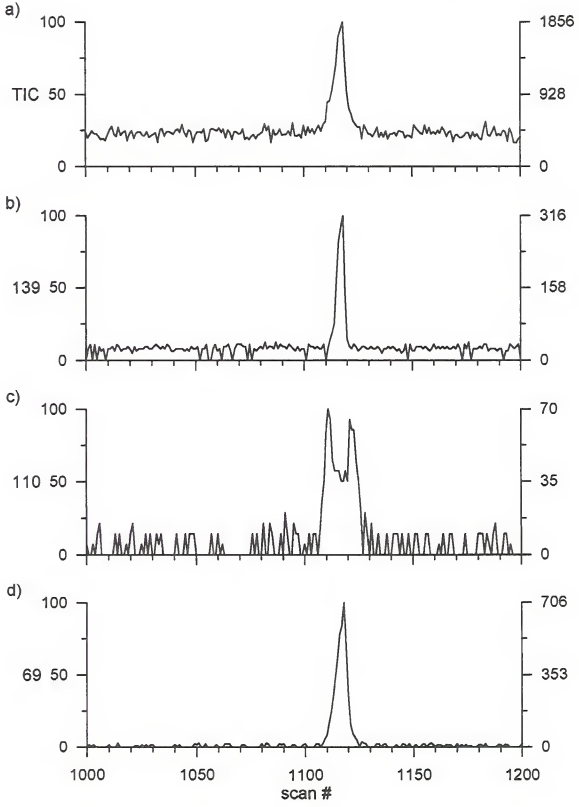
a)
100
TIC 50
0
1856
928
0
b)
100
139 50
0
316
158
0
c)
100
110 50
0
70
35
0
d)
100
69 50
0
706
353
0
1000
1050
1100
1150
1200
scan #

Figure 4-8. Frequency-assignment pre-scan signals. Comparison of (a) the frequency breakdown curve and (b,c) swept frequency ejection curves for m/z 264 of perfluorotributylamine. A frequency sweep rate of ±840 kHz/s and amplitude of 2.0 $V_{p-p}$ was used to eject the mass isolated 134$^+$ ions stored at $q_z$ = 0.3. Labels dv' and dv'' designate the delay associated with energy absorption and ion ejection for the two frequency sweeps.

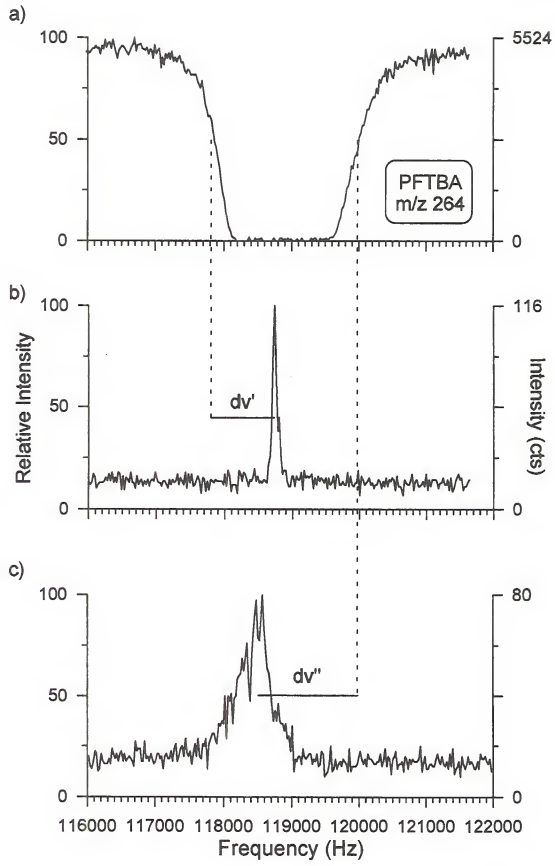
a)
100
50
0
5524
0
PFTBA
m/z 264
b)
100
50
0
116
0
Relative Intensity
Intensity (cts)
dv'
c)
100
50
0
80
0
dv''
116000 117000 118000 119000 120000 121000 122000
Frequency (Hz)

width of the resonance band is ca. 2 kHz wide at half-depth and is centered around 118.9 kHz. Figure 4-8 also shows the frequency pre-scan data for m/z 264 acquired with (a) increasing and (b) decreasing frequency sweeps. The peaks observed for the positive and negative slope frequency sweeps correspond to the frequency at which the m/z 264 ions begin to absorb resonant power and are ejected from the ion trap to the detector. Thus, the frequency sweep data determines the edges of an ion's resonance band. By averaging the frequency of ejection for the two frequency sweeps, the center of the frequency band and the ion's secular frequency of motion is determined.

In practice, a single frequency sweep does not provide enough information to identify an ion's secular frequency of motion. The absolute ejection frequency observed for an ion that has been detected with a frequency sweep depends on several parameters. The amplitude of the frequency sweep affects the rate at which the ion absorbs power from the supplementary AC field. At low amplitudes, an ion absorbs power more slowly and requires more excitation time before it is ejected from the ion trap. At high excitation amplitudes, ions begin to leave the ion trap as soon as the ion begins to come into resonance with the applied field. Figure 4-9 shows the ejection frequencies observed for m/z 156 of bromobenzene as a function of excitation amplitude. The data identified with plus symbols (+) and hollow squares (□) correspond to the ejection frequencies recorded with a frequency scan rate of +225 Hz/ms and -225 Hz/ms, respectively. Note that regardless of the excitation amplitude, the average ejection frequency (identified with triangles △) for the frequency sweeps of opposite slope show close agreement with the center of the ion's resonance band (identified with a solid line ——— ).

Figure 4-9. Frequency for maximum ejection versus resonant excitation voltage for m/z 156 from bromobenzene. The increasing frequency scan data are shown as plus symbols (+), and the decreasing frequency scan data are represented with hollow squares (□). The hollow triangles (△) indicate the average of the two frequency sweep data points and the solid horizontal line ( ——— ) marks the center of the resonance band for m/z 156 determined by manual frequency optimization.

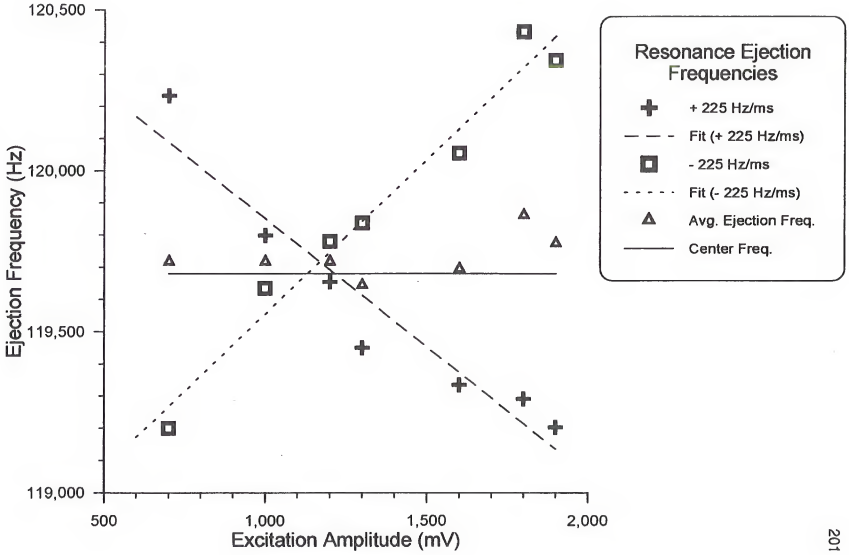
Resonance Ejection Frequencies
+ 225 Hz/ms
Fit (+ 225 Hz/ms)
- 225 Hz/ms
Fit (- 225 Hz/ms)
Avg. Ejection Freq.
Center Freq.
Ejection Frequency (Hz)
120,500
120,000
119,500
119,000
500
1,000
1,500
2,000
Excitation Amplitude (mV)

The frequency sweep rate can also effect the frequency at which ions are ejected from the ion trap. Figure 4-10 shows the relationship between the frequency of ejection and the frequency sweep rate for m/z 156 of bromobenzene. For a positive frequency scan, the ions are ejected earlier as the frequency is swept more slowly. Ions must reach a specific energy before they are ejected from the trap. Slow frequency scans allow ions to absorb sufficient power to cross this barrier before the optimum excitation frequency is reached. A fixed scan rate is used for both frequency pre-scans to eliminate this effect. Higher frequency scan rates have been observed to produce a sharper ion ejection peak shape.

The incorporation of the two frequency sweeps into a frequency-assignment pre-scan (see Figure 4-4) provides a method for determining the frequency of motion for an ion of interest in the ion trap and is the only technique capable of adjusting the frequency of the supplementary AC voltage on the millisecond time scale. A limitation of this method is that the isolated parent ion must be of sufficient intensity to allow detection by the pre-scan. Also, the extra 50 - 70 ms required for the pre-scan to be performed may be a limitation for some applications. Automatically assigned frequencies, the average of two ejection frequencies, agree with those determined by manual procedures with less than 0.1% (100 Hz) deviation, as shown in Figure 4-9. Although the scan program used by this method is complex, the technique has reliably determined the appropriate resonant excitation frequencies for MS/MS.

Figure 4-11 shows three product ion spectra that were acquired using the frequency-assignment pre-scan. Ionization times of (a) 5 ms, (b) 85 ms, and (c) 200 ms duration were used to alter the space charge level in the ion trap. For each ionization time, the frequency assignment pre-scan determined an appropriate

Figure 4-10. Frequency for maximum ejection versus frequency sweep rate for m/z 156 of bromobenzene with an increasing frequency scan. Frequency sweep from 115 kHz to 122 kHz, with an amplitude of 3 $V_{p\text{-}p}$.

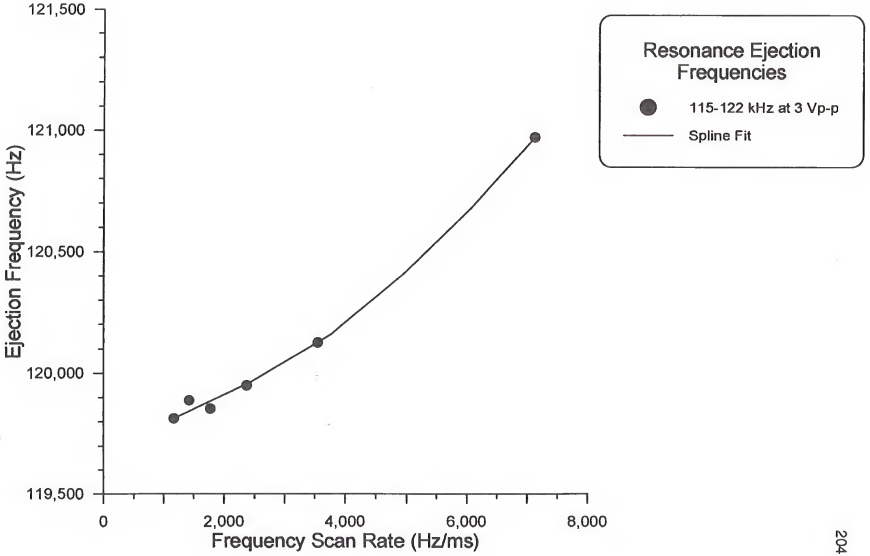
Resonance Ejection Frequencies
115-122 kHz at 3 Vp-p
Spline Fit
121,500
121,000
120,500
120,000
119,500
Ejection Frequency (Hz)
0
2,000
4,000
6,000
8,000
Frequency Scan Rate (Hz/ms)

Figure 4-11. Comparison of three MS/MS product ion spectra obtained using the frequency-assignment pre-scan for m/z 134 of n-butylbenzene at ionization times of (a) 5 ms, (b) 85 ms, and (c) 200 ms. Resonant excitation amplitude and durations were 400 mV and 10 ms, respectively. The excitation frequency used for resonant excitation was determined automatically via the frequency-assignment pre-scan.

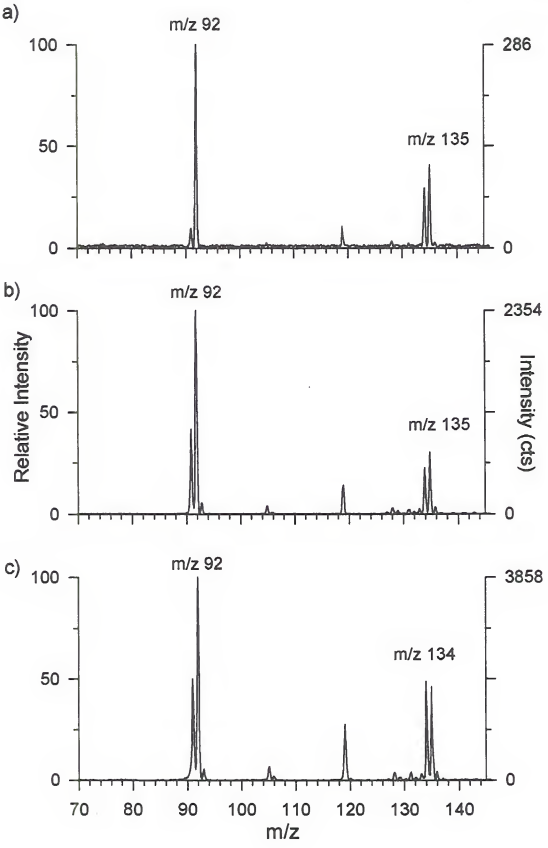
a)
m/z 92
100
50
0
286
m/z 135
0
b)
m/z 92
100
50
0
Relative Intensity
2354
Intensity (cts)
m/z 135
0
c)
m/z 92
100
50
0
3858
m/z 134
0
70
80
90
100
110
120
130
140
m/z

excitation frequency that was used to produce a reliable product ion spectrum. Although the MS/MS efficiencies were not measured directly, the intensity of the parent ($134^+$) and product ions can be compared to the m/z 135 ion intensity remaining. The three MS/MS product spectra are similar to each other except for the intensity ratio of the $91^+$ and $92^+$ ions. The $91^+/92^+$ ratio can be used to gauge the internal energy deposited into m/z 134 prior to dissociation, where higher $91^+/92^+$ ratios indicate higher internal energies. Here, the internal energy deposition into the parent ion increases with ionization time. Because the frequency-assignment pre-scan determines the proper excitation frequency based on the ejection of the parent ion, internal energy deposition is not accounted for. Thus, slight variations in the relative intensities of the product ions would be expected.

Frequency Modulated Broadband Excitation

Broadband excitation compensates for frequency shifts by exciting a range of frequencies that cover the expected magnitude of the frequency shift.[71] On the ITMS, broadband excitation may be implemented by programming the frequency synthesizer to switch between selected frequencies in a phase continuous manner. A typical broadband excitation pulse switches between 1400 discrete frequencies covering a 10 kHz wide range. Centering this broadband excitation signal at 118 kHz excites a 1.2 u wide m/z range at $q_z = 0.3$.

Figure 4-12 shows a chromatogram for 800 pg of n-butylbenzene that was acquired with an MS/MS scan program and broadband excitation. The MS/MS product ion spectra for m/z 134 observed at the top and base of the GC peak show good correlation to each other and to reference product ion spectra for n-butylbenzene. The

Figure 4-12. GC/MS/MS product ion data for m/z 134 of n-butylbenzene (800 pg injected), obtained using broadband excitation over a 10 kHz frequency range centered at 118 kHz. An excitation time and amplitude of 40 ms and 1.2 $V_{p-p}$ were used. The insets show the MS/MS product ion spectra observed at the top and bottom of the chromatographic peak.

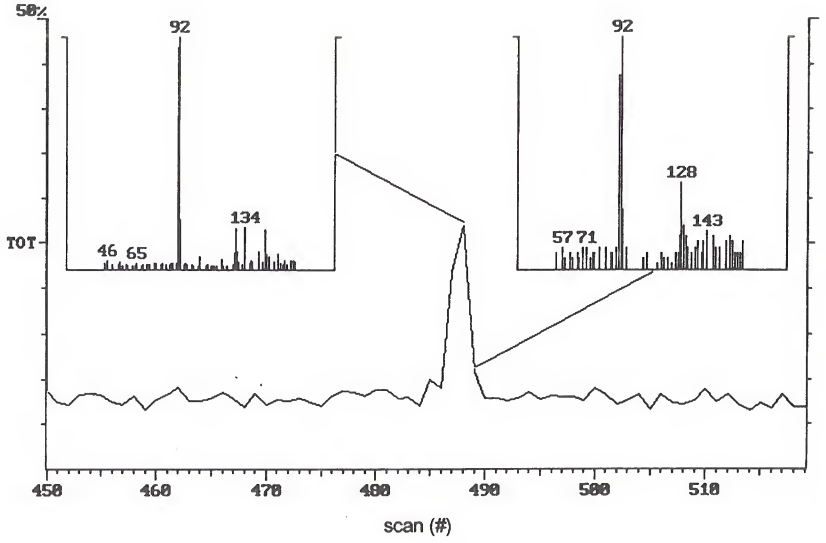
50%
92
134
46 65
TOT
92
128
143
57 71
450
460
470
480
490
500
510
scan (#)

$91^+/92^+$ ratios approach unity in both spectra and suggest that broadband excitation deposits more energy into the parent ion than is typically observed for single frequency excitation. No adjustment of the excitation frequency was required and no frequency shift effects were observed over the GC peak. In contrast, when the experiment was repeated with single frequency resonant excitation, product ions were not observed until the frequency was manually optimized by making repetitive sample injections and attempting different frequencies.

Figure 4-13 (a) shows GC/MS/MS results obtained for the injection of 200 times more of n-butylbenzene (140 ng). Broadband excitation was used to dissociate m/z 134. The chromatographic peak shape is clipped at the top of the peak as a result of space charge caused by the use of too long an ionization time. Note that the product and parent ions for n-butylbenzene are observed in the spectrum recorded on the front of the GC peak, but that these ions are not observed at the top of the peak. Figure 4-13 (b) shows the total and selected ion mass chromatograms for m/z 134 and the sum of m/z 91 and m/z 92. At the sided of the GC peak, the parent and product ions are observed, but in the middle of the GC peak, space charge and ion-molecule reactions result in the loss of ion signal for the parent ion m/z 134. Importantly, broadband excitation was capable of producing product ions whenever m/z 134 was present in the ion trap. However, ion-molecule reactions also produced product ions at m/z 91 and m/z 92 when m/z 134 was absent, as noted by the small peak at scan # 537. Thus, ion-molecule reactions can, in extreme cases, reduce the selectivity of MS/MS on the ion trap.

Qualitatively, the CID efficiencies observed for broadband excitation are 10-40% less than are observed with optimized single frequency resonant excitation. Although

Figure 4-13. GC/MS/MS results obtained for the injection of 140 ng of n-butylbenzene. (a) MS/MS product ion spectra for m/z 134 obtained at different points across the GC peak. (b) The total and selected mass chromatogram for m/z 134 and the sum of m/z 91 and m/z 92.

a)

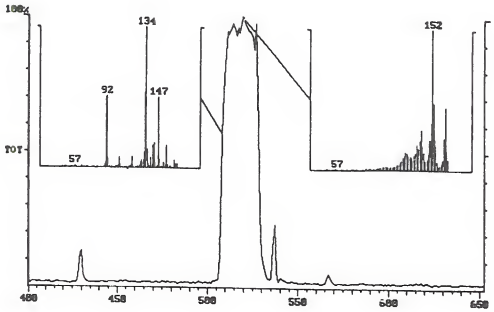
134
92
147
152
57
57
TOT
400
450
500
550
600
650

b)

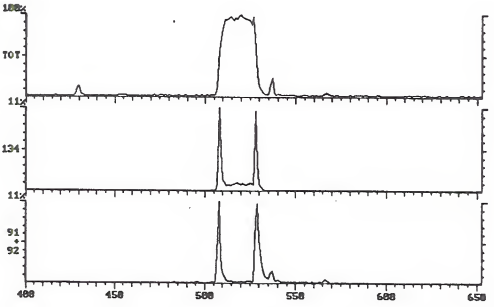
TOT
134
91
92
400
450
500
550
600
650

scan (#)

the frequency pattern that is used to create the broadband signal is designed to distribute the excitation power evenly over the 10 kHz wide excitation envelope, the actual power spectrum may contain irregular power distribution that can lead to ion losses and reduced CID efficiencies. Broadband excitation also requires a 40 ms excitation time and 1-2 V amplitudes to obtain similar spectra to those observed with a 10 ms excitation time and 300-700 mV amplitude using single frequency excitation. The need for longer excitation times and higher voltages is a result of the excitation power being spread over a wider frequency range, and thus less power is put into the ions (which don't absorb all frequencies) per unit time. Despite the reduced CID efficiencies and the need for increased excitation times and amplitudes, broadband excitation may result in higher CID efficiencies for GC/MS/MS because the overall CID efficiency remains constant as the ion's secular frequency of motion shifts.

SWIFT Broadband Excitation

Broadband excitation over a 10 kHz frequency range can also be achieved with the use of SWIFT waveforms. While SWIFT methods have been demonstrated for the CID, isolation and ejection of ions in the ion trap,[95] SWIFT broadband excitation is particularly useful for GC/MS/MS experiments because it is unaffected by shifts in an ion's secular frequency of motion.[73] Unlike frequency modulated methods, the power spectrum for SWIFT broadband excitation exhibits a flat power response over the excited frequency range. Figure 4-14 compares the average power spectrum for a 10 kHz wide SWIFT pulse centered at 100 kHz with the power spectrum for a 100 kHz sine function. The SWIFT power spectrum exhibits a flat power curve with sharp cutoffs at 95 kHz and 105 kHz respectively. SWIFT effects continuous excitation,

Figure 4-14. Comparison of the average power spectra for SWIFT and single frequency resonant excitation signals as measured by a digital spectrum analyzer. (a) Power spectrum of a 10 kHz wide SWIFT pulse centered at 100 kHz. (b) Power spectrum of a 100 kHz sine function.

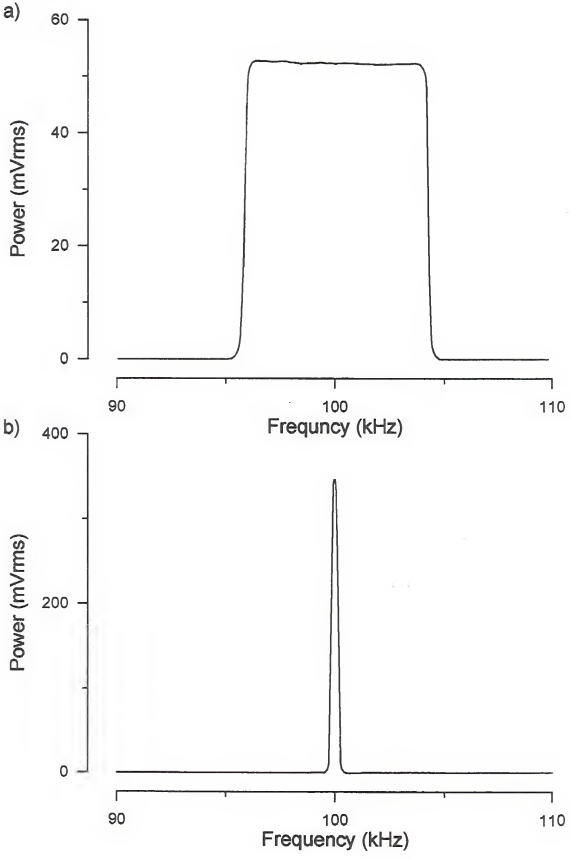
a)
60
40
20
0
Power (mVrms)
90
100
110
Frequncy (kHz)
b)
400
200
0
Power (mVrms)
90
100
110
Frequency (kHz)

meaning that ions that are moving at a particular frequency are excited in a phase continuous manner for the duration of the SWIFT pulse. As a result, the CID efficiency for SWIFT broadband excitation is comparable to single-frequency resonant excitation. The overall MS/MS efficiency, including the SWIFT broadband excitation step, is discussed in chapter 5 of this dissertation.

Qualitatively, SWIFT broadband excitation is simple to adjust and produces reliable CID spectra for GC/MS/MS experiments. The adjustment of the SWIFT excitation amplitude gives the same control over excitation energy that is observed for single frequency CID. Although the duration of the SWIFT excitation waveform is determined by the digitization rate and the number of data points in the SWIFT waveform, these values can be altered to increase or decrease the excitation time. Typical values for a 10 kHz wide SWIFT broadband excitation period are: digitization rate = 500 kHz, data points = 8192, waveform bursts = 3, and excitation amplitude 200-1000 mV. Interestingly, changing to a digitization rate of 1 MHz, 1024 data points, and a burst count of 39 appears to have little affect on the CID spectra that are observed. How these parameters influence ion activation in the ion trap has yet to be characterized. As a general rule, SWIFT settings that excite an ion for 10-50 ms are observed to produce the highest CID efficiencies for MS/MS.

## Summary

The frequency-assignment pre-scan, frequency-modulated broadband excitation, and SWIFT broadband excitation techniques described in this chapter have been developed to compensate for the frequency shifts that can reduce the CID efficiency as the number of ions in the ion trap change. The frequency-assignment

pre-scan is the only technique capable of measuring an ion's secular frequency of motion on the millisecond time scan. However, a disadvantage of this approach is the complexity of the scan function and additional scan time required by the pre-scan. Additionally, the technique has not been characterized in terms of sensitivity. Frequency-modulated broadband excitation has been demonstrated on a standard ITMS using modified instrument control software as a simple method for compensating for the frequency shifts that occur during GC/MS/MS experiments. Frequency-modulated broadband excitation exhibits reduced CID efficiencies and requires increased excitation times and amplitudes compared to manually optimized single frequency excitation. However, for GC/MS/MS experiments where manual optimization is infeasible, broadband excitation may result in higher CID efficiencies for GC/MS/MS because the overall CID efficiency remains constant as the ion's secular frequency of motion shifts. Finally, SWIFT is shown to be a versatile ion activation method capable of producing flat broadband excitation spectrum. This method can be implemented using commercial hardware with the availability of mathematical programming tools that simplify the development of SWIFT software. Of the three techniques described, broadband excitation using SWIFT pulses appears to offer the most potential for effecting ion activation in GC/MS/MS experiments.

# CHAPTER 5
# A BENCHTOP ION TRAP FOR GC/MS/MS

## Introduction

Chapters 2, 3, and 4 of this dissertation discuss several of the problems that have limited the extension of the ion trap's capabilities to include MS/MS on-line with chromatography. In general, these problems stem from the rapid fluctuations in partial pressure that occur as analytes elute out of the chromatographic column and pass into the mass analyzer. These dynamic pressure changes influence the proper adjustment of the ionization, isolation, ion activation, and ion detection parameters, and introduce the need for real-time optimization during a chromatographic run. Another problem that arises with GC sample introduction is that short GC peaks do not provide sufficient time for tuning the MS/MS scan program parameters, such as the RF amplitude and DC voltages used to isolate the parent m/z. For these reasons, most ion trap MS/MS experiments have utilized batch inlet systems instead of GC because they provide a constant flow of analyte that eliminates the need for real-time optimization and allows time for manual adjustment of the ion trap scan program.

This chapter describes the construction and characterization of an ion trap mass spectrometer that overcomes many of the problems that have restricted the ion trap's use for GC/MS/MS analyses. In this work, MS/MS capabilities were added to a commercial GC/MS ion trap so that GC/MS/MS experiments could be performed.

Instrument control software was developed that creates pre-tuned scan functions that include the ionization, isolation, fragmentation, and detection stages of EI and CI MS/MS experiments. The standard automatic ionization control techniques, AGC for EI and ARC for CI, were also adapted for GC/MS/MS so that samples that range from the low picogram to high nanogram levels could be analyzed with a single experiment. RF/DC ion isolation capabilities were added to the instrument to facilitate two-step isolation and other RF/DC techniques. Single frequency resonant excitation and SWIFT broadband excitation capabilities have been incorporated into the benchtop ion trap to provide a variety of ion activation techniques.

The performance of the new ion trap has been evaluated using standards and complex mixtures. A comparison of GC/MS and GC/MS/MS has been performed in terms of the linear dynamic range (LDR), limit of detection (LOD), and signal-to-noise (S/N) characteristics. The use of GC/MS/MS for complex mixture analysis is demonstrated using acylcarnitines present in liver tissue. Example results are also shown for the analysis of cocaine, petroleum, and barbiturate samples. Limitations of the current approach for GC/MS/MS are also discussed.

## Instrumentation

### GC/MS Hardware

The GC/MS/MS ion trap constructed for this study was based on the Finnigan MAT ITS-40 GC/MS ion trap. The primary components of the instrument include an A200S autosampler, a Varian model 3400 GC, and a microprocessor controlled ion trap detector. A one inch diameter heated stainless steel transfer line positions the end of the GC column inside the ion trap without the use of a splitter. The GC

components include a Varian 3400 splitless injector and a 30 meter 0.25 DB5-MS column with a helium carrier gas pressure of 9 psi. The ITS-40 ion trap electrodes share the same hyperbolic geometry ($r_o$ = 10.00 mm and $z_o$ = 7.07 mm) that are common to all of the commercial ion traps that are based the Finnigan MAT design. These electrodes are mounted in a stretched geometry ($z_o$ = 7.83 mm) with two quartz spacers placed between the endcap and ring electrodes. The analog signals applied to the ion trap are similar to those used on the ITD and ITMS instruments except that a drive and axial modulation frequency of 1.0 MHz and 485 kHz are used respectively. An Intel 80186C embedded microprocessor with 512 Kbytes of RAM is used to control the timing of the scan program, collect and centroid the mass spectral data, communicate with the host PC data system, and regulate the heater and vacuum systems.

Hardware Modifications

Figure 5-1 shows a block diagram of the ITS-40 instrument, including the hardware components that were added to implement MS/MS. A 3/4 inch i.d. cajon fitting was welded to the ITS-40 vacuum chamber to allow the connection of a Bayerd-Alpert type ion gauge (Granville Phillips). The location of the pressure gauge allows the pressure in the electron multiplier region of the vacuum system to be measured. The pressures (uncorrected for Helium) observed in this region without the addition of helium carrier gas is $1.2 \times 10^{-7}$ torr when the system is free of leaks. With the addition of helium carrier gas into the ion trap an observed gauge reading of $1.5 \times 10^{-5}$ torr was recorded. This corresponds to approximately $1.0 \times 10^{-3}$ torr within the ion trap when conductance limits and ion gauge correction factors are accounted for.

Figure 5-1. Block diagram of a modified ITS40 GC/MS/MS ion trap. Samples are injected into the gas chromatograph by an autosampler. Following chromatographic separation, samples elute into the ion trap where they are mass analyzed. MS/MS product ions scans are performed by the ion trap's embedded microprocessor and MS/MS software. The arbitrary waveform generator is used to produce the SWIFT broadband excitation signals that effect CID in the ion trap. The dipolar excitation circuit sums the SWIFT and axial modulation signals and splits the result into two signals that have a phase difference of 180 degrees. These signals are connected to the ion trap endcap electrodes. A personal computer provides a user interface to control the instrument and perform data processing.

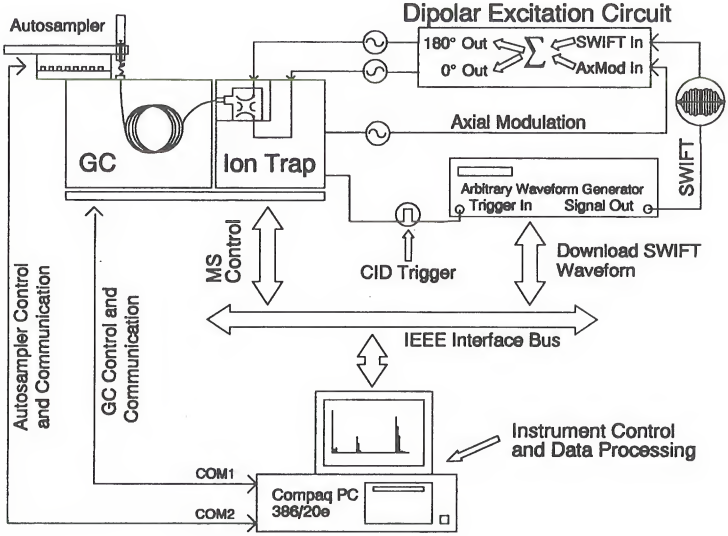
Dipolar Excitation Circuit
Autosampler
180° Out
0° Out
SWIFT In
AxMod In
Axial Modulation
GC
Ion Trap
Arbitrary Waveform Generator
Trigger In
Signal Out
SWIFT
MS Control
CID Trigger
Download SWIFT Waveform
Autosampler Control and Communication
GC Control and Communication
IEEE Interface Bus
Instrument Control and Data Processing
COM1
COM2
Compaq PC 386/20e

An active circuit was constructed to perform the mixing and phase inversion of axial modulation and SWIFT dipolar excitation signals. Figure 5-2 shows a schematic diagram of the circuit that consists of two operational amplifiers (AD488) that mix the supplementary AC voltages into two signals of equal magnitude that are phase shifted by 180°. These signals are then passed through two capacitors to remove residual DC offsets and are connected to the endcap electrodes. Two 4W 50 Ω ceramic resistors act as sinks, removing excess RF voltage that feeds back into the circuit through capacitive coupling of the ring and endcap electrodes. In practice, the AD488 operational amplifier must be connected to a large heat sink and cooled by forced air to protect the chip from overheating. An alternative high power/high speed operational amplifier (Apex PA09) could be used to eliminate the need for the extra cooling. However, these chips costs several hundreds dollars each while the AD488 cost less than five dollars and works reliably when it is cooled properly. The frequency response of the active dipolar excitation circuit remains flat from 10 kHz to 10 MHz and exhibits less than a 2° phase distortion between the two signal outputs. The maximum output amplitude for the circuit is 15 $V_{p\text{-}p}$.

The SWIFT excitation signal is produced by a commercial arbitrary waveform generator (Stanford Research Systems model# DS345) that is capable of generating a 16,000 point arbitrary waveform with digitization rates from 1 Hz to 40 MHz. The SWIFT arbitrary waveforms are downloaded from the personal computer (PC) to the DS345 via a general purpose interface bus (GPIB) that connects the data system PC, the ITS-40, and the DS345 arbitrary waveform generator. The amplitude, duration, and rate of the SWIFT waveform can be controlled from the front panel or via the GPIB interface. The synchronization of the SWIFT waveform with the timing of the scan

Figure 5-2. Schematic diagram of the active dipolar excitation circuit used to mix the supplementary AC voltages into two signals of equal magnitude that are phase shifted by 180°.

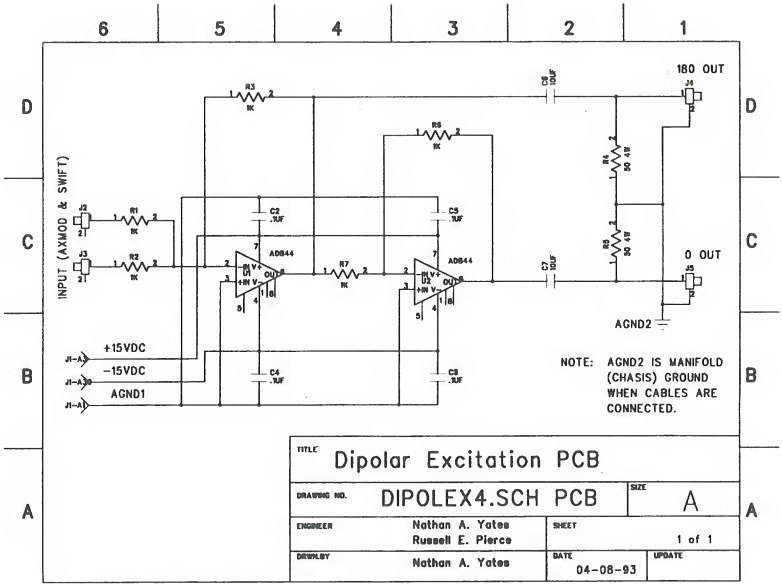
6
5
4
3
2
1
D
C
B
A
INPUT (AXMOD & SWIFT)
J3
J3
R1
1K
R2
1K
R3
1K
R6
1K
R7
1K
C2
.1UF
C5
.1UF
C4
.1UF
C3
.1UF
C6
10UF
C7
10UF
AD844
U1
AD844
U2
+IN V
-IN V
OUT
R4
90.4 1%
R5
90.4 1%
180 OUT
J4
0 OUT
J5
AGND2
+15VDC
-15VDC
AGND1
J1-A
NOTE: AGND2 IS MANIFOLD (CHASIS) GROUND WHEN CABLES ARE CONNECTED.
TITLE
Dipolar Excitation PCB
DRAWING NO.
DIPOLEX4.SCH PCB
SIZE
A
ENGINEER
Nathan A. Yates
Russell E. Pierce
SHEET
1 of 1
DRAWN BY
Nathan A. Yates
DATE
04-08-93
UPDATE

program is accomplished by a TTL trigger that is generated by ITS-40 scan acquisition processor electronics.

## Software

### Scan Editor and Acquisition Software

Software was written using the ITS-40 source code to allow the instrument's scan acquisition processor to implement the user defined EI and CI MS/MS scan programs utilized in these studies. In particular, a scan editor that is similar in function to the ITMS scan editor was developed. The ITS-40 firmware was modified to allow for the implementation of the scan programs that are created with the scan editor. In addition, the acquisition software, that coordinates the timing and control of the autosampler, GC, and MS for each scheduled injection, was modified to include the activation of multiple MS/MS scan function programs at particular times during a chromatographic separation.

Scan programs are created by linking scan tables together that specify the triggering, amplitude, frequency and duration of the voltages that are applied to the ion traps electrodes during each step of the scan program. Figure 5-3 shows the scan editor software interface that is used to created each step of the MS/MS scan programs on the ITS40. The user can chose to enter the RF and DC voltages with either the RF and DC DAC values directly, or have the program calculate the proper settings required to move a m/z to a particular point on the Mathieu stability diagram by entering $a_z$ and $q_z$ values. By controlling the RF and DC voltage in this fashion, a scan program can be automatically scaled to the m/z of interest by simply changing the m/z value in each scan table.

Figure 5-3. Screen captures for the scan editor software interface used to create AGC-EI/MS/MS and ARC-CI/MS/MS scan programs. Scan tables 12 (left) and 14 (right) show the RF ramp and DC pulse tables used in the AGC-EI/MS/MS product ion scan program for m/z 182.

RF ramp Table

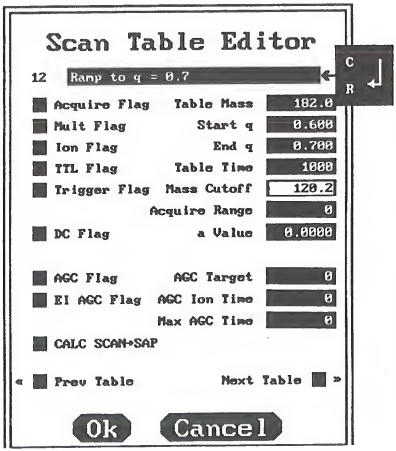


RF/DC Table

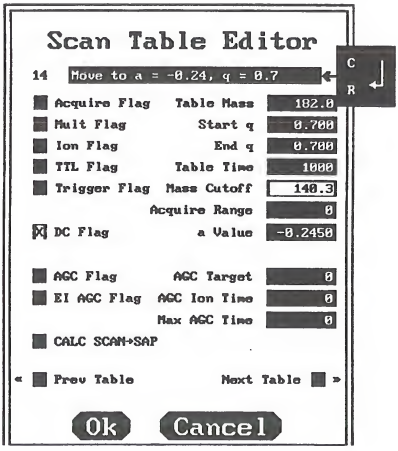

Table 5-1. AGC-EI/MS/MS scan program list.

| # | Table Comment | m/z | Start $q_z$ | End $q_z$ | Start DAC | End DAC | DCV $a_z$ | Time ms | Misc. |
|---|---|---|---|---|---|---|---|---|---|
| 1 | trigger-agc | | | | 0 | 0 | | 0 | |
| 2 | pre-ion-agc | | | | 125 | 125 | | 2.96 | |
| 3 | ionize-agc | | | | 125 | 125 | | 3.94 | gate on |
| 4 | post-ion-agc | | | | 125 | 125 | | 4.08 | |
| 5 | mult-on-agc | | | | 125 | 316 | | 5.09 | |
| 6 | acquire-agc | | | | 316 | 4095 | | 6.86 | gate on |
| 7 | trigger | 182 | 0.00 | 0.00 | 0 | 0 | | 8.28 | calc |
| 8 | pre-ion | 182 | 0.13 | 0.13 | 125 | 125 | | 8.42 | |
| 9 | ionize | 182 | 0.13 | 0.13 | 125 | 125 | | 8.62 | gate on |
| 10 | post-ion | 182 | 0.13 | 0.13 | 125 | 125 | | 13.60 | |
| 11 | RF ramp 1 | 182 | 0.13 | 0.60 | 125 | 591 | | 13.91 | |
| 12 | RF ramp 2 | 182 | 0.60 | 0.70 | 591 | 651 | | 14.92 | |
| 13 | pause | 182 | 0.70 | 0.70 | 651 | 651 | | 15.40 | |
| 14 | high m/z ejct. | 182 | 0.70 | 0.70 | 651 | 651 | -.245 | 15.90 | DC on |
| 15 | RF ramp 3 | 182 | 0.07 | 0.85 | 651 | 790 | | 17.38 | |
| 16 | pause | 182 | 0.85 | 0.85 | 790 | 790 | | 17.92 | |
| 17 | low m/z ejct. | 182 | 0.85 | 0.85 | 790 | 790 | 0.008 | 18.42 | DC on |
| 18 | RF ramp 4 | 182 | 0.85 | 0.30 | 790 | 278 | | 20.91 | |
| 19 | SWIFT-CID | 182 | 0.30 | 0.30 | 278 | 278 | | 21.42 | TTL on |
| 20 | mult-on | 182 | 0.30 | 0.30 | 278 | 278 | | 61.48 | |
| 21 | acquire | | | | 258 | 1688 | | 63.50 | data on |
| 22 | shut down | | | | 0 | 0 | | 103.76 | |

Figure 5-4 and Table 5-1 show the timing diagram and scan table listing for the AGC-EI/MS/MS scan program that was used in these studies. For GC/MS experiments, standard scan programs, as created by the commercial ITS-40, were used. Scan tables 1-6 consist of the trigger, pre-ionization, ionization, post-ionization,

Figure 5-4. Ion trap scan program used to acquire GC/MS/MS EI mass spectra on a modified ITS40. The AGC pre-scan (A) sets the ionization time used during period I, the parent ion is mass selected using two-step RF/DC isolation during period M, CID is accomplished during period C with three SWIFT broadband excitation bursts that excite a 10 kHz range of frequencies from 102 kHz - 112 kHz, and the resulting product ions are mass analyzed during period S. A supplementary AC voltage frequency of 485 kHz is applied during period S to effect axial modulation.

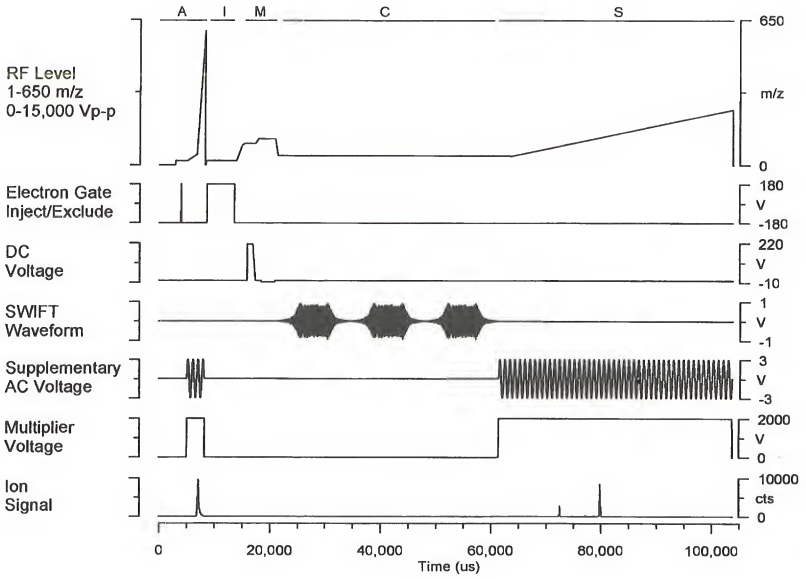
A
I
M
C
S
RF Level
1-650 m/z
0-15,000 Vp-p
650
m/z
0
Electron Gate
Inject/Exclude
180
V
-180
DC
Voltage
220
V
-10
SWIFT
Waveform
1
V
-1
Supplementary
AC Voltage
3
V
-3
Multiplier
Voltage
2000
V
0
Ion
Signal
10000
cts
0
0
20,000
40,000
60,000
80,000
100,000
Time (us)

multiplier warm up/background mass ejection, acquisition, end, and calculation tables that make up the AGC pre-scan. Briefly, the relative number of ions formed by the 200μs ionization time employed in scan table 3 are measured using the 25,000 u/s RF ramp acquisition shown in scan table 6. Scan table five serves to eject low m/z ions below a variable "background m/z" prior to the AGC acquisition. Scan table 7 estimates the ionization time required to increase the observed ion signal to the "target value" shown in scan table 6. Scan tables 8-11 perform the trigger, pre-ionization, ionization, and post-ionization steps of the MS/MS scan, using the ionization time that was determined by the AGC pre-scan. Scan tables 12-19 are used to implement the sequence of RF ramps, DC pulses, and pause tables that make up the two-step isolation stage of the MS/MS scan. The pause tables that follow the RF ramps and the DC pulses decrease ion losses by allowing the ions trajectories to stabilize prior to moving onto the next stage of the scan. Scan tables 20-21 consist of an RF ramp table to bring the parent ion of interest to the $q_z$ (0.3) used for resonant excitation, and a SWIFT-CID table that triggers the arbitrary waveform via a TTL signal. Typical amplitudes and durations of the SWIFT signal were 0.5-1.5 $V_{p-p}$ and 10-40 ms respectively. Scan tables 22-24 perform the multiplier warm up procedure, acquire the mass spectrum of the daughter ions, and end the scan program by setting the applied voltages to zero prior to resetting the MS/MS scan program back to scan table 1. The acquisition table acquires the daughter spectrum at a rate of 5,500 u/s with an axial modulation frequency of 485 kHz.

The scan repetition rate for m/z 182 product ion scan is 8 microscans/s. The data for each microscan are averaged and the resulting analytical scan is centroided and written to the data system. Higher scan repetition rates are typically observed

with MS/MS scan programs relative to full scan EI and CI scan programs because a narrower mass range is acquired.

SWIFT Software

The algorithm used to implement SWIFT has been described in chapter 4 of this dissertation. Briefly, the SWIFT technique calculates the time domain waveform for a tailored frequency domain spectrum by use of the inverse fast Fourier transform (IFFT). Quadratic phase modulation is applied to the frequency domain spectrum prior to performing the IFFT to reduce the dynamic range. The resulting time domain waveform is reflected about its midpoint and apodization of the ends of the waveform is performed with a quarter sine wave window function. Next, the digital waveform that contains the amplitude vs. time data is transferred to the waveform memory of the arbitrary waveform generator. Several seconds are required to transfer a 8192 point waveform over the GPIB.

Software Integration

The modified ITS-40 instrument control software adds the ability to create and execute complex ion trap scan programs that include AGC, two-step isolation, and SWIFT broadband excitation into a computer controlled benchtop GC/MS/MS instrument. The total software control of the autosampler, gas chromatograph, and ion trap mass spectrometer not only simplifies the daily operation of the instrument but provides a means for evaluating the feasibility of this benchtop instrument for performing routine GC/MS/MS analyses automatically.

## Experimental

The instrumental performance of the new GC/MS/MS ion trap was characterized using pure standards and complex mixtures. GC/MS results were also obtained to allow comparison of GC/MS and GC/MS/MS modes of operation. The relevant experimental parameters and key instrumental settings for each set of experiments are outlined in the following sections.

### AGC-EI Calibration Studies

A stock benzophenone solution was prepared by dissolving 18.7 mg of benzophenone in 10 mL of hexane to produce a concentration of 1.87 µg/µL. Eleven calibration standards ranging in concentration from 530 ng/uL to 1.9 pg/uL were prepared by serial dilution 200:700 (v:v). Each standard was prepared in an 800 µL glass vial, sealed with a teflon lined rubber septa and cap, and stored in a freezer to minimize evaporative sample losses prior to use.

Each calibration standard was analyzed 21 times using three ion trap scan programs. Injections 1-7 were analyzed with a standard AGC-EI/MS scan program that collects full scan EI mass spectra from 60 u to 300 u. Injections 8-14 were analyzed with a custom AGC-EI/ISO/MS scan program that included the necessary scan tables to isolate ions between m/z 181 and m/z 183. Injections 15-21 were analyzed with an AGC-EI/MS/MS scan program that included the necessary scan tables required to isolate and fragment ions between m/z 181 and m/z 183. Identical scan tables were used for ionization so that the initial number of ions generated in each of the three scan modes would remain constant for a given sample amount.

Two-step isolation and SWIFT broadband excitation were used to mass select and fragment the parent ions.

Table 5-2 contains the principal acquisition, MS, MS/MS, autosampler, and GC parameters used for the AGC-EI analysis of benzophenone. The samples were analyzed in order of increasing concentration to prevent contamination of the GC injection port by the high concentration standards. Eight clean cycles, containing both solvent flush and sample conditioning steps, were performed between each injection to minimize sample carryover. Ten blank solvent injections were performed at the start and end of the autosampler/acquisition sequence to characterize the background signals and check the column baseline.

For each set of benzophenone standards, a total of 250 GC analyses were performed over a 42 hour period. Automated instrument control software carried out all of the steps involved in the data acquisition process for each vial in the autosampler tray. Post acquisition data processing of the resulting mass chromatographic data was performed manually using the ITS-40's quantitation software to integrate the chromatographic peaks. Peak area and sample amount data was exported from the calibration files and read into a commercial spreadsheet program, Quattro Pro (Borland International Inc., Scotts Valley, CA), that was used to calculate average peak areas and standard deviations. Calibration curves and best fit lines were generated from this spreadsheet data using a commercial graphing package, GRAPHER™ for WINDOWS (Golden Software Inc., Golden, CO).

Table 5-2. AGC-EI parameters for the analysis of benzophenone.

| Acquisition Parameters | |
|---|---|
| Multiplier voltage | -2150 V |
| Manifold temperature | 220 °C |
| Emission current | 100 µA |
| Axial modulation | 485 kHz, 5.0 $V_{p-p}$ |
| Ionization mode | EI |
| Ionization control | automatic |
| Target value | 20,000 |
| Background m/z | 60 u |
| Acquire time | 8 min |
| Filament delay | 200 s |
| Scan acquisition rate | 1000 ms/scan |
| **MS Scan Mode Parameters** | |
| Low m/z | 60 u |
| High m/z | 300 u |
| **MS/MS Scan Mode Parameters** | |
| Low m/z | 60 u |
| High m/z | 250 u |
| SWIFT excitation | 9 bursts, 0.50 $V_{p-p}$, 37 ms |
| SWIFT pattern | 4096 pts, 1 MHz, 107-117 kHz |
| **Autosampler Parameters** | |
| Sample volume | 1.0 µL |
| Air volume | 2.0 µL |
| Clean cycles | 8 counts |
| **GC Parameters** | |
| Column temperature segment 1 | 60 °C, 0.0 °C/min, 1.06 min |
| Column temperature segment 2 | 60 °C, 50.0 °C/min, 3.00 min |
| Column temperature segment 3 | 210 °C, 6.8 °C/min, 2.94 min |
| Column temperature segment 4 | 230 °C, 0.0 °C/min, 1.00 min |
| Injector temperature | 260 °C, 0.0 °C/min, 8.00 min |
| Transfer line temperature | 280 °C, 0.0 °C/min, 8.00 min |
| Splitter valve state 1 | open, T = 0.00 min |
| Splitter valve state 2 | closed, T = 0.01 min |
| Splitter valve state 3 | open, T = 0.70 min |

ARC-CI Calibration Studies

The standards used to generate the CI benzophenone calibration curve were prepared using the same procedure that was used for the EI benzophenone calibration curve. Each standard was injected fifteen times; five ARC-CI/MS, five ARC/CI/ISO/MS, and five ARC-CI/MS/MS acquisitions. Table 5-3 summarizes the instrumental parameters used to collect the CI calibration curve data. The post acquisition data processing was performed with the same procedure used to generate the EI calibration curves.

Fixed Ionization Time Studies

A 6.8 pg/μL benzophenone sample was subjected to EI/MS and EI/MS/MS analyses using variable (AGC) and fixed (150 ms) ionization times respectively. Table 5-4 summarizes the instrumental parameters used for both acquisitions. For the AGC-EI/MS experiment, the average ionization time employed during the elution of the benzophenone was approximately 9.8 ms.

Carnitine Analyses

The analysis of carnitine and acylcarnitines (referred to here as carnitines) by GC/MS involves the formation of tertiarybutyldimethylsilyl (TBDMS) and trimethylsilyl (TMS) carnitine derivatives so that the compounds will have sufficient volatility to pass through the GC. Derivatization of the carnitines used in these studies was performed by the Metabolic Assessment Laboratory, Food Science and Human Nutrition Department, University of Florida, using the procedure reported by Huang.[124]

Table 5-3. ARC-CI parameters for the analysis of benzophenone.

| Acquisition Parameters | |
|---|---|
| Multiplier voltage | -2200 V |
| Manifold temperature | 220 °C |
| Emission current | 10 μA |
| Axial modulation | 485 kHz, 5.0 $V_{p-p}$ |
| Ionization mode | CI, methane |
| Ionization control | automatic |
| Target value | 15,000 |
| Background m/z | 45 u |
| Acquire time | 7 min |
| Filament delay | 200 s |
| Scan acquisition rate | 700 ms/scan |
| **MS Scan Mode Parameters** | |
| Low m/z | 50 u |
| High m/z | 300 u |
| **MS/MS Scan Mode Parameters** | |
| Low m/z | 60 u |
| High m/z | 250 u |
| SWIFT excitation | 9 bursts, 0.40 $V_{p-p}$, 37 ms |
| SWIFT pattern | 4096 pts, 1 MHz, 107-117 kHz |
| **Autosampler Parameters** | |
| Sample volume | 1.0 μL |
| Air volume | 2.0 μL |
| Clean cycles | 8 counts |
| Injection delay | 3 s |
| **GC Parameters** | |
| Column temperature segment 1 | 60 °C, 0.0 °C/min, 1.00 min |
| Column temperature segment 2 | 60 °C, 50.0 °C/min, 3.00 min |
| Column temperature segment 3 | 210 °C, 6.8 °C/min, 2.94 min |
| Injector temperature | 260 °C, 0.0 °C/min, 8.00 min |
| Transfer line temperature | 280 °C, 0.0 °C/min, 8.00 min |
| Splitter valve state 1 | open, T = 0.00 min |
| Splitter valve state 2 | closed, T = 0.01 min |
| Splitter valve state 3 | open, T = 0.70 min |

Table 5-4. Fixed EI parameters for the analysis of benzophenone.

| Acquisition Parameters | |
|---|---|
| Multiplier voltage | -2200 V |
| Manifold temperature | 220 °C |
| Emission current | 100 µA |
| Axial modulation | 485 kHz, 5.0 $V_{p-p}$ |
| Ionization mode | EI |
| Ionization control | automatic (MS), fixed (MS/MS) |
| Target value | 10,000 (MS) |
| Background m/z | 50 u |
| Acquire time | 7 min |
| Filament delay | 200 s |
| Scan acquisition rate | 1000 ms/scan |
| **MS Scan Mode Parameters** | |
| Low m/z | 50 u |
| High m/z | 300 u |
| **MS/MS Scan Mode Parameters** | |
| Low m/z | 60 u |
| High m/z | 250 u |
| SWIFT excitation | 9 bursts, 0.60 $V_{p-p}$, 37 ms |
| SWIFT pattern | 4096 pts, 1 MHz, 107-117 kHz |
| **Autosampler Parameters** | |
| Sample volume | 1.0 µL |
| Air volume | 2.0 µL |
| Clean cycles | 8 counts |
| Injection delay | 3 s |
| **GC Parameters** | |
| Column temperature segment 1 | 60 °C, 0.0 °C/min, 1.00 min |
| Column temperature segment 2 | 60 °C, 50.0 °C/min, 3.00 min |
| Column temperature segment 3 | 210 °C, 6.8 °C/min, 2.94 min |
| Injector temperature | 260 °C, 0.0 °C/min, 8.00 min |
| Transfer line temperature | 280 °C, 0.0 °C/min, 8.00 min |
| Splitter valve state 1 | open, T = 0.00 min |
| Splitter valve state 2 | closed, T = 0.01 min |
| Splitter valve state 3 | open, T = 0.70 min |

Carnitine standards were prepared by dissolving 1 mg of carnitine in 2 mL of 1:1 (v:v) MeOH/$CHCl_3$ solution. Table 5-5 contains the names, abbreviations, molecular weights, and on-column derivatized molecular weights for the carnitine standards that were analyzed by GC/MS and GC/MS/MS.

A silation cocktail is prepared by mixing 20 μL of N-(tert-butyldimethylsilyl)-methyltrifluoroacetamide (MTBSTFA), 2 μL of 10% 2,2-dimethoxypropane (DMP) in $CH_2Cl_2$, 4 μL of 10% 2,4,6-trimethyl-pyridine (TMP) in $CH_2Cl_2$, and 2 μL of 10% trimethyliodosilane (TMIS) in $CH_2Cl_2$. For samples containing longer chain acylcarnitines (C>10) 2-4 μL of N-methyl-N-(trimethylsilyl)trifluoroacetamide (MSTFA) is added to the silation cocktail to promote complete conversion of the acylcarnitines to their TBDMS and TMS derivatives.

Liquid samples were prepared by transferring a 100 μL aliquot to an autosampler vial and allowing the sample to dry for 2 h in a vacuum desiccator over $P_2O_5$/NaOH. Tissue samples were subject to homogenization, methanol/chloroform extraction, and centrifugation prior to being dried over $P_2O_5$/NaOH. Derivatization of the dried samples was performed by adding 25 μL of freshly prepared silation cocktail and allowing each sample to stand at room temperature for five minutes. Derivatives stored for extended period of time were kept in a freezer. Carnitine standards and samples were further diluted 1:100 in methylene chloride prior to analysis.

Table 5-6 contains the principal acquisition, MS, MS/MS, autosampler, and GC parameters used in the carnitine analysis. Injection amounts specified for each standard assume complete derivatization and no sample losses.

Table 5-5. Summary of carnitine test mixture.

| Compound | Abbreviation | MW | On-column MW |
|---|---|---|---|
| carnitine | C | 162 | 375 |
| carnitine chloride | CC | 197 | 375 |
| acetyl-carnitine | AC | 174 | 303 |
| propionyl-carintine | PP | 188 | 317 |
| isobutyral-carnitine | B | 202 | 331 |
| α-methyl butyryl-carnitine | a | 216 | 345 |
| isovaleryl-carnitine | V | 216 | 345 |
| octanoyl-carnitine | O | 258 | 387 |
| palmitoyl-carnitine | PM | 370 | 499 |

ARC-CI Cocaine Analyses

Cocaine standards and hair samples that were spiked with the deuterated drug ($d_3$-cocaine) were supplied by Dr. Henry Scholtz of Psychemedics (Culver City, CA 90230). The concentration of five cocaine standards ranged from 0.1 ng/μL to 2.5 ng/μL, each containing 0.5 ng/μL of the deuterated internal standard. Hair samples were extracted from an enzyme digest. The total sample volume for each sample was 20 μL. Table 5-7 contains the principal acquisition, MS, MS/MS, autosampler, and GC parameters used for the cocaine analysis. The accidental use of 10 clean cycles for the initial injections caused 15 μL of each sample to be lost in the sample waste container.

AGC-EI Petroleum Analyses

Table 5-8 contains a summary of the instrumental parameters used for the analysis of several petroleum samples. Kerosene, gasoline, and oil samples were

Table 5-6. Summary of instrument parameters for the analysis of carnitine.

| | |
|---|---|
| **Acquisition Parameters** | |
| Multiplier voltage | -1950 V |
| Manifold temperature | 220 °C |
| Emission current | 100 µA |
| Axial modulation | 485 kHz, 3.5 $V_{p-p}$ |
| Ionization mode | EI |
| Ionization control | automatic |
| Target value | 25,000 |
| Background m/z | 50 u |
| Acquire time | 13 min |
| Filament delay | 250 s |
| Scan acquisition rate | 1000 ms/scan |
| **MS Scan Mode Parameters** | |
| Low m/z | 40 u |
| High m/z | 650 u |
| **MS/MS Scan Mode Parameters** | |
| Low m/z | 60 u |
| High m/z | 375 u |
| SWIFT excitation | 4 bursts, 1.20 $V_{p-p}$, 37 ms |
| SWIFT pattern | 4096 pts, 500 kHz, 107-117 kHz |
| **Autosampler Parameters** | |
| Sample volume | 2.0 µL |
| Air volume | 2.0 µL |
| Clean cycles | 10 counts |
| Injection delay | 3 s |
| **GC Parameters** | |
| Column temperature segment 1 | 120 °C, 0.0 °C/min, 2.00 min |
| Column temperature segment 2 | 120 °C, 20.0 °C/min, 9.50 min |
| Column temperature segment 3 | 310 °C, 0.0 °C/min, 1.5 min |
| Injector temperature | 260 °C, 0.0 °C/min, 13.00 min |
| Transfer line temperature | 280 °C, 0.0 °C/min, 13.00 min |
| Splitter valve state 1 | open, T = 0.00 min |
| Splitter valve state 2 | closed, T = 0.01 min |
| Splitter valve state 3 | open, T = 0.50 min |

Table 5-7. Summary of parameters for the analysis of cocaine.

| | |
|---|---|
| **Acquisition Parameters** | |
| Multiplier voltage | -1950 V |
| Manifold temperature | 220 °C |
| Emission current | 10 μA |
| Axial modulation | 485 kHz, 3.5 $V_{p-p}$ |
| Ionization mode | CI, methane |
| Ionization control | automatic |
| Target value | 25,000 |
| Background m/z | 50 u |
| Acquire time | 13 min |
| Filament delay | 250 s |
| Scan acquisition rate | 1000 ms/scan |
| **MS Scan Mode Parameters** | |
| Low m/z | 180 u |
| High m/z | 370 u |
| **MS/MS Scan Mode Parameters** | |
| Low m/z | 60 u |
| High m/z | 375 u |
| SWIFT excitation | 9 bursts, 0.60 $V_{p-p}$, 37 ms |
| SWIFT pattern | 4096 pts, 1 MHz, 107-117 kHz |
| **Autosampler Parameters** | |
| Sample volume | 1.5 μL |
| Air volume | 2.0 μL |
| **GC Parameters** | |
| Column temperature segment 1 | 120 °C, 0.0 °C/min, 1.00 min |
| Column temperature segment 2 | 120 °C, 35.0 °C/min, 2.85 min |
| Column temperature segment 3 | 220 °C, 0.0 °C/min, 0.25 min |
| Column temperature segment 4 | 220 °C, 10.0 °C/min, 3.00 min |
| Column temperature segment 5 | 250 °C, 0.0 °C/min, 4.00 min |
| Column temperature segment 6 | 250 °C, 25.0 °C/min, 2.40 min |
| Injector temperature | 260 °C, 0.0 °C/min, 13.00 min |
| Transfer line temperature | 250 °C, 0.0 °C/min, 13.00 min |
| Splitter valve state 1 | open, T = 0.00 min |
| Splitter valve state 2 | closed, T = 0.01 min |
| Splitter valve state 3 | open, T = 0.50 min |

Table 5-8. ARC-EI parameters for the analysis of petroleum.

| Acquisition Parameters | |
|---|---|
| Multiplier voltage | -2150 V |
| Manifold temperature | 220 °C |
| Emission current | 100 µA |
| Axial modulation | 485 kHz, 3.5 $V_{p-p}$ |
| Ionization mode | EI |
| Ionization control | automatic |
| Target value | 10,000 |
| Background m/z | 60 u |
| Acquire time | 23 min |
| Filament delay | 175 s |
| Scan acquisition rate | 700 ms/scan |
| **MS Scan Mode Parameters** | |
| Low m/z | 50 u |
| High m/z | 400 u |
| **MS/MS Scan Mode Parameters** | |
| Low m/z | 45 u |
| High m/z | 400 u |
| SWIFT excitation | 9 bursts, 0.90 $V_{p-p}$, 37 ms |
| SWIFT pattern | 4096 pts, 1 MHz, 107-117 kHz |
| **Autosampler Parameters** | |
| Sample volume | 1.0 µL |
| Air volume | 2.0 µL |
| Clean cycles | 4 counts |
| Injection delay | 3 s |
| **GC Parameters** | |
| Column temperature segment 1 | 50 °C, 0.0 °C/min, 1.00 min |
| Column temperature segment 2 | 50 °C, 10.0 °C/min, 21.00 min |
| Column temperature segment 3 | 260 °C, 0.0 °C/min, 1.00 min |
| Injector temperature | 260 °C, 0.0 °C/min, 23.00 min |
| Transfer line temperature | 280 °C, 0.0 °C/min, 23.00 min |
| Splitter valve state 1 | open, T = 0.00 min |
| Splitter valve state 2 | closed, T = 0.01 min |
| Splitter valve state 3 | open, T = 0.70 min |

prepared by diluting each petroleum sample in hexane. The final sample dilution factor was 1:100 (v:v).

ARC-CI Barbiturate Analyses

A barbiturate standards mixture containing 1 μg/μL of barbital (MW = 184), butobarbital (MW = 212), amobarbital (MW = 226), pentobarbital (MW = 226), and secobarbital (MW = 238) was purchased from Merck. The standards were diluted with hexane 1:100 (v:v) and subject to GC/MS and GC/MS/MS analysis using the instrumental parameters contained in Table 5-9.

## Results and Discussion

The performance of the GC/MS/MS ion trap developed in this work has been evaluated by a series of experiments. Benzophenone standards were used to characterize the limit of detection, sensitivity, and linear dynamic range of the instrument for several operation modes including EI, CI, MS, and MS/MS. Example analyses were also performed on acylcarnitine, cocaine, petroleum, and barbiturate samples to test the selectivity and applicability of ion trap GC/MS/MS for a variety of samples. The results of each of these experiments are summarized in the following sections.

Benzophenone was used as a test compound to measure the performance of the ion trap's EI/MS/MS and CI/MS/MS capabilities because it exhibited sufficient $M^+$ and $[M+H]^+$ intensity for CI and EI MS/MS studies. Both the molecular ion and the protonated benzophenone were chosen for CID experiments because they could be isolated without fragmentation and dissociated with resonant excitation techniques.

Table 5-9. Summary of parameters for the analysis of barbiturates.

| Acquisition Parameters | |
|---|---|
| Multiplier voltage | -2150 V |
| Manifold temperature | 220 °C |
| Emission current | 10 μA |
| Axial modulation | 485 kHz, 3.5 $V_{p-p}$ |
| Ionization mode | CI, methane |
| Ionization control | automatic |
| Target value | 5,000 |
| Background m/z | 50 u |
| Acquire time | 8 min |
| Filament delay | 300 s |
| Scan acquisition rate | 1000 ms/scan |
| **MS Scan Mode Parameters** | |
| Low m/z | 50 u |
| High m/z | 301 u |
| **MS/MS Scan Mode Parameters** | |
| Low m/z | 50 u |
| High m/z | 301 u |
| SWIFT excitation | 9 bursts, 0.80 $V_{p-p}$, 37 ms |
| SWIFT pattern | 4096 pts, 1 MHz, 107-117 kHz |
| **Autosampler Parameters** | |
| Sample volume | 1.0 μL |
| Air volume | 2.0 μL |
| Clean cycles | 15 counts |
| **GC Parameters** | |
| Column temperature segment 1 | 50 °C, 0.0 °C/min, 1.00 min |
| Column temperature segment 2 | 50 °C, 50.0 °C/min, 3.80 min |
| Column temperature segment 3 | 240 °C, 15.0 °C/min, 2.00 min |
| Column temperature segment 4 | 270 °C, 10.0 °C/min, 1.20 min |
| Injector temperature | 280 °C, 0.0 °C/min, 8.00 min |
| Transfer line temperature | 280 °C, 0.0 °C/min, 8.00 min |
| Splitter valve state 1 | open, T = 0.00 min |
| Splitter valve state 2 | closed, T = 0.01 min |
| Splitter valve state 3 | open, T = 0.50 min |

Some ions, such as those observed for alkanes, fragment so readily that it is difficult to isolate them without dissociation. It is important to note that the EI and CI MS/MS calibration curves that were generated in this study represent the first detailed look at the linearity of MS/MS on the quadrupole ion trap. Previous studies have relied on the use of internal standards to eliminate non-linearities from MS/MS experiments

AGC-EI Calibration Studies

Figure 5-5 shows the EI mass spectrum for the injection of 3.5 ng of benzophenone (MW = 182). The base peak at m/z 105 corresponds to ionized benzophenone that has lost a neutral phenyl group. Alternatively, the ion at m/z 77 corresponds to the loss of a positively charged phenyl group from ionized benzophenone. An intense molecular ion at m/z 182 is also observed in the EI mass spectrum for benzophenone. The peak at m/z 51 appears throughout the chromatographic separation and is believed to be due to the presence of residual solvent in the injection port. The smaller ions surrounding the molecular ion were not definitively identified. However, the peak at m/z 183 is a combination of the protonated benzophenone and the contribution of the $^{13}C$ isotope. The peak observed at m/z 181 may be the result of a rearrangement followed by the loss of hydrogen. The low intensity ions near m/z 152 have been previously identified as the biphenylene ion which is formed by rearrangement and loss of neutral CO.[125] In general, the full scan EI spectrum obtained with the ion trap is comparable to benzophenone spectra obtained on other types of mass spectrometers.

The MS/MS product ion spectrum for m/z 182 of benzophenone is shown in Figure 5-6. Two-step isolation was used to isolate a 3 u window covering m/z 181 to

Figure 5-5. Background subtracted AGC-EI/MS spectrum of 3.56 ng of benzophenone (MW = 182) and structure showing fragmentation of the carbon-carbon bond $\alpha$ to the carbonyl to yield the two major fragment ions.

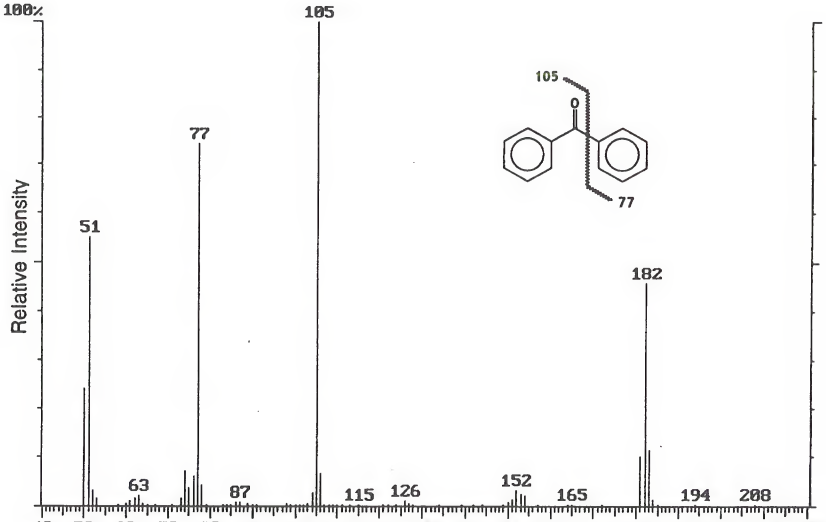
100%
105
77
51
182
63
87
115
126
152
165
194
208
Relative Intensity
40 50 60 70 80 90 100 110 120 130 140 150 160 170 180 190 200 210 220
m/z
105
O
77

Figure 5-6. Background subtracted AGC-EI/MS/MS $182^+$ product ion spectrum of 3.56 ng of benzophenone (MW = 182).

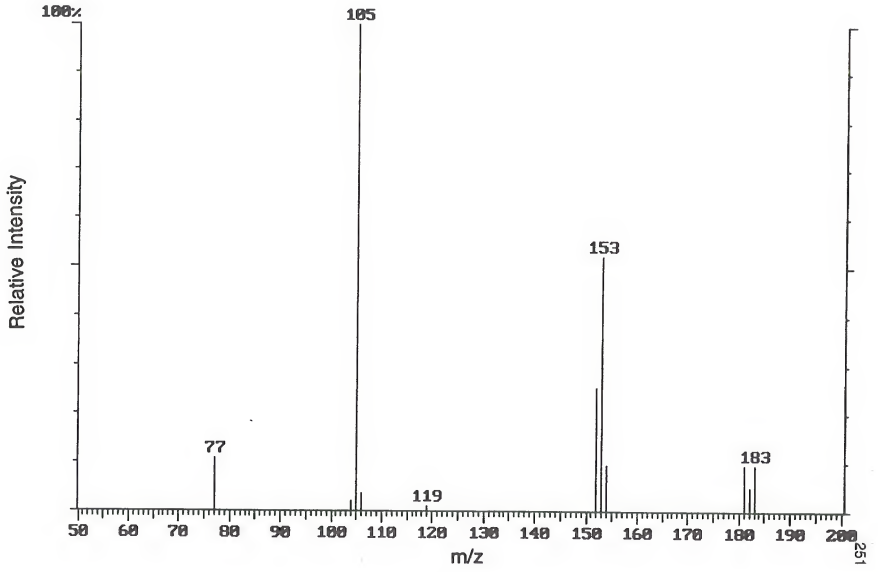
100%
105
153
77
183
119
Relative Intensity
50 60 70 80 90 100 110 120 130 140 150 160 170 180 190 200
m/z
251

m/z 183 prior to broadband excitation of m/z 182. Although it was possible to completely isolate m/z 182 and eject m/z 181 and m/z 183, large losses in parent ion signal were observed. The inability of the two-step isolation method to isolate a single m/z contradicts results discussed in chapter 3 that were obtained with the ITMS instrument. It is believed that the difficulties associated with isolating a single m/z on the modified ITS-40 were due to an error in the MS/MS software. The RF drive frequency used to calculate the Mathieu parameters was entered incorrectly, and created errors in the instruments $a_z$ and $q_z$ calculations. This error was corrected after the data for this manuscript was collected. Broadband excitation using the SWIFT technique was employed to excite a 10 kHz wide frequency range centered at 112 kHz which correspond to a 1.7 u wide mass range centered at m/z 182. Interestingly, the intensity of the parent ion, m/z 182, is lower than the intensity of the peaks at m/z 181 and m/z 183. This indicates that although SWIFT broadband excitation excites more than a single u, it can be utilized as a selective excitation technique.

The product ions observed for $182^+$ include $77^+$, $105^+$, and $153^+$. As was observed in the full scan EI mass spectrum (Figure 5-5), the $77^+$ and $105^+$ ions, $C_6H_5^+$ and $C_6H_5CO^+$, arise from cleavage $\alpha$ to the carbonyl; the $152^+$, $153^+$, and $154^+$ ions, $C_{12}H_8^+$, $C_{12}H_9^+$, and $C_{12}H_{10}^+$, arise from rearrangement and loss of $H_2CO$, HCO, and CO. The rearrangement ions are observed as the major ions in the CID spectrum, compared to the full scan spectrum. Also, the peak at m/z 51 in the full scan mass spectrum is not observed in the product ion spectrum for m/z 182. While this suggests that it is not a benzophenone fragment ion, $51^+$ could be formed by a high energy fragmentation pathway that is not accessed by the limited energy deposited by

resonant excitation. Compared to the full scan mass spectrum, the product ion spectrum contains fewer spurious peaks and exhibits a higher S/N ratio.

Figure 5-7 shows the AGC-EI/MS, AGC-EI/ISO, and AGC-EI/MS/MS calibration curves that were obtained for benzophenone standards that range in concentration from 1.9 pg/μL to 530 ng/μL. The AGC-EI/MS data points represent the chromatographic peak area for the molecular ion, m/z 182, that was obtained with a standard AGC-EI segmented scan program. The AGC-EI/ISO/MS data points correspond to the chromatographic peak area for ions between m/z 182 and m/z 183 that were detected with an AGC-EI scan program that included the isolation of ions between m/z 181 and m/z 183. The AGC-EI/MS/MS data points show the chromatographic peak area for the product ions $77^+$, $105^+$, and $153^+$ that was measured using an AGC-EI/MS/MS scan program. For each sample amount, the number of ions formed in the trap during ionization was held constant regardless of the scan mode that was used. Thus, the differences in the number of ions detected reflects the ion losses that occurred as a result of the different scan modes.

Comparison of the AGC-EI/MS and AGC-EI/ISO/MS calibration curves in Figure 5-7 demonstrates that the efficiency of isolation, $E_{iso}$, for two-step isolation of m/z 182 is approximately 95 % when a 3 u wide isolation window is selected. The sum of the peak areas for m/z 182 and m/z 183 were plotted for the AGC-EI/ISO/MS results to compensate for the conversion of $182^+$ to $183^+$ that is caused by self-CI. Large sample amounts combined with the longer ion storage times used in AGC-EI/ISO/MS scans programs increase the probability of ion-molecule reaction processes like self-CI.

Comparison of the AGC-EI/ISO/MS and AGC-EI/MS/MS calibration curves shown in Figure 5-7 demonstrates that the overall collision induced dissociation

Figure 5-7. Calibration curve for benzophenone (MW = 182). Each data point represents seven replicate injections. Error bars correspond to ± 2 standard deviations. AGC-EI/MS data (●) correspond to the peak area observed for m/z 182 without isolation or CID. AGC-EI/ISO/MS data (◯) correspond to the isolated peak for m/z 182 and m/z 183 without CID. AGC-EI/MS/MS data (▲) correspond to total peak area for the product ions m/z 77, m/z 105, and m/z 153 of m/z 182. AGC-EI/MS and AGC-EI/ISO/MS fit results are calculated for data points between 0.1 ng and 1000 ng. AGC-EI/MS/MS fit results are calculated for data points between 0.002 ng and 1000 ng.

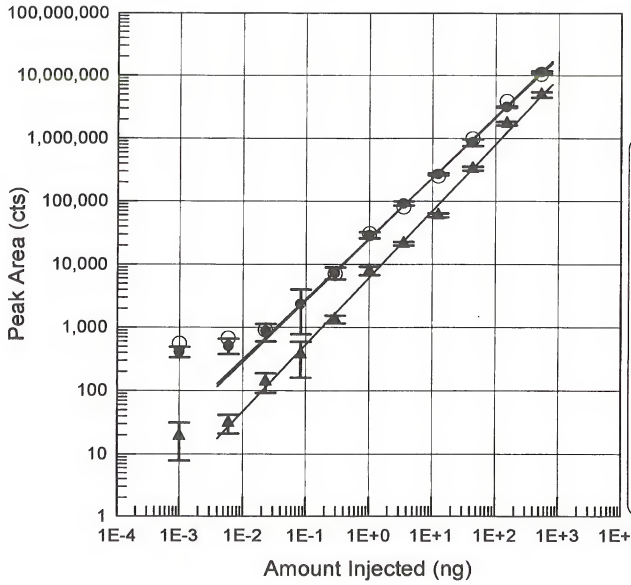


## Calibration Curve Benzophenone products m/z 182

**Fit Results**

●
AGC-EI/MS
m/z 182
log(cts)=0.985*log(ng)+10.14
correlation coef. = 0.998

○
AGC-EI/ISO/MS
m/z 182-183
log(cts)=.9727*log(ng)+10.12
correlation coef. = 0.997

▲
AGC-EI/MS/MS
m/z 77, 105, 153
log(cts)=1.058*log(ng)+8.71
correlation ceof. = 0.995

efficiency, $E_{CID}$, is approximately 20% at the lower sample amounts and 50% at higher sample amounts. This assumes that the three ions plotted, m/z 77$^+$, 105$^+$, and 153$^+$, make up the majority of the product ions that are formed, which is the case.

The overall MS/MS efficiency, $E_{MSMS}$, reflects the ion losses that occur during both the ion isolation and ion excitation stages of the MS/MS experiment and is calculated as the product of $E_{ISO}$ and $E_{CID}$. Thus, for the dissociation of the molecular ion of benzophenone, m/z 182, the overall MS/MS efficiency is approximately 33%. It is significant that CID is the least efficient step since $E_{CID}$ is a measure of the efficiency of the excitation method and the ease with which a particular ion can be dissociated. For the ion trap, the $E_{CID}$ has been observed to approach 100% for ions that dissociate readily, such as the molecular ion of n-butylbenzene. Thus, $E_{CID}$ and $E_{MSMS}$ often decrease for ions that require larger excitation amplitudes to affect dissociation, as is the case for benzophenone.

The linearity of the three log-log calibration curves shown in Figure 5-7 was measured as the slope of the best fit line, where a slope of unity corresponds to a perfectly linear data set. For the AGC-EI/MS, AGC-EI/ISO/MS and AGC/MS/MS calibration curves, the slopes of the best fit lines were 0.985, 0.973, and 1.058, respectively. Visual inspection was used to eliminate data points that clearly fell off of the best fit line. Correlation coefficients of 0.998, 0.997, and 0.995 signify that there is good agreement between the data points and the best fit calibration line. An important difference between the overlapping AGC-EI/MS and AGC-EI/ISO/MS curves and the AGC-EI/MS/MS curves is that the slopes are less than unity and greater than unity, respectively. This is not believed to be an isolated example, since high AGC-EI/MS/MS slopes have been observed in other calibration curves. An explanation of

this effect is that the AGC-EI/MS and AGC-EI/ISO/MS curves level off at the higher sample amounts as the ion traps upper detection limit is reached. Large sample amounts often produce space charge conditions, even when AGC is employed, and can reduce the detection efficiency of the ion trap. For MS/MS experiments, the intensity of each individual product ion is typically much lower than the original parent ion signal. Thus, space charge is reduced in MS/MS experiments and the detection saturation effects would not be observed until larger sample amounts were examined. While this explanation has not been confirmed, it makes sense that MS/MS experiments would be less sensitive to space charge phenomena because the total number of ions is reduced before the mass spectrum is acquired.

The error bars shown in Figure 5-7 indicate ± 2σ standard deviations for seven sample injections. The precision of the peak area measurements is comparable for the three scan modes. As would be expected, the magnitude of the error bars increase as sample amounts decrease. The data points for the 82 pg injections exhibit much larger error bars than any of the other injection that fall within the linear dynamic range of the instrument. In additions, no data were obtained for the AGC-EI/ISO/MS injections at the 82 pg level. Although the source of these anomalies is not known, it appears that the error may have been connected to the 82 pg standard because data for the remaining 224 injections show good precision and reproducibility.

A linear dynamic range from 23.5 pg to 530 ng is observed for the AGC-EI/MS and AGC-EI/ISO/MS calibration curves shown in Figure 5-7. The LDR for the AGC-EI/MS/MS scan mode spans from 6.7 pg to 530 ng. As was observed, MS/MS experiments are expected to produce a lower the limit of detection (LOD) for any analyses that is limited by chemical noise. Although the amount of chemical noise

present in the benzophenone standards is expected to be small, MS/MS can reduce background signals due to the injection port, GC column, and solvent, and can enhance the S/N ratio for the detection of benzophenone.

Figure 5-8 shows the mass chromatogram for the three primary ions detected with (a) an AGC-EI/MS scan program and (b) an AGC-EI/MS/MS scan program for the injection of 23 pg of benzophenone. The chromatographic peak located at scan 412 is due to benzophenone while the other peaks in the AGC-EI/MS mass chromatogram are background interferences. The AGC-EI/MS/MS chromatogram is free of background interferences and has a S/N ratio that approaches infinity. Difficulty in detecting the level of background noise in the MS/MS chromatogram complicates the practical estimation of the LOD because the true background signal is so small that it is not recorded by the data system. In practice, the LOD's for benzophenone have been approximated by the smallest sample amount that produced a characteristic product ion spectrum and a measurable chromatographic peak; 23 pg.

Figure 5-9 shows (a) a background subtracted AGC-EI/MS mass spectrum and (b) a background subtracted AGC-EI/MS/MS mass spectrum for the benzophenone peaks shown in Figure 5-8 (a) and (b). The AGC-EI/MS spectrum shows three large peaks at m/z 77, m/z 105, and m/z 182 that correspond to benzophenone. Two peaks are observed in the AGC-EI/MS/MS spectrum, m/z 150 and m/z 153. While both spectra provide sufficient information for the identification of benzophenone, it is important to point out that without the use of background subtraction, the AGC-EI/MS spectrum would have been difficult to observe amongst an abundance of background signals while the AGC-EI/MS/MS spectrum could be clearly identified without the use of background subtraction. Clearly, MS/MS increases the selectivity of the analyses

Figure 5-8. EI ion chromatograms for benzophenone. (a) AGC-EI/MS and (b) AGC-EI/MS/MS chromatogram for 23 pg of benzophenone. Selected ion chromatogram for the three predominant EI and product ions are plotted for AGC-EI/MS and AGC-EI/MS/MS scan modes.

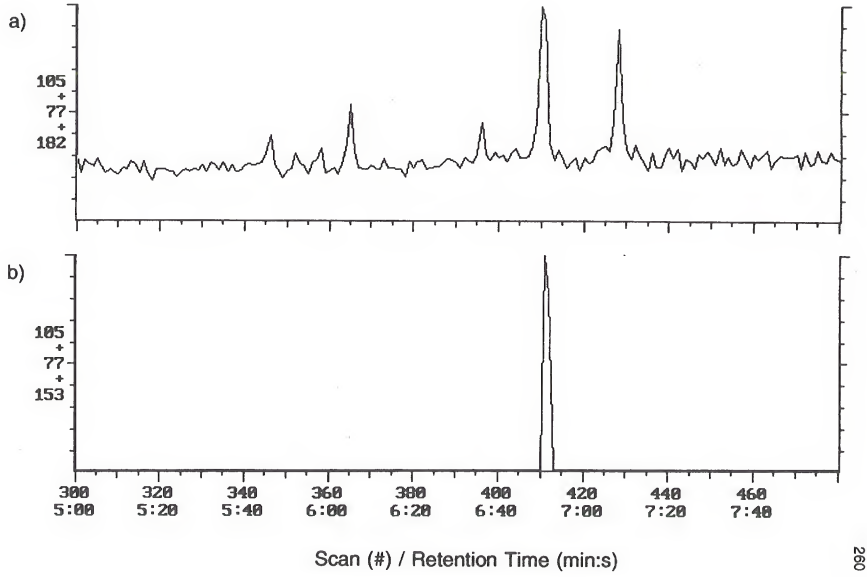
a)
105
+
77
+
182
b)
105
+
77
+
153
300
5:00
320
5:20
340
5:40
360
6:00
380
6:20
400
6:40
420
7:00
440
7:20
460
7:40
Scan (#) / Retention Time (min:s)

Figure 5-9. Background subtracted spectra for 23 pg of benzophenone. (a) AGC-EI/MS full-scan and (b) AGC-EI/MS/MS product ion scan for m/z 182.

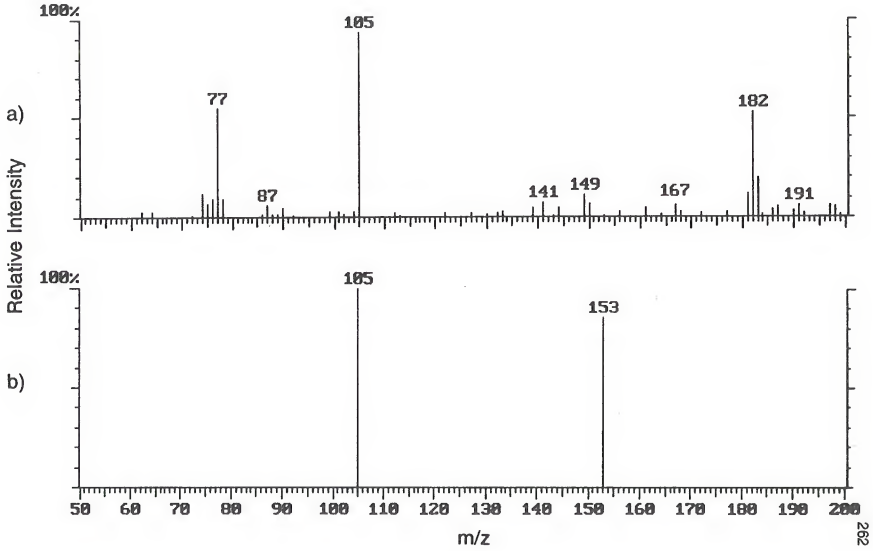
a)
b)
Relative Intensity
100%
100%
105
77
87
141
149
167
182
191
105
153
50
60
70
80
90
100
110
120
130
140
150
160
170
180
190
200
m/z
262

and simplifies the detection of the benzophenone relative to single stage MS experiments.

AGC-CI/MS/MS Calibration Studies

Figure 5-10 shows three chemical ionization calibration curves that were obtained for benzophenone using a standard ARC-CI/MS scan program, an ARC-CI/ISO/MS scan program that includes two-step isolation of m/z 183, and an ARC-CI/MS/MS scan program that includes two-step isolation and SWIFT broadband excitation of m/z 183. A software error resulted in the omission of two data points from the ARC-CI/MS calibration curve and one data point from the ARC-CI/ISO/MS calibration curve. $E_{ISO}$ = 90% and $E_{CID}$ = 60% for the protonated benzophenone which corresponds to an overall $E_{MSMS}$ = 54%. This is higher than the $E_{MSMS}$ that was observed for the EI experiments. The higher CID efficiencies indicate that protonated benzophenone dissociates more readily than the molecular ions formed by EI. The slopes of the best fit lines show good correlations for the ARC-CI/MS, ARC-CI/ISO/MS, and ARC-CI/MS/MS scan modes. Surprisingly, all three slopes were approximately 0.91, corresponding to a non-linear calibration curve. Since the same slope is observed for standard ARC-CI/MS and ARC-CI/MS/MS experiments, the non-linearity is believed to be the result of the chemical ionization event and not a result of MS/MS. Similarly, the linear dynamic range observed for the ARC-CI/MS data is less than that of the AGC-EI/MS data from Figure 5-7. The observation that CI resulted in a reduced LDR relative to EI is surprising at first, but can be explained when space charge is considered. For large sample amounts, ARC forms a fixed number of reagent ions and reduces the length of the CI reaction time to limit the number of CI sample ions

Figure 5-10. Calibration curve for benzophenone (MW = 182). Each data point represents five replicate injections. Error bars correspond to ± 2 standard deviations. ARC-CI/MS data (●) correspond to the peak area observed for m/z 183 without isolation or CID. ARC-CI/ISO/MS data (◯) correspond to the isolated peak for m/z 183 without CID. ARC-CI/MS/MS data (▲) correspond to total peak area for the product ions m/z 91, and m/z 105 of m/z 182. Fit results are calculated for data points between 0.1 ng and 20 ng.

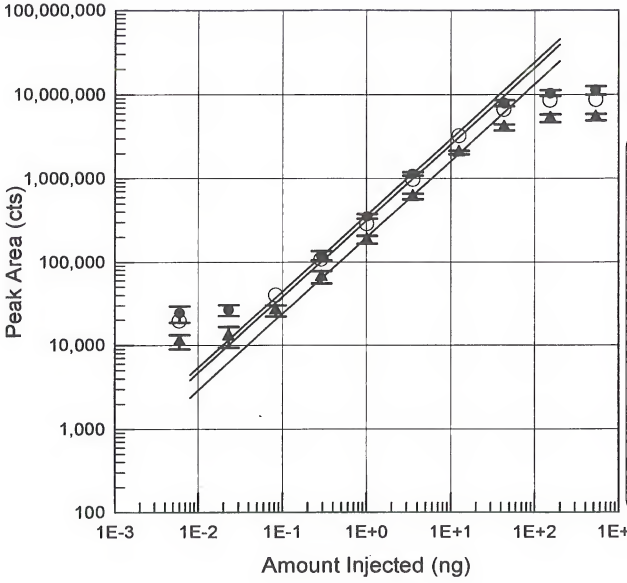


## Calibration Curve Benzophenone products m/z 183

**Fit Results**

ARC-CI/MS
m/z 183
log(cts)=0.9119*log(ng)+12.8
coef. of determ. = 0.998

ARC-CI/ISO/MS
m/z 183
log(cts)=.9110*log(ng)+12.6
coef. of. determ. = 0.996

ARC-CI/MS/MS
m/z 91, 105
log(cts)=0.9154*log(ng)+12.1
ceof. of determ. = 0.997

that are formed. For small sample amounts, the same number of CI reagent ions are allowed to react for a longer period of time to produce more CI sample ions. ARC assumes that the number of CI reagent ions that are formed and stored in the ion trap greatly outnumber the sample molecules present in the ion trap. However, if a large excess of CI reagent ions is not present, the conversion of CI reagent ions into CI sample ions would become less efficient as the sample amount increased and the reaction time decreased. The presence of EI fragment ions that are formed during the CI reagent ion formation period would also result in ARC calculating a reduction in the CI reaction time and decrease the number of CI sample ions that are formed. Both of these effects would result in calibration curves that have a slope that is less than unity as is indicated in Figure 5-10. The EI fragment ions and reduced reaction times may also explain why the upper portion of the calibration curve begins to level off above 40 ng. The non-linear calibration curves shown here would definitely limit the utility of chemical ionization with the ion trap when external standards are employed. However, the fact that ion isolation and collision induced dissociation does add additional non-linearities is a promising result.

Figure 5-11 shows two background subtracted mass spectra for 290 pg of benzophenone that was detected using (a) an ARC-CI/MS scan program and (b) an ARC-CI/MS/MS scan program that isolates and dissociates the protonated benzophenone at m/z 183. The base peak for the ARC-CI/MS spectrum is the protonated molecular at m/z 183, and the other ions in the spectrum constitute the background signal that was not eliminated by background subtraction. The base peak for the ARC-CI/MS/MS spectrum is m/z 105. It is likely that the structure of the 105$^+$, $C_6H_5CO^+$, arises from the loss of $C_6H_6$. An important characteristic of the two spectra

Figure 5-11. Background subtracted spectra for 290 pg of benzophenone. (a) ARC-CI/MS full-scan and (b) ARC-CI/MS/MS product ion scan for m/z 183.

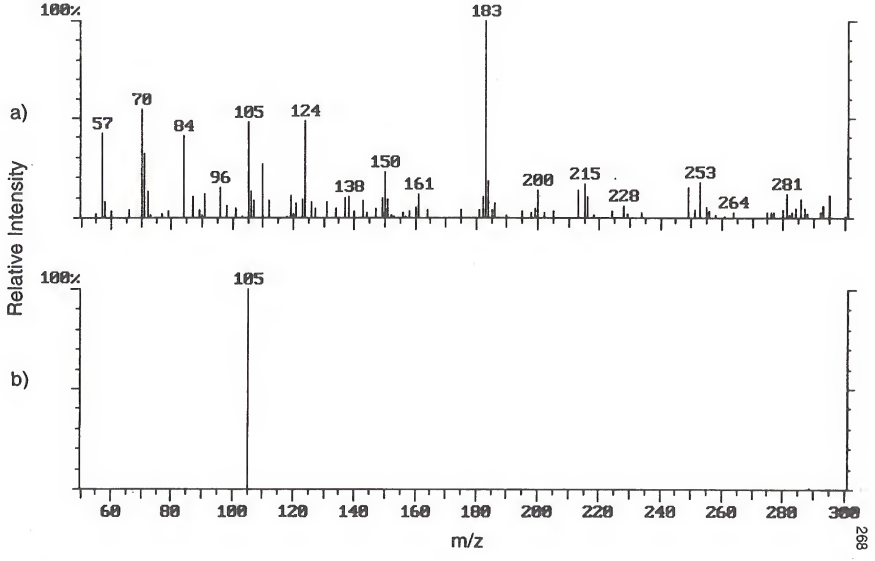
100%
183
70
a)
57
84
105
124
96
150
138
161
200
215
228
253
264
281
Relative Intensity
100%
105
b)
60
80
100
120
140
160
180
200
220
240
260
280
300
m/z
268

is that the ARC-CI/MS/MS spectrum is free of chemical noise relative to the ARC-CI/MS spectrum. This demonstrates that the added selectivity provided by MS/MS can improve the clarity of the mass spectra, even when the amount of chemical noise is low. A particular advantage to CI MS/MS experiments where the protonated molecular is selected as the parent ion is that both molecular weight and structural information is obtained in a single scan.

Figure 5-12 shows two mass chromatogram for the injection of 290 pg of benzophenone that was detected using (a) an ARC-CI/MS scan program and (b) an ARC-CI/MS/MS scan program that isolates and dissociates the protonated benzophenone at m/z 183. The peak at scan 537 in the ARC-CI/MS chromatogram and scan 375 in the ARC-CI/MS/MS spectrum is the benzophenone peak. The ARC-CI/MS chromatographic peak exhibits a S/N ratio of approximately ten and the ARC-CI/MS/MS peak has a S/N ratio that approaches infinity because no background signal was detected. The difference in chromatographic peak shape is attributed to the difference in scan repetition rate between the ARC-CI/MA and ARC-CI/MS/MS scan programs. The longer ARC-CI/MS/MS scan program results in fewer analytical scans acquired every second. Thus, the ARC-CI/MS/MS peak profile is distorted due to the limited number of scans that were acquired over the chromatographic peak.

Fixed Ionization Time Studies

The benzophenone results presented in the previous two sections have compared GC/MS and GC/MS/MS results using the automatic ionization control routines to automatically adjust the ionization time. The use of AGC and ARC assured that the initial number of sample ions was fixed for a given sample amount. Although

Figure 5-12. CI ion chromatograms for benzophenone. (a) ARC-CI/MS and (b) ARC-CI/MS/MS chromatogram for 290 pg of benzophenone. Selected ion chromatograms for the $[M+1]^+$ ion, $183^+$, and product ion $105^+$ are plotted for ARC-CI/MS and ARC-CI/MS/MS scan modes.

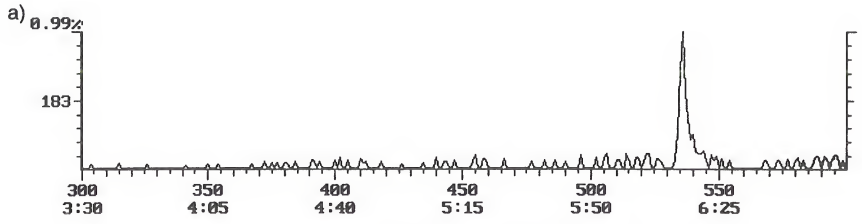
a)
0.99%
183
300
3:30
350
4:05
400
4:40
450
5:15
500
5:50
550
6:25
Scan (#) / Retention Time (min:s)

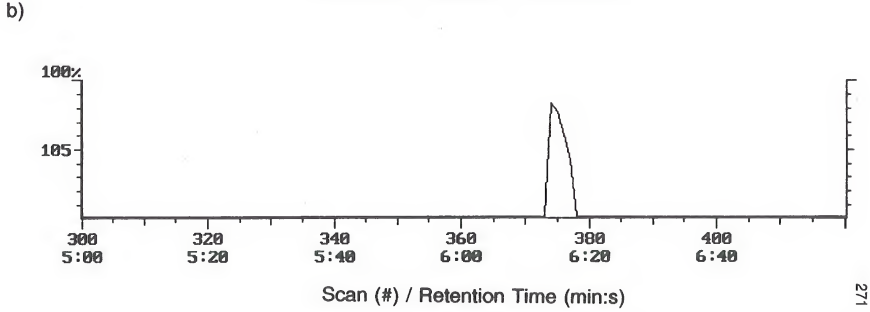
b)
100%
105
300
5:00
320
5:20
340
5:40
360
6:00
380
6:20
400
6:40
Scan (#) / Retention Time (min:s)

this allowed direct comparison of the GC/MS and GC/MS/MS data, it does not demonstrate the additional sensitivity that can be afforded for trace analyses using GC/MS/MS and extended ionization times. It is well appreciated that the sensitivity (as defined by the number of ions detected for a given amount of sample) of the ion trap can be enhanced by augmenting the ionization time to increase the number of ions that are produced during the ionization event. However, the gains in sensitivity that can be obtained by increasing the ionization time are limited by space charge which results in a loss of performance. The most common manifestation of space charge is observed in a loss of resolution and detection efficiency during the selective instability scan. For full-scan MS, where all of the ions are detected, this space charge limit is commonly reached with ionization times ranging from 10 ms to 25 ms. For GC/MS/MS, where all of the ions that are analyzed come from a single parent m/z, longer ionization times can be employed before the space charge affects resolution and detection efficiency. Since the isolation stage of an MS/MS experiment eliminates all but one m/z following ionization, the total number of ions in the ion trap is reduced prior to detection. This allows longer ionization times to be used before space charge limits the resolution and detection efficiency of the selective instability scan.

Figure 5-13 shows two mass chromatograms for the injection of 6.7 pg of benzophenone that were detected using (a) an AGC-EI/MS scan program that had an average ionization time of 5 ms and (b) an EI/MS/MS scan program that had a 150 ms ionization period. Benzophenone eluted from the GC column between scan 375 and scan 380. The background subtracted product ion spectrum (see inset) shows a base peak at m/z 105 and a less intense ion at m/z 77. Clearly, the use of a 150 ms ionization time for the EI/MS/MS scan program increased the number of ions produced

Figure 5-13. Benzophenone EI ion chromatograms for the three predominant EI and $182^{+}$ product ions are plotted for AGC-EI/MS and EI/MS/MS scan modes. (a) AGC-EI/MS and (b) 150 ms fixed ionization time EI/MS/MS, chromatograms for 6.7 pg of benzophenone. AGC selected ionization times ranged between 4 ms and 6 ms. Inset shows the averaged MS/MS product ion spectra observed for m/z 182 and m/z 183 of benzophenone.

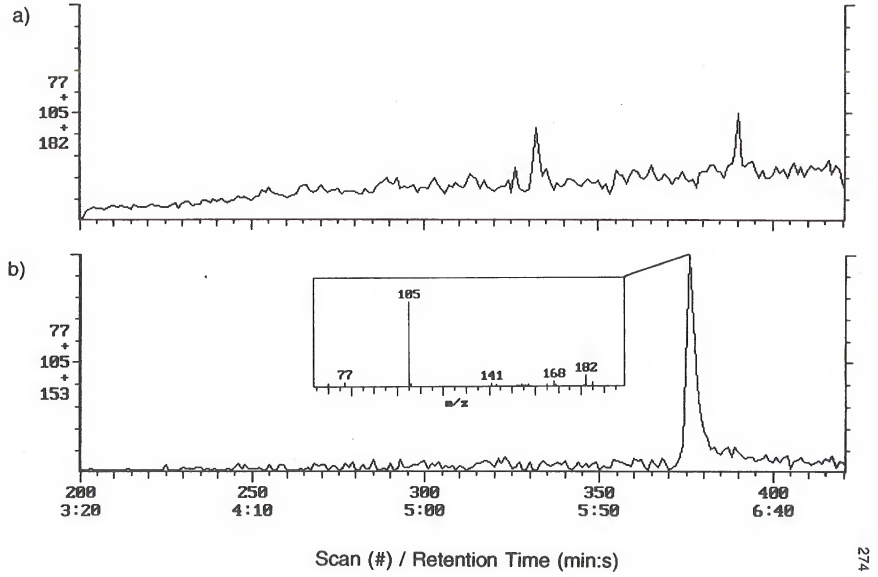
a)
77
+
105
+
182
b)
77
+
105
+
153
105
77
141
168
182
m/z
200
3:20
250
4:10
300
5:00
350
5:50
400
6:40
Scan (#) / Retention Time (min:s)
274

and allowed benzophenone to be detected. The use of an EI/MS scan program with a 150 ms ionization time produced gross space charge conditions and prevented benzophenone from being detected. The EI/MS/MS spectrum observed for benzophenone exhibits several differences from the EI/MS/MS spectrum shown in Figure 5-6. In particular, the intensity of the m/z 105 peak is higher for the extended ionization spectrum relative to the peak at m/z 77. One explanation for the elevated $105^+$ peak is that the extended ionization time provides sufficient time for self-CI to produce the protonated benzophenone which predominantly dissociates to from $105^+$. Differences in the relative intensity of product ions can also be the result of different ion trap pressures, excitation conditions, or background subtraction procedures. It is important to emphasize that increasing the ionization time to increase MS/MS sensitivity only works when small sample amounts are present. The use of long ionization times with large sample amounts can result in gross space charge conditions which reduce ion trap performance. One disadvantage associated with the use of long ionization times is that the LDR is reduced by several orders of magnitude. For benzophenone, the 150 ms ionization time calibration curve could not be approximated by linear fit methods.

Carnitine Analyses

Figure 5-14 shows the CI full scan mass spectrum and structure for the N-demethylated tertiarybutyldimethylsilyl derivative of isobutyrylcarnitine. Demethylation occurs on-column, removing one of three methyl groups from the basic terminus of the acylcarnitine derivative. The molecular weight of the resulting compound for the tertiarybutyldimethylsilyl (TBDMS) derivative of N-demethylated isobutyrylcarnitine is

Figure 5-14. Background subtracted ARC-CI/MS mass spectrum and structure for the N-demethylated tertiarybutyldimethylsilyl derivative of isobutyrylcamitine (MW = 331).

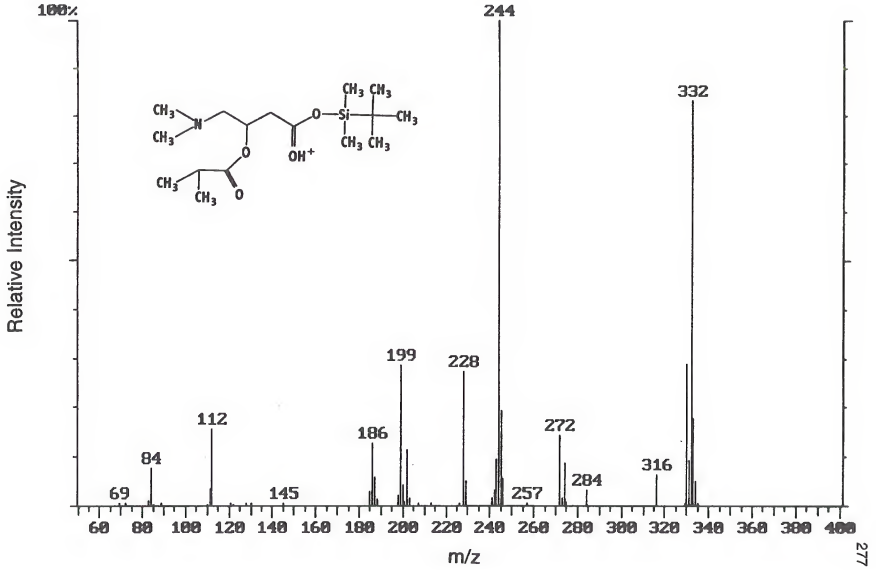
100%
Relative Intensity
244
332
199
228
112
186
272
84
316
284
69
145
257
60 80 100 120 140 160 180 200 220 240 260 280 300 320 340 360 380 400
m/z
277

331 u. The ion trap CI mass spectra for all acylcarnitine derivatives are characterized by abundant protonated molecular ([M+1]$^+$) and are often accompanied by several EI and CI fragment ions. A mixture of CI and EI ions is commonly observed in ion trap CI spectra as a result of the initial EI event that is used to create the CI reagent ions. Characteristic fragment ions that were observed for eight of the nine carnitine derivatives listed in Table 5-5 include 244$^+$ 186$^+$, 112$^+$, and 84$^+$. All of these ions may be accounted for by the fragmentation pathway presented in Figure 5-15. A similar mechanism has been suggested for the fragmentation of acyl N-demethylcarnitine propyl esters.[126] This mechanism shows that the 186$^+$ and both the 112$^+$ and 84$^+$ ions are formed by separate pathways. The 186$^+$ ion is formed by the loss of $Me_2N{=}CH_2$ from the basic terminus. Both the 112$^+$ and the 84$^+$ ions are formed from an intermediate that has lost the TBDMS derivative from the C-terminus. Interestingly, when the 186$^+$ ion was dissociated with an MS/MS experiment, it formed product ions including 112$^+$ and 84$^+$. This result contradicts the pathways proposed in Figure 5-15 and suggests that the 186$^+$ ion may also correspond to a second structure arising from the loss of $CH(CH_3)_3$.

Since the 186$^+$, 112$^+$, and 84$^+$ ions were observed to be characteristic for acylcarnitines regardless of chain length, a 186$^+$ product ion scan was used to screen for acylcarnitines present in both a test mixture and spiked liver tissue extract. Figure 5-16 shows the total ion chromatogram and selected mass chromatograms for 186$^+$, 112$^+$, and 84$^+$ for the analysis of the nine carnitines listed in Table 5-5. Potential carnitine candidates were identified as peaks that contained ion signal for m/z 186, m/z 112, and m/z 84. Figure 5-17 shows the chromatograms that were recorded for the same sample with an MS/MS product ion experiment for m/z 186. Clearly, the MS and

Figure 5-15. Fragmentation pathways for N-demethylated tertiarybutyldimethylsilyl derivatives of acylcarnitines. Adapted from Huang et al.[125]

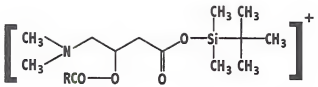

M+

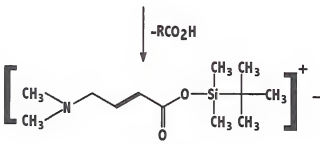

-RCO2H



m/z 244

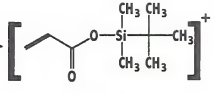

m/z 186

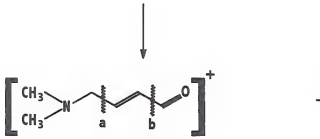

m/z 112

-CO

b

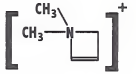

m/z 84

a

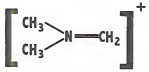

m/z 58

Figure 5-16. AGC-EI/MS chromatograms for nine carnitine standard TBDMS derivatives. Carnitine candidate peaks exhibit ion signal in the 186*, 112* and 84* ion chromatograms.

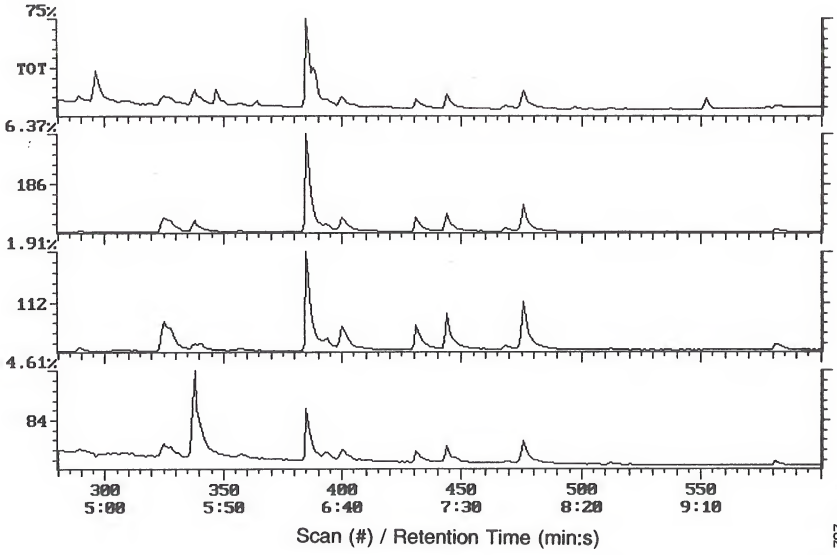
75%
TOT
6.37%
186
1.91%
112
4.61%
84
300
5:00
350
5:50
400
6:40
450
7:30
500
8:20
550
9:10
Scan (#) / Retention Time (min:s)

Figure 5-17. AGC-EI/MS/MS chromatograms for nine carnitine standard TBDMS derivatives. Carnitine candidate peaks exhibit 186* product ion signal in the 112* and 84* ion chromatograms.

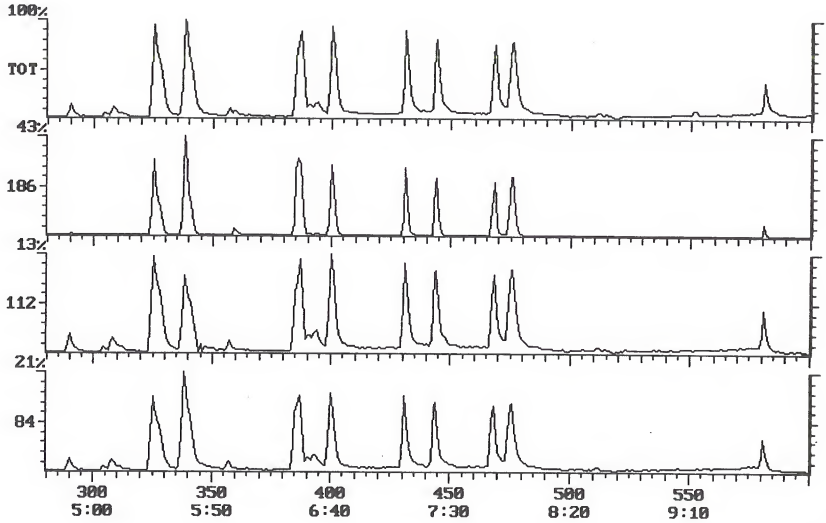
100%
TOT
43%
186
13%
112
21%
84
300
5:00
350
5:50
400
6:40
450
7:30
500
8:20
550
9:10
Scan (#) / Retention Time (min:s)

MS/MS data obtained for the carnitine test mixture demonstrate the usefulness of MS/MS scan modes when screening for compounds of similar structure. Identification of each of the potential carnitine peaks on the basis of retention time or molecular weight was not possible because neither the pure standards nor chemical ionization capabilities were available when these studies were performed.

Figures 5-18 and Figure 5-19 show the EI/MS and EI/MS/MS chromatogram for a liver tissue sample that was spiked with the carnitine standards listed in Table 5-5. The parent ion for the MS/MS experiment again was $186^+$. Of the many GC peaks that are present in the EI/MS total ion chromatogram, only a few low abundance peaks contain the $186^+$, $112^+$ and $84^+$ ions that are indicative of the carnitine derivatives. The EI/MS/MS chromatograms show several peaks at m/z 186 that fragment to form product ions at m/z 112 and m/z 84. The increase in S/N ratio that is observed in the EI/MS/MS chromatogram is a result of the selectivity of the MS/MS experiment and use of longer ionization times. The MS/MS product ion spectra of the $186^+$ ion observed for the carnitine candidate peaks are similar to one another because $186^+$ is a fragment ion (see Figure 5-15) that has lost the variable part of the carnitine species and exhibit few unique characteristics that can be used to identify the different carnitine derivatives in the liver sample. Interestingly, the analysis of an unspiked liver sample extract using the EI/MS/MS $186^+$ product scan revealed two clear acylcarnitine candidate peaks, presented in Figure 5-20 (located between scans 386-390 and scans 465-470), with retention times that match two of the carnitine candidate peaks in the spiked liver tissue. These peaks could not be observed using EI/MS alone and may be evidence of endogenous levels of carnitines in liver tissue.

Figure 5-18. AGC-EI/MS chromatograms for a TBDMS derivitized liver tissue extract containing nine carnitine standards. Carnitine candidate peaks exhibit ion signal in the $186^+$, $112^+$ and $84^+$ ion chromatograms.

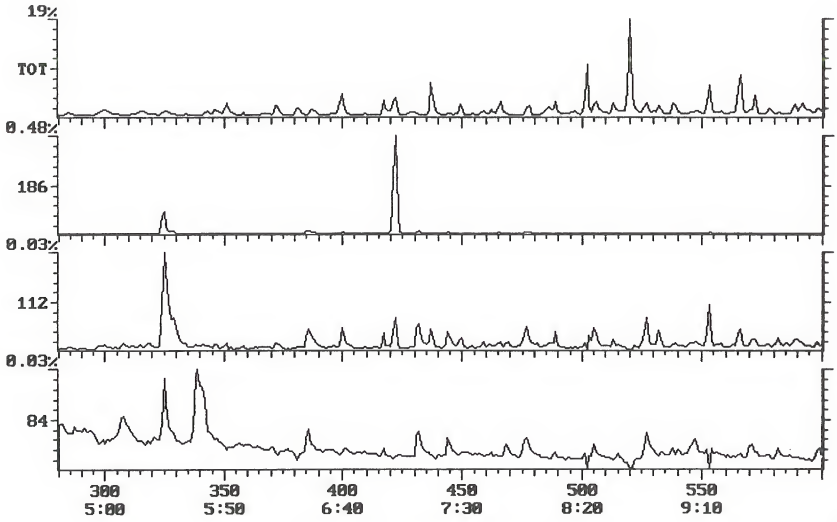
19%
TOT
0.48%
186
0.03%
112
0.03%
84
300
5:00
350
5:50
400
6:40
450
7:30
500
8:20
550
9:10
Scan (#) / Retention Time (min:s)

Figure 5-19. AGC-EI/MS/MS chromatograms for a TBDMS derivitized liver tissue extract containing nine carnitine standard. Carnitine candidate peaks exhibit $186^+$ product ion signal in the $112^+$ and $84^+$ ion chromatograms.

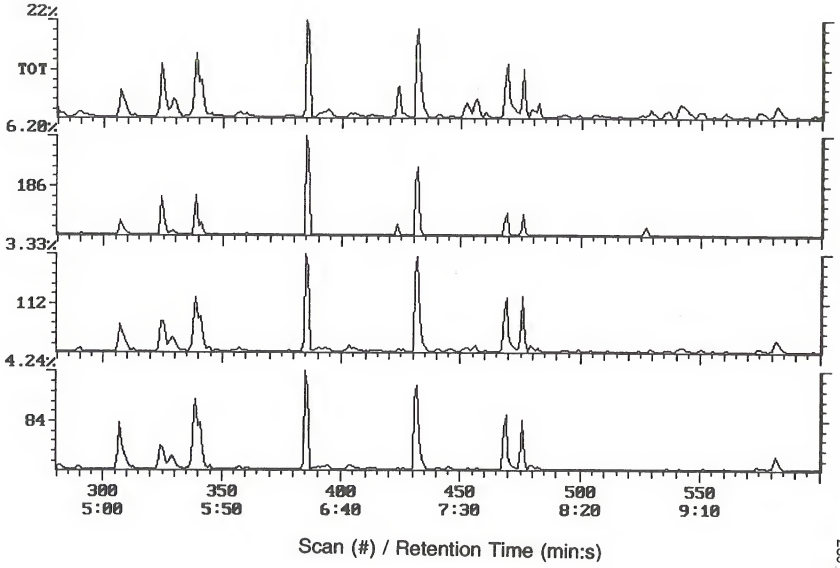
22%
TOT
6.20%
186
3.33%
112
4.24%
84
300
5:00
350
5:50
400
6:40
450
7:30
500
8:20
550
9:10
Scan (#) / Retention Time (min:s)

Figure 5-20. AGC-EI/MS/MS chromatograms for a TBDMS derivitized liver tissue extract. Carnitine candidate peaks exhibit $186^+$ product ion signal in the $112^+$ and $84^+$ ion chromatograms.

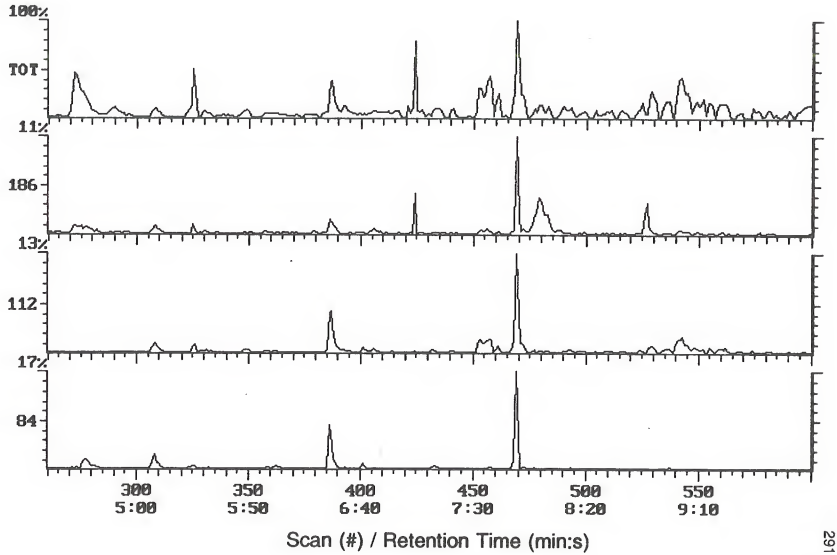
100%
TOT
11%
186
13%
112
17%
84
300
5:00
350
5:50
400
6:40
450
7:30
500
8:20
550
9:10
Scan (#) / Retention Time (min:s)

Additional GC/MS/MS Analyses

Figure 5-21 compares (a) the CI/MS background subtracted mass spectrum and (b) the CI/MS/MS background subtracted mass spectrum for the injection of 1.25 ng of cocaine. The $[M+1]^+$ ion at m/z 304 was selected as the parent ion for the MS/MS product ion experiment. The primary fragment ion observed for cocaine was m/z 182 which corresponds to the loss of a neutral benzoyl group ($C_7H_6O_2$). A limitation of the current GC/MS/MS software is that the automatic scaling of the ARC-CI/MS/MS scan function did not isolate m/z 304 correctly. Several manual adjustments and repetitive injections were required before the parent ion was isolated and the SWIFT excitation amplitude was adjusted correctly for the formation of product ions. For samples of limited volume, such as the cocaine samples, the need for manual adjustments and repetitive sample injections was a serious problem. However, the source of these difficulties appears to be the limited precision of the ITS-40 electronics and RF calibration procedures, which were originally intended for GC/MS use. As more precise instrumentation is developed, the ability to automatically calibrate and tune ion trap MS/MS scan programs should improve.

A second limitation of the current ion trap configuration are ion-molecule reactions that can occur when sample amounts and background neutral sample pressures are high. Figure 5-22 shows the AGC-EI/MS ion chromatogram for m/z 134 that was obtained for the injection of a petroleum oil sample that was diluted in hexane 1:100 (v:v). To determine if any of the peaks present in the oil sample were due to n-butylbenzene (MW = 134), m/z 134 was selected as the parent ion for an MS/MS product ion experiment. Figure 5-23 shows the background subtracted mass spectrum

Figure 5-21. Background subtracted CI spectra for 1.25 ng of cocaine (MW = 303). (a) ARC-CI/MS full-scan and (b) ARC-CI/MS/MS product ion scan for m/z 304.

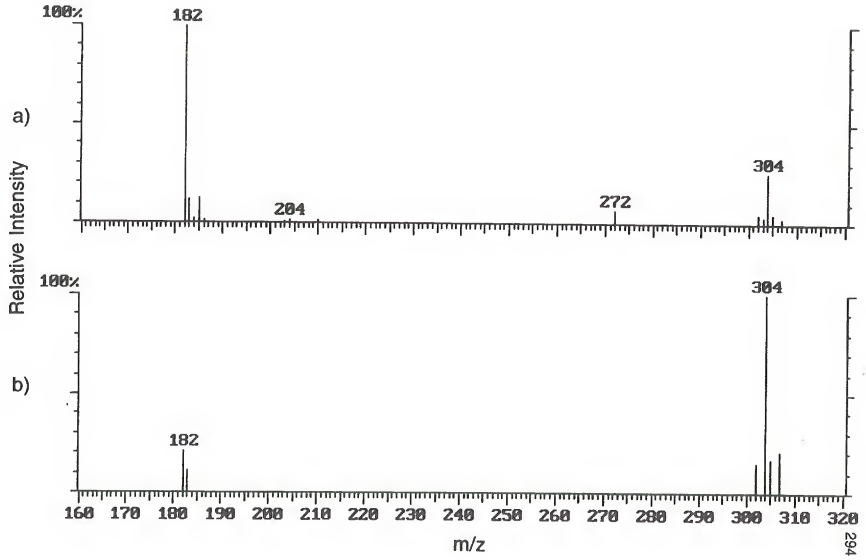
100%
182
a)
304
204
272
Relative Intensity
100%
304
b)
182
160 170 180 190 200 210 220 230 240 250 260 270 280 290 300 310 320
m/z
294

Figure 5-22. AGC-EI/MS chromatogram for the injection of petroleum oil that was diluted 1:100 (v:v) in hexane. The 134$^+$ ion chromatogram shows candidate peaks for n-butylbenzene (MW = 134).

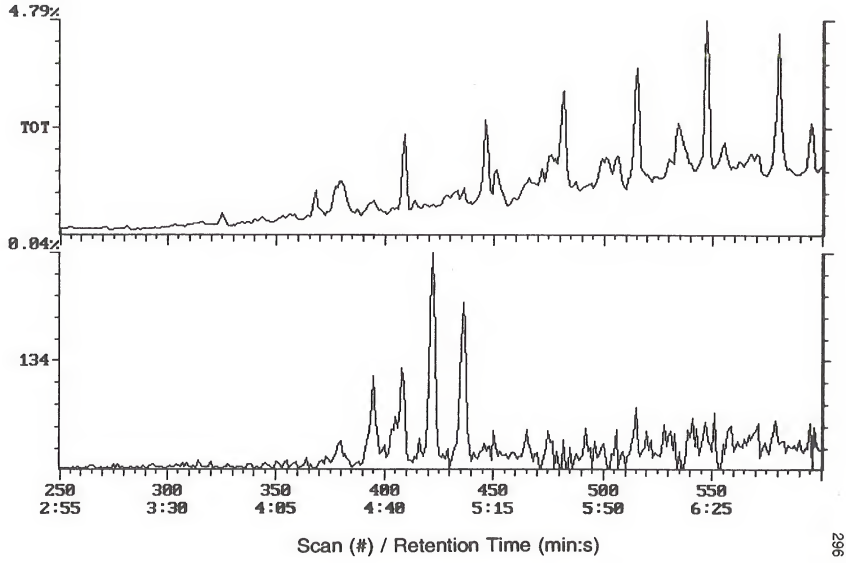
4.79%
TOT
0.04%
134
250
2:55
300
3:30
350
4:05
400
4:40
450
5:15
500
5:50
550
6:25
Scan (#) / Retention Time (min:s)
296

Figure 5-23. AGC-EI/MS/MS background subtracted mass spectrum for the injection of petroleum oil that was diluted 1:100 (v:v) in hexane. The ions above m/z 136 are the result of ion-molecule that involve the isolated parent ions $133^+$, $134^+$, and $135^+$ and neutral oil sample molecules.

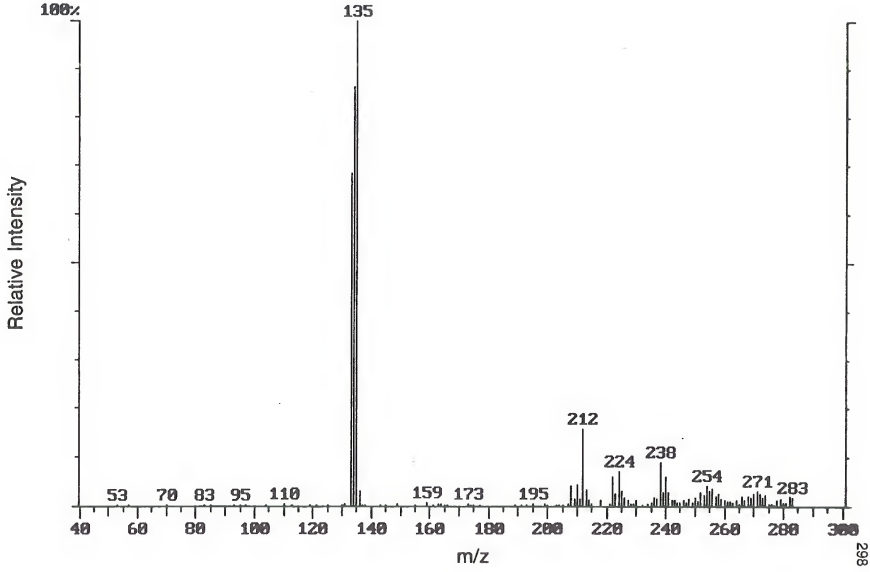
100%
135
Relative Intensity
212
224
238
254
271
283
53
70
83
95
110
159
173
195
40
60
80
100
120
140
160
180
200
220
240
260
280
300
m/z
268

for the isolated parent ion $134^+$ for the oil sample examined in Figure 5-22. Note that two-step isolation was adjusted to isolate ions between m/z 133 and m/z 135. The ions that appear above m/z 200 were determined to be the result of ion-molecule reactions that occurred after the isolation step of the MS/MS scan program. The formation of anomalous peaks in MS/MS spectra complicates both target and unknown analyses and reduces the selectivity of MS/MS detection. One method for reducing ion-molecule reaction is to use a physically separate ion source and ion trap analyzer.

The CI/MS/MS capabilities of the ion trap allow molecular weight verification and structural confirmations to be obtained in a single experiment. To demonstrate this, a barbiturate test mixture containing 2 ng of barbital (MW = 184), butobarbital (MW = 212), amobarbital (MW = 226), pentobarbital (MW = 226), and secobarbital (MW = 238) was assayed by ARC-CI/MS and ARC/CI/MS/MS. Figure 5-24 shows the total ion chromatogram that was obtained using a standard ARC-CI/MS scan program, including the identities of each of the peaks and the structures of the two isomers amobarbital and pentobarbital. The CI/MS full scan mass spectra for amobarbital and pentobarbital show abundant $[M+1]^+$ peaks at m/z 227 and several EI fragment ions which are commonly observed in ion trap CI spectra. Figure 5-25 shows the total ion chromatogram and m/z 227 product ion spectra that were obtained with an ARC-CI/MS/MS experiment. The ARC-CI/MS/MS chromatogram shows two chromatographic peaks which correspond to both of the barbiturates that have a molecular weight of 226 u, amobarbital and pentobarbital. The product ion spectra for the protonated barbiturates display different characteristic fragment ions. Amobarbital dissociates to produce product ions at m/z 141, m/z 156, and m/z 184 that are less intense than the remaining parent ion intensity. Pentobarbital dissociates more readily

Figure 5-24. Total ion chromatogram for a barbiturate test mixture containing five barbiturates at 2 ng/μL level that was analyzed with a ARC-CI/MS scan program. The inset shows the chemical structures of the two isomers amobarbital and pentobarbital.

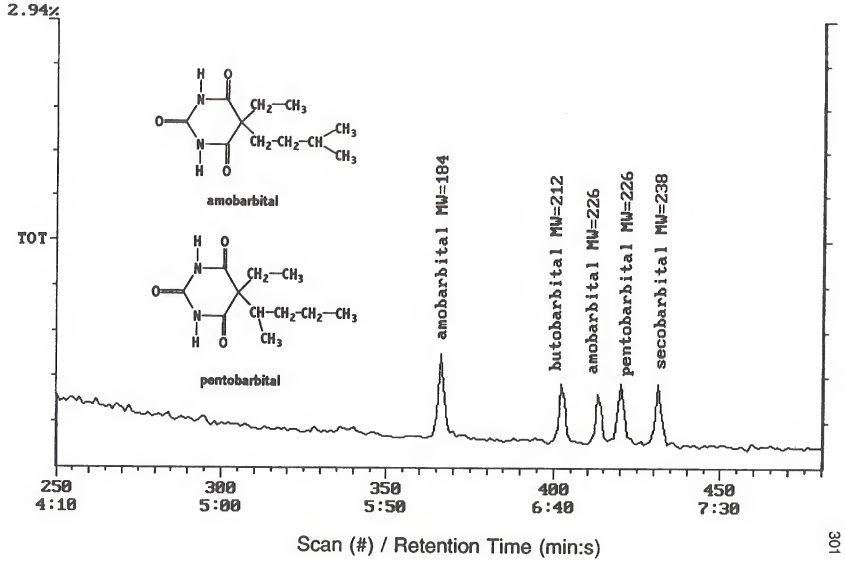
2.94x
TOT
amobarbital
pentobarbital
amobarbital MW=184
butobarbital MW=212
amobarbital MW=226
pentobarbital MW=226
secobarbital MW=238
250
4:10
300
5:00
350
5:50
400
6:40
450
7:30
Scan (#) / Retention Time (min:s)

Figure 5-25. Total ion chromatogram for a barbiturate test mixture containing five barbiturates at 2 ng/μL level that was analyzed with a ARC-CI/MS/MS $227^{+}$ product ion scan program. The insets shows the product ion spectra obtained for the two isomers amobarbital and pentobarbital.

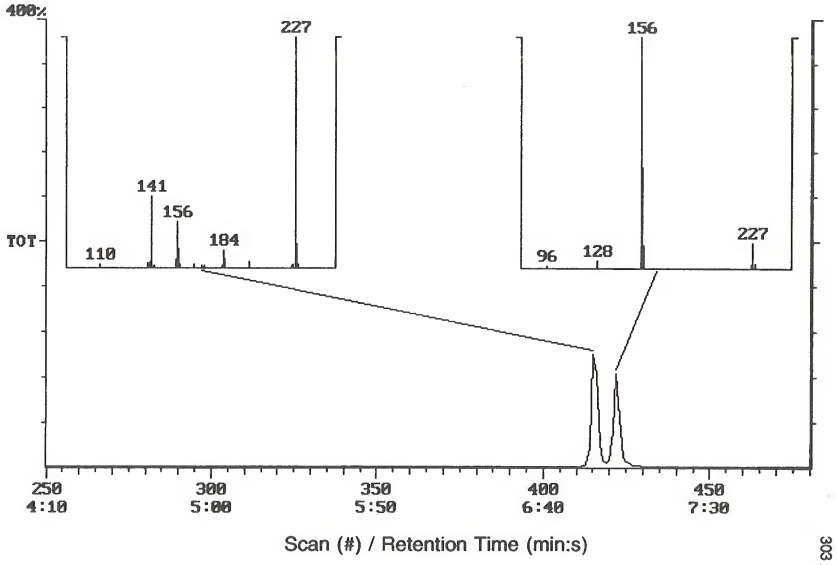
400%
TOT
227
141
156
184
110
156
227
96
128
250
4:10
300
5:00
350
5:50
400
6:40
450
7:30
Scan (#) / Retention Time (min:s)

and forms an intense product ion at m/z 156. Comparison of Figures 5-24 and 5-25 also demonstrates the increased selectivity that can be achieved with MS/MS relative to MS alone. The ARC-CI/MS/MS chromatogram contains two peaks as opposed to the five peaks that are observed in the ARC-CI/MS chromatogram. In additions, the S/N ratio observed for the ARC-CI/MS/MS chromatogram is greater than the S/N ratio of the ARC-CI/MS chromatogram.

## Summary

The instrumentation demonstrated in this study represents the first successful coupling of gas chromatography and tandem mass spectrometry on the quadrupole ion trap. The combination of automatic ionization control, two-step isolation, and SWIFT broadband excitation was used to solve many of the problems that have limited the utility of GC/MS/MS on the quadrupole ion trap. In particular, the use of automatic ionization control allows samples of unknown concentrations to be analyzed without the need for repetitive sample injections that were previously needed to adjust the ionization time. Two-step isolation is observed to be a reliable technique for mass selecting the parent ion prior to CID and also serves to reduce space charge effects that limit ion trap performance. SWIFT broadband excitation is found to be a reliable method for affecting CID over a chromatographic peak regardless of the ions exact frequency of motion. The automated instrument control software that allowed non-standard scan programs to be implemented on the ITS-40 also enhanced the instrument's capabilities and simplified many of the complex adjustments that have been associated with ion trap MS/MS experiments.

The results illustrated in this chapter identify several of the strengths and weaknesses of ion trap GC/MS/MS instrumentation. First, the EI and CI MS/MS results for benzophenone demonstrate that comparable product ion spectra can be obtained for sample amounts that range from the low picogram to the high nanogram levels. Second, the linearity and linear dynamic range observed for ion trap GC/MS/MS is equivalent to or better than that of GC/MS. Third, the added selectivity of ion trap MS/MS experiments is shown to lower the detection limits for trace analyses and improve the confidence of identifications. Finally, the use of extended ionization times in conjunction with MS/MS is found to improve the ion trap's sensitivity for sample amounts that are at or below the detection limits of GC/MS.

Example applications presented in this chapter highlight several potential advantages and limitations of ion trap GC/MS/MS. For the analysis of camitines, ion trap MS/MS is observed to be a useful screening tool for compounds of like structure. The additional sensitivity of MS/MS also allowed several camitine candidates to be detected in the spiked and endogenous liver samples that could not be observed by GC/MS alone. Ion trap MS/MS can also provide useful structural information that can be used to assign fragmentation pathways for gas phase ions. In addition, reproducible product ion spectra were obtained for cocaine and barbiturate samples via GC/MS/MS. Ion-molecule reactions were identified as a potential limitation of ion trap GC/MS/MS for complex mixture analysis, such as the identification of trace analytes in petroleum samples. An instrumental limitation of the current GC/MS/MS was the accuracy with which a single m/z could be isolated prior to CID, although the development of improved electronics and refined calibration software is expected to solve this problem.

# CHAPTER 6
# CONCLUSIONS AND FUTURE WORK

Based on the success of these investigations, it is very likely that ion trap instruments will begin to be utilized as "high performance" tandem mass spectrometers as well as inexpensive GC/MS detectors. The significance of this work is three-fold. First, the development of methods that allow the GC/MS/MS capabilities of the ion trap to be realized is important in that it advances the analytical capabilities of an instrument that is expected to be the mass spectrometer of choice for the next century. Second, the study of new methods of mass analysis and ion excitation has offered new insight into the fundamental relationships that underlie the ion trap's operation as a mass spectrometer. Third, the construction of a reliable GC/MS/MS ion trap is significant in that it has provided the first measurements of ion trap GC/MS/MS performance.

A systematic approach was used to identify the effect of GC sample introduction on each of the four stages of the MS/MS experiment; ionization, isolation, excitation, and detection. Automatic ionization control, used to minimize space change and increase sensitivity, was observed to be a necessity for the analysis of samples that have a wide range of analyte concentrations. Two-step isolation was demonstrated as a new, more efficient, method of isolating a parent ion that requires less optimization than traditional RF/DC methods. SWIFT broadband excitation was identified to be the most efficient and reliable technique for effecting CID of a parent

ion over a GC peak out of three ion excitation methods studied. MS/MS was observed to enhance ion detection relative to that of MS alone, by minimizing the detection of chemical interferences and by reducing space charge conditions. An important aspect of this work is that the instrumentation that was developed included all of these features, making it uniquely capable to evaluate the figures of merit for ion trap GC/MS/MS.

Automatic ionization control techniques, AGC for EI and ARC for CI, allowed samples of varying concentration to be analyzed without manual adjustment of the principal ionization parameters; ionization and reaction time. GC/MS/MS calibration curves obtained using AGC and ARC exhibited a linear response for sample amounts from the low picogram and high nanogram range. A limitation of these techniques is that they use the total ion signal to calculate ionization times. This procedure can prematurely limit MS/MS sensitivity when large numbers of background ions are present in the full-scan spectrum. The development of automatic ionization control methods that base the ionization time used for MS/MS experiments on the intensity of the isolated parent ion would be expected to increase the sensitivity of MS/MS above that of MS for complex mixtures. Background ions that reduce the ionization times calculated by AGC and ARC could also be reduced with the implementation of selective ion injection methods that fill the ion trap with the MS/MS parent ion.

The ion-molecule reactions observed between mass selected parent ions and neutral background molecules are shown to reduce the selectivity of ion trap MS/MS and complicate the interpretation of product ion spectra. These effects may be minimized in future studies by removing the background neutral molecules from the ion

trap. Two potential solutions to these problems are the use of ion injection or pulsed valve sample introduction.

Ion isolation was shown to be a critically important step for ion trap MS/MS experiments because the isolation of a m/z or narrow m/z range greatly reduces the number of ions present in the ion trap. This serves to reduce space charge effects that can cause frequency shifts, loss of detection efficiency, reduced mass accuracy, and limited resolution. Ion isolation also fulfills the first requirement of the MS/MS experiment, mass analysis of the parent ion. CID experiments alone do not exhibit the S/N benefits of MS/MS.

Two new figures of merit were defined and test procedures were developed to quantitatively evaluate ion isolation techniques. Using these tools, apex and two-step isolation where characterized. Two-step isolation was shown to be more efficient than apex isolation. Future studies that characterize other isolation techniques, such as resonant ejection and selective injection methods, may offer new advantages for MS/MS and lend insight into the different means available for performing mass analysis with ion traps. An important shortcoming of this work was the ion trap's inability to reproducibly isolate a single m/z with high efficiency during GC/MS/MS experiments. The difficulties encountered with isolation of one m/z are believed to be the result of imprecise calibration of the Mathieu parameters $a_z$ and $q_z$, as well as the inaccuracies of the ITS40 ion trap electronics. The developments and demonstration of methods that can achieve unit mass isolation over a GC peak without manual optimization is a necessary step if ion trap GC/MS/MS is to be widely applicable.

The excitation of ions was demonstrated using three techniques, the frequency-assignment pre-scan, frequency modulated broadband excitation, and SWIFT

broadband excitation. Of these, SWIFT broadband excitation was viewed as the most practical method for effecting CID over a chromatographic peak. However, little is known about the motion of ions that are excited with SWIFT waveforms compared to the motion of ions excited by single frequency techniques. Close examination of the effects of the many SWIFT parameters may produce more efficient or selective excitation techniques and could also provide insight into the ion excitation process.

The use of frequency sweep techniques, such as the frequency-assignment pre-scan, offer new methods and opportunities for studying ion motion, ion activation, and ion detection. In particular, the profiles of the peaks that are detected with frequency sweeps exhibit many differences that may provide information about ion trajectories and losses during ion activation. The rate with which ions absorb resonant power could also be studied using frequency sweeps.

The GC/MS/MS ion trap developed in this study was used to demonstrate reproducible CID over GC peaks. Linear calibration curves were obtained for EI and CI GC/MS/MS experiments without the use of internal standards. Comparable product ion spectra were obtained for sample amounts in the low picogram and high nanogram range without manual adjustment of the ion trap scan program. The measurement of both molecular weights and characteristic CID spectra in a single experiment was demonstrated using CI/MS/MS. Instrument control software was developed that simplified the steps involved in performing GC/MS/MS experiments.

In conclusion, this work clearly demonstrates that ion traps are capable performing GC/MS/MS experiments. However, before ion trap GC/MS/MS receives widespread use, the utility of ion trap GC/MS/MS for solving real analytical problems must be demonstrated and reliable commercial instruments must be available. One

goal that was not possible to accomplished in this work was the development of refined GC/MS/MS ion trap applications. Certainly, much can be learned about the use of ion trap GC/MS/MS by developing assays for a wide range of applications. In particular, using the ion trap for a large number GC/MS/MS analyses, such as would be required to verify the analysis of acylcarnitines, and comparison of the results with those obtained by traditional methods, would enhance the results presented in this study.

REFERENCE LIST


1. Louris, J. N., Cooks, R. G., Syka, J. E. P., Kelley, P. E., Stafford, G. C. & Todd, J. F. J. *Anal. Chem.* 59, 1677-1685 (1987).

2. March, R. E. & Hughes, R. J. *Quadrupole Storage Mass Spectrometry* (Wiley, New York, 1989).

3. Stafford, G. C., Kelley, P. E., Syka, J. E. P., Reynolds, W. E. & Todd, J. F. J. *Int. J. Mass Spectrom. Ion Processes* 60, 85-98 (1984).

4. March, R. E. *Int. J. Mass Spectrom. Ion Processes* 118/119, 71-135 (1992).

5. Todd, J. F. J *Mass. Spectrom. Rev.* 10, 3-52 (1991).

6. Reiser, H. P., Julian Jr., R. K. & Cooks, G. R. *Int. J. Mass Spectrom. Ion Processes* 121, 49-63 (1992).

7. Franzen, J. *Int. J. Mass Spectrom. Ion Processes* 130, 15-40 (1994).

8. Johnson, J. V., Pedder, R. E. & Yost, R. A. *Int. J. Mass Spectrom. Ion Processes* 106, 197-212 (1991).

9. Johnson, J. V., Pedder, R. E., Yost, R. A. & Story, M. S. *United States Patent* 5075547, 1-8 (1991).

10. Schwartz, J. C., Syka, J. E. P. & Jardine, I. *J. Am. Soc. Mass Spectrom.* 2, 198-204 (1991).

11. Williams, J. D. & Cooks, R. G. *Rapid Commun. Mass Spectrom.* 6, 524-527 (1992).

12. Morand, K. Reiser, H. Williams, J. D. Julian, R. & Cooks, R. G. "Factors Affecting Mass Measurement Accuracy in the Quadrupole Ion Trap" *Personal Communication* (1992).

13. Stafford, G. C., Kelley, P. E. & Stephens, D. R. *United States Patent* 4540884, 1-14 (1985).

14. Stafford, G. C., Kelley, P. E. & Bradford, D. C. *Am. Lab.* 15(6), 51-52, 54-57 (1983).

15. Eichelberger, J. W., Bellar, T. A., Donnelly, J. P. & Budde, W. L. *J. Chromatogr. Sci.* 28, 460-467 (1990).

16. Lim, H. K., Sakashita, C. O. & Foltz, R. L. *Rapid Commun. Mass Spectrom.* 2, 129-131 (1988).

17. Philp, R. P., Lewis, C. A., Campbell, C. & Johnson, E. *Org. Geochem.* 14, 183-187 (1989).

18. Louris, J. N., Amy, J., Ridley, T., Kascheres, C. & Cooks, R. G. *Proceedings of the 35th ASMS Conference on Mass Spectrometry and Allied Topics* Atlanta, GA, 769-770 (1987).

19. Syka, J. E. P., Louris, J. N., Kelley, P. E., Stafford, G. C. & Reynolds, W. E. *United States Patent* 4736101, 1-12 (1988).

20. Louris, J. N., Brodbelt, J. S., Cooks, R. G., Glish, G. L., Van Berkel, G. J. & McLuckey, S. A. *Int. J. Mass Spectrom. Ion Processes* 96, 117-137 (1990).

21. Strife, R. J. & Simms, J. R. *Anal. Chem.* 61, 2316-2319 (1989).

22. Todd, J. F. J., Penman, A. D., Thorner, D. A. & Smith, R. D. *Rapid Commun. Mass Spectrom.* 4, 108-113 (1990).

23. Morand, K. L., Cox, K. A. & Cooks, R. G. *Rapid Commun. Mass Spectrom.* 6, 520-523 (1992).

24. Brodbelt, J. S., Liou, C. C. & Donovan, T. *Anal. Chem.* 63, 1205-1209 (1991).

25. McLuckey, S. A., Van Berkel, G. J., Glish, G. L., Huang, E. C. & Henion, J. D. *Anal. Chem.* 63, 375-383 (1991).

26. Glish, G. L., Goeringer, D. E., Asano, K. G. & McLuckey, S. A. *Int. J. Mass Spectrom. Ion Processes* 94, 15-24 (1989).

27. McLuckey, S. A., Glish, G. L. & Van Berkel, G. J. *Int. J. Mass Spectrom. Ion Processes* 106, 213-235 (1991).

28. Johnson, J. V., Yost, R. A., Kelley, P. E. & Bradford, D. C. *Anal. Chem.* 62, 2162-2172 (1990).

29. Strife, R. J., Simms, J. R. & Lacey, M. P. *J. Am. Soc. Mass Spectrom.* 1, 265-271 (1990).

30. Brodbelt, J. S., Louris, J. N. & Cooks, R. G. *Anal. Chem.* 59, 1278-1285 (1987).

31. Louris, J. N., Syka, J. E. P. & Kelley, P. E. *United States Patent* 4686367, 1-14 (1987).

32. Weber-Grabau, M., Bradshaw, S. C. & Syka, J. E. P. *United States Patent* 4771172, 1-7 (1988).

33. Shetty, H. U., Daly, E. M., Greig, N. H., Rapoport, S. I. & Soncrant, T. T. *J. Am. Soc. Mass Spectrom.* 2, 168-173 (1991).

34. De Jong, E. G., Maes, R. A. A. & Van Rossum, J. M. *J. Pharm. Biomed. Anal.* 6, 987-993 (1988).

35. Strife, R. J., Kelley, P. E. & Weber-Grabau, M. *Rapid Commun. Mass Spectrom.* 2, 105-109 (1988).

36. Kaiser, R. E., Cooks, R. G., Syka, J. E. P. & Stafford, G. C. *Rapid Commun. Mass Spectrom.* 4, 30-33 (1990).

37. Louris, J. N., Amy, J. W., Ridley, T. Y. & Cooks, R. G. *Int. J. Mass Spectrom. Ion Processes* 88, 97-111 (1989).

38. Williams, J. D., Reiser, H. -P., Kaiser, R. E. & Cooks, R. G. *Int. J. Mass Spectrom. Ion Processes* 108, 199-219 (1991).

39. Louris, J. N., Brodbelt-Lustig, J. S., Kaiser, R. E. & Cooks, R. G. *Proceedings of the 36th ASMS Conference on Mass Spectrometry and Allied Topics* San Diego, CA, 968-969 (1988).

40. Schwartz, J. C. & Cooks, R. G. *Proceedings of the 36th ASMS Conference on Mass Spectrometry and Allied Topics* San Diego, CA, 634-635 (1988).

41. McLuckey, S. A., Glish, G. L. & Van Berkel, G. J. *Proceedings of the 38th ASMS Conference on Mass Spectrometry and Allied Topics* Tucson, AZ, 512-513 (1990).

42. Pedder, R. E., Yost, R. A. & Weber-Grabau, M. *Proceedings of the 37th ASMS Conference on Mass Spectrometry and Allied Topics* Miami, FL, 468-469 (1989).

43. Eckenrode, B. A., Glish, G. L. & McLuckey, S. A. *Int. J. Mass Spectrom. Ion Processes* 99, 151-167 (1990).

44. Fales, H. M., Sokoloski, E. A., Pannell, L. K., Quan-L, P, Klayman, D. L., Lin, A. J., Brossi, A., & Kelley, J. A. *Anal. Chem.* 62, 2494-2501 (1990).

45. Kaiser, R. E., Cooks, R. G., Moss, J. & Hemberger, P. H. *Rapid Commun. Mass Spectrom.* 3, 50-53 (1989).

46. Kaiser, R. E., Louris, J. N., Amy, J. W. & Cooks, R. G. *Rapid Commun. Mass Spectrom.* 3, 225-229 (1989).

47. Williams, J. D., Cox, K., Morand, K. L., Cooks, R. G. & Julian, R. K.,Jr. *Proceedings of the 39th ASMS Conference On Mass Spectrometry and Allied Topics* Nashville, TN, 1481-1482 (1991).

48. Cooks, R. G., Cox, K., Williams, J. D., Morand, K. L. & Julian, R. K.,Jr. *Proceedings of the 39th ASMS Conference On Mass Spectrometry and Allied Topics* Nashville, TN, 469-470 (1991).

49. Goeringer, D. E., Whitten, W. B., Ramsey, J. M., McLuckey, S. A. & Glish, G. L. *Anal. Chem.* 64, 1434-1439 (1992).

50. Weber-Grabau, M. *United States Patent* 4818869, 1-8 (1989).

51. Yates, N. A., Yost, R. A., Bradshaw, S. C. & Tucker, D. B. *Proceedings of the 39th ASMS Conference On Mass Spectrometry and Allied Topics* Nashville, TN, 1489-1490 (1991).

52. Tucker, D. B., Hameister, C. H., Bradshaw, S. C., Hoekman, D. J. & Weber-Grabau, M. *Proceedings of the 36th ASMS Conference on Mass Spectrometry and Allied Topics* San Diego, CA, 628-629 (1988).

53. Fulford, J. E., Hoa, D. N., Hughes, R. J., March, R. E., Bonner, R. F. & Wong, G. J. *J. Vac. Sci. Technol.* 17, 829-835 (1980).

54. Creasar, C. S., McCoustra, M. R. S. & O'Neil, K. E. *Org. Mass Spectrom.* 26, 335-338 (1991).

55. Strife, R. J. & Simms, J. R. *J. Am. Soc. Mass Spectrom.* 3, 372-377 (1992).

56. Arnold, N. S., Kalousek, P., McClennen, W. H., Gibbons, J. R., Maswadeh, W. & Meuzelaar, H. L. C. *Proceedings of the 38th ASMS Conference on Mass Spectrometry and Allied Topics* Tucson, AZ, 613-614 (1990).

57. Bruns Weller, E. & Tillmanns, U. *GIT Fachz. Lab.* 33, 1159-1160, 1162 (1989).

58. Canela, A. M. & Muehleisen, H. *J. Chromatogr.* 456, 241-249 (1988).

59. Fuerst, P., Krueger, C., Meemken, H. A. & Groebel, W. *J. Chromatogr.* 405, 311-317 (1987).

60. Evans, S., Smith, R. D. & Wellby, J. K. *Int. J. Mass Spectrom. Ion Processes* 60, 239-249 (1984).

61. Pereira, W. E., Rostad, C. E. & Leiker, T. J. *Anal. Chim. Acta* 228, 69-75 (1990).

62. De Boer, D., De Jong, E. G & Maes, R. A. A. *Rapid Commun. Mass Spectrom.* 4, 181-185 (1990).

63. Horman, I., Traitler, H. & Aeschlimann, J. *J. High Resolut. Chromatogr.* 12, 308-315 (1989).

64. Aggazzotti, G., Predieri, G., Fantuzzi, G. & Benedetti, A. *J. Chromatogr.* 416, 125-130 (1987).

65. Anon., *Anal. Rep.* 16-18, (1987).

66. Leloux, M. S. & Maes, R. A. A. *Biological Mass Spectrometry* 20, 382-388 (1991).

67. Leloux, M. S., De Jong, E. G. & Maes, R. A. A. *J. Chromatogr.* 488, 357-367 (1989).

68. Genin, E. & Lehrer, M. *Analusis* 16, 54-57 (1988).

69. Horman, I. & Traitler, H. *Biomed. Environ. Mass Spectrom.* 18, 1016-1022 (1989).

70. Van Berkel, G. J. & Goeringer, D. E. *Anal. Chim. Acta* 277, 41-54 (1993).

71. Yates, N. A., Yost, R. A., Bradshaw, S. C. & Tucker, D. B. *Proceedings of the 39th ASMS Conference On Mass Spectrometry and Allied Topics* Nashville, TN, 132-133 (1991).

72. Chappel, C. G., Creaser, C. S., Stygal, J. W. & Shepherd, M. J. *Biological Mass Spectrometry* 21, 688-692 (1992).

73. Yates, N. A., Griffin, T. P. & Yost, R. A. *Proceedings of the 41st ASMS Conference on Mass Spectrometry and Allied Topics* San Francisco, CA, 125 (1993).

74. Schachterle, S. & Brittain, R. D. *Proceedings of the 41st ASMS Conference on Mass Spectrometry and Allied Topics* San Francisco, CA, 639 (1993).

75. Creaser, C. S., Mitchell, D. S., O' Neill, K. E. & Trier, K. J. *Rapid Commun. Mass Spectrom.* 4, 217-221 (1990).

76. Galletti, G. C., Traldi, P. & Bonaga, G. *Rapid Commun. Mass Spectrom.* 3, 241-243 (1989).

77. Galletti, G. C., Marotti, M., Piccaglia, R., Pelli, B. & Traldi, P. *Flavour Fragrance J.* 4, 155-159 (1989).

78. Stafford, G. C., Taylor, D. T., Bradshaw, S. C., Syka, J. E. P. & Uhrich, M. *Proceedings of the 35th ASMS Conference on Mass Spectrometry and Allied Topics* Atlanta, GA, 775-776 (1987).

79. Todd, J. F. J., Waldren, R. M. & Mather, R. E. *Int. J. Mass Spectrom. Ion Phys.* 345, 325-349 (1980).

80. Vedel, F. & Andre, J. *Int. J. Mass Spectrom. Ion Processes* 65, 1-22 (1985).

81. Chattopadhyay, A. P. & Ghosh, P. K. *Int. J. Mass Spectrom. Ion Phys.* 49, 253-263 (1983).

82. Pannell, L. K., Pu, Q. L., Fales, H. M., Mason, R. T. & Stephenson, J. L. Jr. *Anal. Chem.* 61, 2500-2503 (1989).

83. McLuckey, S. A., Glish, G. L., Asano, K. G. & Van Berkel, G. J. *Anal. Chem.* 60, 2312-2314 (1988).

84. Vedel, F., Vedel, M. & March, R. E. *Int. J. Mass Spectrom. Ion Processes* 108, R11-R20 (1991).

85. Vedel, F., Vedel, M. & March, R. E. *Int. J. Mass Spectrom. Ion Processes* 99, 125-138 (1990).

86. Eades, D. M. & Yost, R. A. *Rapid Commun. Mass Spectrom.* 6, 573-578 (1992).

87. Kleintop, B. L., Yost, R. A. & Abolin, C. R. *J. Am. Soc. Mass Spectrom.* 3, 85-88 (1992).

88. Pedder, R. E., Johnson, J. V. & Yost, R. A. *Proceedings of the 40th ASMS Conference on Mass Spectrometry and Allied Topics* San Francisco, CA, 1761-1762 (1993).

89. Kelley, P. E., Hoekman, D. J., Bradshaw, S. C. & Stiller, S. W. *Proceedings of the Pittsburgh Conference on Analytical Chemistry and Applied Spectroscopy* Atlanta, GA March 8, 1081 (1993).

90. Olson, E. S. & Diehl, J. W. *Anal. Chem.* 59, 443-448 (1987).

91. Ratnayake, W. M. N., Timmins, A., Ohshima, T. & Ackman, R. G. *Lipids* 21, 518-524 (1986).

92. Watson, J. T. *Introduction To Mass Spectrometry - Second Edition* (Raven Press, New York, 1985) 121-152.

93. McLuckey, S. A., Goeringer, D. E. & Glish, G. L. *J. Am. Soc. Mass Spectrom.* 2, 11-21 (1993).

94. Eades, D. M., Yates, N. A. & Yost, R. A. *Proceedings of the 39th ASMS Conference On Mass Spectrometry and Allied Topics* Nashville, TN, 1491-1492 (1991).

95. Julian, R. K. & Cooks, R. G. *Anal. Chem.* 65, 1827-1833 (1993).

96. Buttrill, S. E., Shaffer, B., Karnicky, J. & Arnold, J. T. *Proceedings of the 40th ASMS Conference on Mass Spectrometry and Allied Topics* San Francisco, CA, 1015-1016 (1993).

97. Yates, N. A., Eades, D. M., Jones, J. A., Booth, M. M., Stephenson, J. L., Griffin, T. P., & Yost, R. A. *J. Am. Soc. Mass Spectrom.* (1994). (submitted)

98. Chen, L., Wang, T-C. L., Ricca, T. L. & Marshall, A. G. *Anal. Chem.* 59, 449-454 (1987).

99. Schwartz, J. C. & Jardine, I. *Rapid Commun. Mass Spectrom.* 6, 313-317 (1992).

100. McLuckey, S. A., Glish, G. L. & Asano, K. G. *Anal. Chim. Acta* 225, 25-35 (1989).

101. Bier, M. E., Winkler, P. C. & Herron, J. R. *J. Am. Soc. Mass Spectrom.* 4, 38-46 (1992).

102. Pinkston, J. D., Delaney, T. E., Morand, K. L & Cooks, R. G. *Anal. Chem.* 62, 1571 (1992).

103. Van Berkel, G. J., Glish, G. L. & McLuckey, S. A. *Anal. Chem.* 62, 1284-1295 (1990).

104. Booth, M. M, Stephenson, J. L. J. & Yost, R. A. *Proceedings of the 41st ASMS Conference on Mass Spectrometry and Allied Topics* San Francisco, CA, 198 (1993).

105. Berberich, D. W., Hail, M. E., Johnson, J. V., Yost, R. A. *Int. J. Mass Spectrom. Ion Processes.* 94:115-147 (1989).

106. Todd, J. F. J, Penmann, A. D., Thorner, D. A. & Smith, R. D. *Proceedings of the 38th ASMS Conference on Mass Spectrometry and Allied Topics* Tucson, AZ, 532-533 (1990).

107. Johnson, J. V., Pedder, R. E. & Yost, R. A. *Rapid Commun. Mass Spectrom.* 6, 760-764 (1992).

108. McLuckey, S. A., Goeringger, D. E. & Glish, G. L. *Anal. Chem.* 64, 1455-1460 (1992).

109. Lammert, S. A. & Cooks, R. G *Rapid Commun. Mass Spectrom.* 6, 528-530 (1992).

110. Wang, M. & Wells, G. *Proceedings of the 41st ASMS Conference on Mass Spectrometry and Allied Topics* San Francisco, CA, 474 (1993).

111. Kelley, P. E., Stafford, G. C. & Syka, J. E. P. *United States Patent* 4749860, 1-7 (1988).

112. Creaser, C. S., Mitchell, D. S., O'Neill, K. E. & Trier, K. J. *Rapid Commun. Mass Spectrom.* 4, 217-221 (1990).

113. Einhorn, J., Kenttamaa, H. I. & Cooks, R. G. *J. Am. Soc. Mass Spectrom.* 2, 305-313 (1991).

114. Hart, K. J., McLuckey, S. A. & Glish, G. L. *J. Am. Soc. Mass Spectrom.* 3, 680-682 (1992).

115. Einhorn, J., Duffault, J. M., Virelizier, H. & Tabet, J. C. *Rapid Commun. Mass Spectrom.* 2, 112-115 (1988).

116. Yates, N. A. & Yost, R. A. *Ion Catcher Mass Spectrometer Software User Manual* University of Florida Copyright (1992).

117. Gronowska, J., Paradisi, C., Traldi, P. & Vettori, U. *Rapid Commun. Mass Spectrom.* 4, 306-313 (1990).

118. March, R. E., McMahon, A. W., Londry, F. A., Alfred, R. L., Todd, J. F. J. & Vedel, F. *Int. J. Mass Spectrom. Ion Processes* 95, 119-156 (1989).

119. March, R. E., McMahon, A. W., Allinson, E. T., Londry, F. A., Alfred, R. L., Todd, J. F. J. & Vedel, F. *Int. J. Mass Spectrom. Ion Processes* 99, 109-124 (1990).

120. March, R. E., Londry, F. A., Alfred, R. L., Todd, J. F. J., Penman, A. D., Vedel, F. & Vedel, M. *Int. J. Mass Spectrom. Ion Processes* 110, 159-178 (1991).

121. Gallant, J. A. *Electrical Design News* November 9, 95-104 (1989).

122. Press, W. H. Teukolsky, S. A. Vetterling, W. T. & Flannery, B. P. *Numerical Recipes in C* (Cambridge University Press, New York, 1992).

123. Yost, R. A., Enke, C. G., McGilvery, D. C., Smith, D., & Morrison, J. D., *Int. J. Mass Spectrom. Ion Phys.* 30(2), 127-136 (1979).

124. Huang, Z. -H. Gage, D. A. Beiber, L. L & Sweeley, C. C. *Personal Communication* (1992).

125. Srzic, D., Martinovic, S., Vujanic, P. & Meic, Z. *Rapid Commun. Mass Spectrom.* 7, 163-166 (1993).

126. Huang, Z. -H., Gage, D. A., Beiber, L. L & Sweeley, C. C. *Anal. Biochem.* 199, 98-105 (1991).

## BIOGRAPHICAL SKETCH

Nathan Andrew Yates, son of Kerin N. Yates and John T. Yates Jr., was born in Silver Spring, Maryland, on April 27, 1966. He graduated from Sandy Spring Friends School in 1984. From 1984 to 1988 he attended Allegheny College in Meadville, Pennsylvania, where he graduated with a Bachelor of Science degree in chemistry. While at Allegheny, he was an active member of the Delta Tau Delta fraternity. During the summers of 1986 and 1987, Nate worked at the National Institute of Standards and Technology, in Gaithersburg, Maryland. His internship, under the guidance of Dr. Alan Fried, involved the development of an $NO_x$ calibration apparatus for chemiluminescence, tunable diode laser, and gas phase titration instrumentation. For his senior research project at Allegheny, Nate constructed a computer controlled spectrofluorometer for measuring the room temperature excitation/emission surfaces of motor oils.

In August 1988, Nate began his graduate work in analytical chemistry at the University of Florida under the direction of Dr. Richard A. Yost. In 1990, a six month industrial cooperative program at Finnigan Corporation, San Jose, California, allowed Nate to pursue his engineering interest while developing instrument control software for commercial mass spectrometers. Dr. George C. Stafford and Mr. Stephen C. Bradshaw of Finnigan Corporation supervised his work and taught Nate the programming skills that were used for his graduate studies. On June 15, 1991, Nate married Jan Sallach, whom he had met his freshman year in college. As a graduate

student, he was awarded the Kenan analytical award sponsored by Union Carbide and a fellowship given by the Shell Oil Company.

Upon completion of his graduate research, Nate accepted a postdoctoral position in the Biological Mass Spectrometry Laboratory at the University of Virginia, Charlottesville, Virginia. Under the direction of Dr. Donald F. Hunt and Dr. Jeffrey Shabanowitz, Nate has begun to study the sequences and fragmentation pathways for biologically important peptides.

I certify that I have read this study and that in my opinion it conforms to acceptable standards of scholarly presentation and is fully adequate, in scope and quality, as a dissertation for the degree of Doctor of Philosophy.

Richard A. Yost, Chairman
Professor of Chemistry

I certify that I have read this study and that in my opinion it conforms to acceptable standards of scholarly presentation and is fully adequate, in scope and quality, as a dissertation for the degree of Doctor of Philosophy.

Charles L. Beatty
Professor of Materials Science and Engineering

I certify that I have read this study and that in my opinion it conforms to acceptable standards of scholarly presentation and is fully adequate, in scope and quality, as a dissertation for the degree of Doctor of Philosophy.

Samuel O. Colgate
Associate Professor of Chemistry

I certify that I have read this study and that in my opinion it conforms to acceptable standards of scholarly presentation and is fully adequate, in scope and quality, as a dissertation for the degree of Doctor of Philosophy.

Anna Brajter-Toth
Associate Professor of Chemistry

I certify that I have read this study and that in my opinion it conforms to acceptable standards of scholarly presentation and is fully adequate, in scope and quality, as a dissertation for the degree of Doctor of Philosophy.

James D. Winefordner
Graduate Research Professor of Chemistry

This dissertation was submitted to the Graduate Faculty of the Department of Chemistry in the College of Liberal Arts and Sciences and to the Graduate School and was accepted as partial fulfillment of the requirement for the degree of Doctor of Philosophy.

April, 1994

_____

Dean, Graduate School